Experimental and Theoretical Study of Carbon Dynamics in an Algal-Bacterial Co-Culture

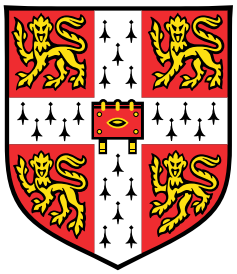

Hannah Laeverenz Schlogelhofer

Department of Physics
University of Cambridge

This dissertation is submitted for the degree of
Doctor of Philosophy

Gonville and Caius College October 2018

Declaration

This dissertation is the result of my own work and includes nothing which is the outcome of work done in collaboration except as declared in the Preface and specified in the text. It is not substantially the same as any that I have submitted, or, is being concurrently submitted for a degree or diploma or other qualification at the University of Cambridge or any other University or similar institution except as declared in the Preface and specified in the text. I further state that no substantial part of my dissertation has already been submitted, or, is being concurrently submitted for any such degree, diploma or other qualification at the University of Cambridge or any other University or similar institution except as declared in the Preface and specified in the text. It does not exceed the prescribed word limit of 60,000 words for the Degree Committee of the Department of Physics.

Hannah Laeverenz Schlogelhofer
October 2018

Acknowledgements

I especially thank my supervisor Dr Ottavio Croze for his kind support, encouragement and guidance throughout my PhD. I also thank my second supervisor Professor Alison Smith for her support and advice, particularly on the biological aspects of my project.

I have thoroughly enjoyed the interdisciplinary nature of my PhD, which has allowed me the pleasure of interacting with researchers from a wide range of disciplines and backgrounds. I thank François Peaudecerf, who has provided valuable guidance on mathematical modelling. The model I have developed during my PhD is based on François' work on microbial mutualisms and has benefited greatly from his advice. I am hugely grateful to Dr Rachel Foster and the members of her group at Stockholm University, who provided valuable guidance and advice regarding SIMS. I also thank Matrin Whitehouse, Kerstin Lindén and others at the NordSIM facility, who were incredibly welcoming and provided great help with my SIMS experiments. I acknowledge Professor Howard Griffiths and Dr Moritz Meyer who provided helpful advice about stable isotope labelling and the Godwin lab, in particular James Rolfe, for running IRMS analysis on my samples. I thank members of the Biological and Soft Systems group, especially Di Jin, Theresa Jakuszeit and Camille Febvre, for helpful discussions and being wonderful colleagues. I am grateful to Alison Smith's group for sharing their knowledge and experience in algal research, especially Vaibhav Bhardwaj who first introduced me to microbiological techniques and the biology of mutualisms, and Freddy Bunbury whose work has prompted many stimulating discussions. I also thank Dr Nalin Patel and Dr Sian Dutton for their support.

My PhD has been as much an experience in personal growth as it has been in academic development and for that I greatly appreciate the support from several people but in particular my PhD supervisors and Dr Karishma Jain. I also especially thank my amazing family who provide constant encouragement and my good friend Yassen Abbas for his wonderful support. I am also incredibly grateful for all I have gained from the inspiring and supportive women I have met through the Homeward Bound network.

Finally, I would like to thank the NanoDTC for giving me the funding and opportunity to carry out this work. I also acknowledge the Winton Programme for the Physics of Sustainability and Gonville and Caius College for the travel grants they have awarded me.

Abstract

Microbial communities are an important component of biogeochemical cycles in ecosystems across our planet. Photosynthetic phytoplankton perform carbon fixation, converting carbon dioxide into organic molecules. Some of these organic molecules are released by the phytoplankton and can be subsequently metabolised by heterotrophic bacteria, therefore heterotrophic bacteria play an important role in determining the fate of fixed carbon. In order to understand how carbon is transported within ecosystems it is important to study the metabolic processes, like photosynthesis, respiration and inter-species nutrient exchange, which underpin the microbial contribution to the carbon cycle. The multitude of species and interactions that exist within a natural microbial community makes studying specific inter-species nutrient dynamics challenging. The approach of this thesis is to use a two species co-culture in order to reduce complexity and increase control over experimental parameters. As a result, it becomes possible to study the carbon exchange between algae and bacteria in detail.

This thesis considers the co-culture between a vitamin B_{12}-dependent alga, the *metE7* mutant of *Chlamydomonas reinhardtii*, and a B_{12}-producing, heterotrophic bacterium, *Mesorhizobium loti*. The interaction between these two species is a type of mutualism, because both species benefit from the presence of the other. The bacteria provide B_{12} to the algae and in exchange the bacteria are able to metabolise some of the organic carbon molecules produced by the algae. The carbon dynamics were studied experimentally using stable isotope labelling and Secondary Ion Mass Spectrometry (SIMS), providing temporal measurements at the single cell level of the carbon assimilation by the algae and its transfer to bacteria.

In the mathematical ecology of interacting species, competition and predator-prey dynamics have been studied more extensively than cooperation. Models that are used to describe interacting species are typically at the population level and only relatively recently have nutrient dynamics been included more explicitly. Creating models that encode our current understanding of metabolic processes means that it is possible to test how well these processes are able to account for experimental observations. Extending a model that was previously developed to describe a mutualism at a distance, the carbon dynamics in the algal-bacterial co-culture were described mathematically by considering algal photosynthesis, organic car-

bon exchange, bacterial respiration and bacterial inorganic carbon metabolism. The model was used to fit carbon isotope labelling dynamics measured experimentally using SIMS, and thus to test our understanding of the carbon dynamics in an algal-bacterial co-culture. Additionally, the model was used to predict potential origins of the temporal evolution of the single-cell distributions observed in the SIMS measurements. The predictive power of the model is illustrated by examining the effect of changing an initial condition or model parameter, providing examples of possible experiments that could further test the model.

Table of contents

List of figures

List of tables

Chapter 1

Introduction

1.1 Microbial ecology: networks and nutrient cycles

Microorganisms are microscopic life forms that include bacteria, microalgae, archaea and protists. Microbial ecology examines how microorganisms interact with each other, their environment and other living organisms (Atlas *et al.*, 1998). Studying microbial interactions is important to better understand the interspecies conflicts and partnerships that exist within microbial communities and their ecological impact (Hom *et al.*, 2015; Momeni *et al.*, 2011; Phelan *et al.*, 2012). Figure 1.1 summarises all possible pairwise interactions that can exist between two species and includes three possible outcomes for the individual species involved: positive, negative or neutral (Faust *et al.*, 2012; Holland *et al.*, 2009). Natural and synthetic microbial communities are widely seen to hold enormous biotechnological potential for novel industrial, medical and environmental applications (Goers *et al.*, 2014; Kouzuma *et al.*, 2015; Zomorrodi *et al.*, 2016).

Biogeochemical cycling describes the movement and transformation of materials by physical, chemical and biochemical processes that occur on a global scale impacting the geology, ecology and environment of our planet (Atlas *et al.*, 1998). All living organisms contribute to biogeochemical cycles, but microorganisms play a particularly major role because of their ubiquity, abundance and metabolic diversity (Atlas *et al.*, 1998). The study of microorganisms and microbial ecology spans many length scales, including the study of subcellular biochemical processes, population dynamics, microbial communities and global biogeochemistry (Brussaard *et al.*, 2016; Shou *et al.*, 2015). Integrating understanding across these different scales is an important area of research for uncovering insights into how microorganisms engage with their environment (Brussaard *et al.*, 2016). Recent technological advances, including techniques like high throughput sequencing, proteomics and metabolomics, allow for the diversity and function of microbial communities to be catalogued

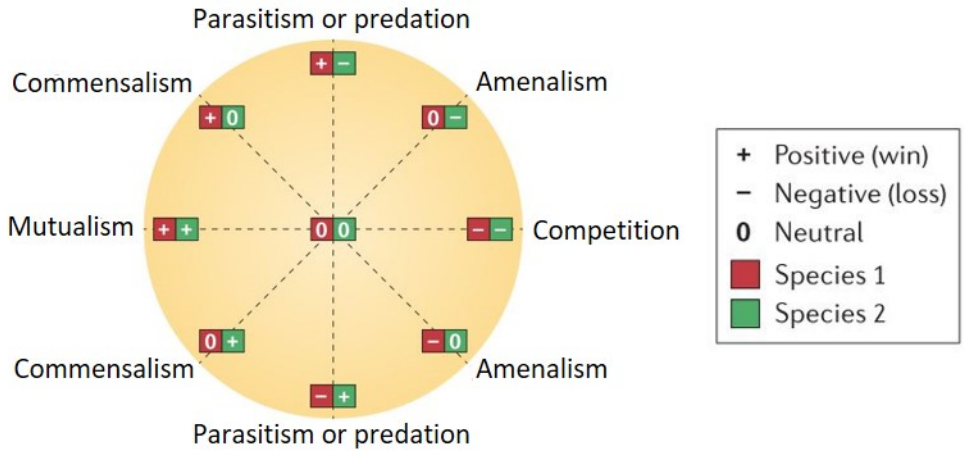

Figure 1.1 **Types of ecological interactions**. Reproduced from Faust *et al.* (2012), this diagram summarises all possible pairwise interactions, which have three possible outcomes for an interaction partner: positive (+), negative (-) or neutral (0). For example parasitism or predation is when one species benefits at the expense of the other, giving '+-', whereas a mutualism is when both species benefit from the interaction, giving '++'.

in an extraordinary level of detail. This kind of 'omics' data represents a snapshot of the species, genes, metabolites and activities present in a given microbial community (Antwis *et al.*, 2017; Widder *et al.*, 2016). An ongoing challenge is to go beyond cataloguing and to uncover mechanistic understanding that can convert experimental data into fundamental insights (Brussaard *et al.*, 2016; Widder *et al.*, 2016). One approach is to combine experiments and theory to build models for predicting the function of dynamically changing microbial communities (Clark *et al.*, 2017; Momeni *et al.*, 2011; Phelan *et al.*, 2012; Widder *et al.*, 2016; Zaccaria *et al.*, 2017). There are many sources of complexity in biological systems, for example they have a large number of interacting parts, intrinsic heterogeneity and can span a wide range of length and time scales (Shou *et al.*, 2015). Due to the complexity of the interactions within natural microbial communities, it can be useful to use simplified communities for reduced complexity and increased control over experimental parameters (Momeni *et al.*, 2011; Widder *et al.*, 2016). The advantage of such artificial communities is the possibility for more systematic hypothesis testing of ecological mechanisms like metabolic interactions, temporal dynamics and spatial structure (Widder *et al.*, 2016). This can contribute to creating a more complete and nuanced understanding of how microorganisms impact and are impacted by their environment, and how interactions between species influence population dynamics, community function and evolution (Momeni *et al.*, 2011; Widder *et al.*, 2016). Figure 1.2 gives an overview of the scope of microbial ecology research and how the field draws on different modelling approaches and experimental data.

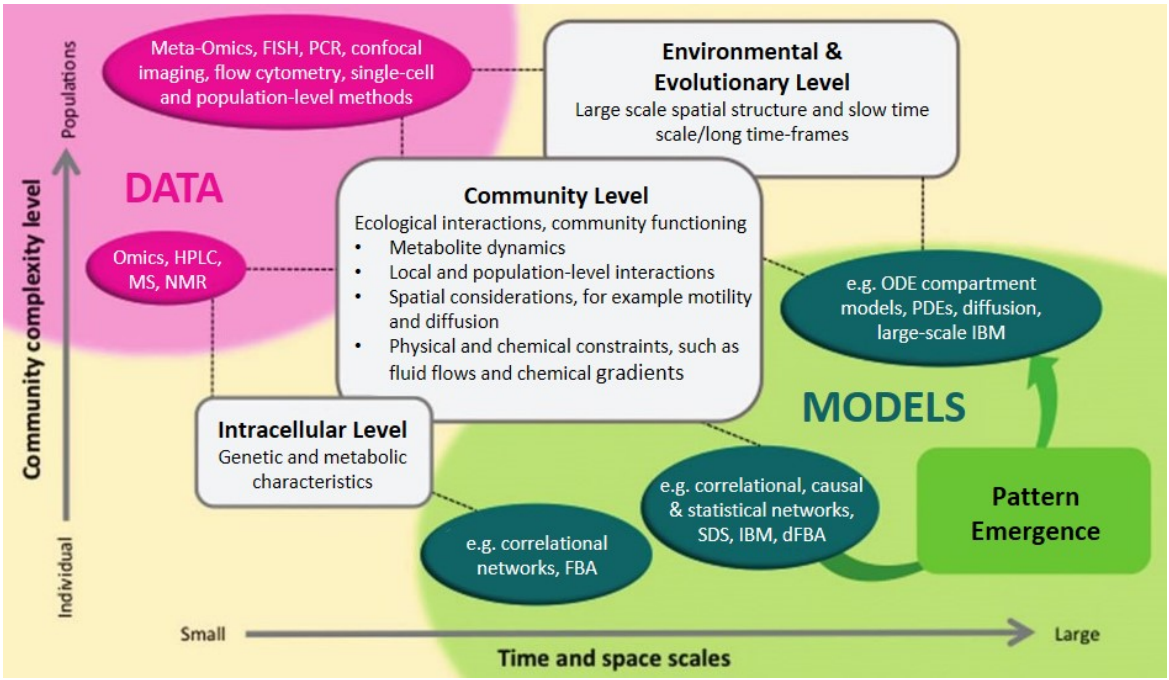

Figure 1.2 **Microbial ecology: from individuals to populations, experiments to models**. Adapted from Widder *et al.* (2016), this schematic summarises some current research questions in microbial ecology and illustrates how data and modelling complement one another. The research areas (white boxes) are plotted according to their microbial community complexity and temporal or spatial scale, with links to the different forms of data (pink) and modelling approaches (green) used. Pattern emergence is the collective behaviour obtained by transitioning from describing individuals to populations. Abbreviations: (d)FBA, (dynamic) flux balance analysis; SDS, stochastic dynamical systems; IBM, individual-based models; PDEs, partial differential equations; ODE, ordinary differential equation; FISH, fluorescence in-situ hybridisation; PCR, polymerase chain reaction; HPLC, high-performance liquid chromatography; MS, mass spectrometry; NMR, nuclear magnetic resonance.

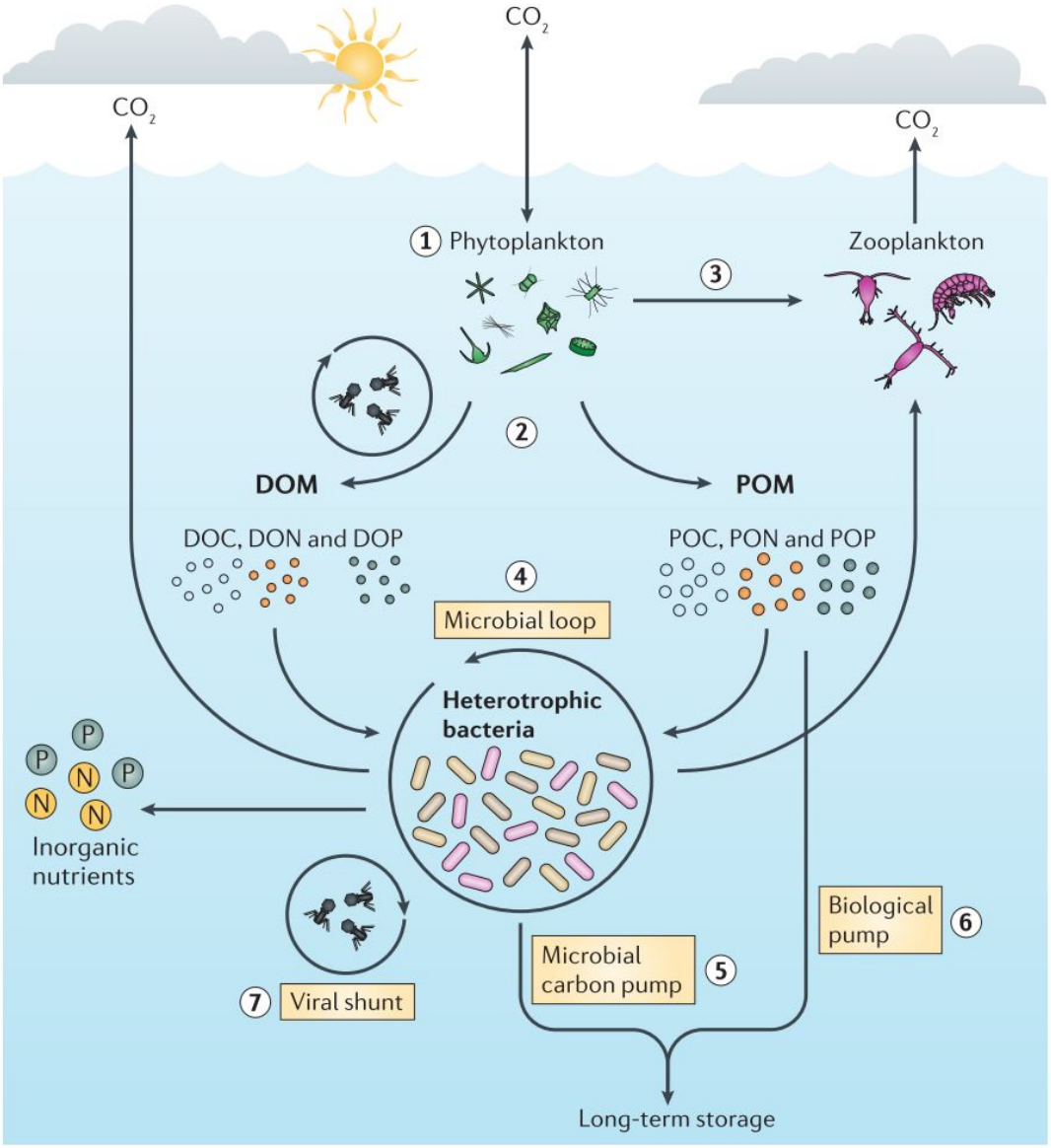

Figure 1.3 **The microbial contribution to the carbon cycle**. Reproduced from Buchan *et al.* (2014), this schematic shows the role of microorganisms in the oceanic carbon cycle. (1) Phytoplankton convert inorganic carbon to organic carbon by photosynthesis and (2) release dissolved organic matter (DOM, including dissolved organic carbon (DOC), nitrogen (DON) and phosphorous (DOP)) and particulate organic matter (POM, including particulate organic carbon (POC), nitrogen (PON) and phosphorous (POP)). (3) Zooplankton grazers consume phytoplankton and bacteria. (4) The release of CO_2 during respiration and the recycling of organic matter by heterotrophic bacteria make up the microbial loop. (5) The microbial carbon pump involves the sequestration of organic matter that resists further degradation or uptake by microbes and (6) the biological pump refers to the sinking of phytoplankton derived POM from the ocean surface to the ocean depths. (7) The contributions to POM and DOM from viral-mediated cell lysis is referred to as the viral shunt.

1.1.1 The microbial contribution to the carbon cycle

The activities of microorganisms affect the accessibility of carbon and the chemical potential energy of organic compounds available to the biosphere (Atlas *et al.*, 1998). Figure 1.3 summarises the many carbon transformation and recycling processes that occur in microbial communities, which form the basis of food webs in both aquatic and terrestrial environments (Buchan *et al.*, 2014). Phytoplankton are the photosynthetic microorganisms, like cyanobacteria and microalgae, found in aqueous environments. Phytoplankton are estimated to have a total global carbon biomass that is only 1-2% of the total global carbon biomass of plants, and yet these microscopic organisms are responsible for about 40% of photosynthetic carbon fixation (P. G. Falkowski, 1994). Using techniques such as isotope labelling, chromatography and mass spectrometry, studies have shown that organic molecules can be exuded by living microalgal cells or released during algal cell lysis (Bjørnsen, 1988; Durham *et al.*, 2015; Grossart *et al.*, 2007; Hellebust, 1958; Larsson *et al.*, 1979). Heterotrophic bacteria play an important role in determining the fate of this fixed carbon because they can degrade and recycle organic matter (Atlas *et al.*, 1998; Bjørnsen, 1988; Buchan *et al.*, 2014; Hellebust, 1958).

1.2 The role of carbon in algal and bacterial metabolism

Carbon is fundamental to all living organisms because it is an essential elemental building block for biological structures and is used as a means of storing energy (Andrews, 2017). Metabolism refers to the biochemical reactions that allow cells to incorporate nutrients from their environment, obtain energy from them and transform them into cellular machinery and architecture. These processes allow the cell to grow, repair damage and construct new cells. Cellular metabolism can be categorised into four types of biochemical reactions: fuelling, biosynthesis, polymerisation and assembly reactions (Andrews, 2017). The fuelling reactions, like photosynthesis and respiration, generate the energy carrying molecule adenosine triphosphate (ATP) from adenosine diphosphate (ADP), create reducing power in the form of NADPH (the reduced form of nicotinamide adenine dinucleotide phosphate) and produce metabolite precursors. These products go on to drive the biosynthesis reactions that create the building blocks needed for polymerisations, which produce the cellular macromolecules like DNA and proteins. Finally, these macromolecules are used by assembly reactions to construct the cellular features (Andrews, 2017).

There are four main groups of carbon molecules that make up the cellular biomass. Firstly, there are the sugars and polysaccharides, which are often used to store carbon and energy reserves in the form of starch or glycogen. Secondly, the amino acids that form proteins

and are the building blocks for the cellular machinery and architecture. The fatty acids and lipids are required as major components of cell membranes, as well as being another form of carbon and energy storage. Lastly, cells use nucleic acids to store and transfer information (Madigan *et al.*, 2019).

ATP is the energy currency of biological systems. This molecule stores and transports energy in the form of chemical potential energy, which is released by hydrolysis of the third phosphate group, a process that regenerates the lower energy molecule ADP. For long-term energy storage organisms produce organic molecules (like glucose or starch) that can be catabolised as a source of ATP when required (Madigan *et al.*, 2019). Organisms can be categorised based on how they obtain energy and what their source of carbon is. Phototrophs contain pigments that convert light energy into ATP, whereas chemotrophs require chemicals to drive the production of ATP (Madigan *et al.*, 2019). There are two classes of chemotrophs, chemolithotrophs use inorganic chemicals and chemoorganotrophs use organic chemicals (Madigan *et al.*, 2019). In terms of their source of carbon, autotrophs can use carbon dioxide as their sole carbon source, whereas heterotrophs need organic carbon (Madigan *et al.*, 2019). By these definitions, microalgae are photoautotrophs because they are photosynthetic, and therefore able to harness energy from light and incorporate carbon dioxide into their biomass.

1.2.1 *Chlamydomonas reinhardtii* and *Mesorhizobium loti*

The microbial species used in this thesis are *Chlamydomonas reinhardtii* and *Mesorhizobium loti*. Therefore the following sections focus on the carbon metabolic processes that are most relevant to these species. *C. reinhardtii* is a single-celled green alga that is commonly used as a model organism in laboratory studies (Harris, 2009). *C. reinhardtii* can grow phototrophically, meaning it photosynthetically assimilates carbon dioxide; heterotrophically, meaning it can grow in the dark with an organic carbon source; or mixotrophically, meaning it can be grown in the light and with an organic carbon source (Harris, 2009). *M. loti* is a member of the group of bacteria known as rhizobia, which are soil bacteria and often form nitrogen fixing symbiosis with leguminous plants (Kaneko *et al.*, 2000). The bacterium *M. loti* is an example of a chemoorganotroph and heterotroph because it relies on organic molecules for both its energy and carbon source.

1.2.2 Algal carbon metabolism

The metabolic processes of algae that involve carbon include photosynthesis, the carbon concentrating mechanism, respiration and biosynthesis reactions. This section briefly summarises algal photosynthesis and the carbon concentrating mechanism of *C. reinhardtii*, since

an understanding of these processes provides helpful insights into the algal carbon dynamics that significantly contribute to the co-culture and are modelled in chapter 3.

Photosynthesis and carbon fixation

Photosynthesis is the process that allows organisms to convert light energy into chemical bond energy and involves two sets of reactions, which are summarised in figure 1.4. The *light-reactions* harness light energy to split water, producing oxygen, protons and electrons. Electron and proton transfer through the photosynthetic machinery of the thylakoid membrane creates electrochemical gradients that are used for the synthesis of ATP and for the reduction of $NADP^+$ to produce NADPH. The light reactions can be summarised as

$$2\,H_2O + 2\,NADP^+ + 3\,ADP + 3\,P_i + \text{light} \longrightarrow 2\,NADPH + 2\,H^+ + 3\,ATP + O_2, \quad (1.1)$$

where P_i corresponds to inorganic phosphate and ADP is adenosine diphosphate (Kurepin *et al.*, 2017).

The second set of photosynthesis reactions are the *light-independent* reactions, these make up the Calvin cycle (also known as the C3 carbon reduction cycle) and require the chemical energy of ATP and the reducing power of NADPH to drive the synthesis of carbohydrates from CO_2 (Kurepin *et al.*, 2017). The Calvin cycle consists of three stages with a net reaction given by

$$CO_2 + 2\,NADPH + 2\,H^+ + 3\,ATP \longrightarrow CH_2O + H_2O + 2\,NADP^+ + 3\,ADP + 3\,P_i. \quad (1.2)$$

The first step is carboxylation, in which the enzyme Rubisco catalyses the fixation of CO_2 to the acceptor molecule ribulose 1,5-bisphosphate (RuBP) and forms the first stable compound in the cycle, 3-phosphoglycerate (3PGA), a three-carbon sugar (P. Falkowski *et al.*, 2007). The second step is the reduction phase, which produces triose phosphate (G3P) and the final phase regenerates the CO_2 acceptor molecule, RuBP (Harris, 2009).

Three turns of the Calvin cycle (i.e. 3 molecules of carbon dioxide) are required to fix enough net carbon to export one G3P molecule from the cycle, which is then used as the precursor metabolite for further carbon based metabolism. The carbohydrates produced from photosynthetic carbon fixation can be polymerised and the resulting polymeric carbohydrates are used to store carbon and energy. For *C. reinhardtii*, starch (a polymer of glucose) accumulates in the chloroplast during the light phase and is degraded in the dark (Harris, 2009).

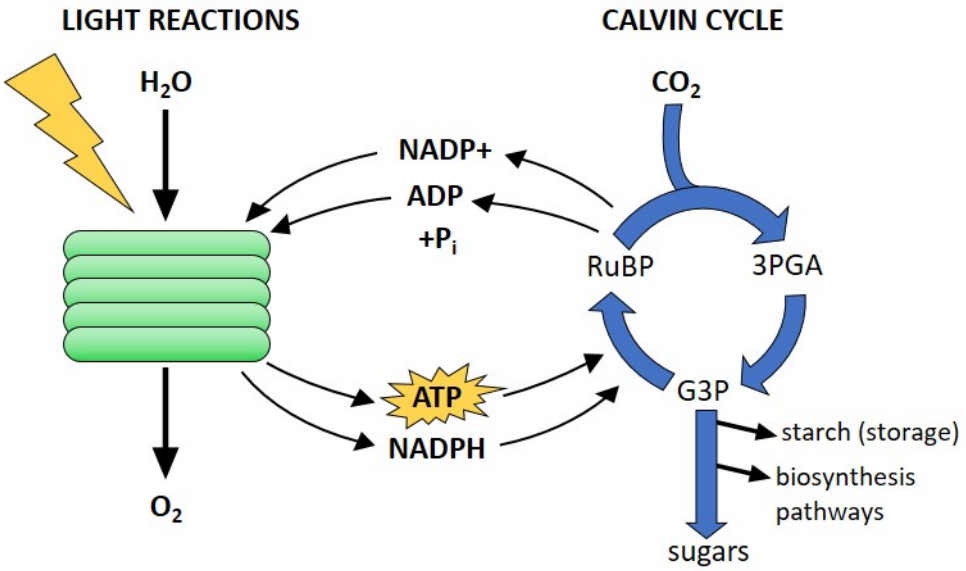

Figure 1.4 **Overview of the metabolic processes involved in photosynthesis**. The light reactions occur in the thylakoid, where light energy is harnessed to split water, electrochemical gradients are created to produce ATP and protons reduce $NADP^+$ to NADPH. The Calvin cycle uses ATP and NADPH to fix carbon from carbon dioxide in three stages: carbon fixation to produce 3-phosphoglycerate (3PGA), reduction to produce triose phosphates (G3P) and then regeneration of ribulose 1,5-bisphosphate (RuBP).

The carbon concentrating mechanism

In the atmosphere, carbon dioxide is found as a gas, but when in aqueous solution carbon dioxide undergoes a series of equilibrium reactions with water, meaning that aqueous inorganic carbon exists in three different forms, CO_2, HCO_3^- and CO_3^{2-}. The relative abundances depend on pH as plotted in figure 1.5 (P. Falkowski *et al.*, 2007), which shows that at pH 7 approximately 80 % of dissolved inorganic carbon is HCO_3^-. *C. reinhardtii*, like many other microalgae and cyanobacteria, has a carbon concentrating mechanism that allows them to use HCO_3^- as well as CO_2 for photosynthesis (figure 1.6) (Harris, 2009; Jungnick *et al.*, 2014). This process is activated at low levels of CO_2 (for example, under standard atmospheric conditions) and it involves proteins that allow for the efficient uptake of HCO_3^- into the cell, carbonic anhydrases for the conversion to CO_2 and transport proteins for the localisation of CO_2 in the pyrenoid, where Rubisco is located, which catalyses the carbon fixation reaction of photosynthesis (Jungnick *et al.*, 2014).

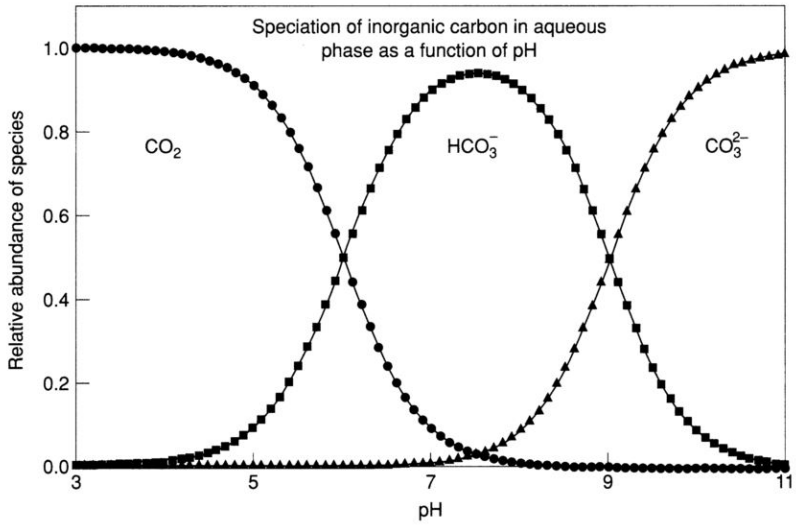

Figure 1.5 **Relative amounts of the different forms of inorganic carbon at equilibrium**. Taken from (P. Falkowski *et al.*, 2007), this plot shows how the relative amounts of CO_2, HCO_3^- and CO_3^{2-}, in aqueous environments at equilibrium, depends on pH.

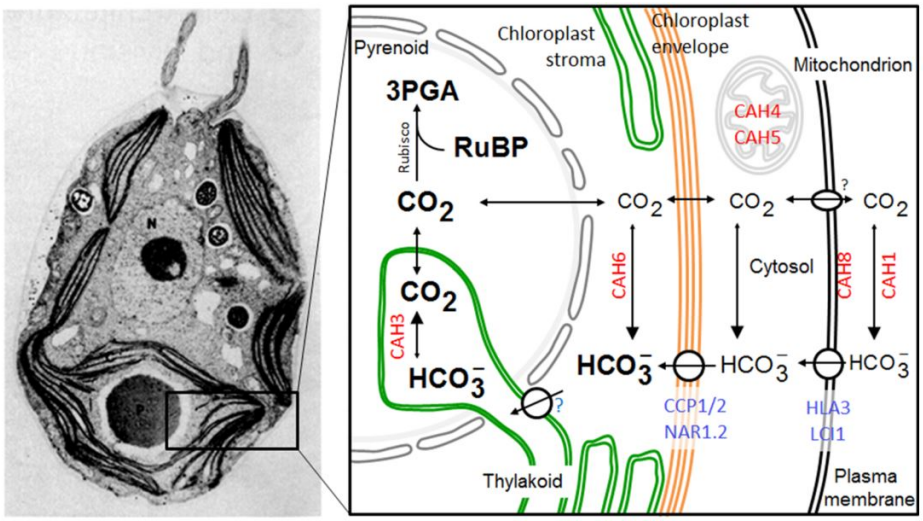

Figure 1.6 **The carbon concentrating mechanism in *C. reinhardtii***. Taken from Jungnick *et al.* (2014), this is an illustration of the process for the inorganic carbon uptake and conversion of HCO_3^- to CO_2 in *C. reinhardtii*. LCI1, HLA3, CCP1/2 and NAR1.2 are transporter proteins and CAH1, CAH3, CAH4/5, CAH6 and CAH8 are carbonic anhydrase enzymes. This process results in the concentration of carbon dioxide in the pyrenoid, where the enzyme Rubisco for carbon fixation is located, and therefore allows *C. reinhardtii* to make use of bicarbonate as an inorganic carbon source for photosynthesis.

1.2.3 Carbon metabolic processes of heterotrophic bacteria

Respiration and bacterial growth efficiency

Fundamental to the growth of heterotrophic bacteria is the production of ATP using organic molecules as their source of energy (Stowers, 1985). Heterotrophic bacteria can use respiration or fermentation to translate the chemical bond energy of organic carbon into the more universal store of chemical energy in biological systems, ATP. Glycolysis is the series of chemical reactions that transforms glucose into pyruvate, following which, in the presence of oxygen, respiration fully oxidises pyruvate via the citric acid cycle to produce carbon dioxide. In anaerobic conditions, fermentation uses pyruvate as an electron acceptor to achieve redox balance and the fermentation products are subsequently discarded (Madigan *et al.*, 2019). Fast-growing rhizobia are able to use a broad range of hexoses, pentoses, disaccharides, trisaccharides, and organic acids to drive the formation of ATP (Stowers, 1985). Heterotrophic bacteria not only require organic carbon as a source of energy but also as a supply of carbon as an elemental building block for cellular material. A measure for the amount of anabolic (biosynthetic, energy-requiring) activity relative to the catabolic (energy-yielding) activity is given by the bacterial growth efficiency (BGE), which is defined as the amount of biomass produced per unit of organic carbon consumed (Carlson *et al.*, 2007). BGE can be defined by the equation

$$\eta' = \frac{BP}{BP + BR}, \tag{1.3}$$

where BP is the bacterial biomass production and BR is the bacterial respiration. Estimates of BGE for bacteria in aquatic environments range from <0.05 to 0.6 (Giorgio *et al.*, 1998). The BGE can be affected by nutrient availability, as well as the quality and quantity of organic matter (Carlson *et al.*, 2007).

Glycerol metabolism

Glycerol can support the growth of both fast and slow growing rhizobia (Stowers, 1985). The metabolism of glycerol proceeds via glycerol kinase and glycerolphosphate dehydrogenase, producing G3P that is further metabolized to pyruvate, which is used in the citric acid cycle to generate ATP (Stowers, 1985).

Inorganic carbon assimilation by heterotrophic bacteria

The traditional view for the metabolism of heterotrophic bacteria is that they are unable to metabolise inorganic carbon, however many studies show that heterotrophic bacteria

assimilate carbon dioxide in carboxylation reactions during biosynthesis (Werkman *et al.*, 1942a,b). Therefore, a heterotroph is defined as an organism that cannot use carbon dioxide as its *only* source of carbon (Hesselsoe *et al.*, 2005; Roslev *et al.*, 2004; Slade *et al.*, 1942; Werkman *et al.*, 1942a). Isotope labelling studies have used carbon dioxide assimilation by heterotrophic bacteria as a measure of metabolic activity and have shown that the extent of carbon dioxide assimilation depends on the organic substrate used (Hesselsoe *et al.*, 2005; Roslev *et al.*, 2004).

1.3 Algal-bacterial interactions

Algal-bacterial interactions are important to understand from an evolutionary and ecological standpoint, but also because of their potential in industrial applications (Ramanan *et al.*, 2016). Potential applications include wastewater treatment, bloom control, aquaculture feed or to improve algal cultivation and harvesting in biotechnological applications of algae for high value chemicals (Kouzuma *et al.*, 2015; Ramanan *et al.*, 2016).

An algal-bacterial interaction can be classed as a nutrient exchange, signal transduction or gene transfer (Kouzuma *et al.*, 2015). Interactions between algae and bacteria range from parasitic, where one species benefits at the expense of the other, to mutualistic, where both species benefit (see figure 1.1) (Cole, 1982; Faust *et al.*, 2012; Ramanan *et al.*, 2016). The focus of the work in this thesis is on the nutrient exchange in an algal-bacterial mutualism. Algae can supply organic matter to bacteria, which can involve several processes: bacteria may parasitise algal cells, use organic material exuded by algae or obtain nutrients from the decomposition of dead cells (Buchan *et al.*, 2014; Cole, 1982; Hellebust, 1958). Although decomposition can be considered as the primary role of heterotrophic bacteria within an ecosystem, they can also promote algal growth (Ramanan *et al.*, 2016). Nitrogen fixation, phosphorous regeneration, vitamin synthesis and feedback of carbon dioxide are all examples of how bacteria can contribute to algal growth and survival (Amin *et al.*, 2012; Cole, 1982; Hom *et al.*, 2015). The specific nature of an interaction can be affected by environmental conditions and nutrient availability (Gurung *et al.*, 1999; Hoek *et al.*, 2016; Liu *et al.*, 2012; Ramanan *et al.*, 2016). For example, a co-culture between an alga and a heterotrophic bacterium shifted between commensalism for carbon and competition for phosphorous, depending on the light intensity and nutrient supply (Gurung *et al.*, 1999). Liu *et al.* (2012) observed that the addition of carbon stimulated bacterial growth and as a result decreased the nutrient availability for algae. Therefore, it is important to understand the nutrient exchanges and dependencies that underpin algal-bacterial interactions in order to better predict the effects of changes in environmental conditions.

1.3.1 Algae and vitamin B_{12}

Vitamin B_{12}, hereafter referred to as B_{12}, contains a central cobalt ion (figure 1.7a) and so is also referred to as cobalamin (Warren *et al.*, 2002). Studies suggest that more than half of algal species require B_{12} for methionine synthesis, i.e. out of 326 species surveyed, 171 were found to require B_{12} (Croft *et al.*, 2005). Methionine is an amino acid and therefore an essential building block for proteins. There are two pathways for the final step of methionine synthesis in algae, which are illustrated in figure 1.7b (Croft *et al.*, 2005; Helliwell *et al.*, 2011). Vitamin B_{12} dependent algae lack the METE pathway and so only have the METH pathway for the conversion of homocysteine to methionine (Croft *et al.*, 2005; Helliwell *et al.*, 2014, 2011, 2013). Figure 1.8 shows how B_{12} dependence is spread across the whole algal kingdom with no phylogenetic patterns, which suggests that B_{12} dependence has evolved independently several times (Helliwell *et al.*, 2015, 2011, 2013). The evolution of vitamin dependency is typically due to the loss of the vitamin synthesis pathway after the species have already developed a metabolic requirement for the vitamin (Helliwell *et al.*, 2013). However, the B_{12} dependence of algae appears to have evolved differently, with species becoming dependent on B_{12} when their metabolism relies on it as an enzyme cofactor (Croft *et al.*, 2005; Helliwell *et al.*, 2013). B_{12} is the most structurally complex vitamin and, as far as it is known, only some prokaryotes are capable of synthesising it (Helliwell *et al.*, 2013; Warren *et al.*, 2002). Therefore, B_{12}-dependent algae rely on B_{12}-producing prokaryotes for their B_{12} requirements (Helliwell *et al.*, 2013; Kazamia *et al.*, 2012b).

Experimental evolution of B_{12} dependence: *C. reinhardtii metE7*

Helliwell *et al.* (2015) cultured the alga *C. reinhardtii*, which has both the METE and METH pathways for methionine synthesis, in media containing B_{12} and after approximately 500 generations the evolution of a B_{12} dependent mutant was observed. This novel phenotype had stunted growth in the absence of B_{12} and was therefore named 'S-tpye'. Further analysis revealed the genetic cause of this new 'S-type' phenotype to be an insertion of a type II Gulliver-related transposable element (GR-TE) into the *METE* gene. On some occasions when 'S-type' cells were further grown on agar plates without B_{12} the stunted colonies reverted back to the wild-type phenotype due to the loss of the GR-TE insertion. From 'S-type' colonies that showed no reversion, the seventh clone tested lacked the GR-TE insertion except for a 9 base-pair footprint sequence. This in-frame insertion corresponds to the inclusion of three extra amino acids in a conserved region of the *METE* gene resulting in a stable B_{12} dependent mutant, named *metE7*. It is this *metE7*-mutant of *C. reinhardtii* that

is used in this thesis. Growth of *C. reinhardtii metE7* can be rescued either by the addition of B_{12} or B_{12} producing bacteria (Helliwell *et al.*, 2015).

Although at first the loss of function of the *METE* gene may seem like an evolutionary disadvantage because it reduces the flexibility of *C. reinhardtii*'s metabolism, there is an energetic advantage for using the B_{12} dependent METH form of methionine synthase because it has an approximately 50-100 fold higher catalytic activity than the B_{12} independent METE form (Bertrand *et al.*, 2013). When viewed on the level of the microbial community, algae that are dependent on an external source of B_{12} are likely to be found in close proximity to B_{12} producing organisms, which in turn benefit from the photosynthetic activity of algae that converts inorganic carbon into energy rich organic molecules.

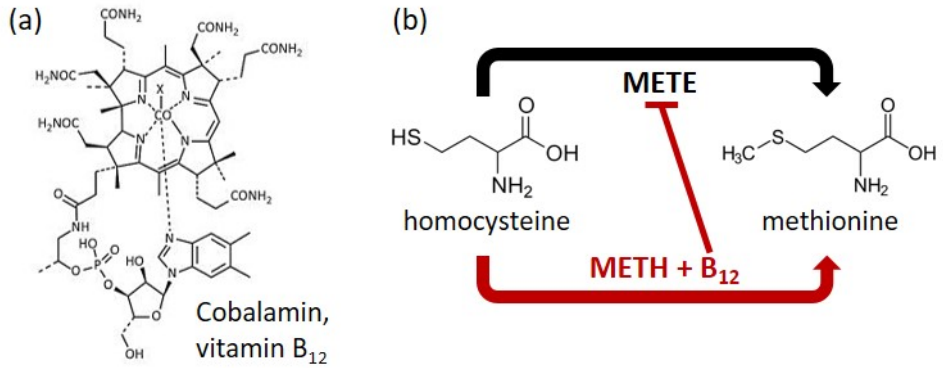

Figure 1.7 **The role of vitamin B_{12} in methionine synthesis**. (a) Reproduced from (Helliwell *et al.*, 2013), this is the chemical structure of cobalamin (vitamin B_{12}). The X group, i.e. the upper ligand, can be a cyano (CN), methyl (CH_3), hydroxyl (OH) or 5'-deoxyadenosyl group, with the corresponding vitamin called cyanocobalamin, methylcobalamin, hydroxocobalamin or adenosylcobalamin respectively. (b) There are two potential pathways for the final step of methionine synthesis in algae. The METE enzyme does not require B_{12}, whereas METH is dependent on the vitamin as a cofactor. In the presence of B_{12} the *metE* gene is repressed. The catalytic activity of the METH enzyme is about 50-100 fold greater than for METE (Bertrand *et al.*, 2013). Algae are dependent on an external source of B_{12} when they only have the METH pathway available.

1.3.2 The B_{12} algal-bacterial mutualism

Algae are photosynthetic and therefore able to fix inorganic carbon. It has been proposed that the organic carbon they produce can be used by heterotrophic bacteria as a nutrient source in exchange for vitamin B_{12} (Kazamia *et al.*, 2012b), forming the basis for an algal-bacterial mutualism. Kazamia *et al.* (2012b) showed that in the laboratory there is a direct interaction between the B_{12} requiring green alga *Lobomonas rostrata* and the rhizobial bacterium *M.*

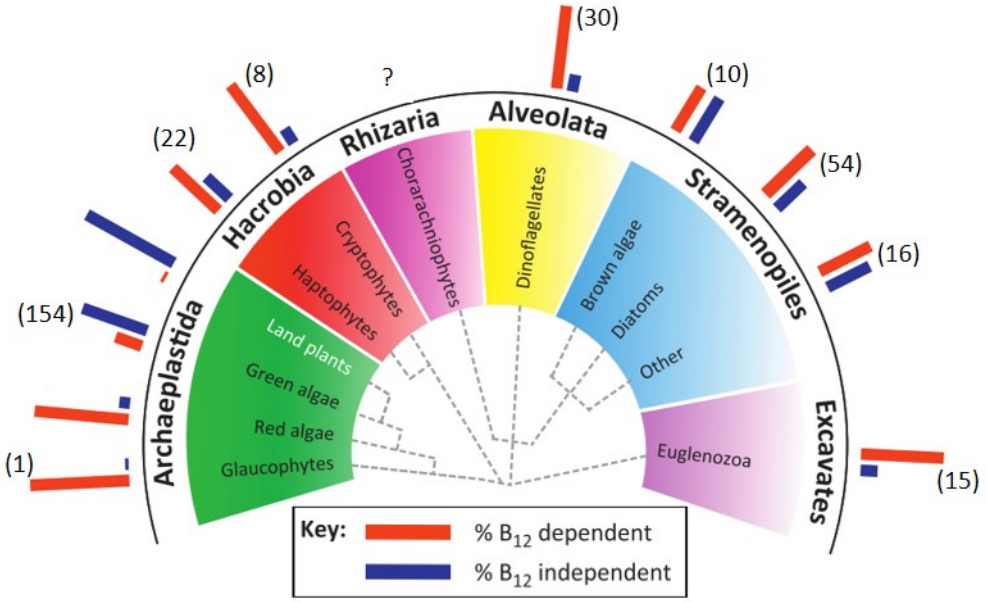

Figure 1.8 **The spread of vitamin B_{12} dependence in algae**. Reproduced from (Helliwell *et al.*, 2013), this diagram shows the eukaryotic tree of life for the super groups that contain photosynthetic lineages. These results are based on a survey of 326 algal species (land plants were not part of the survey, but do not require B_{12}) (Helliwell *et al.*, 2011). The numbers in brackets give the total number of species surveyed within each group and the bar charts indicate the percentage of these surveyed species that are known to require B_{12} (red), and those that do not (blue).

loti. The bacteria provide cobalamin in exchange for organic carbon molecules produced by the algae. The two organisms form a stable co-culture with an equilibrium ratio of algae to bacteria converging to about 1:30, which is perturbed when B_{12} or an organic carbon source is added to the culture (Kazamia *et al.*, 2012b). Grant *et al.* (2014) developed mathematical models to investigate different mechanisms for this nutrient exchange, which suggest that release of B_{12} during bacterial cell lysis is not sufficient to account for the observed co-culture dynamics and that a successful model is able to describe a change in behaviour when B_{12} or an organic carbon source are added to the growth media. The algal and bacterial populations are still able to support one another even when they are grown spatially separated on agar (Kazamia *et al.*, 2012b) or in two separate flasks connected with a diffusive channel (F. J. Peaudecerf *et al.*, 2018), meaning that the populations are physically separated but can still exchange chemicals via diffusion. This suggests that the diffusion of nutrients between the two populations is sufficient to sustain the mutualism, physical association is not required.

The co-culture system used for the work described in this thesis uses the experimentally evolved, B_{12} dependent alga *C. reinhardtii metE7* and the B_{12} producing, heterotrophic

bacterium *M. loti*. Helliwell *et al.* (2015) demonstrated that *M. loti* was able to produce sufficient B_{12} to support the growth of *C. reinhardtii metE7* even when growth medium without an organic carbon source was used (Helliwell *et al.*, 2015). These results imply that for this co-culture system algal growth is dependent on B_{12} produced by bacteria and bacterial growth is dependent on algal photosynthate (Helliwell *et al.*, 2015).

1.4 Stable isotopes and microbial ecology

Stable isotope studies, for example source-to-sink tracer experiments or natural abundance analyses, are an important tool used in several research areas including biogeochemistry and ecology (Boschker *et al.*, 2002; Jiang *et al.*, 2014; Peterson *et al.*, 1987). Tracking isotopically labelled compounds is an effective way of measuring nutrient fluxes, relationships between interacting microbial species and microbial physiology (Orphan *et al.*, 2009; Widder *et al.*, 2016). The focus here is on carbon because it is the exchange of carbon in algal-bacterial co-cultures that is of particular interest in this thesis.

The most abundant form of carbon is ^{12}C, which makes up about 98.9 % of naturally occurring carbon. The stable isotope ^{13}C constitutes about 1.1 % and the natural abundance of the radioactive isotope ^{14}C is <0.0001 % (P. Falkowski *et al.*, 2007). The isotope ratio defines the amount of ^{13}C relative to ^{12}C as given by

$$R = \frac{^{13}C}{^{12}C}. \tag{1.4}$$

The atomic fraction of ^{13}C is defined as the amount of ^{13}C relative to the total carbon and is defined as

$$f = \frac{^{13}C}{^{13}C + ^{12}C} = \frac{R}{1+R}. \tag{1.5}$$

The ^{13}C enrichment is often expressed as $\delta^{13}C$, which is defined as

$$\delta^{13}C = \left(\frac{R_{sample}}{R_{standard}} - 1\right) 1000\ ‰, \tag{1.6}$$

with R_{sample} and $R_{standard}$ the isotope ratios for the sample of interest and a standard respectively (P. Falkowski *et al.*, 2007). The $\delta^{13}C$ value is a measure of the isotope ratio relative to a standard, in parts per thousand. The commonly used standard for carbon isotope measurements and the one used in this thesis, is Pee Dee Belemnite (PDB), which has an isotope ratio of $R_{standard} = 0.01124$ (Craig, 1957).

1.4.1 Isotopic fractionation and natural abundance

In chemical reactions the collision frequency, which affects the reaction rate, is greater for lighter isotopes than for heavier isotopes, meaning that ^{12}C is more likely to undergo a reaction than ^{13}C. This process is called isotopic fractionation and leads to variation in the natural abundance isotope ratios for different carbon pools (P. Falkowski *et al.*, 2007). When considering a particular chemical reaction, the isotopic fractionation factor is defined as

$$\alpha = \frac{R_{substrate}}{R_{product}} \tag{1.7}$$

with $R_{substrate}$ and $R_{product}$ the isotope ratios of the substrate and product respectively for the reaction of interest at equilibrium (P. Falkowski *et al.*, 2007).

Understanding the process of isotopic fractionation allows natural abundance studies to use small differences in isotope ratios to acquire information about biological processes (Peterson *et al.*, 1987). Variation in the extent of isotopic fractionation among primary producers occurs because of differences in the inorganic substrate, fixation pathways, or environmental and physiological conditions (Boschker *et al.*, 2002). Heterotrophic organisms generally have carbon isotope ratios similar to their food source(s) and the isotope ratios of specific biomarkers can be used to study these organic matter sources (Boschker *et al.*, 2002).

1.4.2 Isotope labelling

Isotope labelling experiments involve artificially enriching the isotope content of a specific substrate and then monitoring the isotope enrichment over time for different components of the system. This allows the nutrient fluxes within a particular microbial community to be identified and can be used to quantify the rates of these fluxes. For example, microbial decomposition can be studied using ^{13}C enriched organic matter, specific microbial processes can be linked to community structure by introducing a particular ^{13}C enriched compound or coupling between primary producers and heterotrophic bacteria can be investigated using ^{13}C enriched carbon dioxide (Boschker *et al.*, 2002).

Two quantitative approaches are typically used to obtain estimates for the net nutrient assimilation rates. Firstly, a method described in detail by Montoya *et al.* (1996) for quantifying nitrogen fixation considers the net nitrogen assimilated by an organism as the amount of nitrogen assimilated relative to the total nitrogen content. The derivation for the assimilation rate, v_{net} in units h^{-1}, is outlined below and has been used in relatively recent work to quantify the carbon and nitrogen fixation rates of free living cyanobacteria (Eichner *et al.*, 2017; Foster *et al.*, 2013). For clarity, a ^{13}C labelling experiment is considered for the

derivation, but the same approach can be used for any isotope labelling experiment. The total carbon biomass concentration after an incubation time t can be defined as

$$c\,(t) = c_0 + \Delta c, \tag{1.8}$$

with c_0 the initial concentration and Δc the concentration of assimilated carbon. A similar expression can be written for the concentration of ^{13}C in the biomass at time t,

$$c^{13}\,(t) = c_0^{13} + \Delta c^{13}, \tag{1.9}$$

with c_0^{13} the initial ^{13}C concentration and Δc^{13} the concentration of assimilated ^{13}C. Using the definition of the atomic fraction of ^{13}C in equation (1.5), equation (1.9) can be rewritten as

$$f\,(t)\;\; c\,(t) = f_0\; c_0 + f_s\; \Delta c, \tag{1.10}$$

with f_0 and $f\,(t)$ the atomic fraction of ^{13}C in the organism at time zero and time t respectively, and f_s the atomic fraction of ^{13}C in the labelled carbon source, assumed to be constant. The net carbon assimilation defined relative to the total carbon biomass concentration, using equations (1.8) and (1.10), is given by

$$\frac{\Delta c}{c\,(t)} = \frac{f\,(t) - f_0}{f_s - f_0}. \tag{1.11}$$

From this, the net carbon assimilation rate, in units h^{-1}, is given by

$$v_{net} = \frac{1}{t}\left(\frac{f\,(t) - f_0}{f_s - f_0}\right). \tag{1.12}$$

This approach to quantifying carbon assimilation relies on the assumption that there is no carbon loss, the change in the total carbon content of the organism is small and the carbon assimilation is linear in time. This approach is therefore most suitable for experiments with short incubation times.

An alternative approach was outlined by Popa *et al.* (2007), which involves a two component mixing model to derive an expression for the net assimilation rate. The net carbon assimilation Fx_{net} is defined as the fraction of carbon in the sampled organism taken up from the labelled source (F_s) relative to the fraction of carbon in the sampled organism remaining

from the initial carbon content of the organism (F_0) at time t. This gives the equation

$$Fx_{net} = \frac{F_s}{F_0}. \tag{1.13}$$

The atomic fraction of ^{13}C in the sampled organism at time t is given by

$$F_{minor} = F_0\ f_0 + F_s\ f_s, \tag{1.14}$$

with f_0 and f_s the atomic fraction of ^{13}C in the organism at time zero and in the labelled carbon source respectively. The atomic fraction of ^{12}C in the sampled organism at time t is given by

$$F_{major} = F_0\,(1 - f_0) + F_s\,(1 - f_s)\,. \tag{1.15}$$

The atomic fraction of ^{13}C is defined as the amount of ^{13}C relative to the total carbon (f in equation (1.5)) and therefore using equations (1.14) and (1.15) the following expression for the atomic fraction of ^{13}C in the sampled organism at time t is obtained

$$f\,(t) = \frac{F_{minor}}{F_{major} + F_{minor}} = \frac{F_0\ f_0 + F_s\ f_s}{F_0 + F_s}. \tag{1.16}$$

Rearranging equation (1.16) and using the definition for Fx_{net} in equation (1.13), the following expression for the net carbon assimilation was derived

$$Fx_{net} = \frac{f\,(t) - f_0}{f_s - f\,(t)}, \tag{1.17}$$

and the net carbon assimilation rate, in units h^{-1}, is given by

$$v_{net} = \frac{1}{t}\left(\frac{f\,(t) - f_0}{f_s - f\,(t)}\right). \tag{1.18}$$

This method still assumes that carbon assimilation is linear in time, but it does not rely on the assumption that there is no carbon loss from the organism, meaning that it can be used more generally and is more suitable for longer time frames. This method for quantifying the net carbon and nitrogen assimilation was recently used by Arandia-Gorostidi *et al.* (2016) to study the effect of temperature and physical attachment on the carbon and nitrogen fluxes between phytoplankton and heterotrophic bacteria. The results suggest that an increase in temperature increases the carbon and nitrogen fluxes between the two species, which is further enhanced by cell-to-cell attachment.

The distinction between the two expressions for the net carbon assimilation rate v_{net} is in the denominator, i.e. $(f_s - f_0)$ in equation (1.12) for the Montoya *et al.* (1996) method and $(f_s - f(t))$ in equation (1.18) for the Popa *et al.* (2007) method. This means that the difference between the two estimates for v_{net} increases for longer time periods as $f(t)$ deviates more from the initial value f_0.

1.4.3 Stable isotope analysis using mass spectrometry

Bulk analysis using Isotope Ratio Mass Spectrometry

Isotope Ratio Mass Spectrometry (IRMS) determines the abundance of isotopes in a sample measured relative to a standard, as defined by $\delta^{13}C$ in equation (1.6) (Brenna *et al.*, 1997). Several different sample preparation techniques can be used in conjunction with IRMS, the two most common are elemental analysers (EA-IRMS) used for bulk measurements of the average isotopic signal for the entire sample and gas chromatographs (GC-IRMS) used for measuring the isotopic signals of individual compounds from a sample mixture (Boschker *et al.*, 2002; Muccio *et al.*, 2009). In this work EA-IRMS is used because it is the overall carbon isotope content that is of interest.

In EA-IRMS the bulk sample, weighed and contained in a tin or silver capsule, is placed into the elemental analyser, where it is combusted at elevated temperatures under a flow of oxygen to produce the gases NO_x, CO_2, SO_2 and H_2O (Brenna *et al.*, 1997; Muccio *et al.*, 2009). For carbon isotope ratio analysis, a helium gas stream carries the combusted sample into a reduction chamber where nitrous oxides are converted into N_2 and excess O_2 is removed (Brenna *et al.*, 1997; Muccio *et al.*, 2009). A chemical trap then removes water and a gas chromatograph separates CO_2 and N_2 (Brenna *et al.*, 1997; Muccio *et al.*, 2009). The resulting effluent from the elemental analyser is then analysed for its stable isotope content using IRMS, which involves ionisation by electron beams to generate positive ions that are mass-analysed using a magnetic sector and multiple ion detectors that allow for the simultaneous and continuous analysis of the specific masses of interest (Brenna *et al.*, 1997).

Single cell analysis using Secondary Ion Mass Spectrometry

Secondary Ion Mass Spectrometry (SIMS) is a highly sensitive mass spectrometry technique that allows for quantitative, spatial analysis of isotope content for a sample area at micrometer resolution. SIMS directs a high energy, focused primary ion beam towards the sample surface, which causes ionised particles to be ejected from the sample. Using an electric field, the charged particles are captured and accelerated, forming a secondary ion beam that is passed

through a mass spectrometer, which analyses the secondary ions according to their mass-to-charge ratio (Boxer *et al.*, 2009; Gao *et al.*, 2015; Musat *et al.*, 2012; Wagner, 2009). The primary ion beam is raster scanned across the sample area of interest, meaning that the data collected at each position contributes to a 2-dimensional map of the mass spectrometry analysis. Technological improvements led to the development of NanoSIMS, which operates under the same principles as SIMS but can achieve a higher spatial resolution (Gao *et al.*, 2015; Musat *et al.*, 2012). The work in this thesis uses SIMS measurements obtained with a Cameca IMS 1280 instrument, a schematic of which is shown in figure 1.9.

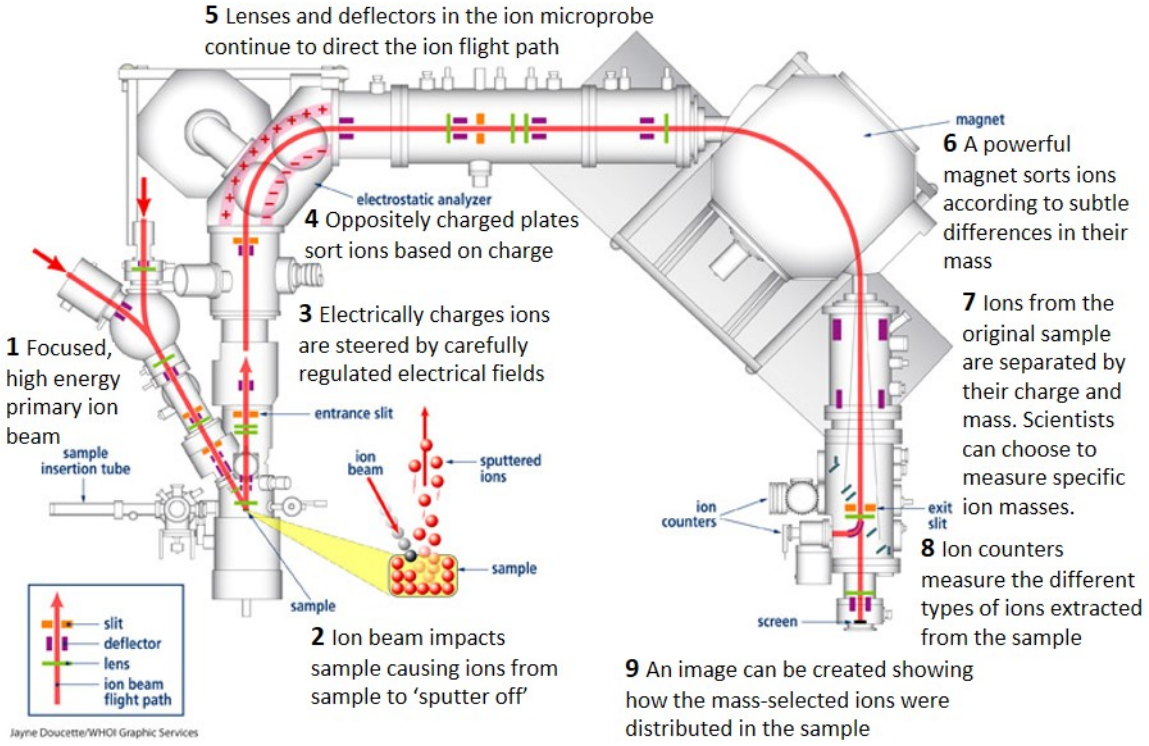

Figure 1.9 **Schematic of the Cameca IMS 1280**. Adapted from (Doucette, 2004), this diagram shows the different components within a SIMS instrument and describes the steps involved in obtaining a measurement.

1.5 Mathematical modelling in microbial ecology

In chapter 3 a mathematical model is developed to describe the carbon dynamics in an algal-bacterial co-culture. There are several different approaches to modelling microbial populations and communities; the most common are summarised in table 1.1, but these are not mutually exclusive and a mathematical model may combine two or more them (Clark *et al.*, 2017; Song *et al.*, 2014; Widder *et al.*, 2016; Zaccaria *et al.*, 2017). The co-culture model in this thesis assumes a well mixed co-culture, corresponding to a homogeneous distribution of algae, bacteria and nutrients. A kinetic growth model for the B_{12}-dependent growth of algae is coupled to the DOC-dependent growth of bacteria. The resulting co-culture model aims to achieve a nutrient explicit description of an algal-bacterial mutualism that does not rely on detailed metabolic fluxes, but is able to capture the population growth and nutrient dynamics. The following sections briefly summarise some mathematical models of microbial growth and interspecies interactions that are relevant to the work described in this thesis.

1.5.1 Modelling nutrient dependent microbial growth

The growth rate of a microbial population is typically density dependent. At low population densities and when nutrients are not limiting, growth can be modelled as an exponential growth rate, however as the population continues to grow negative interactions within the population begin to dominate and the growth rate decreases towards zero (Atlas *et al.*, 1998). This logistic microbial population growth can be described by the equation

$$\frac{dN}{dt} = \mu\, N \left(1 - \frac{N}{K_N}\right), \tag{1.19}$$

with N the population density, μ the exponential growth rate and K_N the carrying capacity, i.e. the maximum population density at which point the growth rate is zero.

Microbial growth rate is often limited by the availability of nutrients, which can be accommodated by introducing a nutrient dependent equation for μ. The Monod model is the form typically used in kinetic models of microbial growth. The Monod growth rate equation, similar to the Michaelis–Menten equation for enzyme kinetics, is defined as

$$\mu = \mu_{max} \left(\frac{S}{K_S + S}\right), \tag{1.20}$$

with μ_{max} the maximum growth rate, S the concentration of the growth limiting nutrient and K_S the half-saturation concentration, meaning when $S = K_S$ the growth rate is half the

maximum value (Monod, 1949). Equation (1.20) describes an increase in growth rate for an increasing external nutrient concentration, but with a limiting maximum growth rate for high values of S.

An alternative approach to the Monod model is the Droop cell quota model, which describes the growth rate as dependent on the nutrient availability inside a cell. The Droop model originated as an empirical description for the relationship between the cell quota Q, defined as the amount of a particular nutrient (like vitamin B_{12} or phosphorous) within a cell, and the organism's growth rate, μ (Droop, 1968; Flynn, 2008). The Droop model defines the nutrient dependent growth rate as

$$\mu = \mu_{max}\left(1 - \frac{Q_m}{Q}\right), \tag{1.21}$$

with Q_m the cell quota value below which the growth rate becomes negative, and μ_{max} the theoretical maximum growth rate as $Q \to \infty$ (Droop, 1968; Flynn, 2008).

In general, growth is likely a function of both the external and internal nutrient concentrations. At a mechanistic level, the cell quota model is most appropriate when nutrient redistribution within the cell is possible (Flynn, 2008). A Droop model requires the nutrient uptake and transport kinetics to be incorporated such that an equation to describe how the cell quota changes with time can be obtained. Therefore a Monod model is generally simpler to construct. For the co-culture model in this thesis, a Monod description of nutrient-dependent growth rate is used. It is assumed that the Monod model is sufficient because in the co-culture the limiting nutrient is provided by the interaction partner and therefore the limiting step is likely to be the nutrient production and uptake rather than internal mechanisms.

1.5.2 Modelling microbial interactions

In theoretical ecology, the dynamics of microbial communities are typically modelled using coupled differential equations that describe the microbial species abundances (Zomorrodi *et al.*, 2016). The Lotka–Volterra models, originally developed for competition and predator-prey dynamics, are popular in ecology because of their relative simplicity (Shou *et al.*, 2015). These models reduce each pairwise interaction into a single parameter, the magnitude of which determines the strength of the interaction (Okuyama *et al.*, 2008). The simplest model for a mutualism is based on the Lotka-Volterra equations, with positive interaction coefficients to represent the 'win-win' interaction and carrying capacities to limit the populations to a maximum size (Murray, 2002). An alternative approach is to model the species carrying capacity as a function of its interaction partner, i.e. for a mutualistic interaction the carrying

capacity increases in the presence of the interaction partner (Grant *et al.*, 2014; Yukalov *et al.*, 2012).

In contrast to pairwise models, which only consider the fitness effects of microbial interactions, mechanistic models explicitly consider the interaction mediators as model variables (Momeni *et al.*, 2017). Although most work examines contact-dependent interactions, for which Lotka-Volterra type pairwise models can be equivalent to mechanistic models, when interactions are chemically mediated Momeni *et al.* (2017) showed that one type of equation cannot capture the full diversity of microbial interactions. Therefore it is important to develop nutrient explicit models that describe the interaction mediators explicitly in order to test understanding of the underlying mechanisms driving an interaction, discover what conditions allow for pairwise models to be appropriate and to obtain improved population level equations for modelling microbial interactions (Momeni *et al.*, 2017).

Therefore it is important to create models that encapsulate the nutrient dynamics that exist within microbial communities in order to better understand these interactions and the effect of changes in community structure or environmental conditions. Additionally, nutrient explicit models have the potential to improve our understanding of the microbial contribution to biogeochemical cycles such that they can be better incorporated into global models.

Table 1.1 **A summary of the most commonly used mathematical approaches in microbial ecology**. These descriptions, advantages and limitations of different types of mathematical models are largely based on the recent review article by Widder *et al.* (2016).

Description	Advantages	Limitations
Population dynamic models. Global empirical functions describe changes in species abundance and the effect of biological and environmental factors (Widder *et al.*, 2016; Zaccaria *et al.*, 2017).	Can successfully capture the temporal trajectories of populations within a community (Widder *et al.*, 2016).	Typically do not address the underlying mechanisms that account for observations (Widder *et al.*, 2016).
Stoichiometric models. Metabolic fluxes defined using chemical stoichiometry. Dynamic flux balance analysis is used to couple microbial growth with the chemical environment (Widder *et al.*, 2016).	Contains an extensive amount of detail that enables researchers to link genotypes to phenotypes (Zaccaria *et al.*, 2017).	Under-determination is common, meaning that experimentally observable variables cannot fully constrain model parameters (Zaccaria *et al.*, 2017).
Kinetic growth models. Uses population growth as a function of chemical concentrations. Community models couple several such equations, one for each species (Widder *et al.*, 2016).	Conceptually simple, computationally tractable and provides dynamical predictions (Widder *et al.*, 2016).	Need knowledge about the key species and interaction mediators. How parameters are determined affects the model reliability (Widder *et al.*, 2016).
Causal and correlational networks. Networks are tools for representing and analysing systems of interactions. Nodes represent microorganisms, edges between them their interactions (Widder *et al.*, 2016).	Used to predict community properties, like metabolic dependencies, keystone species and the effects of perturbations (Faust *et al.*, 2012).	Can be challenging to distinguish between direct and indirect interactions (Faust *et al.*, 2012).
Individual-based models. These describe the behaviour of individual microbial cells and the local interactions are used to predict global community dynamics (Widder *et al.*, 2016).	Can model the effects of complex environments and test the consistency of assumed single cell behaviour with population data. (Hellweger *et al.*, 2016).	Can be very complex, so not viable for studying large systems. Experimental data is not always enough to validate the model (Hellweger *et al.*, 2016).
Spatially resolved approaches. Microorganisms often exist in spatially structured environments, like biofilms. Spatially resolved models represent space explicitly (Widder *et al.*, 2016; Zaccaria *et al.*, 2017).	Spatial structure is important for the system dynamics when motility or chemical diffusion is significant (Widder *et al.*, 2016; Zaccaria *et al.*, 2017).	Can be complex, so it is often reasonable to use well-mixed models that assume homogeneous distributions of species and chemicals (Zaccaria *et al.*, 2017).
Evolutionary game theory. Considers strategic decision making in a group of competitors, resulting in conflict and cooperation (Widder *et al.*, 2016).	Addresses how microbial strategies and their frequencies within a population change over time (Hummert *et al.*, 2014; Widder *et al.*, 2016).	Can be a challenge to quantify fitness effects (Zomorrodi *et al.*, 2016). Usually gives relative rather than absolute population sizes (Hummert *et al.*, 2014).

1.6 Thesis outline

This thesis explores the potential of using isotope labelling experiments to parametrise and test nutrient-explicit models of microbial interactions. Stable isotope labelling combined with Secondary Ion Mass Spectrometry (SIMS) and mathematical modelling is used to examine the carbon dynamics in an algal-bacterial co-culture. The chosen microbial system for this work is a mutualistic co-culture between the B_{12}-dependent *metE7* mutant of *C. reinhardtii* and the B_{12}-producing, heterotrophic bacterium *M. loti*. Additional experiments with axenic cultures, i.e. where only a single organism is present, supplement the co-culture results and provide a useful test for the bacterial components of the model.

Chapter 2 combines stable carbon isotope labelling and SIMS to obtain evidence of the photosynthetic carbon fixation of algae and the bacterial uptake of algal derived carbon in a co-culture. For axenic bacteria, the effect of organic carbon availability on inorganic carbon assimilation was investigated. Moreover, by obtaining SIMS measurements of the carbon isotope content of single cells at different time-points, the temporal evolution of the ^{13}C-enrichment of single cells demonstrated the heterogeneity within a microbial population.

Chapter 3 describes a nutrient-explicit co-culture model that couples B_{12}-dependent growth of algae and organic carbon dependent growth of bacteria. The model also incorporates algal photosynthesis, algal exudation of organic carbon resulting from excess photosynthesis, bacterial respiration and bacterial inorganic carbon assimilation. Therefore, the model is able to connect metabolic processes to the interdependent growth of algae and bacteria. The isotope labelling dynamics are derived from the nutrient and growth dynamics. Mathematical analysis provides parameter constraints and analytical solutions that are used to discuss how the model connects the growth and isotope labelling dynamics.

In chapter 4 the co-culture model from chapter 3 is parametrised by fitting the model to experimental data from chapter 2. The quality of the fits is used to evaluate the successes and limitations of the model. The fully parametrised model is used to investigate the single-cell heterogeneity of carbon dynamics within a bacterial population grown both axenically and in co-culture. Model predictions are also explored by considering the effect of different initial conditions and model parameters on the growth and isotope labelling dynamics.

Chapter 5 summarises the overall conclusions of the work presented in this thesis. Potential future directions for further experiments and model development are also discussed.

Chapter 2

Time-resolved, single cell measurements of microbial carbon uptake and exchange

2.1 Introduction

Photosynthetic phytoplankton are major contributors to global carbon fixation and an important step in the carbon cycle is the release of organic compounds by phytoplankton and the subsequent degradation of these molecules by heterotrophic bacteria (figure 1.3) (Bjørnsen, 1988; Buchan *et al.*, 2014; Hellebust, 1958). However, as discussed in section 2.2.3, nutrient transfer is rarely one sided. Many different species of algae are dependent on an external source of vitamin B_{12} (Croft *et al.*, 2005), which can be provided by some species of heterotrophic bacteria that in turn rely on algae as their source of organic carbon (Kazamia *et al.*, 2012b). This type of pairwise interaction is an example of a mutualism, where both species benefit from the presence of the other. The B_{12}-dependent *metE7* mutant of *C. reinhardtii* (see section 1.3.1 for details) and the B_{12}-producing, heterotrophic bacterium *M. loti* were used for the work described in this chapter. This algal-bacterial co-culture system between *C. reinhardtii metE7* and *M. loti* was established in Professor Alison Smith's research group at the Department of Plant Sciences, University of Cambridge (Helliwell *et al.*, 2015). Helliwell *et al.* (2015) used growth experiments to show that *M. loti* is able to produce enough B_{12} to support the growth of *C. reinhardtii metE7*. This chapter sets out to experimentally investigate the carbon dynamics in this algal-bacterial co-culture by measuring the bacterial uptake of DOC produced by algae, as well as the inorganic carbon assimilation for algae and bacteria grown axenically. This was achieved through combining stable isotope labelling and Secondary Ion Mass Spectrometry (SIMS). Isotope labelled substrates are assimilated into the cellular biomass and SIMS measurements provide quantitative analysis of the isotopic

enrichment for algal and bacterial cells, which can be used to analyse the metabolic activity of single cells.

Isotope Ratio Mass Spectrometry (IRMS) was used for bulk stable isotope analysis, however relatively large sample volumes are needed in order to achieve the minimum dry mass required for IRMS. In contrast, SIMS is a single cell analysis technique and therefore much smaller samples are needed, which allows for more regular sample extraction from microbial cultures of interest. Since this work aims to investigate temporal trends, it was important to be able to reliably obtain stable isotope analysis at several time points and so SIMS analysis is the focus here. Moreover, for IRMS analysis the bacterial and algal biomass fractions of a co-culture sample need to be pre-separated before analysis, whereas SIMS is able to distinguish between algal and bacterial cells in the same sample. In addition, SIMS was used in this work because it has the potential to reveal single cell heterogeneity that bulk measurements are unable to access. Lastly, SIMS can be used to obtain spatial information, which is not exploited in this work, but could be used in future as a way to investigate the effect of spatial heterogeneity on microbial metabolic activity. Therefore, the work in this thesis, which explores how SIMS and mathematical modelling can be combined, could help make steps towards a spatio-temporal analysis of nutrient fluxes in microbial communities.

2.1.1 SIMS and microbial ecology

Over the last decade, there have been many studies that combine stable isotope labelling with SIMS and NanoSIMS to address questions in microbial ecology (Abreu *et al.*, 2016; Boxer *et al.*, 2009; Gao *et al.*, 2015; Herrmann *et al.*, 2007; Musat *et al.*, 2012, 2016; Wagner, 2009; Wessel *et al.*, 2013). When environmental or cultured samples are incubated with isotope labelled nutrients, such as $H^{13}CO_3$ or $^{15}N_2$, the isotope ratio images obtained using SIMS can be used to analyse single cell metabolic activity. Therefore, SIMS is a powerful technique for investigating microbial nitrogen and carbon fixation, as well as nutrient transfer within microbial communities. Figure 2.1 shows an example result obtained using SIMS to analyse the carbon and nitrogen fixation and exchange for two cyanobacterial cells (Musat *et al.*, 2012). When studying microbial communities from the environment, stable isotope labelling and SIMS measurements are often combined with genetic methods like fluorescence in situ hybridisation (FISH), allowing the metabolic function to be related to cell identity (Musat *et al.*, 2012, 2016; Orphan *et al.*, 2009). In recent years SIMS and NanoSIMS have been used to investigate the effect of physical attachment on carbon and nitrogen fluxes between bacteria and microalgae (Arandia-Gorostidi *et al.*, 2016; Samo *et al.*, 2018), to obtain evidence of the carbon and nitrogen exchange between two partners of a newly established synthetic algal-bacterial mutualism (De-Bashan *et al.*, 2016) and to study the microbial carbon cycle

dynamics in Antarctic glacial environments (Smith *et al.*, 2017). Although the main focus of using SIMS for biological studies is on carbon and nitrogen, Raina *et al.* (2017) used NanoSIMS and ^{34}S isotope labelling to study the contribution of phytoplankton-bacteria interactions to the sulfur cycle and to image the sub-cellular distribution of sulfur within algal cells.

The bulk properties of a microbial population do not necessarily reflect the internal dynamics that exist within a community or the intrinsic variability of single cell metabolism (Kiviet *et al.*, 2014; Wagner, 2009). The capability of SIMS to measure elemental composition at single cell resolution means that it can be used to explore this single cell heterogeneity (Gao *et al.*, 2015; Musat *et al.*, 2012; Wagner, 2009).

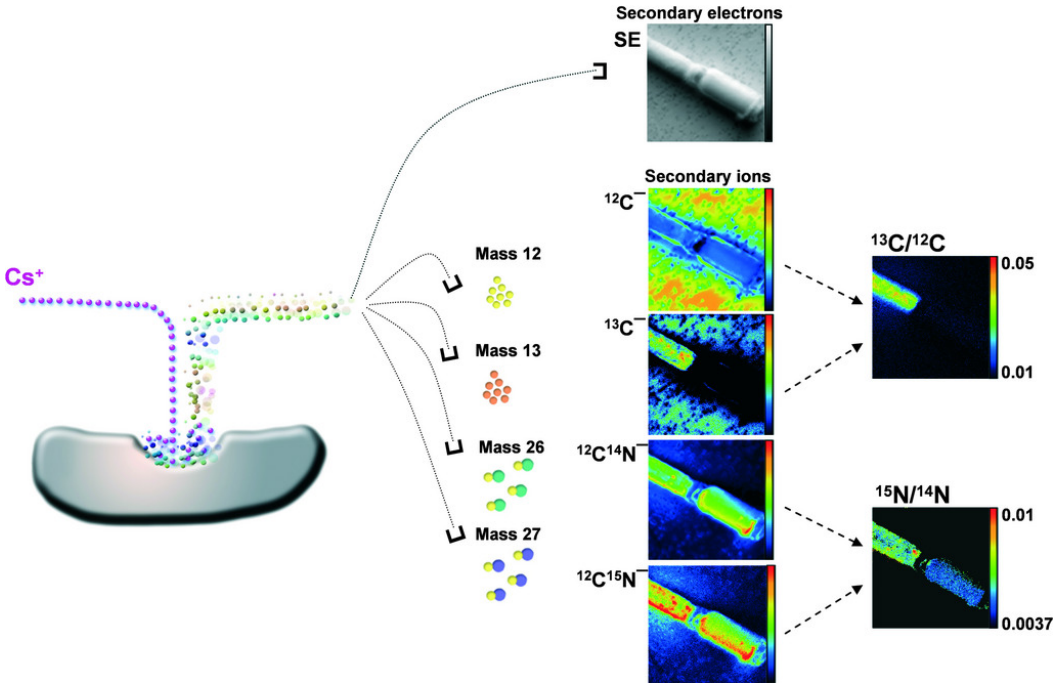

Figure 2.1 **Example NanoSIMS analysis of cyanobacteria**. Reproduced from (Musat *et al.*, 2012), this figure shows a diagram illustrating the use of NanoSIMS to measure the carbon and nitrogen isotope ratios for microbial cells. The sample is bombarded with a Cs^+ primary ion beam and the resulting secondary ions are collected and analysed using mass spectrometry. This example is for cyanobacteria that have been incubated for 6 h under light conditions and with $H^{13}CO_2$ and $^{15}N_2$. The resulting isotope ratio images for $^{13}C/^{12}C$ and $^{15}N/^{14}N$ show two types of differentiated cyanobacterial cells: a vegetative cell (photosynthetically active) and a heterocyst cell (nitrogen fixing). The vegetative cell has a high enrichment of both ^{13}C and ^{15}N, whereas the adjacent heterocyst cell shows only a small enrichment of ^{15}N because of the fast transfer of newly fixed nitrogen from the heterocyst to vegetative cells. The apparent absence of ^{13}C enrichment for the heterocyst is due to the slower transfer of carbon to the heterocyst from the vegetative cells.

2.2 Materials and methods

2.2.1 Culturing algae and bacteria

Algal and bacterial strains

C. reinhardtii metE7 (Helliwell *et al.*, 2015) and *M. loti* (MAFF 303099) were provided by Prof Alison Smith's research group at the Department of Plant Sciences, University of Cambridge. *M. loti* was originally a gift from Prof Allan Downie, John Innes Centre, UK (Kazamia *et al.*, 2012b).

Growth conditions

Cultures of both *C. reinhardtii metE7* and *M. loti* alone and in co-culture were grown at 25 °C, shaking at 120 rpm and in a 12 h-12 h light-dark cycle. During the light period the light intensity of the photosynthetically active radiation (PAR) was measured to be approximately 70 $\mu mol\, m^{-2}\, s^{-1}$ using a Skye PAR sensor (SKP 215). The growth medium used for all cultures was TRISmin, with the addition of cyanocobalamin (referred to as B_{12} throughout this thesis), glycerol and sodium bicarbonate where needed. TRISmin is a minimal medium, which means that algae grow phototrophically. Details of the chemical components of TRISmin are given in appendix A.1.

Cell density measurements

For cell density measurements of algae a Beckman Coulter counter (Z2 model) was used. A volume of 9.9 mL Coulter isoton II diluent (purchased from Beckman Coulter) was added to a 100 µL sample taken from a well-mixed culture, resulting in a 100 fold dilution. The sample was gently mixed and the Beckman Coulter counter set to measure 0.5 mL of the diluted sample and count particles in a 3.5-11.5 µm size range. From these measurements the cell densities in units of $cells\, mL^{-1}$ were calculated.

Viable counts were used to monitor the growth of both the algal and bacterial populations. First a series of 10-fold dilutions were carried out by taking 20 µL of the previous dilution and mixing it with 180 µL of sterile water. In this way dilutions from 1-10^{-3} for algae and 1-10^{-8} for bacteria were obtained. Relevant dilutions were chosen such that approximately 10-100 colonies would result. An aliquot of 20 µL from the chosen dilutions were spotted onto TY agar plates (appendix A.2) as separate drops and the plates were tilted back and forth to create streaks along the agar in order to disperse the cells, such that the colonies were easier to distinguish (Jett *et al.*, 1997). The plates were left to dry in the flow hood

before incubation. For algal colonies, the plates were incubated in continuous light at 25 °C for approximately 5 days. For bacterial colonies, the plates were incubated in the dark at 30 °C for approximately 2 days. The plates were monitored daily to ensure that the colonies were not overgrowing and merging. Two independent viable counts were obtained for each time-point and the results converted to values for the population size in units of colony forming units per unit volume (cfu mL^{-1}).

2.2.2 Work-flow for the stable isotope labelling cultures

Dissolved sodium ^{13}C-bicarbonate (Sigma-Aldrich $NaH^{13}CO_3$, 98 atom % ^{13}C) was used for the stable isotope labelling of cultures. Table 2.1 summarises the cultures grown for the experiments described in this chapter and the concentrations of glycerol, B_{12} and sodium ^{13}C-bicarbonate added to TRISmin media for each culture. The glycerol concentrations are given in units of % v/v and the B_{12} concentrations in ng L^{-1}. Figure 2.2 shows the culture work-flow for the stable isotope labelling experiments. A sample taken from the 600 mL axenic pre-culture of algae was washed and then re-suspended in 1 L of fresh media containing 100 ng L^{-1} B_{12} and 5 mM $NaH^{13}CO_3$. This pre-labelling culture of algae was grown for 48 h. An axenic pre-culture of bacteria was grown in media with 0.1 % glycerol, which was then sampled, washed and re-suspended in 750 mL fresh media with 5 mM $NaH^{13}CO_3$, to which 250 mL of pre-labelled algae was added to initiate the co-culture.

In order to confirm that an increase in ^{13}C content measured in co-cultured bacteria was due to the uptake of algal-derived carbon, control cultures of axenic bacteria were grown with 5 mM $NaH^{13}CO_3$ and different concentrations of unlabelled glycerol. The isotope labelling dynamics of these cultures were used to measure the assimilation of inorganic carbon by bacteria and to investigate whether this depends on growth rate (i.e. does an increase in the glycerol/DOC concentration, which increases the growth rate, affect inorganic carbon assimilation?).

Samples were taken at different time-points for monitoring the population growth using viable counts, for bulk isotope analysis using IRMS (see appendix C) and for single-cell isotope analysis using SIMS. Samples were also taken from the unlabelled algal and bacterial pre-cultures to measure the natural abundance of ^{13}C.

A preliminary experiment for the stable isotope labelling and SIMS analysis was carried out for an algal pre-labelling culture, a labelled co-culture and an axenic culture of bacteria with 0.1 % glycerol. The results of these preliminary experiments are presented in appendix B, where they are compared to the results from the final SIMS experiment. The preliminary experiment was used to test the experimental work-flow and it was from the preliminary results that DIC (dissolved inorganic carbon) uptake by axenic bacteria was observed, so

it became interesting to investigate this further using different concentrations of glycerol. The results from the two sets of SIMS experiments show the same trends in the isotope labelling dynamics and therefore illustrate the reproducibility of the measurements obtained. Unlabelled controls for the axenic algal culture and the co-culture were included in the preliminary experiments and showed the expected result of natural abundance for both algae and bacteria.

Table 2.1 **List of cultures grown for the SIMS experiments**. A complete list of the cultures grown as part of the stable isotope labelling experiments described in this chapter. The growth medium used for all cultures was TRISmin with the addition of B_{12}, glycerol and sodium bicarbonate as listed in this table. The glycerol concentrations are given in units of % v/v and the B_{12} concentrations in $ng\,L^{-1}$. These cultures were grown in 2 L conical flasks except for the pre-cultures, which were grown in 1 L flasks.

Cultures for the preliminary experiment	Volume (mL)	B_{12} ($ng\,L^{-1}$)	Glycerol (%)	Sodium bicarbonate
Algal pre-culture	600	1000		
Axenic algae (pre-labelling)	1000	100		5 mM $NaH^{13}CO_3$
Axenic algae (unlabelled)	1000	100		5 mM $NaHCO_3$
Bacterial pre-culture	400		0.1	
Axenic bacteria (0.1% glycerol)	1000		0.1	5 mM $NaH^{13}CO_3$
Labelled co-culture	1000			5 mM $NaH^{13}CO_3$
Unlabelled co-culture	1000			5 mM $NaHCO_3$
Cultures for the final experiment	Volume (mL)	B_{12} ($ng\,L^{-1}$)	Glycerol (%)	Sodium bicarbonate
Algal pre-culture	600	1000		
Axenic algae (pre-labelling)	1000	100		5 mM $NaH^{13}CO_3$
Bacterial pre-culture	400		0.1	
Axenic bacteria (0.1% glycerol)	1000		0.1	5 mM $NaH^{13}CO_3$
Axenic bacteria (0.01% glycerol)	1000		0.01	5 mM $NaH^{13}CO_3$
Axenic bacteria (0.001% glycerol)	1000		0.001	5 mM $NaH^{13}CO_3$
Axenic bacteria (no glycerol)	1000			5 mM $NaH^{13}CO_3$
Labelled co-culture	1000			5 mM $NaH^{13}CO_3$

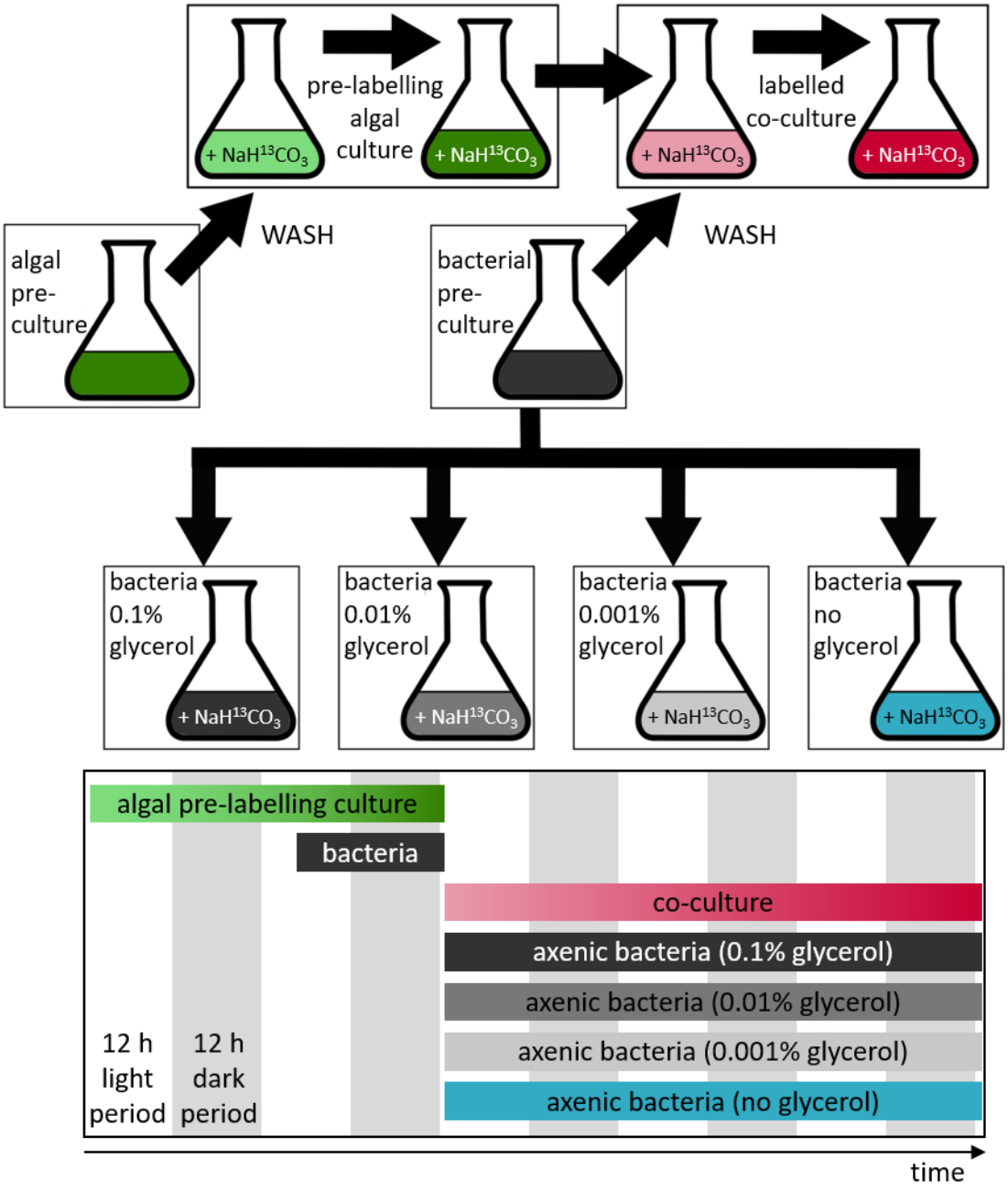

Figure 2.2 **Work-flow for the stable isotope labelling cultures**. Schematic overview and time-line of the stable-isotope labelling cultures using the alga *C. reinhartii metE7* and the bacterium *M. loti*, as described in detail in the text. The vertical white and grey bars indicate the 12 h light and 12 h dark periods respectively. Samples were taken at different time-points for single cell carbon isotope analysis using SIMS and for bulk carbon isotope analysis of the algal and bacterial biomass using IRMS.

2.2.3 Chemistry of dissolved inorganic carbon

This section briefly discusses inorganic carbon dynamics for aqueous solutions and isotopic fractionation processes. The aim here is to better understand the contribution of these processes to the carbon isotope labelling dynamics in the experiments described in this chapter.

Sodium bicarbonate

Sodium bicarbonate dissolves in water, forming bicarbonate ions $HCO_3{}^-$ that enter a set of equilibrium reactions

$$H_2CO_3 \rightleftharpoons HCO_3{}^- + H^+, \tag{2.1}$$

$$CO_2 + H_2O \rightleftharpoons H_2CO_3. \tag{2.2}$$

The different forms of inorganic carbon that are present in an aqueous solution (i.e. $HCO_3{}^-$, H_2CO_3 and CO_2) can be grouped together as DIC (dissolved inorganic carbon), and their relative concentrations depend on pH (see figure 1.5). At high pH, an additional inorganic carbon species $CO_3{}^{2-}$ would need to be considered, however the pH of the cultures grown for the experiments described in this work was always below pH 8, and therefore the concentration of $CO_3{}^{2-}$ is assumed to be negligible (Greenwood *et al.*, 1997). The equilibrium constant for the equilibrium between H_2CO_3 and $HCO_3{}^-$ in equation (2.1) is given by

$$K_1 = \frac{\left[HCO_3{}^-\right]\left[H^+\right]}{[H_2CO_3]} = 2.5 \times 10^{-4}\,\mathrm{mol\,L^{-1}} \text{ (Greenwood } \textit{et al.}\text{, 1997).} \tag{2.3}$$

For the equilibrium between CO_2 and H_2CO_3 in equation (2.2) the equilibrium constant is given by

$$K_2 = \frac{[H_2CO_3]}{[CO_2]} = 1.7 \times 10^{-3} \text{ (Housecroft } \textit{et al.}\text{, 2008).} \tag{2.4}$$

The total DIC concentration is equal to the sum of the concentrations of the different inorganic carbon components, such that

$$[\mathrm{DIC}] = [CO_2] + [H_2CO_3] + \left[HCO_3{}^-\right]. \tag{2.5}$$

Using equations (2.5), (2.3) and (2.4) and the definition $\mathrm{pH} = -\log\left[H^+\right]$, the relationship between the CO_2 concentration and pH is defined as

$$[CO_2] = \frac{[\mathrm{DIC}]}{1 + K_2 + K_2\,K_1\,10^{pH}}. \tag{2.6}$$

From this, the CO_2 concentration that results from dissolving 5 mM of sodium bicarbonate at 25 °C was estimated to be 0.65 mM (i.e. for $[\mathrm{DIC}] = 5\,\mathrm{mM}$, $K_1 = 2.5 \times 10^{-4}\,\mathrm{mol\,L^{-1}}$ (Greenwood *et al.*, 1997), $K_2 = 1.7 \times 10^{-3}$ (Housecroft *et al.*, 2008) and using the initial pH for the experimental cultures, measured to be approximately 7.2).

Atmospheric carbon dioxide

Gaseous carbon dioxide dissolves in water. Henry's law is a gas law, which states that the concentration of the dissolved gas, $[CO_2]$, is proportional to the partial pressure of the gas, p_{CO_2}, as defined by

$$[\mathrm{CO_2}] = K_H\, p_{\mathrm{CO_2}}, \tag{2.7}$$

with K_H the Henry's law constant, which is approximately $10^{-1.47}$ for carbon dioxide in water at 25 °C (Butler, 1991). The partial pressure of carbon dioxide in the atmosphere is approximately 3.6×10^{-4} atm (Hobbs, 2000), therefore, using equation (2.7), the concentration of dissolved carbon dioxide coming from gaseous carbon dioxide in the air was estimated to be 12 µM. Using the equilibrium relations defined by equations (2.3) and (2.4), the concentration of H_2CO_3 and HCO_3^- due to dissolved carbon dioxide from the air were estimated to be 20 nM and 80 µM respectively, meaning that the total concentration for DIC due to dissolved atmospheric carbon dioxide is about 92 µM.

Total DIC

For the growth media used in the experiments described in this chapter, there are two sources of DIC: sodium bicarbonate and atmospheric carbon dioxide. Although the atomic fraction of ^{13}C for the sodium bicarbonate added to the media is known (i.e. 98 atom % ^{13}C), the exact atomic fraction of ^{13}C for the total DIC is unknown due to the constant exchange of carbon between the different forms of inorganic carbon in the media and atmospheric carbon dioxide. Nonetheless, it is likely that the DIC has a high atomic fraction of ^{13}C because the estimated contribution to the DIC from dissolved atmospheric carbon dioxide is 92 µM, which is about two orders of magnitude smaller than the 5 mM concentration of sodium bicarbonate dissolved in the media.

Isotopic fractionation

As mentioned in section 1.4.1, isotopic fractionation is the process by which variation in the isotope ratio ($^{13}C/^{12}C$) between different forms of carbon is observed, which is due to different reaction rates for the two carbon isotopes for processes involving bonds to

carbon or different carbon transport rates (Farquar *et al.*, 1989; Ohkouchi *et al.*, 2015). For the equilibrium between dissolved bicarbonate and gaseous carbon dioxide the isotopic fractionation factor is defined as

$$\alpha_{HCO_3^-/CO_2(g)} = \frac{R_{HCO_3^-}}{R_{CO_2(g)}}, \tag{2.8}$$

with $R_{HCO_3^-}$ and $R_{CO_2(g)}$ the isotope ratios for dissolved bicarbonate and gasous carbon dioxide respectively. The value of $\alpha_{HCO_3^-/CO_2(g)}$ is 1.0079 at 25 °C (Mook *et al.*, 1974), which is very close to 1. This is small compared to the isotope ratio of the dissolved ^{13}C-bicarbonate relative to natural abundance for atmospheric carbon dioxide: $1.0079 \ll R_{H^{13}CO_3^-}/R_{CO_2(g)} \approx 49/0.011 \approx 4,455$. Therefore, for the stable isotope analysis discussed in this chapter, isotopic fractionation effects were considered negligible.

2.2.4 SIMS sample preparation

Figure 2.3 gives an overview of the steps required to prepare samples for SIMS analysis. Further details of each of these sample preparation steps are given below.

Chemical fixation

Cell culture samples were chemically fixed using formaldehyde. For every 10 mL of sample volume, 0.54 mL of 37-41% (w/v) formaldehyde was added to reach a final formaldehyde concentration of about 2 % (w/v). The sample was gently vortexed and then incubated at 4-6 °C for 1 h. To remove the fixative, the sample was washed twice by centrifugation followed by re-suspension in 1X PBS buffer (i.e. phosphate buffered saline solution consisting of 10 mM Na_2HPO_4 and 150 mM NaCl). The sample was then centrifuged for a third time and finally re-suspended in a 1:1 by volume mix of 1X PBS buffer and 96 % ethanol solution. Samples were stored in the fridge (4-6 °C) until further use.

Cell staining and vacuum filtration

In order to be able to visualise the distribution of algal and bacterial cells on the membrane filter, SYTO9 green fluorescent nucleic acid stain (taken from a Molecular Probes LIVE/DEAD BacLight bacterial viability kit) was used for both bacterial and algal cells. Per 1 mL of sample, 1.5 µL of 3.34 mM SYTO9 was added, the sample was then incubated in the dark and at room temperature for 15 min. An appropriate sample volume was chosen for vacuum filtration in order to achieve an even distribution of cells on the filter, which meant choosing a volume that contained 0.5×10^5 to 2×10^5 cfu for algae and 1×10^7 to 1×10^8 cfu for

bacteria. Isopore membrane filters with a pore size of 0.22 µm and diameter 25 mm (Merck Millipore) were pre-sputtered with ~20 nm gold coating, using a BioRad SEM Coating System, and cells were then deposited on these gold-coated filters by vacuum filtration using a Charles Austen Capex 8C vacuum pump.

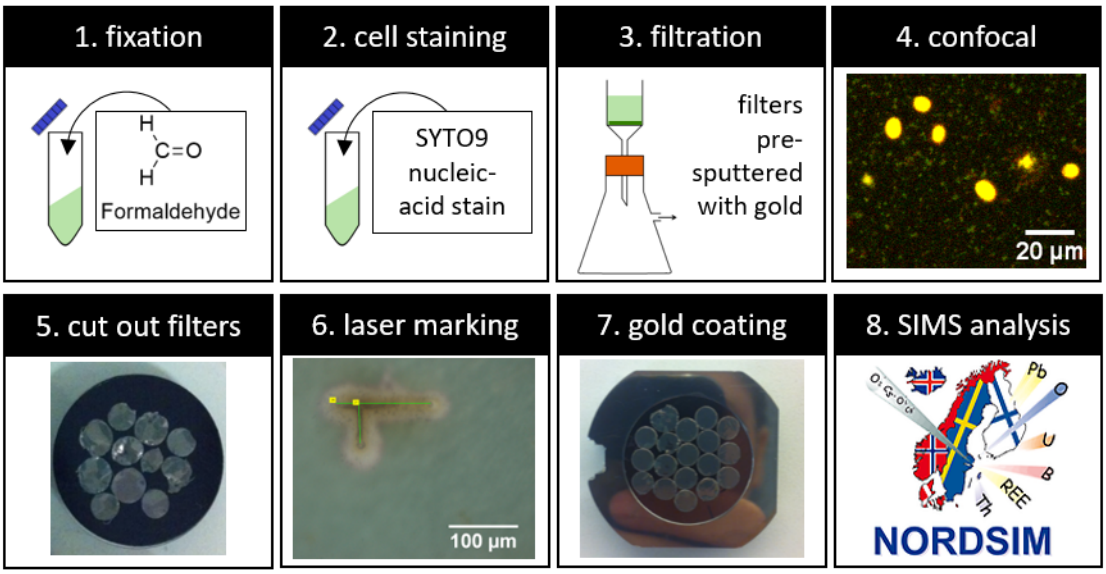

Figure 2.3 **Sample preparation for SIMS**. An overview of the steps involved in preparing microbiological samples for analysis by Secondary Ion Mass Spectrometry. (1) The samples were first fixed with formaldehyde and then washed to remove the chemical fixative. (2) The cells were stained with a fluorescent nucleic acid stain, SYTO9. (3) Vacuum filtration was used to deposit the cells onto a membrane filter, with a pore size of 0.22 µm and which had been pre-sputtered with gold. (4) Confocal microscopy was used to confirm an even distribution of cells on the filter. (5) A hole punch was used to cut the filters into 4-6 mm disks. (6) Using a Zeiss laser micro-dissection microscope, the filters were marked with a laser and epifluorescence images of algal chlorophyll fluorescence were taken. The fluorescence images were matched with the carbon isotope images obtained using SIMS. (7) The samples were sputter coated with gold to ensure conductivity of the samples. (8) SIMS analysis was conducted using the Cameca IMS 1280 at the NordSIM facility at the Swedish Museum of Natural History in Stockholm.

Confocal microscopy

It is important that samples prepared for SIMS are flat, as an uneven sample can result in unreliable measurements (Watrous *et al.*, 2011). An Olympus Fluoview laser scanning confocal microscope (FV1200) was used to image the filter samples and to ensure an even distribution of cells. A 473 nm excitation laser was used and fluorescence emission was detected in two channels; 490-525 nm to detect the green fluorescence of the SYTO9 nucleic acid stain and 560-660 nm to detect the chlorophyll autofluorescence of algae. Figure 2.4 is an example of a confocal z-stack image for a co-culture sample obtained during preliminary experiments, which shows an even distribution of algal and bacterial cells across the filter in a relatively uniform layer. The orthogonal views obtained from a series of z-stack images (with a 2 µm step size) confirmed that the algal and bacterial cells were not piled on top of one another, meaning that the vacuum filtration achieved an approximate monolayer of cells. Figure 2.5 shows example confocal microscopy images for the axenic and co-culture samples prepared for SIMS, which further confirm that an even distribution of cells was achieved.

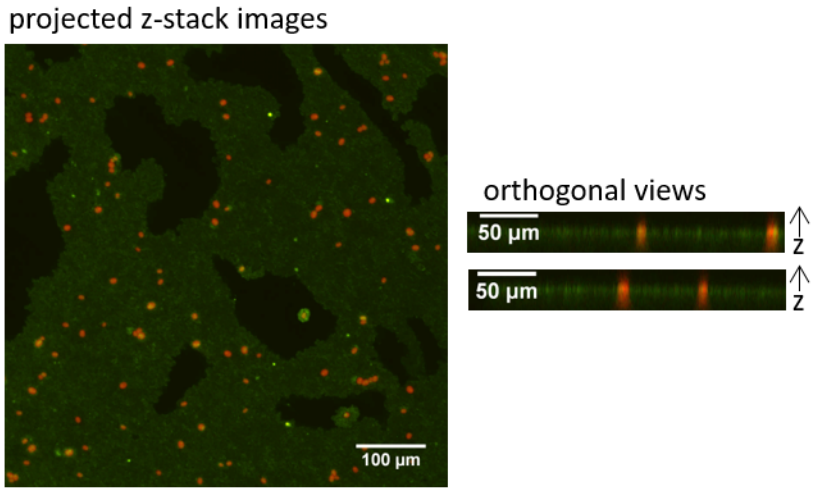

Figure 2.4 **Confocal z-stack images for a co-culture sample**. A 473 nm excitation laser was used and fluorescence emission was detected in two channels; 490-525 nm to detect the fluorescence of the SYTO9 nucleic acid stain (green) and 560-660 nm to detect the chlorophyll autofluorescence of algae (red). The projected image was obtained by the summation of eight images taken at a 2 µm separation in the z direction. The orthogonal views were obtained in Image J and show the xz projection of the confocal z-stack.

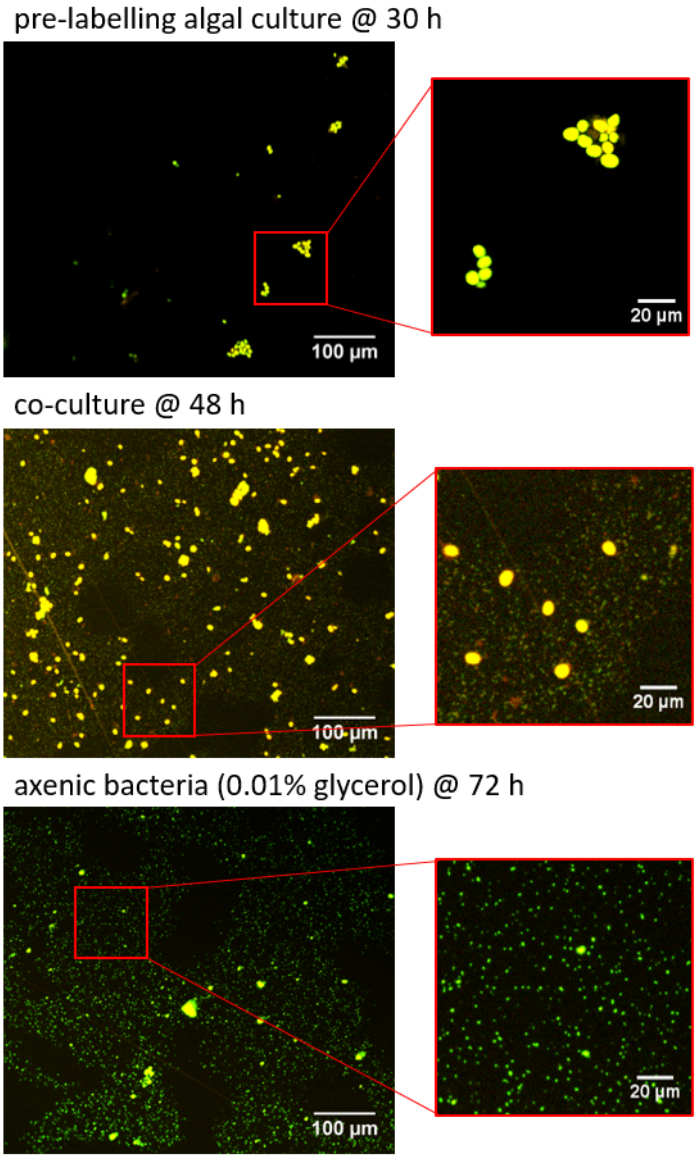

Figure 2.5 **Example confocal microscopy images**. For comparison of the different types of cultures, example confocal microscopy images are shown here for a sample of the pre-labelling algal culture, the co-culture and an axenic bacterial culture. A 473 nm excitation laser was used and fluorescence emission was detected in two channels: 490-525 nm to detect the fluorescence of the SYTO9 nucleic acid stain (green); and 560-660 nm to detect the chlorophyll autofluorescence of algae (red). The yellow regions indicate where red and green overlap and therefore show the areas where both chlorophyll and SYTO9 fluorescence are present.

Laser marking and gold coating

A single hole punch was used to cut out 4-6 mm disks from the filter samples. Following this, a Zeiss laser micro-dissection microscope (Zeiss LSM710-NLO housed at the LCI facility of the Karolinska Institute, Stockholm) was used to laser-mark the filter samples and to image the autofluorescence of the algal chlorophyll using the FITC and Rhodamine filter sets. The laser markings could be seen with the camera of the SIMS instrument, and so the SIMS measurements could be matched to chosen sample areas corresponding to particular algal cells in the fluorescence images. Figure 2.6 shows an example comparison between the fluorescence image of a laser mark and the camera view of the SIMS instrument. After laser-marking the filter samples, they were placed on a conductive sticky tape and mounted onto a glass disk to be placed in the sample holder of the SIMS instrument. The samples were then sputter coated with gold at the NordSIM facility to ensure conductivity of the sample.

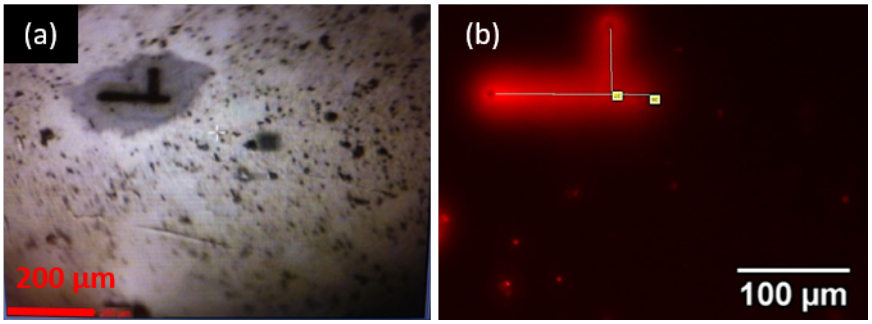

Figure 2.6 **Laser markings were used to locate specific algal cells for SIMS analysis**. (a) The camera view of the SIMS instrument, in which it is challenging to identify regions with algal and bacterial cells, but a laser mark is clearly visible. (b) A fluorescence image of the region around a laser mark obtained using the Rhodamine filter set, which shows the laser mark and the chlorophyll fluorescence of nearby algal cells. Fluorescence images were used to navigate around the filter and to locate regions of interest for SIMS analysis.

Epifluorescence microscopy after SIMS analysis

After the SIMS measurements were complete the samples were imaged with an Olympus BX60 epifluorescence microscope using the 460-490 nm excitation filter and the 510 nm dichromatic beamsplitter for imaging the fluorescence emission. These images were used to confirm which algal cells were analysed and therefore was helpful during the selection of algal cell areas in the SIMS analysis. Figure 2.7 shows an example of the imaging work-flow, which started with fluorescence imaging of the algal cells in relation to a laser mark, followed by SIMS analysis of a selected 35 µm square area of the sample and finally fluorescence

microscopy to confirm which algal cells were analysed. Since chlorophyll fluorescence was still observed after SIMS analysis, this suggests that the SIMS measurements did not raster scan through the depth of the whole algal cells.

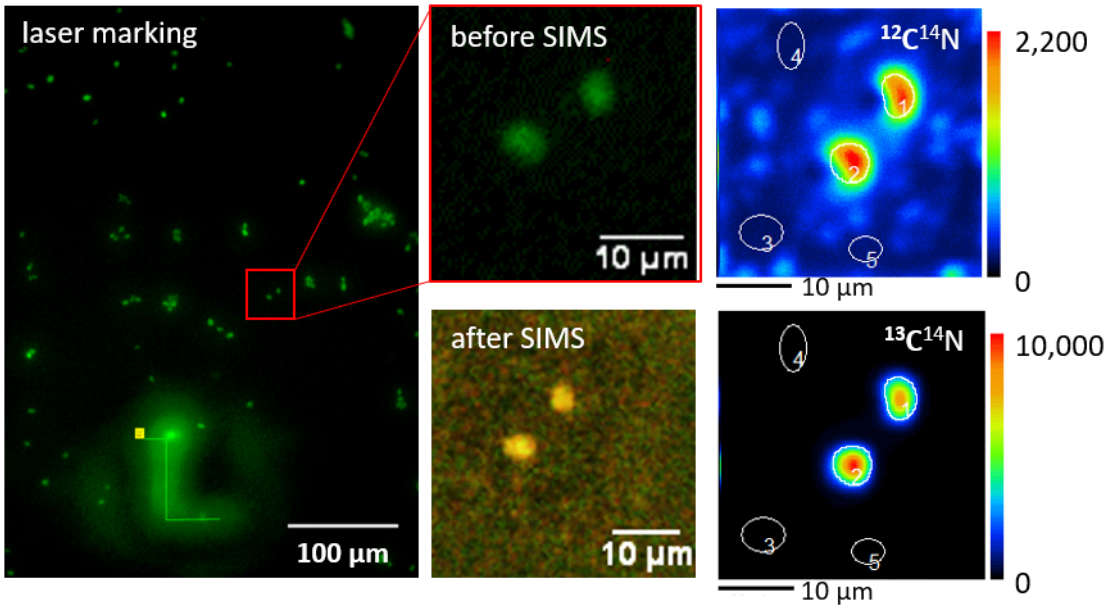

Figure 2.7 **Laser-marking and fluorescence imaging was used to identify specific algal cells for SIMS analysis**. These are example images for a sample taken from the co-culture at 48 h. A fluorescence image using the FITC filter set was obtained for the chlorophyll fluorescence of algal cells in the same field of view as a laser mark. This was then used as a reference to select a 35 µm square area for SIMS analysis, after which another chlorophyll fluorescence image was obtained to confirm which algal cells had been analysed. The fluorescence images were used to guide the selection of the algal cell regions of interest in the SIMS images (areas 1 and 2 are the algal cell areas used for analysis and areas 3, 4 and 5 were used for background measurements). The colour maps indicate the scale for the SIMS measurements in units of secondary ion counts, which were accumulated over 100 scans.

2.2.5 Secondary Ion Mass Spectrometry

Secondary Ion Mass Spectrometry (SIMS) analysis was carried out using the Cameca IMS 1280 (figure 1.9) at the NordSIM facility in the Department of Geosciences at the Swedish Museum of Natural History in Stockholm. The instrument uses a Gaussian focussed primary ion beam of cesium ions (Cs^+). For selected positions on the filter sample, 45×45 µm square areas were pre-sputtered for 10 s with a beam of 3 nA. Within this pre-sputtered region, 100 scans of a 35×35 µm square area were measured using a ~60-80 pA primary ion beam, which has a spot size of approximately 1 µm. The secondary ion mass peaks were measured using

an ion counting electron multiplier in peak hopping mode with a 44 ns electronically gated dead-time. The count times for the $^{12}C^{14}N^-$, $^{12}C^{15}N^-$ (not used in subsequent analysis) and $^{13}C^{14}N^-$ secondary ion peaks were 1, 0.5 and 2 s respectively. A mass resolution ($M/\Delta M$) of approximately 6000 for the preliminary experiments and 7000 for the final experiments was used; a mass resolution of 6000-7000 was sufficient in resolving both the $^{12}C^{14}N^-$ and $^{13}C^{14}N^-$ peaks. The SIMS measurements were run once for bacterial cells and repeated 1-8 times for each algal cell.

2.2.6 Data analysis using the WinImage software

Data analysis using the WinImage software (Cameca) was used to calculate the isotope ratios ($^{13}C/^{12}C$) for single cells of algae and bacteria from the SIMS measurements. For bacterial cells (figure 2.8), the elliptical tool in the WinImage software was used to select regions of interest (ROIs) in the $^{12}C^{14}N$ image. The isotope ratio $\left(R = {}^{13}C/{}^{12}C\right)$ for each cell was calculated by taking the mean value for the 100 scans of SIMS measurements, from which the atomic fraction of ^{13}C, i.e. $f = {}^{13}C/\left({}^{13}C + {}^{12}C\right)$, was calculated using

$$f = \frac{R}{1+R}. \tag{2.9}$$

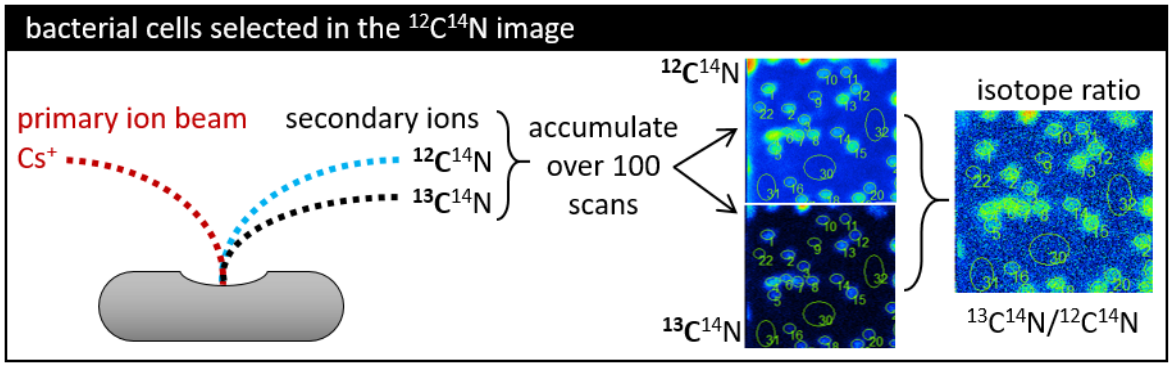

Figure 2.8 **SIMS analysis work-flow for bacterial cells**. SIMS measures the $^{13}C^{14}N$ and $^{12}C^{14}N$ ion counts across a 35×35 µm square area. Using the WinImage software, the counts were accumulated over 100 scans and the $^{12}C^{14}N$ image was used to select regions of interest (ROIs) corresponding to bacterial cells. The isotope ratio per cell was calculated as the mean of 100 scans.

For algae (figure 2.9), the SIMS results for highly labelled cells show an inhomogeneous distribution of the different carbon isotopes. Therefore, in order to select algal cells in a way that is not biased towards a particular carbon isotope, a linear combination image was created by a simple addition of the two isotope counts $\left(1\cdot{}^{12}C^{14}N + 1\cdot{}^{13}C^{14}N\right)$, which gives the

total distribution of carbon across the area scanned. By comparing this with the fluorescence images, the ROIs corresponding to algal cells were selected. The isotope ratio (R) was calculated by taking the mean for the 100 scans of each measurement, from which the atomic fraction of ^{13}C was calculated using equation (2.9). For the preliminary experiment only one measurement of 100 scans was completed, whereas for the final experiment 2-8 repeated measurements for each algal cell was obtained.

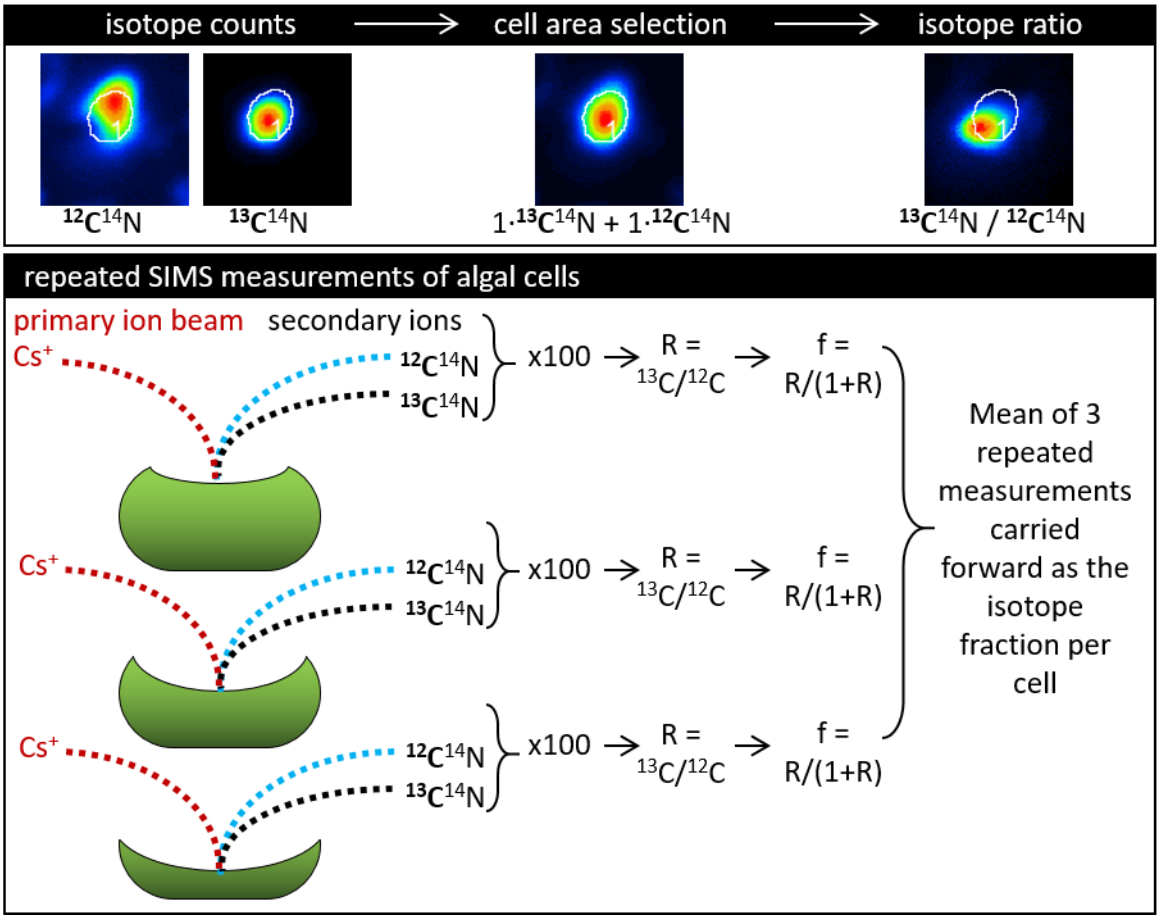

Figure 2.9 **SIMS analysis work-flow for algal cells**. SIMS measures the $^{13}C^{14}N$ and $^{12}C^{14}N$ ion counts across a 35 µm square area. Using the WinImage software, the counts were accumulated over 100 scans. For the SIMS images of algal cells, a linear combination image $\left(1 \cdot {}^{12}C^{14}N + 1 \cdot {}^{13}C^{14}N\right)$ was used to select the algal cell areas while comparing with fluorescence images for an indication of cell size and shape. The isotope ratio per cell was calculated as the mean of 100 scans. In the final experiment this was repeated 2-3 times to get a measurement for the atomic fraction of ^{13}C, i.e. f, at different depths within the algal cell. For single cells of algae, f was calculated as the mean for these 2-3 measurements.

2.3 Results

2.3.1 Depth analysis

Secondary Ion Mass Spectrometry (SIMS) is a destructive technique, meaning that through the process of measurement, as the primary ion beam scans across the sample, the biomass of the cells is gradually degraded. For each measurement, the area of interest was raster scanned 100 times and each subsequent scan collected cellular material from deeper into the cell. Figure 2.10 shows that after the first measurement most of the bacterial biomass was lost from the sample and therefore one measurement was sufficient in sampling the bacterial biomass for analysis of its carbon isotope content.

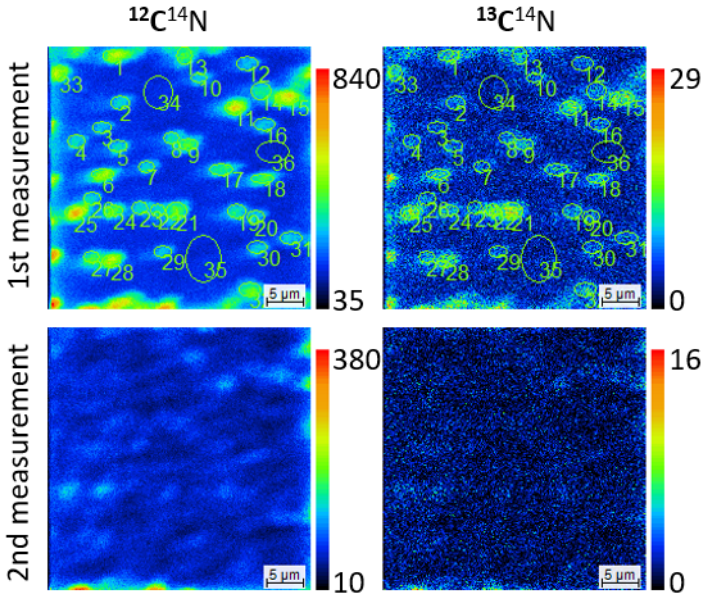

Figure 2.10 **Repeated SIMS scan for bacterial cells**. Example SIMS results for the $^{12}C^{14}N$ and $^{13}C^{14}N$ isotope images obtained from two measurements at the same sample location. The colour maps indicate the scale for the SIMS measurements in units of secondary ion counts, which were accumulated over 100 scans.

The algal cells were approximately 10 times larger than the bacterial cells, therefore the first measurement resulted in only partial degradation of the algal biomass. To investigate how the carbon isotope enrichment of algal cells changes with depth, eight repeated measurements were taken for selected sample areas. The results are plotted in figure 2.11a and suggest that the ^{13}C-enrichment of algal cells was not homogeneous. Figure 2.11b shows the difference between the third and first measurements of the atomic fraction of ^{13}C ($\Delta f = f_3 - f_1$) relative to the mean of three repeated measurements taken for the same

algal cells (mean $= (f_1 + f_2 + f_3)/3$). These results showed that the ^{13}C-enrichment can increase or decrease for repeated measurements. It was too time intensive to acquire eight measurements for each algal cell, therefore, in order to have a measurement that is representative of the whole cell, the mean of the first three repeated measurements was taken as the value for f of an individual algal cell (with the exception of two cells for the 6 h sample of the pre-labelling culture of algae, for which only two repeated measurements were taken and therefore f for these two cells was calculated as the mean of only two repeated measurements).

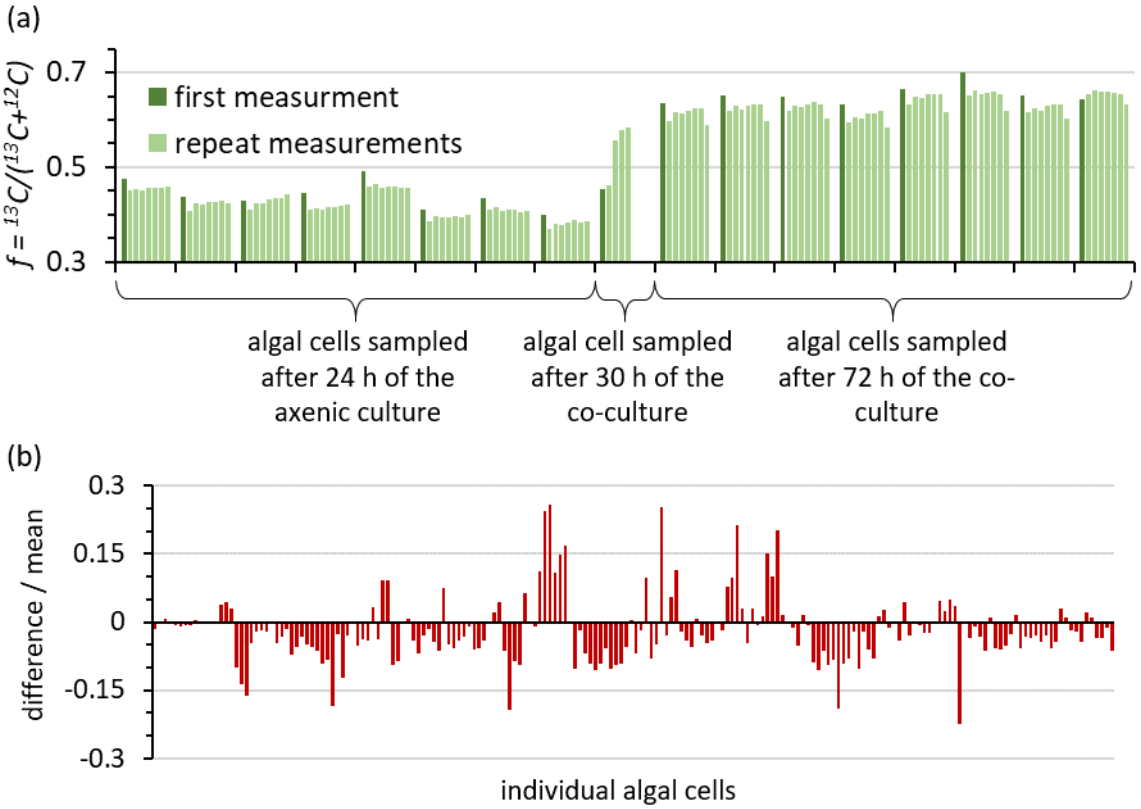

Figure 2.11 **Depth analysis of algal cells**. (a) The atomic fraction of ^{13}C in algal cells taken for eight 'depth-positions'. (b) The difference between the atomic fraction of ^{13}C in algal cells obtained from the third and first 'depth-positions' ($\Delta f = f_3 - f_1$) relative to the mean (mean $= (f_1 + f_2 + f_3)/3$).

2.3.2 Scattering effect for highly labelled algae

In the preliminary SIMS experiment for the labelled co-culture, some of the areas of the filter sample analysed contained a mix of algal and bacterial cells, while other areas analysed contained only bacterial cells. Figure 2.12 compares the mean and standard deviation of the atomic fraction of ^{13}C in bacterial cells that lie within scan areas containing at least one labelled algal cell and those that only had bacterial cells in the scan area. When the scan area contained a labelled algal cell the f values for bacterial cells in that area were both higher and more variable. As the cesium ion beam is scanned across the sample, the cellular material is sputtered away to produce secondary ions for SIMS analysis. If a highly labelled algal cell is in the area scanned, some of the highly labelled algal biomass may not be captured as secondary ions, but instead be scattered in the region around the algal cell on the filter. This could explain the observed increase in f for bacterial cells analysed in the same area as a labelled algal cell. As a result of this observation, for the subsequent analysis described in this chapter, only bacteria from scanned areas that did not contain labelled algae were considered.

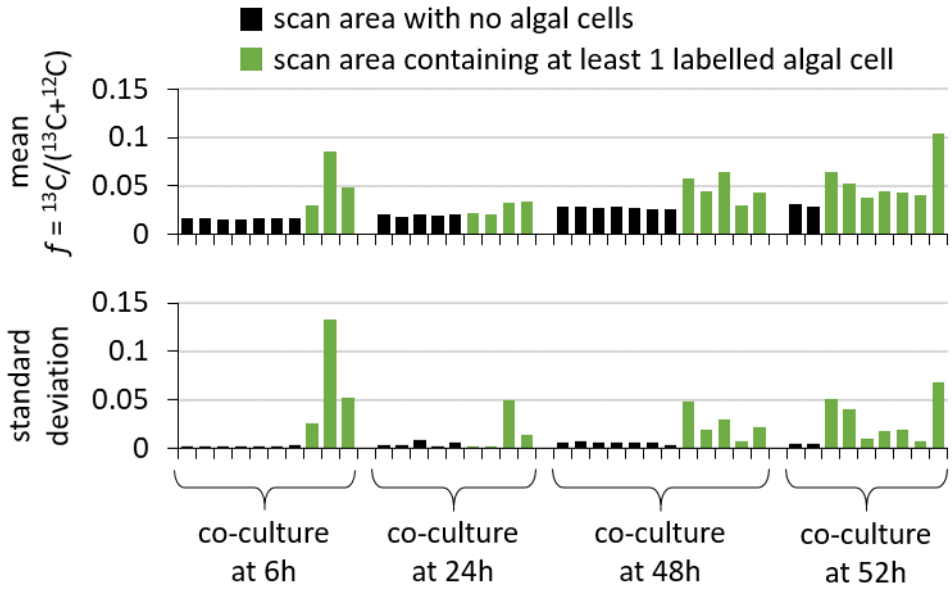

Figure 2.12 **Scattering effect associated with highly labelled algal cells**. These plots compare the mean and standard deviation of the atomic fraction of ^{13}C in bacterial cells within SIMS scan areas that do not contain a highly labelled algal cell (black bars) and areas that do contain at least one highly labelled algal cell (green bars). When the scan area contains a labelled algal cell, the atomic fractions of ^{13}C in bacterial cells are both higher and tend to be more variable.

2.3.3 Dilution effect - comparing bulk and single cell measurements

Isotope Ratio Mass Spectrometry (IRMS) was used for bulk analysis of the carbon isotope content of the algal and bacterial biomass sampled from the different cultures. It was not possible to obtain IRMS measurements for every time-point because for some samples not enough dry mass was obtained. The IRMS results are given in detail in appendix C and they confirm the trends observed for the SIMS results discussed in this chapter.

The sample preparation for SIMS analysis involved chemical fixation and staining. Both of these processes introduced unlabelled carbon into the cells and therefore diluted the atomic fraction of ^{13}C. As established by Musat *et al.* (2014), the relationship between the atomic fraction measured by SIMS (f_{SIMS}) and the atomic fraction for the sample before chemical fixation and staining (f) is

$$f = f_{SIMS} + D\,(f_{SIMS} - f_{ch})\,, \tag{2.10}$$

where D is the dilution factor and f_{ch} is the atomic fraction of ^{13}C in the chemical fixative, and the nucleic acid stain, which are both assumed to be at natural abundance, i.e. $f_{ch} = 0.0108$.

The samples for IRMS analysis did not undergo any chemical fixation or staining, so the IRMS results for the atomic fraction of ^{13}C were assumed to be the true, undiluted value of f. To estimate the dilution factor D, the SIMS results f_{SIMS} were compared with the bulk measurements obtained by IRMS (i.e. $f_{IRMS} = f$). Figure 2.13 compares the IRMS and SIMS results, and plots the results of using the curve fitting application in Matlab to fit equation (2.10) to the experimental data. The fit results are summarised in table 2.2. The estimated dilution factor for algae is $D_a = 0.04$, for which the 95 % confidence bound is greater than the value for D_a (table 2.2), meaning that the estimate for the dilution factor for algae was close to zero, but with a relatively high error. For bacteria, the fit was carried out both with and without including the 72 h sample from the co-culture. There is reason to doubt the validity of the quantitative value of the IRMS result for this co-culture sample, it might be higher than the true value for bacteria due to contamination with biomass debris from highly labelled algae that was not removed by the filtration step. Therefore, the dilution factor for bacteria carried forward for subsequent analysis was the value obtained when only the results for samples taken from axenic cultures were used, i.e. $D_b = 1.29$ (table 2.2).

To obtain estimates for the undiluted atomic fraction of ^{13}C, the SIMS results for the single cell measurements were '*dilution corrected*' using equation (2.10) and the dilution factors $D_a = 0.04$ for algal cells and $D_b = 1.29$ for bacterial cells. The chemical fixation and nucleic acid staining dilute the atomic fraction of ^{13}C to a greater extent for bacteria than for algae. This is likely to be because the bacterial cells are approximately 10 times smaller than

the algal cells and therefore have a greater surface area to volume ratio, which could account for the greater relative uptake of the chemical fixative and nucleic acid stain.

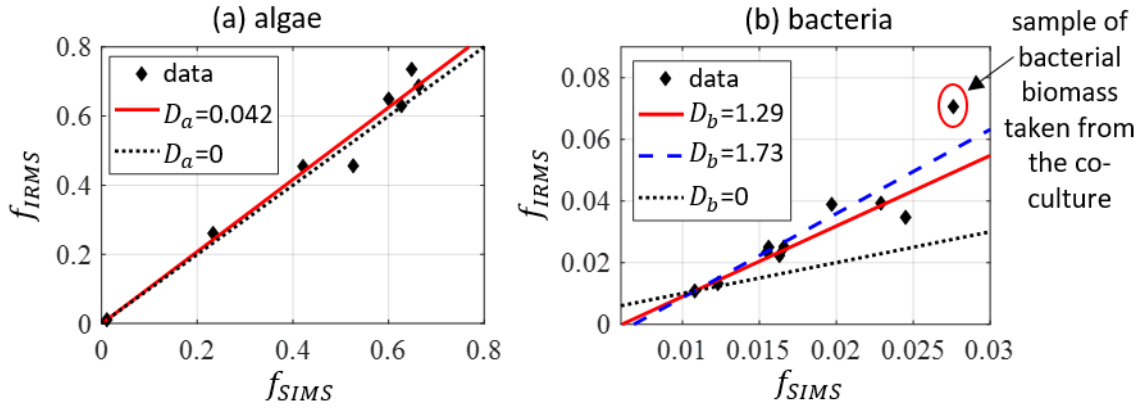

Figure 2.13 **The dilution effect**. The atomic fraction of ^{13}C obtained by IRMS and SIMS analysis plotted against one another (black diamonds). The lines show the results of the least squares fit of equation (2.10), using $f_{ch} = 0.0108$. (a) For algae the fit gave a dilution factor of $D_a = 0.042$ (red, solid line). (b) For samples of bacteria, the fit to obtain the dilution factor, D_b, was done both with (blue, dashed line, $D_b = 1.73$) and without (red, solid line, $D_b = 1.29$) the co-culture sample included. In both plots, the $D = 0$ case is plotted (black, dotted line), which shows that if there was no dilution effect the IRMS and SIMS results would be expected to give the same results. The dilution effect results in SIMS measurements providing an underestimate of the true, undiluted f.

Table 2.2 **The dilution factor results**. The dilution factor, D, was obtained from a least squares fit of equation (2.10) using the curve fitting application in Matlab and with $f_{ch} = 0.0108$. This table lists the results for D, the 95 % confidence bounds, the number of points in the fit, n, and the least square displacements, R^2. For bacteria, two fits were performed - one with and one without the co-culture sample included.

	D	95 % confidence bound	n	R^2
Algae	0.04	$\pm$ 0.07	8	0.968
Bacteria	1.73	$\pm$ 0.55	10	0.837
Bacteria (without the co-culture sample)	1.29	$\pm$ 0.41	9	0.840

2.3.4 Axenic bacteria assimilate dissolved inorganic carbon

M. loti was grown in axenic cultures with 5 mM $NaH^{13}CO_3$ and different concentrations of unlabelled glycerol. A higher concentration of glycerol results in a faster growth rate and a higher carrying capacity (figure 2.14a-b). Even when there is no glycerol added to the growth medium, bacterial growth is still observed, which is likely to be due to the bacteria having an internal store of carbon as a result of the pre-culture being grown with a high concentration (0.1 %) of glycerol.

For each time-point 80-190 cells were analysed and the f values were corrected for the dilution effect using $D_b = 1.29$ (section 2.3.3). Figure 2.14c-d and table 2.3 show the mean f for bacteria cells sampled from the axenic cultures, and figure 2.15 shows histogram plots for the single-cell measurements of f acquired for the different time-points. During the SIMS analysis there were a few fields of view that contained region(s) of a size comparable to bacterial cells but with a relatively high atomic fraction of ^{13}C. These regions might correspond to bacteria with a relatively high DIC assimilation rate in the first 6 h of the cultures grown with no glycerol and 0.001 % glycerol, which would suggest that there could be a small sub-population of bacteria that consume a large amount of DIC compared to the population average. However more data would be required to make this conclusion because these regions with high f values could be the result of an experimental artefact, for example cross-contamination between samples. The rare occurrence of cross-contamination can occur during sample preparation or inside the SIMS instrument. Sputtering with the primary ion beam could cause material from one sample to be deposited on a neighbouring sample, or due to the close proximity of the first lens to the sample surface, material from one sample can land on the mechanical structure of the lens and subsequently be re-deposited onto a different sample (Deline, 1983; McPhail *et al.*, 2009). For the purposes of this work, points were considered outliers and not included in the calculation of the mean if they had an atomic fraction of ^{13}C greater than $f_{max} = p_2 + 4 \cdot (p_2 - p_1)$, where p_1 and p_2 are the 25th and 75th percentile respectively. The outliers are indicated on the histogram plots with red stars (figure 2.15).

During the first 24 hours all four cultures were in the exponential growth phase and the bacteria reached a higher ^{13}C-enrichment when grown with a higher concentration of glycerol (figure 2.14). Only the inorganic carbon was labelled (i.e. $NaH^{13}CO_3$), therefore an increase in f for bacteria suggests that they can metabolise DIC (dissolved inorganic carbon). The data implies that a higher glycerol concentration results in the bacteria having a higher exponential growth rate and taking up a larger proportion of DIC. For the bacteria grown with 0.1 and 0.01 % glycerol, a peak in f is observed, which is particularly prominent for the 0.1 % glycerol culture (figure 2.14d). A decrease in f is observed for the stationary growth

phase, which implies that although the bacterial population size has reached a constant, the culture is still active in terms of its carbon dynamics.

The single cell measurements obtained from SIMS analysis show that the bacteria from the pre-culture have a narrow distribution of f at natural abundance (figure 2.15 and table 2.3). During the initial 24 hours of the axenic cultures, as the bacterial population grows exponentially, the mean f increases and the single cell distribution of f broadens, as seen in the histogram plots in figure 2.15 and the increasing standard deviation values in table 2.3. This broadening could be due to the heterogeneity of growth, carbon uptake and/or respiration rates within a population. For bacteria in a high concentration (0.1 %) of glycerol, during the stationary phase of the culture, between the 24 h and 72 h time-points, the mean f decreases and there is a distribution narrowing for the single-cell measurements. Different potential origins for the observed temporal evolution of these single cell distributions of f are discussed in more detail in chapter 4 using a mathematical model of bacterial carbon dynamics.

Table 2.3 **SIMS results for the axenic cultures of *M. loti***. This table lists the number of bacterial cells included in the analysis and the mean, standard deviation and standard error in the mean for the dilution corrected ($D_b = 1.29$, section 2.3.3), single cell measurements of the atomic fraction of ^{13}C $\left(f = {}^{13}C/\left({}^{13}C + {}^{12}C\right)\right)$ for bacteria grown with different concentrations of unlabelled glycerol and 5 mM $NaH^{13}CO_3$.

Culture	Time (h)	No. of cells	Mean f	Standard deviation	Standard error
Bacterial pre-culture	0	86	0.0108	0.0005	0.00006
0.1 % glycerol	6	103	0.0338	0.0045	0.0004
	24	86	0.0421	0.0070	0.0008
	48	137	0.0240	0.0031	0.0003
	72	102	0.0217	0.0027	0.0003
0.01 % glycerol	6	83	0.0316	0.0035	0.0004
	24	90	0.0385	0.0052	0.0006
	72	83	0.0311	0.0056	0.0006
0.001 % glycerol	6	96	0.0207	0.0028	0.0003
	24	185	0.0234	0.0033	0.0002
	72	106	0.0217	0.0036	0.0004
No glycerol	6	84	0.0125	0.0010	0.0001
	24	147	0.0132	0.0010	0.00008
	72	163	0.0143	0.0013	0.0001

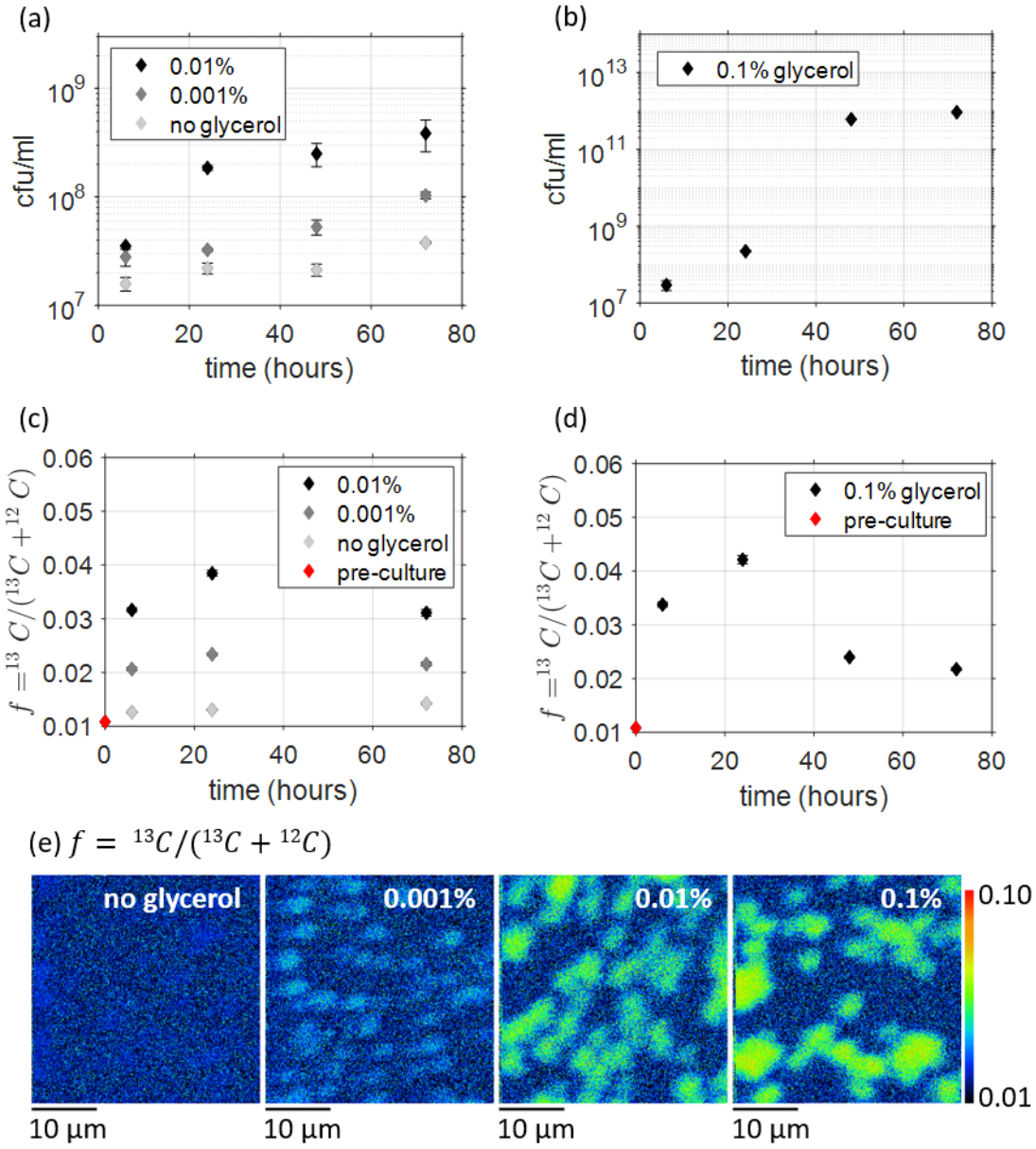

Figure 2.14 **Growth and SIMS results for the axenic cultures of *M. loti* showing uptake of DIC**. The results presented in these figures are for the four different axenic cultures of bacteria that were grown with (a, c) no, 0.001 % and 0.01 % glycerol, and (b, d) 0.1 % glycerol; all of which grown with 5 mM $NaH^{13}CO_3$. (a, b) Bacterial growth plotted as the mean and standard error of two viable count measurements. (c, d) The mean atomic fraction of ^{13}C for dilution corrected ($D_b = 1.29$, section 2.3.3) SIMS measurements of samples taken at different time-points. The standard error values are smaller than the size of the plotted points. (e) Example images of the atomic fraction of ^{13}C in bacterial cells obtained using SIMS analysis of the 24 h samples. The colour map shows the scale for the atomic fraction of ^{13}C $\left(f = {}^{13}C/\left({}^{13}C + {}^{12}C\right)\right)$ between 0.01 and 0.10.

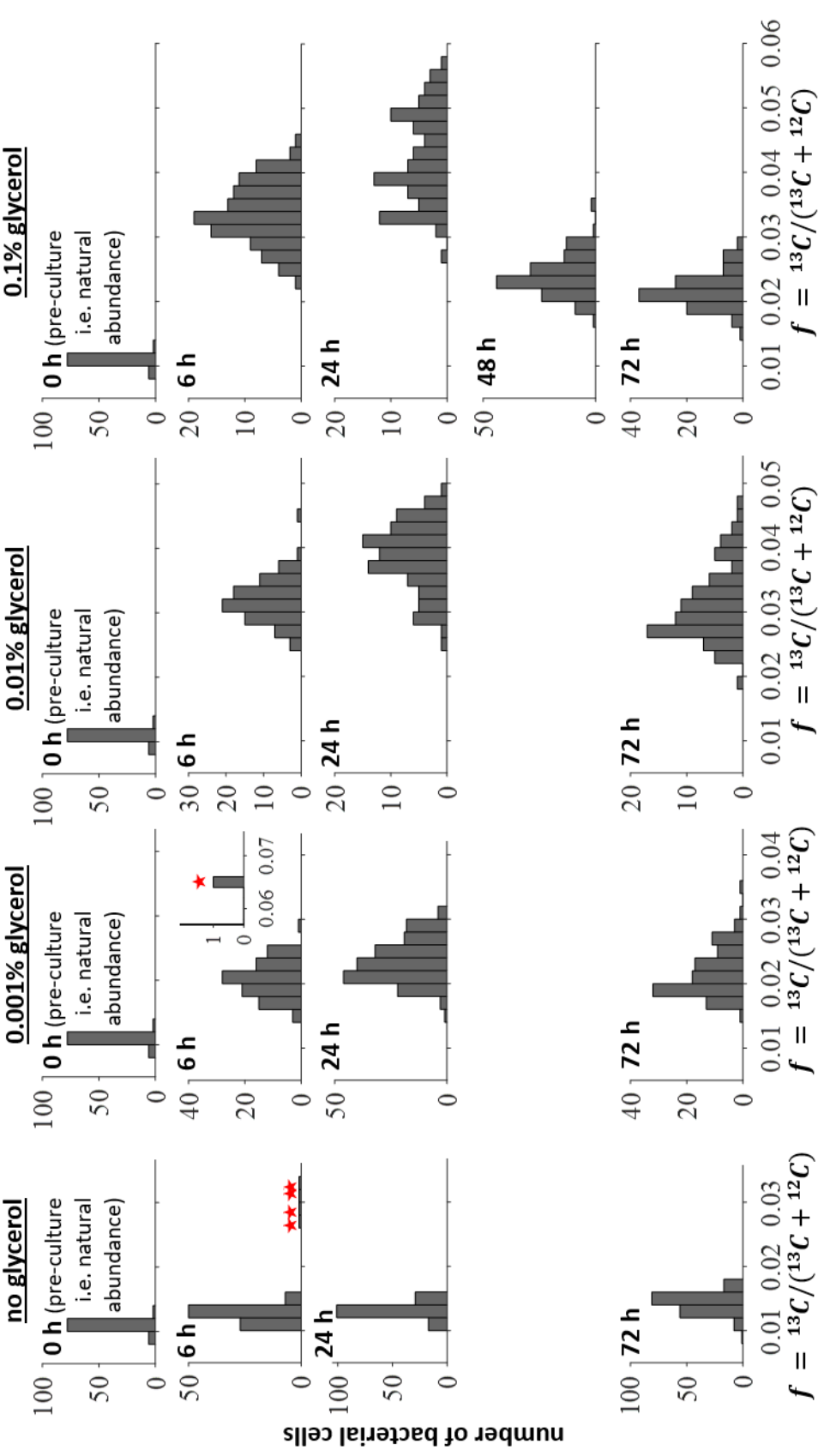

Figure 2.15 **Distributions of the atomic fraction of ^{13}C for *M. loti* grown axenically in different glycerol concentrations**. Histogram plots showing the dilution corrected ($D_b = 1.29$, section 2.3.3) SIMS results for the single cell measurements of bacterial samples taken from axenic cultures grown with different concentrations of unlabelled glycerol and 5 mM $NaH^{13}CO_3$. The red stars indicate the points that were considered outliers from the distribution and therefore excluded from the calculation of the mean (i.e. 4 points for the 6 h sample from the no glycerol culture and 1 point for the 6 h sample from the 0.001 % glycerol cultures).

2.3.5 Axenic algae: the pre-labelling culture

The B_{12} dependent *metE7* mutant of *C. reinhardtii* was grown axenically for 48 hours in media containing 5 mM $NaH^{13}CO_3$, which provides a ^{13}C-enriched inorganic carbon source for photosynthesis. As described in detail in section 2.2.3, the dissolved sodium bicarbonate enters an equilibrium and therefore both $H^{13}CO_3^-$ and $^{13}CO_2$ are available. *C. reinhardtii* has a carbon concentrating mechanism and so can take up bicarbonate, as well as carbon dioxide, for photosynthesis.

The algal population growth was monitored using both Coulter counts and viable counts (figure 2.16a). Coulter counts give a measure of the total cell density of a culture, whereas viable counts estimate how many of these cells are actively growing. There was approximately a factor of 10 difference between the two measurements, which suggests that a significant proportion of the algal cells were not viable and therefore not active in the culture. This goes some way to explaining the observation that the SIMS results for a few cells at all time-points were close to natural abundance, these are highlighted in red in figure 2.17. The presence of cells close to natural abundance throughout the 48 h culture imply that some cells are not accumulating DIC at any point in the culture and are therefore either dead or continuously dormant. This sub-population of algal cells could be interesting to explore further, but here, in order to obtain an estimate of the mean atomic fraction of ^{13}C for the algal cells that are active in the carbon dynamics of the culture, the cells with atomic fractions close to natural abundance were not included in the analysis. The fraction of cells close to natural abundance relative to the total number of algal cells analysed ranged between 20-40 %, which is less than what would be expected from the factor of 10 difference between the viable and Coulter count results for the cell density. This could be because not enough cells were analysed in the SIMS experiment to be able to obtain a representative sample. Alternatively, the viable count measurements underestimated the number of active cells because it only measured viability in relation to growth on TY agar plates, and therefore the number of cells that were actively growing in the liquid cultures may be different. If this is the case, it is likely to be a systematic error, so although the viable counts might not give quantitative measurements of the cell density for growing cells, it can be used for measuring population growth between different time-points.

The results from the SIMS analysis of algal cells in the pre-labelling culture were corrected for the dilution effect using $D_a = 0.04$ (section 2.3.3). The results are shown in table 2.4 and figure 2.16b-c. Throughout the culture the mean atomic fraction of ^{13}C in algae increases, indicating that as the algae grow and photosynthesise they are utilising the ^{13}C-enriched DIC. After 48 h the algal cells have become approximately 60 % enriched with ^{13}C.

The rate of ^{13}C enrichment of algae was observed to be faster during the light period, i.e. the gradients ($\Delta f/\Delta t$) calculated by interpolation between 0-6 h and 24-30 h time-points are greater than for 6-24 h and 30-48 h (figure 2.16b and table 2.5). This is likely to be because it is only during the light period that the algae are able to photosynthesise and therefore it could be concluded that most of the DIC assimilation occurs during the light period. However, further experiments and more time-points would be required to test this observation fully.

The SIMS results also suggest that the rate of ^{13}C-enrichment of algae decreases and f begins to plateau as the culture progresses (figure 2.16b and table 2.5). As the atomic fraction of ^{13}C in algae approaches that of DIC, the labelling rate would be expected to slow down, since the atomic fraction of ^{13}C would be reaching an equilibrium. If this were the main contribution to the observed decrease in labelling rate, then this would imply that the atomic fraction of ^{13}C in DIC is about 0.6-0.7, which could be due to the equilibrium between the different forms of inorganic carbon, as described in section 2.3.3. Another factor that could contribute to this observation is that carbon storage within algae might cause it to take longer for the cells to become enriched with ^{13}C, which is explored in chapter 4. Additionally, isotopic fractionation associated with carbon assimilation by algae, due to different rates of carbon transport and carbon fixation for the two isotopes (^{13}C and ^{12}C) because of their different masses, should be considered. The isotopic fractionation factor is defined as

$$\alpha_{a/\mathrm{CO_2}} = \frac{R_a}{R_{\mathrm{CO_2}}}, \tag{2.11}$$

with R_a and $R_{\mathrm{CO_2}}$ the isotope ratios for algae and carbon dioxide respectively. For *C. reinhardtii*, isotopic fractionation decreases as growth rate increases, with $\alpha_{a/\mathrm{CO_2}}$ between 0.992 and 0.976 for growth rates between 0.6 and 0.1 day^{-1} (Ohkouchi *et al.*, 2015; Takahashi *et al.*, 1991). This is a relatively small effect, i.e. if carbon dioxide has an isotope ratio of 0.9, the equilibrium isotope ratio for algae would be expected to be between 0.893 and 0.878, therefore isotopic fractionation is unlikely to be the cause for the observed decrease in the rate of ^{13}C-enrichment for axenic algae.

Table 2.4 **SIMS results for the axenic culture of *C. reinhardtii metE7***. This table lists the number of algal cells included in the analysis and the mean, standard deviation and standard error in the mean for the dilution corrected ($D_a = 0.04$, section 2.3.3), single cell measurements of the atomic fraction of ^{13}C $\left(f = {}^{13}C / \left({}^{13}C + {}^{12}C\right)\right)$ for algae in the axenic culture grown with 5 mM $NaH^{13}CO_3$.

Culture	Time (h)	No. of cells	Mean f	Standard deviation	Standard error
Algal pre-culture	0	12	0.0111	0.00005	0.00002
Axenic culture (pre-labelling)	6	5	0.242	0.035	0.016
	24	11	0.438	0.036	0.011
	30	7	0.569	0.050	0.019
	48	19	0.624	0.037	0.008

Table 2.5 **The rate of ^{13}C-enrichment calculated for different time-periods of the axenic culture of *C. reinhardtii metE7***. This table lists the results for the rate of ^{13}C-enrichment ($\Delta f / \Delta t$) calculated by taking a linear interpolation between the dilution corrected ($D_a = 0.04$, section 2.3.3) results for the atomic fraction of ^{13}C at different time-points. The quoted errors are estimated from error propagation calculations taken from the standard errors in the mean for the atomic fractions of ^{13}C.

Time period	0 h to 6 h	6 h to 24 h	24 h to 30 h	30 h to 48 h
Light/dark period	6 h light	6 h light, 12 h dark	6 h light	6 h light, 12 h dark
Δt (h)	6	18	6	18
Δf	0.23 ± 0.02	0.20 ± 0.02	0.13 ± 0.02	0.05 ± 0.02
$\frac{\Delta f}{\Delta t}$ (h^{-1})	0.038 ± 0.003	0.011 ± 0.001	0.022 ± 0.004	0.003 ± 0.001

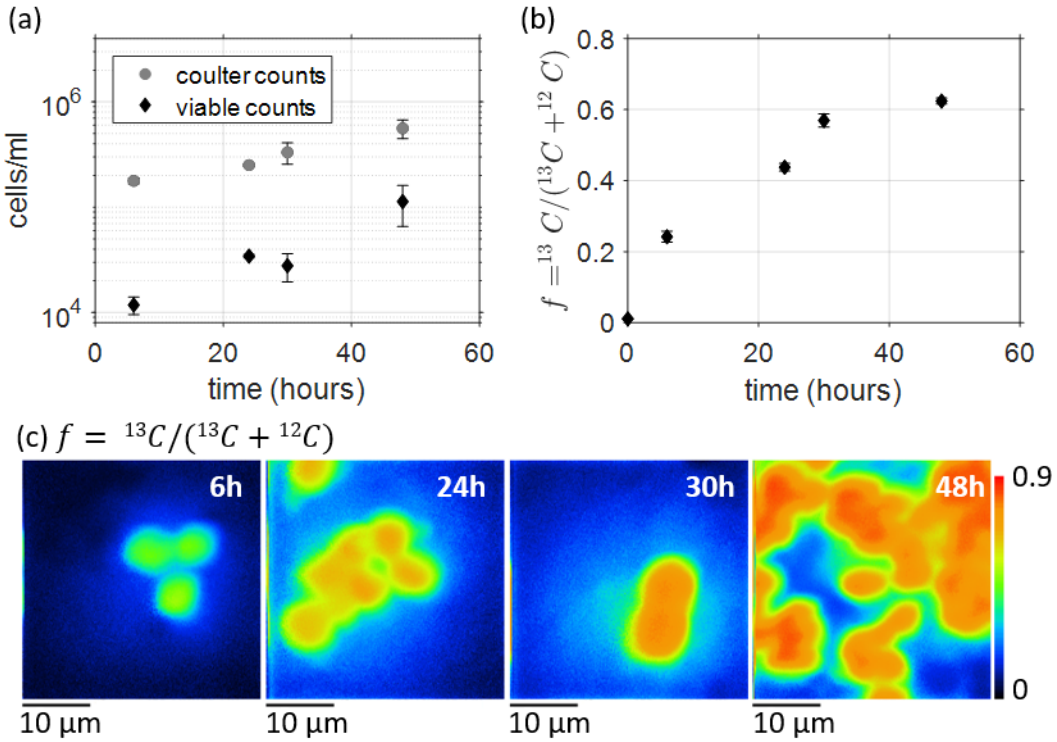

Figure 2.16 **Growth and SIMS results for the axenic culture of *C. reinhardtii metE7***. (a) Algal growth measured using Coulter counts (cells mL^{-1}) and viable counts (cfu mL^{-1}). Mean and standard error for three Coulter counter measurements and two viable count measurements. (b) The mean atomic fraction of ^{13}C for the dilution corrected ($D_a = 0.04$, section 2.3.3) SIMS measurements. Error bars show the standard error, which are hardly visible because the standard errors are small compared to the size of the plotted points. (c) Example images of the atomic fraction of ^{13}C in algal cells obtained by SIMS analysis of algae sampled at different time-points of the axenic, pre-labelling culture. The colour map shows the scale for the atomic fraction of ^{13}C, i.e. $f = {}^{13}C/\left({}^{13}C + {}^{12}C\right)$ between 0 and 0.9.

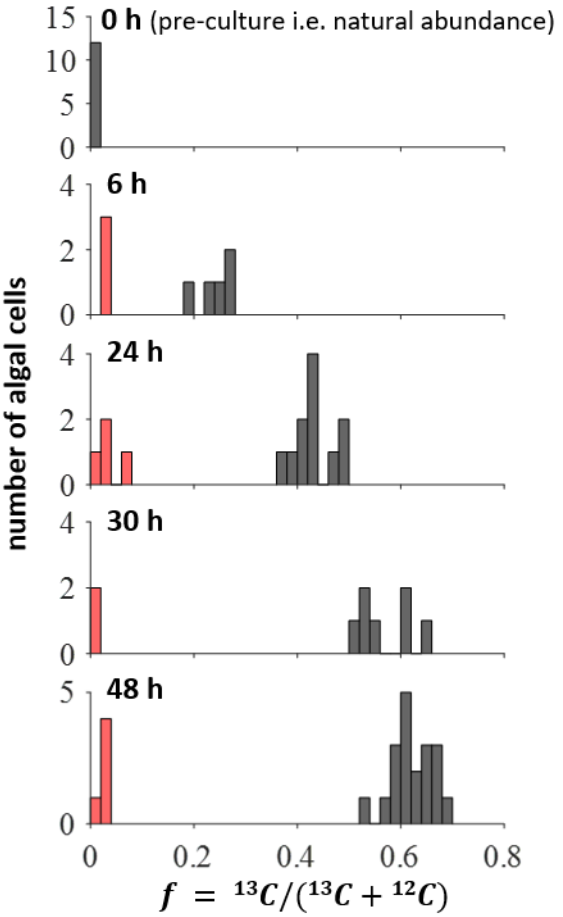

Figure 2.17 **Distributions of the atomic fraction of ^{13}C in *C. reinhardtii metE7* cells in an axenic culture**. Histogram plots showing the dilution corrected ($D_a = 0.04$, section 2.3.3) SIMS results for single cell measurements of the atomic fraction of ^{13}C in algal cells taken from the axenic (pre-labelling) culture grown with 5 mM $NaH^{13}CO_3$. The red bars indicate the algal cells that were not included in the calculation of the mean because they were close to natural abundance and therefore considered inactive.

2.3.6 Exchange of carbon in an algal-bacterial co-culture

A co-culture was inoculated with *M. loti* and *C. reinhardtii metE7* and grown with 5 mM $NaH^{13}CO_3$. The algae came from a pre-labelled culture (i.e. the axenic culture described in section 2.3.5) and were not washed, meaning that the dissolved organic carbon (DOC) exuded by algae during the pre-labelling culture was carried forward into the co-culture. This allowed for the best chance of observing the uptake of algal derived carbon by bacteria in the co-culture since the time-scale for the DOC to become available to the bacteria was unknown.

Population growth is observed for both the algal and bacterial populations in the co-culture (figure 2.18a-b). This implies that the algae were able to grow using B_{12} produced by bacteria and bacteria were growing on organic carbon produced by algae. However, the bacterial growth for the co-culture is comparable with the axenic culture of bacteria grown without glycerol (figure 2.18b), so the growth results for the 72 h time-period of the co-culture are not enough to show that bacteria are using algal derived DOC.

The atomic fraction of ^{13}C in algae sampled after 48 h of the axenic, pre-labelling culture was measured to be 0.624 ± 0.008 (table 2.4). It was this algal population that was used to inoculate the co-culture. The dilution corrected ($D_a = 0.04$ and $D_b = 1.29$ for algae and bacteria respectively, section 2.3.3) results from the SIMS analysis of the co-culture are given in figure 2.18c-d and table 2.6. Although the algal population increases, the atomic fraction of ^{13}C in algae remains between about 0.6-0.7 throughout the co-culture. This could be because the atomic fraction of ^{13}C for algae has reached an equilibrium with the atomic fraction of ^{13}C for DIC, which would suggest that the atomic fraction of ^{13}C in DIC is between about 0.6-0.7. Isotopic fractionation associated with biochemical processes within the co-culture could be another contributing factor, however this is likely to have only a small effect (Farquar *et al.*, 1989; Ohkouchi *et al.*, 2015; Takahashi *et al.*, 1991). Additionally, bacterial respiration produces carbon dioxide that starts to dilute the atomic fraction of ^{13}C in DIC, which could be contributing to the observation that during the light period, i.e. as algae photosynthesise, the atomic fraction of ^{13}C in algae decreases (i.e. between 0-6 h, 24-30 h and 48-52 h in figure 2.18c and table 2.6). Further experiments with more time-points and with measurements of the carbon isotope content of the DOC and DIC would be needed to test this hypothesis.

Figure 2.18d compares the carbon isotope dynamics for co-cultured bacteria with the results for axenic bacteria grown without glycerol. Although the two cultures exhibit comparable growth, the bacterial metabolism and labelling dynamics are different. In the axenic culture without glycerol, there is no organic carbon source in the media, so presumably the bacteria are growing on their internal stores and the atomic fraction of ^{13}C in bacteria

increases slightly as they assimilate ^{13}C-enriched DIC. For all axenic cultures of bacteria grown with different concentrations of glycerol (section 2.3.4), the mean f for bacterial cells either plateaued or peaked (figure 2.14). This is in contrast to the steady increase in the mean f for bacteria grown in co-culture with pre-labelled algae (figure 2.18d), which implies that they are able to metabolise ^{13}C-enriched DOC produced by algae as well as potentially assimilating a small amount of ^{13}C-enriched DIC. Overall, the SIMS results given in figure 2.18c-f and table 2.6 demonstrate that *M. loti* takes up carbon molecules produced by *C. reinhardtii metE7*.

The red bars in the histogram plots of the SIMS results for individual algal cells (figure 2.19) indicate the cells that have atomic fraction values close to natural abundance and were therefore not included in the calculation of the mean because they were considered to be inactive (either dead or dormant), meaning they were not contributing to the carbon dynamics of the co-culture. For bacteria, as in the axenic cultures, points were considered outliers and not included in the calculation of the mean if they had a value greater than $f_{max} = p_2 + 4 \cdot (p_2 - p_1)$, where p_1 and p_2 are the 25th and 75th percentile respectively. These outliers (marked with red stars in figure 2.19) with high values for the atomic fraction of ^{13}C could be a result of algal cell debris being mistaken for a bacterial cell, cross-contamination between different samples or it could be bacterial cells that had a particularly high ^{13}C-uptake rate, for example because they became attached to an algal cell at some point during the co-culture. Not enough data was obtained in this work to determine the origins of these outliers.

The single cell distribution for the atomic fraction of ^{13}C in bacterial cells within the co-culture population broadens over time (figure 2.19 and table 2.6). The bacteria start as a narrow distribution at natural abundance and the distribution broadening could be a result of a heterogeneity of growth, carbon uptake and/or respiration rates within the bacterial population that would result in a range of ^{13}C-enrichment rates. In chapter 4 a theoretical description of the co-culture carbon dynamics is used to examine the potential origins of the observed heterogeneity in the single-cell values of f for bacteria.

Table 2.6 **SIMS results for carbon isotope dynamics in the algal-bacterial co-culture**. The table lists the number of cells included in the analysis and the mean, standard deviation and standard error in the mean for the dilution corrected ($D_a = 0.04$ and $D_b = 1.29$ for algae and bacteria respectively, section 2.3.3), single cell measurements of the atomic fraction of ^{13}C $\left(f = {}^{13}C/\left({}^{13}C + {}^{12}C\right)\right)$ for algae and bacteria in the co-culture. The results for the bacterial pre-culture and pre-labelled algae are also included for completeness.

	Time (h)	No. of cells	Mean f	Standard deviation	Standard error
Pre-labelled algae	0	19	0.624	0.037	0.008
Algae in Co-culture	6	7	0.547	0.122	0.046
	24	28	0.689	0.069	0.013
	30	11	0.616	0.044	0.013
	48	19	0.674	0.061	0.014
	52	12	0.651	0.023	0.007
	72	29	0.652	0.046	0.009
Bacterial pre-culture	0	86	0.0108	0.0005	0.00006
Bacteria in co-culture	6	169	0.0157	0.0015	0.00011
	24	192	0.0202	0.0031	0.00022
	30	125	0.0243	0.0036	0.00032
	48	167	0.0324	0.0086	0.00066
	52	143	0.0334	0.0073	0.00061
	72	108	0.0492	0.0121	0.00116

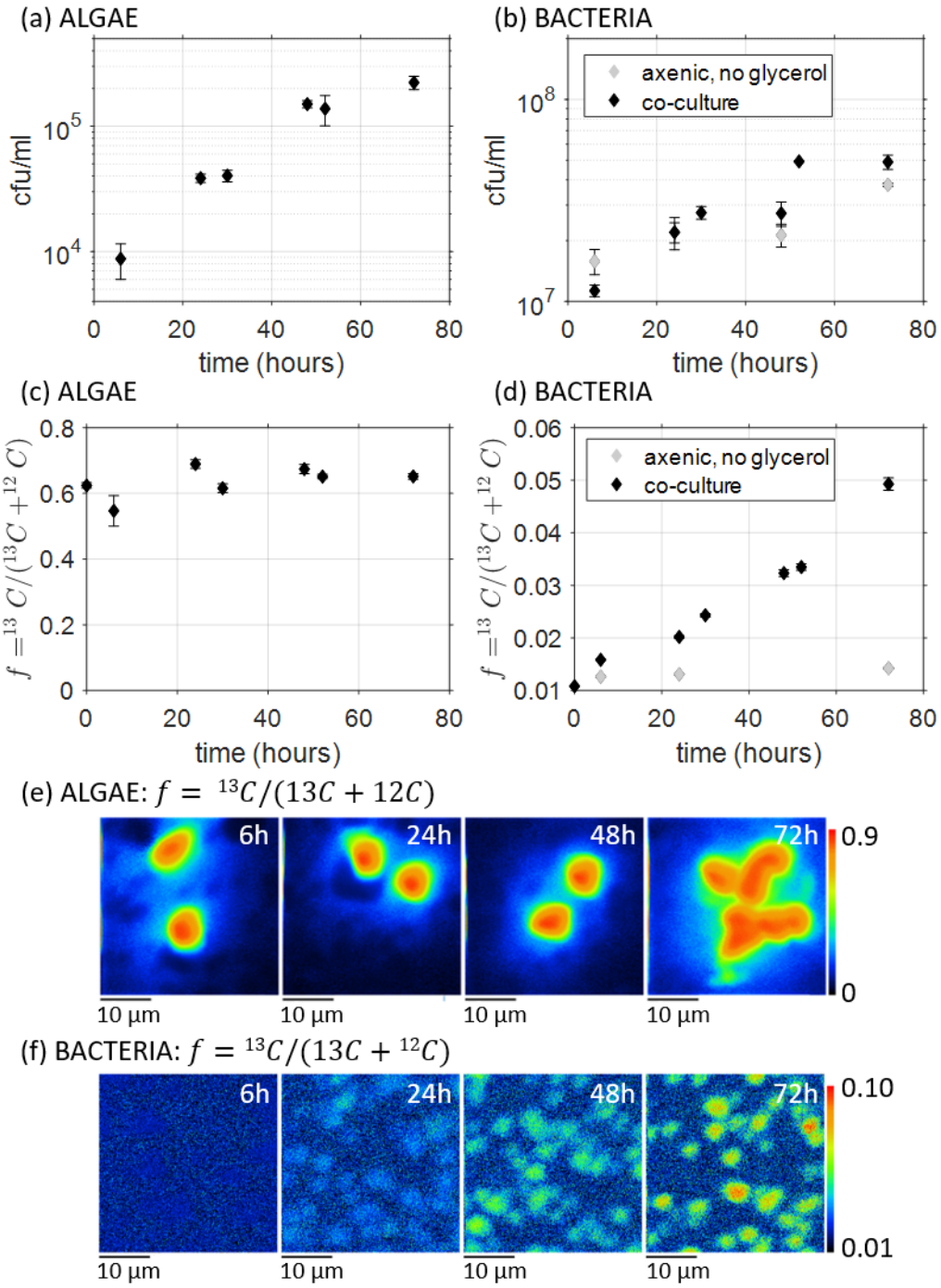

Figure 2.18 **Growth and SIMS results for the algal-bacterial co-culture**. (a) Algal and (b) bacterial growth plotted as the mean and standard error of two viable count measurements. (c) Algal and (d) bacterial ^{13}C enrichment results, i.e. the dilution corrected ($D_a = 0.04$ and $D_b = 1.29$ for algae and bacteria respectively, section 2.3.3) SIMS measurements of the atomic fraction of ^{13}C plotted as the mean and standard error for at least 7 algal cells and 100 bacterial cells per time-point. Error bars corresponding to the standard error in the mean are small compared to the plotted points. Example images for the atomic fraction of ^{13}C in (e) algal and (f) bacterial cells obtained using SIMS analysis, for which the colour maps show the scale.

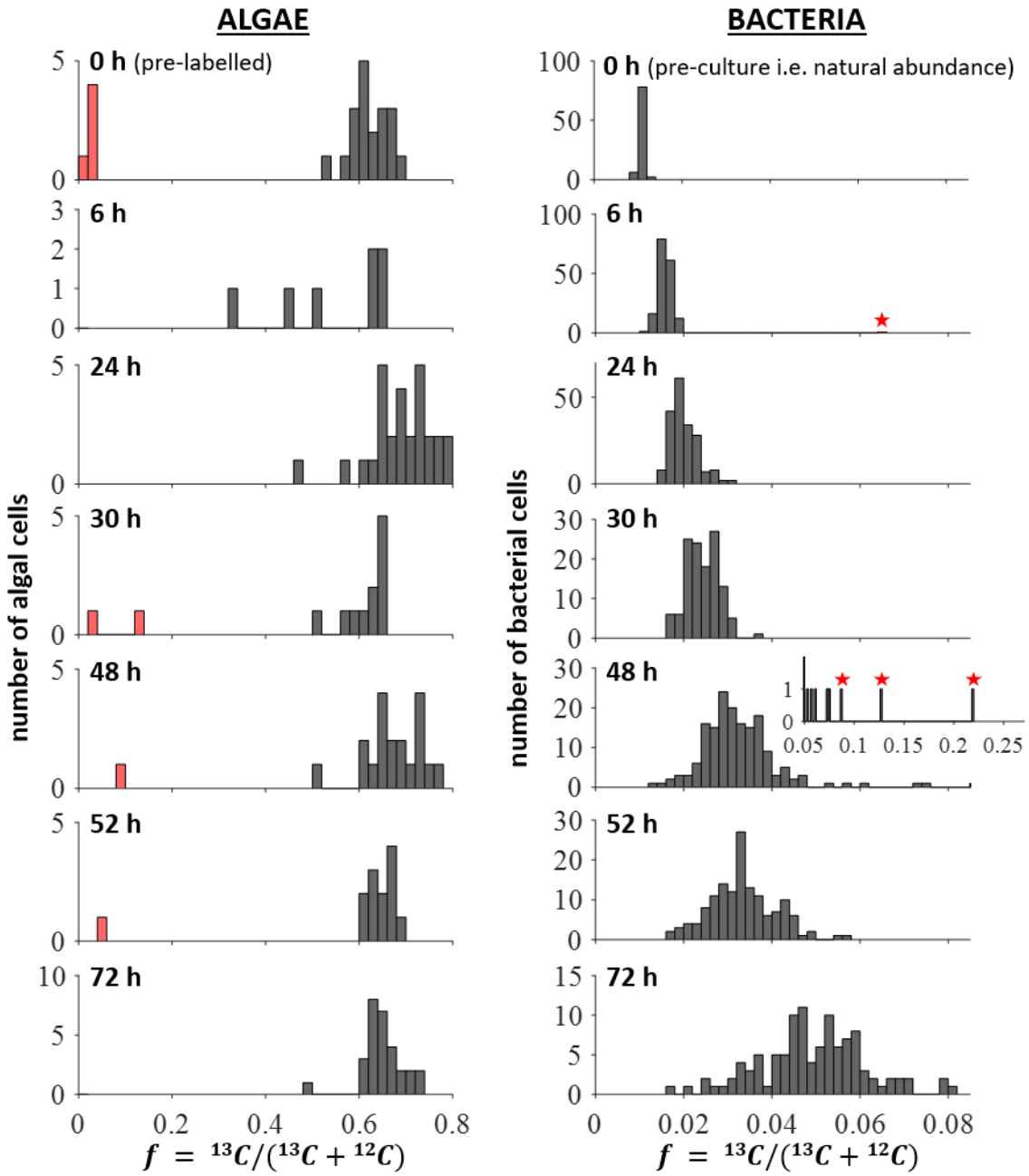

Figure 2.19 **Distributions for the atomic fraction of ^{13}C in algal and bacterial cells in the co-culture**. Histogram plots showing the dilution corrected ($D_a = 0.04$ and $D_b = 1.29$ for algae and bacteria respectively, section 2.3.3) SIMS results for single-cell measurements of the atomic fraction of ^{13}C, i.e. f, for algal (left) and bacterial (right) cells at different time-points of the co-culture. The red bars indicate the algal cells that were not included in the calculation of the mean because they are close to natural abundance and therefore considered inactive. The red stars indicate the bacterial cells that were considered outliers from the distribution and therefore excluded from the calculation of the mean (i.e. 1 point for the 6 h time-point and 3 points for the 48 h time-point).

Carbon assimilation rates for bacteria in the co-culture

A net carbon assimilation rate was calculated for the co-cultured bacteria using the definition of net carbon assimilation as the fraction of carbon in the sampled organism from the ^{13}C enriched source relative to the fraction of carbon in the sampled organism remaining from the initial carbon content (Fx_{net} in equation (1.13)) (Popa *et al.*, 2007). In section 1.4.2 an expression for Fx_{net} is derived and the result gives

$$Fx_{net} = \frac{f(t) - f_0}{f_s - f(t)}, \tag{2.12}$$

with f_0 and $f(t)$ the atomic fraction of ^{13}C in the organism at time zero and at time t respectively, and f_s the atomic fraction of ^{13}C in the ^{13}C enriched source.

The experiments described in this chapter used TRIS buffer in the growth media, which is an organic buffer and created a high background of carbon in the media. Therefore it was not possible to obtain reliable results for the DOC concentrations and isotope measurements for the organic carbon produced by algae. When calculating the net carbon assimilation for co-cultured bacteria $f_s = 0.6$ was used because the pre-labelled algae have an f value of approximately 0.6 (table 2.6). This estimate for f_s means that the results for the net carbon assimilation are unlikely to be quantitatively accurate, but qualitative trends can still be observed.

The results for the net carbon assimilation rate (Fx_{net}/t, in units h^{-1}) for bacteria at different time-points of the co-culture are given in table 2.7 and figure 2.20. These results suggest that in the first 6 h of the co-culture, the bacteria have a relatively fast carbon assimilation rate with a relatively wide single cell distribution. After this relatively quick initial carbon assimilation rate, Fx_{net}/t decreases and between 24 h-72 h the results suggest a small increase in the carbon assimilation rate over time. The co-culture was inoculated with unwashed, pre-labelled algae, meaning that there was an initial, non-zero concentration of ^{13}C enriched DOC. The results for the net carbon assimilation rates in table 2.7 and figure 2.20 could be explained by the bacteria quickly depleting the initial concentration of DOC, after which the bacteria assimilate carbon more slowly because they are relying on new DOC being produced by the co-cultured algae. Over time, as the algal population size increases, it would be expected that the DOC production rate also increases, which could account for the small increase in Fx_{net}/t between 24 h-72 h.

Population growth for bacteria can be described using the exponential growth equation

$$b = b(0)\ e^{\mu_B t}, \tag{2.13}$$

Table 2.7 **Net carbon assimilation rate for bacteria in co-culture with pre-labelled algae**. The net carbon assimilation rate is defined here as Fx_{net}/t (section 1.4.2). This was calculated for each bacterial cell using the dilution corrected ($D_b = 1.29$, section 2.3.3) SIMS results. The table lists the mean and standard deviation for single cell values of Fx_{net}/t, as well as the number of cells included in the analysis (excluding the outliers for the 6 h and 48 h time-points).

Time (h)	No. of cells	Mean Fx_{net}/t (h^{-1})	Standard deviation
6	169	1.4×10^{-3}	4.2×10^{-4}
24	192	6.7×10^{-4}	2.3×10^{-4}
30	125	7.8×10^{-4}	2.1×10^{-4}
48	167	8.0×10^{-4}	3.4×10^{-4}
52	143	7.7×10^{-4}	2.6×10^{-4}
72	108	9.7×10^{-4}	3.3×10^{-4}

where b and $b(0)$ are the bacterial population size at time t and at time zero respectively, and μ_B is the exponential growth rate. Using the LINEST function in Microsoft Excel, the exponential growth rate fit was performed as a linear regression analysis of $\ln(b)$ against t with the gradient equal to μ_B and the intercept equal to $\ln(b(0))$. For the co-culture, the fit result gave estimates $b(0) = 1.2 \times 10^7 \pm 1.5 \times 10^5$ cfu mL^{-1} and $\mu_B = 0.022 \pm 0.005$ h^{-1}. For the axenic culture grown without glycerol, the fit result gave estimates $b(0) = 1.5 \times 10^7 \pm 1.4 \times 10^5$ cfu mL^{-1} and $\mu_B = 0.012 \pm 0.004$ h^{-1}. These results are plotted in figure 2.21.

Assuming exponential growth, a linear relationship between bacterial carbon biomass and population size, a relatively slow rate of carbon loss compared with the rate of carbon uptake for bacteria and short time periods (i.e. $t \ll 1/\mu_B$), it can be shown that Fx_{net}/t gives a reasonable approximation for the growth rate μ_B (see appendix D for details). Comparing the exponential growth rate for bacteria in the co-culture (figure 2.21) with the mean net carbon assimilation rate for the 6 h time-point, i.e. $Fx_{net}/t = 0.0014$ (table 2.7), implies that carbon assimilation of algal photosynthate accounts for approximately 6% of bacterial population growth in the co-culture. The growth rate of axenic bacteria grown without an organic carbon source as a percentage of the growth rate of bacteria in the co-culture is estimated to be 55%. These comparisons between growth and carbon assimilation rates suggest that the uptake of organic carbon produced by algae is responsible for only some of the observed bacterial growth in the co-culture, with the majority of bacterial growth due to internal carbon storage carried forward from the pre-cultured bacteria.

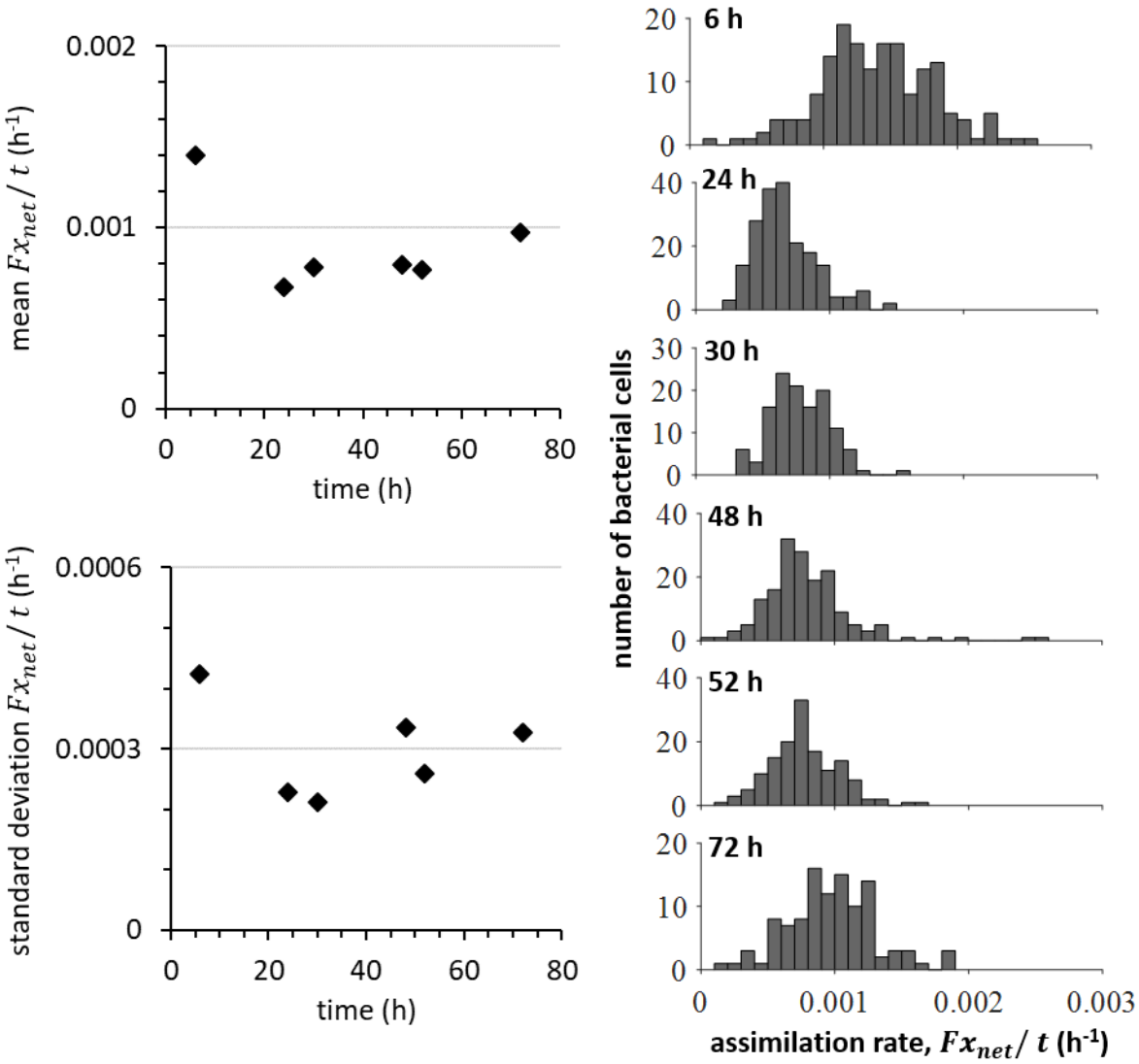

Figure 2.20 **Net carbon assimilation rate for bacteria in co-culture with pre-labelled algae**. The histograms show the results for calculating the net carbon assimilation rate (Fx_{net}/t defined in detail in section 1.4.2) for each individual bacterial cell, using the dilution corrected ($D_b = 1.29$) SIMS results. The mean and standard deviation for the single cell values of Fx_{net}/t were calculated and are plotted against time. The error bars in the Fx_{net}/t plot are the standard errors, which are small compared to the size of the plotted points.

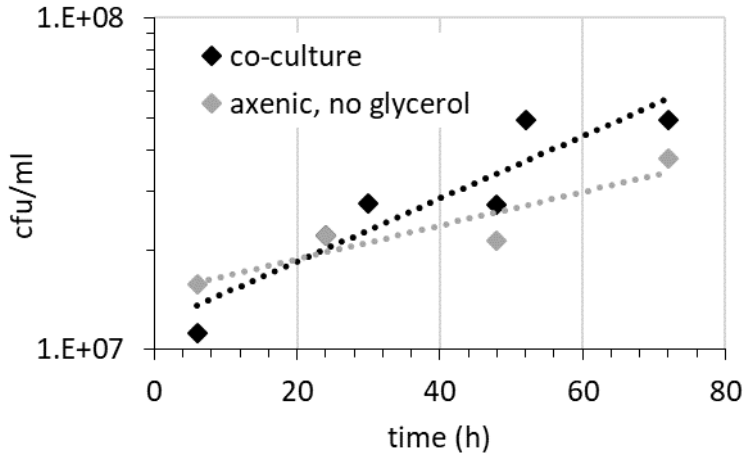

Figure 2.21 **Fit for the exponential growth rate of bacteria**. Plotted points show the viable count results for the growth of *M. loti* in the co-culture (black) and in the axenic culture grown without glycerol (grey). The dotted lines indicate the results obtained from a linear regression analysis of $\ln(b)$ against t using the LINEST function in Microsoft Excel. The fit results give an initial bacterial abundance $b(0) = 1.19 \pm 0.01 \times 10^7$ cfu mL^{-1} and an exponential growth rate $\mu_B = 0.022 \pm 0.005$ h^{-1} for the co-culture and $b(0) = 1.48 \pm 0.01 \times 10^7$ cfu mL^{-1} and $\mu_B = 0.012 \pm 0.004$ h^{-1} for the axenic culture.

2.4 Conclusion and outlook

This chapter set out to study the carbon metabolic activity of both *M. loti* and *C. reinhardtii metE7* in axenic cultures and in co-culture, in order to gain insight into the nature and time-scale of their carbon dynamics. Secondary Ion Mass Spectrometry (SIMS) is a powerful technique for analysing the elemental composition of single cells and therefore, when combined with stable isotope labelling, can be used to measure the metabolic activity at the single cell level. In order to achieve successful and reliable results from SIMS experiments, several technical considerations must be taken into account. In particular, the isotope content may be heterogeneously distributed within the cell and therefore depth analysis should be completed to ensure that a representative amount of biomass is sampled for SIMS analysis. Additionally, SIMS is not a 'clean' technique, which means that not all the material that is sputtered from the sample is captured as secondary ions. Some might be deposited around the cell and therefore a highly labelled cell can contaminate its surrounding area. Therefore, in order to avoid unreliable measurements, it is important to ensure that for samples from a co-culture between a low and a high labelled population of cells, the cells with a low ^{13}C content are only included in the analysis when the scan area does not contain a highly labelled

cell. Lastly, samples for SIMS analysis were chemically fixed and stained with a nucleic acid stain. These processes introduce chemicals into the cells that are unlabelled (i.e. have natural abundance), resulting in a dilution of the atomic fraction of ^{13}C in the cells. Therefore, this dilution effect must be considered if quantitative estimates of the true, undiluted isotope content of the cells are to be determined. The carbon isotope dilution effect was observed to be more significant for bacterial cells than for algal cells, possibly because bacterial cells have a larger surface to volume ratio due to their smaller size, meaning they are likely to have a relatively higher influx of chemicals.

SIMS results for bacterial cells grown axenically with $NaH^{13}CO_3$ and different concentrations of unlabelled glycerol showed that in the exponential phase, a higher concentration of glycerol resulted in a faster growth rate and a higher ^{13}C-enrichment. This suggests that when there is more organic carbon available to bacteria, the population grows faster and also assimilates a relatively greater fraction of inorganic carbon, meaning that the inorganic carbon assimilation depends on growth conditions. Similar observations were also made by Hesselsoe *et al.* (2005) and Roslev *et al.* (2004), whose work showed that the amount of inorganic carbon assimilation by heterotrophic bacteria depends on the type of organic carbon substrate added to the growth media. For high concentrations of glycerol (0.1 % and 0.01 %), the cultures entered the stationary phase of growth within the 72 h time-frame of the experiment. In the stationary growth phase the SIMS results showed a decrease in ^{13}C-enrichment, which is evidence that although the population size reached an equilibrium, the cells were still metabolically active and the carbon dynamics continued.

The results for algae grown axenically with $NaH^{13}CO_3$ showed an increase in the atomic fraction of ^{13}C throughout the 48 h culture. The results also suggested that the carbon fixation rate was faster during the light period, which is as expected because algae photosynthesise in the light and therefore the majority of inorganic carbon assimilation is also expected to occur during the light period. Additionally, it was observed that the apparent ^{13}C-enrichment rate became slower as the culture progressed, which could be due to the inorganic carbon chemistry, i.e. a dilution of the atomic fraction of ^{13}C in dissolved inorganic carbon due to the exchange with unlabelled atmospheric carbon dioxide. The effect of isotopic fractionation associated with algal photosynthesis was estimated and considered to be relatively small. Further experiments, in particular with more time-points and including measurements of the atomic fraction of ^{13}C in dissolved inorganic carbon, would be needed to test these observations.

Unlabelled bacteria were grown in a co-culture with pre-labelled algae. SIMS analysis of samples taken at different time-points of the 72 h co-culture showed that bacteria were taking up algal derived carbon already within the first 6 hours. The ^{13}C-enrichment of bacteria

continued to increase throughout the co-culture. These results are the first direct observations of the carbon exchange from *C. reinhardtii metE7* to *M. loti*. The distribution of single cell values for the atomic fraction of ^{13}C in bacteria in the co-culture broadened overtime, which could be a result of single-cell heterogeneity in growth, carbon uptake and/or respiration rates. These dynamics and their effect on single cell distributions are considered in more detail in chapter 4. The carbon assimilation rates estimated for the co-cultured bacteria suggest that they quickly depleted the DOC carried over from the algal pre-labelling culture and after 6 hours the carbon assimilation rate became slower, which is likely to be because after depleting the initial DOC the bacteria were dependent on the algae as a continuous source of organic carbon. The results for the net carbon assimilation rate and exponential growth rate suggest that carbon assimilation of algal photosynthate accounts for approximately 6% of bacterial population growth in the co-culture and the majority of bacterial growth is likely to be due to internal carbon storage since the pre-cultured bacteria were not completely carbon starved. Unlabelled organic carbon originating from dead algal cells could also account for the discrepancy between growth rate and carbon assimilation rate calculated for the co-cultured bacteria.

There are several metabolic processes that contribute to the carbon cycling in an algal-bacterial mutualism including photosynthesis, respiration and bacterial inorganic carbon uptake. Carbon isotope labelling experiments can give an indication of the metabolic activity of the microorganisms, however a mathematical model is required to link isotope labelling to carbon metabolic dynamics. Chapter 3 describes a mathematical model that has been developed to explicitly model the nutrient dynamics of the algal-bacterial co-culture taking into account the carbon and vitamin B_{12} exchanged between the two species. From this dynamic model, equations for the expected carbon isotope dynamics are derived. Chapter 4 goes on to test this model by carrying out a set of parameter optimisations using the data obtained from the SIMS experiments described in this chapter and then uses the fully parametrised model to explore its predictive power. By bringing together experiments and theory, our understanding of the nutrient dynamics within this two species system can be thoroughly tested.

Chapter 3

Modelling nutrient dynamics in an algal-bacterial co-culture

3.1 Introduction

In order to understand and predict the collective activity of a microbial community it is important to choose an appropriate model to describe the interactions between different species (Momeni *et al.*, 2017; Widder *et al.*, 2016). Ideally, a mathematical model will include the minimum level of detail required to capture the properties of interest, however it can be challenging to know what level of abstraction is appropriate. The simplest approach to modelling ecological interactions is to neglect the interaction mediators and to focus on the population growth dynamics. Lotka-Volterra type models describe the population growth as the sum of a basal growth rate (i.e. growth rate for the species in a monoculture) and pairwise interaction terms, which define the fitness effect resulting from the presence of each of the other species in the community (Murray, 2002). This can be described as the *additivity assumption*, meaning that any indirect effects that arise when a species engages in several interactions are neglected (Momeni *et al.*, 2017). Additionally, Lotka-Volterra type models make a *universality assumption*, meaning that all interactions are described using one type of equation with only the sign and magnitude of the interaction coefficients defining the fitness effect of each species interaction (Momeni *et al.*, 2017). For mutualistic interactions, Lotka-Volterra models use positive interaction coefficients and must include carrying capacities in order to limit the population size to a maximum value (Murray, 2002). For example, an algal-bacterial pairwise mutualism could be described by the following set

of coupled Lotka-Volterra type equations

$$\frac{da}{dt} = r_a\, a \left(1 - \frac{a}{K_a} + k_{ab}\, b\right) \tag{3.1a}$$

$$\frac{db}{dt} = r_b\, b \left(1 - \frac{b}{K_b} + k_{ba}\, a\right) \tag{3.1b}$$

with a and b the algal and bacterial population sizes respectively, r_a and r_b the intrinsic growth rates, K_a and K_b the intrinsic carrying capacities, and k_{ab} and k_{ba} the positive interaction coefficients.

An alternative to Lotka-Volterra population models is a pairwise modelling approach for which the carrying capacity is a function of the interaction partner (Grant *et al.*, 2014; Yukalov *et al.*, 2012). For an algal-bacterial mutualism this gives

$$\frac{da}{dt} = r_a\, a \left(1 - \frac{a}{K_a(b)}\right) \tag{3.2a}$$

$$\frac{db}{dt} = r_b\, b \left(1 - \frac{b}{K_b(a)}\right) \tag{3.2b}$$

with $K_a(b)$ the algal carrying capacity as a function of the bacterial cell density and $K_b(a)$ the bacterial carrying capacity as a function of the algal cell density. Grant *et al.* (2014) used different functional forms for the carrying capacity to investigate different mechanisms of nutrient exchange in an algal-bacterial mutualism.

Pairwise interaction models have been used to construct ecological models for whole communities (Faust *et al.*, 2012), study community stability (Holling, 1973; May, 1973; Okuyama *et al.*, 2008) and predict transitions between different interaction outcomes as conditions change (Holland *et al.*, 2009, 2010). However, Momeni *et al.* (2017) recently demonstrated the limited scope of Lotka-Volterra type pairwise models to qualitatively capture the full diversity of microbial interactions. For example, when interactions are mediated by metabolites, only in some instances (like when a fast equilibrium is assumed) will a mechanistic model map onto a Lotka-Volterra type model (Momeni *et al.*, 2017). Moreover, even when pairwise models can successfully describe population growth dynamics, it is also important to understand how microbial interactions impact biogeochemical cycles. Therefore, developing nutrient explicit models is valuable for two reasons, firstly in order to more realistically capture the diversity of microbial interactions and secondly to assess our interpretation of the metabolic processes that underpin the microbial contribution to nutrient cycles.

This chapter outlines a nutrient explicit mathematical model that aims to capture a mutualistic relationship between algae and bacteria where each provides the other with an essential metabolite. The specific algal-bacterial co-culture that was taken as my focus was one in which algae provide organic carbon to bacteria, and bacteria provide B_{12} to algae. This was chosen because an established experimental system exists for this type of mutualism (see section 1.3.2) (Helliwell *et al.*, 2015; Kazamia *et al.*, 2012b). In chapter 2 experiments were discussed that measure the growth and carbon isotope labelling dynamics for *C. reinhardtii metE7* and *M. loti* both alone and in co-culture, these results are used to parametrise and test the model in chapter 4.

The nutrient explicit model developed in this chapter incorporates algal photosynthesis, algal organic carbon exudation, bacterial respiration and bacterial inorganic carbon assimilation. The model does not go into biochemical detail of the metabolic reactions and therefore may not provide quantitative comparisons with experiment, instead the model aims to capture the essence of the metabolic processes most central to the algal-bacterial co-culture. Bringing the focus of the model to the carbon dynamics meant that the carbon isotope labelling rates could be predicted, which allows the model to be testable in terms of nutrient dynamics as well as population growth. This model was designed to be compared with stable isotope labelling experiments in order to extend our understanding of the key carbon metabolic processes of an algal-bacterial mutualism. Further to this, the aim was to obtain a mathematically tractable model such that characteristic features can be established and the predictive power tested in order to reveal new insights into the relationship between microbial growth and nutrient cycling.

3.1.1 Nutrient explicit models of microbial mutualisms

Nutrient-explicit, or mechanistic, models of microbial interactions describe how species release and consume chemicals, and how these chemicals affect species growth. Models like these give a more realistic interpretation of the ecological interactions than pairwise models, however they are more challenging to construct because a nutrient explicit model involves more equations and parameters, as well as requiring knowledge of the chemical mediators (i.e. what they are and how they are produced and consumed). There are several examples of nutrient-explicit models used to study algal-bacterial interactions. Bai *et al.* (2015) used a kinetic model to study the effect of carbon re-mineralisation by bacteria on algal growth limited by the concentration of inorganic carbon. The model used Monod growth equations and was able to reproduce the experimental observation that the presence of bacteria enhances algal growth, illustrating the important contribution of bacterial respiration to carbon cycling. Van den Meersche *et al.* (2004) used mathematical modelling of growth, carbon and nitrogen

dynamics, together with a ^{13}C tracer experiment to investigate algal-bacterial interactions in an experimental algal bloom and were able to identify three distinct phases of the bloom, each defined by a characteristic flow of nutrients.

F. J. Peaudecerf *et al.* (2018) developed a co-culture model in order to investigate the effect of spatial separation on the interdependent growth of a B_{12} dependent alga and a B_{12} producing bacterium. The model considers an algal and bacterial population that are grown in separate culture vessels, but connected with a diffusive channel through which metabolites can be exchanged. The model describes the B_{12}-dependent growth of algae and DOC-dependent growth of bacteria using Monod growth equations and a carrying capacity term in order to cap the microbial growth in batch cultures to a maximum population size. The model also describes the exchange of B_{12} and DOC through a diffusive channel along with the nutrient production and uptake kinetics for the two microbial populations. The bacterial production of B_{12} and algal production of DOC are modelled to be linearly dependent on the cell density, and constant values for the carbon per bacterial cell and B_{12} per algal cell are assumed to define the rates of nutrient consumption. In this chapter a more complete description of the carbon dynamics was developed by starting from the zero-distance limit of the algal-bacterial co-culture model by F. J. Peaudecerf *et al.* (2018) and then including algal photosynthesis, algal DOC exudation from excess photosynthesis, bacterial growth efficiency and bacterial inorganic carbon assimilation. The Peaudecerf model was extended to include these additional metabolic processes because without them the model is not complete in its description of the carbon dynamics of the co-culture. Most significantly the Peaudecerf model does not consider inorganic carbon, which was the ^{13}C-enriched carbon source used in the stable isotope labelling experiments in chapter 2 and so must be included in any model that aims to be comparable with these experiments.

3.2 The co-culture model

This section establishes a model for an algal-bacterial co-culture that combines nutrient exchange dynamics with algal and bacterial population growth. A particular focus was on obtaining a set of equations for the atomic fraction of ^{13}C in the different carbon pools within the co-culture (i.e. the algal and bacterial carbon biomass, DOC and DIC). Atomic fractions are experimentally accessible and so including them as variables in the model offers scope for being able to test how well the model agrees with experiments, at least in terms of qualitative trends. Inspiration for the model came from metabolic processes and an approach based on chemical reaction kinetics was used to describe the nutrient dynamics. However many simplifying assumptions were necessary since full details of some of the biological

processes underpinning the mutualism are currently unknown (for example the chemical identity of the DOC exchanged and the mechanisms for B_{12} uptake and export). Moreover, reducing mathematical complexity is desirable in order to obtain a tractable model with clear predictions.

3.2.1 The 'basic model': zero-distance limit of the Peaudecerf model

In an algal-bacterial co-culture, the microbial populations are considered to be well-mixed and so effectively zero-distance apart. Therefore, in this work the starting point for developing a carbon-explicit co-culture model was the zero-distance limit of the Peaudecerf model (F. J. Peaudecerf *et al.*, 2018), which is described in this section and called the 'basic model' throughout this thesis because it reduces the co-culture to its essential components - vitamin B_{12} is produced by bacteria and is the limiting factor for algal growth, DOC is produced by algae and is the limiting factor for bacterial growth (see figure 3.1 for an overview of these nutrient exchange dynamics). Carrying capacities are incorporated into the model in order to stop population growth at high cell densities.

The basic model describes algal growth by assuming a Monod dependence on the external vitamin B_{12} concentration v, such that

$$\frac{da}{dt} = \mu_a\, a \left(1 - \frac{a}{K_a}\right)\left(\frac{v}{K_v + v}\right) - \delta_a\, a, \tag{3.3}$$

with a the algal cell density, μ_a the maximum growth rate, K_a the carrying capacity, K_v the half-saturation concentration of B_{12} and δ_a the cell death rate. This description of algal growth does not explicitly consider the internal recycling dynamics of B_{12} and as a result the external concentrations and the half-saturation constant are considered 'pseudo-B_{12} concentrations', which means they cannot necessarily be taken as exact quantitative values when comparing with experiment.

Similarly, the basic model defines bacterial growth by assuming a Monod dependence on the external DOC concentration c_o, such that

$$\frac{db}{dt} = \mu_b\, b \left(1 - \frac{b}{K_b}\right)\left(\frac{c_o}{K_c + c_o}\right) - \delta_b\, b, \tag{3.4}$$

with b the bacterial cell density, μ_b the maximum growth rate, K_b the carrying capacity, K_c the half-saturation concentration of DOC and δ_b the cell death rate. Equation (3.4) assumes that the DOC can be modelled as an effective single carbon source.

The carbon yield for algal and bacterial cells is given by $Y_{a,c}$ and $Y_{b,c}$ respectively, in units of cells per mole of carbon. It is assumed that these are constant, such that the carbon

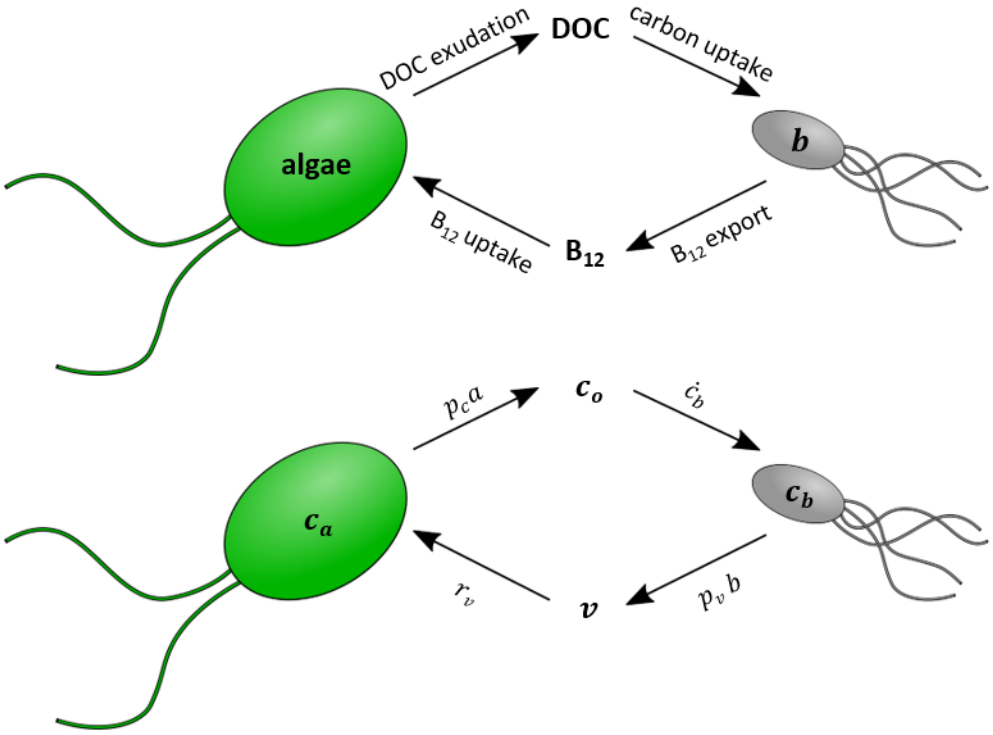

Figure 3.1 **The basic co-culture model**. An overview of the nutrient exchange considered in the basic model used as a starting point for the co-culture model developed in this chapter. Vitamin B_{12} is released by bacteria and required for algal growth, in exchange the bacteria are able to use some of the dissolved organic carbon (DOC) produced by algae.

biomass concentrations (c_a and c_b for algae and bacteria respectively) are

$$c_a = \frac{a}{Y_{a,c}}, \tag{3.5}$$

$$c_b = \frac{b}{Y_{b,c}}, \tag{3.6}$$

where a and b are the algal and bacterial cell densities respectively.

Dissolved organic carbon (DOC) is exuded into the media by algae. The rate of DOC production is assumed to be linearly proportional to the algal cell density with a constant cellular production rate of p_c in units of moles of carbon exuded per cell per unit time. From the Monod description of DOC-dependent bacterial growth in equation (3.4) and the carbon biomass relationship in equation (3.6), the rate of change of the bacterial carbon biomass

concentration, in moles per unit volume per unit time, is defined as

$$\dot{c}_b = \frac{\mu_b\, b}{Y_{b,c}} \left(\frac{c_o}{K_c + c_o} \right), \tag{3.7}$$

with c_o the DOC concentration. The absence of the carrying capacity term means that the bacteria continue to take up DOC when the population reaches carrying capacity. Therefore, in this basic model, the linear relationship between bacterial carbon biomass and cell density (equation (3.6)) only holds true when $b \ll K_b$, i.e. when bacteria are in the exponential growth phase. In section 3.2.3, bacterial respiration is introduced to the model in such a way that maintains a linear relationship between c_b and b even at carrying capacity.

Vitamin B_{12} is produced and released into the media by bacteria. The rate of B_{12} production is assumed to be linearly proportional to the bacterial cell density with a constant cellular production rate of p_v in units of moles of B_{12} released per cell per unit time. From the Monod description of B_{12}-dependent algal growth in equation (3.3), the total B_{12} uptake rate for the whole algal population, in moles per unit volume per unit time, is defined as

$$r_v = \frac{\mu_a\, a}{Y_{a,v}} \left(\frac{v}{K_v + v} \right), \tag{3.8}$$

with v the B_{12} concentration and $Y_{a,v}$ the algal B_{12} yield in units of cells per mole of B_{12} for algae in the exponential growth phase (i.e. when $a \ll K_a$), which is assumed to be a constant. The absence of the carrying capacity term in equation (3.8) means that the algae continue to take up B_{12} when the population reaches carrying capacity.

In this thesis the focus is on describing a co-culture with algal and bacterial population sizes that are small compared to carrying capacity. Although the assumptions of continued DOC and B_{12} uptake and production at carrying capacity may not be supported by experimental evidence, this behaviour of the model at carrying capacity was chosen for mathematical simplicity and continuity, as well as to ensure that the model has a positive fixed point for the DOC and B_{12} concentrations. The main effect of assuming this continued nutrient dynamics is that a population of algae at carrying capacity can still support a growing population of bacteria due to the continued DOC production, and vice versa, bacteria at carrying capacity can support a growing population of algae through continued B_{12} production. Additionally, it means that after the microbial populations reach carrying capacity the DOC and B_{12} concentrations still continue to change until the fixed point is reached, and thus all non-zero initial conditions will eventually reach the non-zero positive fixed point.

For the purposes of this thesis cell death is neglected, meaning that the death rate is assumed to be negligible compared to the growth rate for both the algal and bacterial

populations. This corresponds to the case where $\delta_a \ll \mu_a (1 - a/K_a) v/(K_v + v)$ for algae and similarly $\delta_b \ll \mu_b (1 - b/K_b) c_o/(K_c + c_o)$ for bacteria. Combining the population growth and nutrient dynamics as discussed above, a set of four ODEs are obtained for the algal-bacterial mutualism, which are

$$\frac{da}{dt} = \mu_a \, a \left(1 - \frac{a}{K_a}\right) \left(\frac{v}{K_v + v}\right), \tag{3.9a}$$

$$\frac{db}{dt} = \mu_b \, b \left(1 - \frac{b}{K_b}\right) \left(\frac{c_o}{K_c + c_o}\right), \tag{3.9b}$$

$$\frac{dc_o}{dt} = p_c \, a - \dot{c}_b, \tag{3.9c}$$

$$\frac{dv}{dt} = p_v \, b - r_v. \tag{3.9d}$$

These equations for the 'basic model' are equivalent to the zero-distance, mixed co-culture limit of the Peaudecerf model (F. J. Peaudecerf *et al.*, 2018), assuming negligible death rate.

3.2.2 Algal photosynthesis

In the model discussed so far there has been no explicit consideration of the algal carbon dynamics beyond the carbon biomass conversion relation in equation (3.5). In particular, the internal carbon dynamics and the role of dissolved inorganic carbon (DIC) as the carbon source for algal photosynthesis have been neglected. The aim for this section is not to describe algal carbon metabolism in detail, but to obtain a mathematical description that encapsulates the general and essential characteristics of algal carbon uptake and exudation.

In order to consider how carbon is taken up, used and released by algae, the basic model from section 3.2.1 is extended to include photosynthesis. The model considers photosynthetic carbon fixation as the transformation of DIC into algal biomass, which then has two possible fates, either it contributes to algal growth (i.e. the biosynthesis of new cellular components) and carbon storage, which means it enters the 'stored' component of algal carbon, or the fixed carbon is exuded by algae and enters the media as dissolved organic carbon (DOC). These algal carbon dynamics are summarised in figure 3.2.

The algal growth rate remains as it was defined in section 3.2.1, but now the algal carbon biomass concentration is split into two internal components

$$c_a = c_{a,s} + c_{a,p}, \tag{3.10}$$

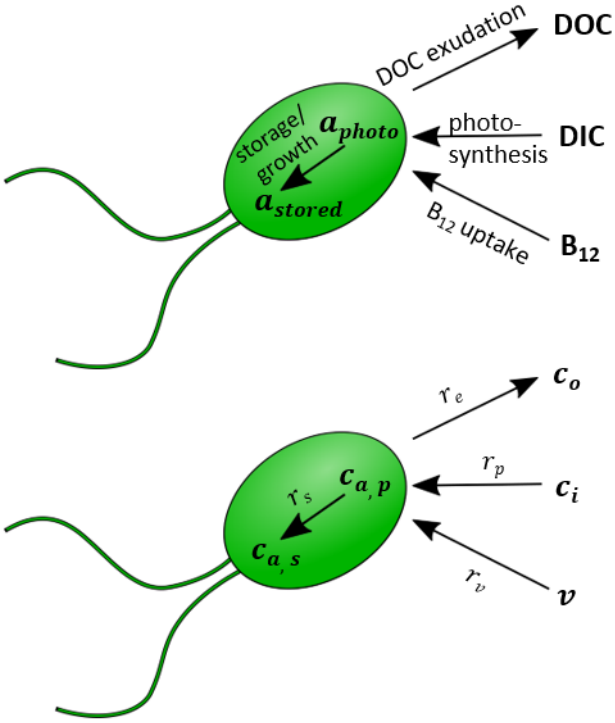

Figure 3.2 **A model for algal carbon dynamics**. This schematic illustrates the metabolic processes incorporated into a mathematical description for the algal carbon dynamics. In particular, photosynthetic DIC assimilation has been incorporated and the algal biomass is considered as two components: a 'photosynthetically active' component ($c_{a,p}$) that contributes to DOC exudation and a 'stored' component ($c_{a,s}$) that corresponds to the algal carbon storage and the carbon required for growth.

with $c_{a,p}$ the concentration of 'photosynthetically active' carbon, corresponding to the assimilated DIC and newly fixed carbon, and $c_{a,s}$ the concentration of 'stored' carbon, meaning the carbon stored in the form of molecules like starch, but also the carbon used for growth and as a building block for the cellular architecture and machinery. A parameter ϕ_s is introduced and defined as

$$\phi_s = \frac{c_{a,s}}{c_a}, \tag{3.11}$$

from which a rate of 'storage' can be defined as a rate proportional to the algal growth rate

$$r_s = \dot{c}_{a,s} = \frac{\phi_s \, \dot{a}}{Y_{a,c}}, \tag{3.12}$$

with $Y_{a,c}$ the total algal carbon yield, assumed to be a constant.

The rate of DOC exudation per cell is defined to be

$$p_c = (1 - \phi_s)\ p'_c, \tag{3.13}$$

where p'_c is assumed to be a constant that can be interpreted as a measure of the rate of DOC exudation per unit of 'photosynthetically-active' algal biomass. The total DOC production rate for the whole algal population, in moles per unit volume per unit time, is

$$r_e = (1 - \phi_s)\ p'_c\ a. \tag{3.14}$$

This means that, as well as an increase in DOC production for a larger algal population, an increase is also expected for a decrease in ϕ_s (i.e. a higher concentration of 'photosynthetically-active' algal carbon).

For simplicity the carbon concentrating mechanism is not considered explicitly. The DIC concentration c_i, is taken as the total concentration of the dissolved bicarbonate and carbon dioxide present in the growth media, both of which can be used by algae for photosynthesis. The total rate of photosynthesis given by r_p, in units of moles per unit volume per unit time, is considered analogous to the inorganic carbon assimilation rate and encapsulates DIC uptake, the carbon concentrating mechanism and carbon fixation. Total carbon conservation is used to obtain the equation

$$r_p = \frac{\dot{a}}{Y_{a,c}} + r_e, \tag{3.15}$$

with $\dot{a}$ the algal population growth rate defined in equation (3.9a).

3.2.3 Bacterial growth efficiency and respiration

The only carbon metabolic process considered for bacteria in the basic model outlined in section 3.2.1 was DOC consumption. However, bacteria must respire in order to generate the energy required for growth, meaning that they will release carbon dioxide (a component of DIC). Therefore, in order to create a more realistic model for bacterial carbon dynamics the basic model from section 3.2.1 is extended to include respiration. The resulting fluxes and pools of carbon considered are sketched in figure 3.3. The DOC-dependent population growth rate for bacteria remains as defined in section 3.2.1 and using equations (3.6) and (3.9b), the rate of change of the bacterial carbon biomass concentration, is defined as

$$\dot{c}_b = \frac{\dot{b}}{Y_{b,c}} = \frac{\mu_b\, b}{Y_{b,c}} \left(1 - \frac{b}{K_b}\right) \left(\frac{c_o}{K_c + c_o}\right). \tag{3.16}$$

Using total carbon conservation, the total bacterial carbon uptake rate, in moles per unit volume per unit time, is given by

$$r_u = \dot{c}_b + r_r, \tag{3.17}$$

with r_r the respiration rate, which corresponds to the total rate of release of inorganic carbon by respiration. The bacterial growth efficiency η' is defined as the ratio of the rate of carbon biomass growth relative to the total carbon uptake rate, giving

$$\eta' = \frac{\dot{c}_b}{r_u}. \tag{3.18}$$

In the logistic model used here, when the bacterial cell density has reached carrying capacity, the net growth is zero ($\dot{c}_b = 0$). It is expected that in this stationary phase the cells remain metabolically active and still turn over carbon (Kolter, 1993; Navarro Llorens *et al.*, 2010), therefore in the model the bacterial growth efficiency becomes zero at carrying capacity such that a non-zero carbon uptake is exactly balanced by the carbon released due to respiration. In order to incorporate this into the model, the bacterial growth efficiency is considered to be dependent on the bacterial population size. The constant η is introduced as the maximum growth efficiency, i.e. the growth efficiency observed in the exponential growth phase, when $b \ll K_b$. As the population grows towards carrying capacity the bacterial growth efficiency η' decreases to zero as

$$\eta' = \eta \left(1 - \frac{b}{K_b}\right). \tag{3.19}$$

From the above discussion of bacterial growth efficiency and respiration, the total rate of DOC uptake by bacteria is defined as

$$r_u = \frac{\mu_b\, b}{\eta\, Y_{b,c}} \left(\frac{c_o}{K_c + c_o} \right). \tag{3.20}$$

Using equations (3.16), (3.17) and (3.20), the total bacterial respiration rate is

$$r_r = \left(1 - \eta \left(1 - \frac{b}{K_b} \right) \right) r_u. \tag{3.21}$$

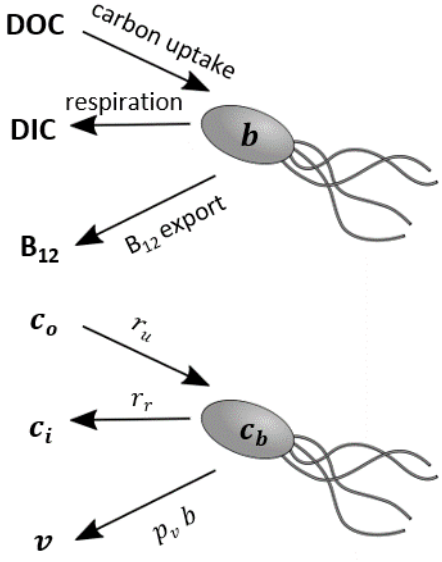

Figure 3.3 **A model for the bacterial carbon dynamics that includes respiration**. A schematic to show the incorporation of bacterial respiration to the biological processes of bacteria included in the model, i.e. in addition to the DOC uptake and B_{12} export of the basic model in section 3.2.1.

3.2.4 Inorganic carbon assimilation by bacteria

The SIMS experiments in section 2.3.4 showed ^{13}C enrichment for bacteria grown axenically with ^{13}C-labelled sodium bicarbonate and unlabelled glycerol. This implies that the bacteria are able to metabolise inorganic carbon. Assimilation of DIC by heterotrophic bacteria has also been observed in other work and has been used as a measure for metabolic activity (Hesselsoe *et al.*, 2005; Roslev *et al.*, 2004). To model this observation, a parameter X is introduced to describe the fraction of total carbon uptake by bacteria that comes from DIC and is defined as

$$X = \frac{r_u^{DIC}}{r_u}, \tag{3.22}$$

with r_u the rate of total carbon uptake by bacteria as defined in equation (3.20) in section 3.2.3 and r_u^{DIC} the DIC uptake rate. This assumes that bacterial growth and carbon uptake are a function of organic carbon availability but independent of the DIC concentration, i.e. DOC is the limiting nutrient for growth and DIC is in excess. The bacterial carbon fluxes that include both respiration and DIC uptake are sketched in figure 3.4.

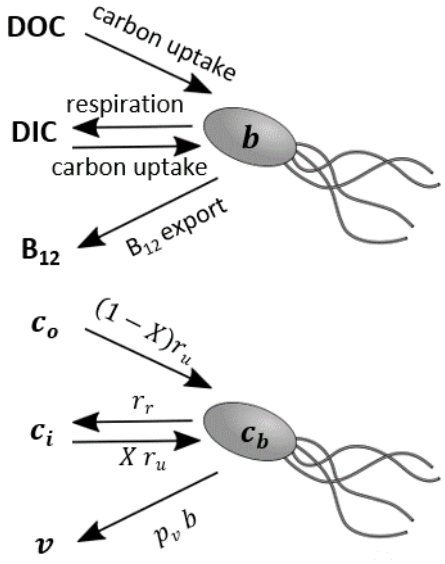

Figure 3.4 **A model for the bacterial carbon dynamics that includes respiration and inorganic carbon assimilation**. An overview of all the metabolic processes included in the model for bacteria, i.e. the addition of bacterial respiration and DIC uptake to the DOC uptake and B_{12} export by bacteria in the basic model discussed in section 3.2.1.

3.2.5 The extended co-culture model

Starting from the basic, nutrient-explicit co-culture model outlined in section 3.2.1, I have introduced the carbon dynamics of the co-culture more explicitly by adding algal photosynthesis, algal DOC exudation from excess photosynthesis, bacterial respiration and bacterial assimilation of DIC. The result is a set of five ODEs defined in equations (3.23). The carbon biomass conversion relations are given in equations (3.24) and the various rates associated with the different nutrient uptake and exchange processes are given in equations (3.25). These nutrient dynamics are summarised in figure 3.5, and the model variables and parameters are summarised in tables 3.1 and 3.2 respectively.

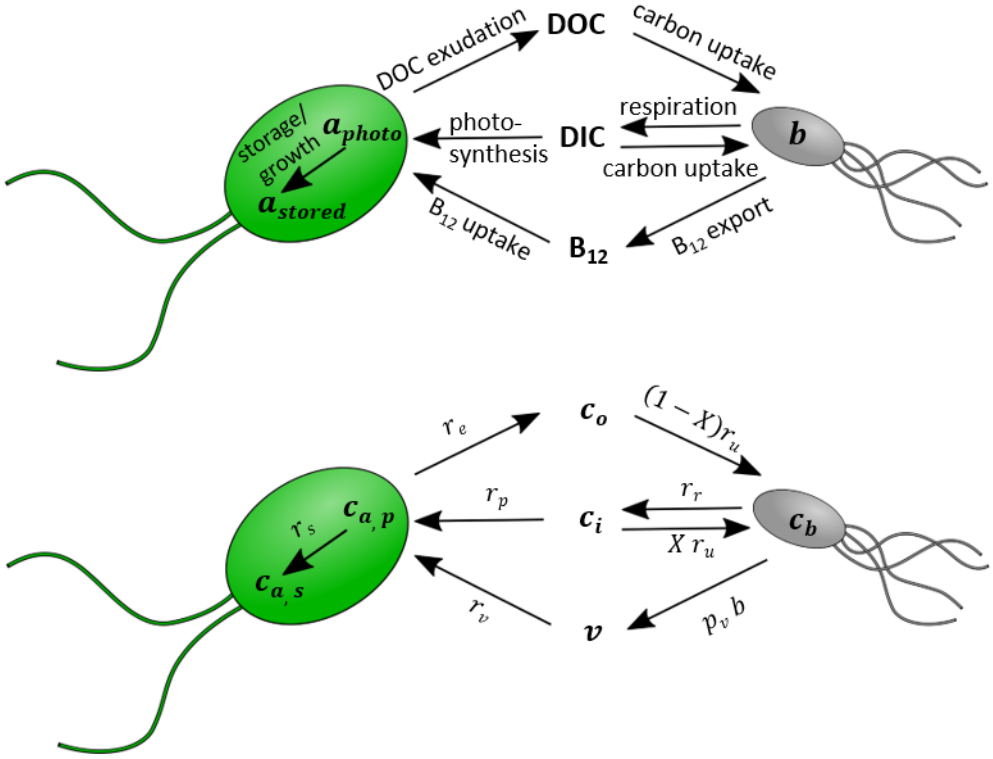

Figure 3.5 **Extended model for the nutrient dynamics and growth rates in an algal-bacterial co-culture**. This schematic shows all the processes considered in the extended co-culture model, i.e. with the addition of algal photosynthesis, algal carbon storage, bacterial respiration and bacterial DIC assimilation to the basic model given in section 3.2.1.

Model ODEs

$$\frac{da}{dt} = \mu_a\, a \left(1 - \frac{a}{K_a}\right) \left(\frac{v}{K_v + v}\right) \tag{3.23a}$$

$$\frac{db}{dt} = \mu_b\, b \left(1 - \frac{b}{K_b}\right) \left(\frac{c_o}{K_c + c_o}\right) \tag{3.23b}$$

$$\frac{dc_o}{dt} = r_e - (1 - X)\, r_u \tag{3.23c}$$

$$\frac{dc_i}{dt} = r_r - X\; r_u - r_p \tag{3.23d}$$

$$\frac{dv}{dt} = p_v\, b - r_v \tag{3.23e}$$

Carbon biomass relations

$$c_a = \frac{a}{Y_{a,c}} \tag{3.24a}$$

$$c_{a,s} = \phi_s\, c_a \tag{3.24b}$$

$$c_{a,p} = c_a - c_{a,s} \tag{3.24c}$$

$$c_b = \frac{b}{Y_{b,c}} \tag{3.24d}$$

Metabolite rates

$$r_s = \phi_s\, \frac{\dot{a}}{Y_{a,c}} \tag{3.25a}$$

$$r_e = (1 - \phi_s)\;\, p_c'\, a \tag{3.25b}$$

$$r_p = \frac{\dot{a}}{Y_{a,c}} + r_e \tag{3.25c}$$

$$r_u = \frac{\mu_b\, b}{\eta\; Y_{b,c}} \left(\frac{c_o}{K_c + c_o}\right) \tag{3.25d}$$

$$r_r = \left(1 - \eta \left(1 - \frac{b}{K_b}\right)\right) r_u \tag{3.25e}$$

$$r_v = \frac{\mu_a\, a}{Y_{a,v}} \left(\frac{v}{K_v + v}\right) \tag{3.25f}$$

Table 3.1 **Summary of model variables**.

Variable	Units	Description
a	$\mathrm{cells\,mL^{-1}}$	Algal cell density
b	$\mathrm{cells\,mL^{-1}}$	Bacterial cell density
c_a	$\mathrm{molC\,mL^{-1}}$	Algal carbon biomass
$c_{a,p}$	$\mathrm{molC\,mL^{-1}}$	'Photosynthetic' algal carbon biomass
$c_{a,s}$	$\mathrm{molC\,mL^{-1}}$	'Stored' algal carbon biomass
c_b	$\mathrm{molC\,mL^{-1}}$	Bacterial carbon biomass
c_o	$\mathrm{molC\,mL^{-1}}$	DOC concentration
c_i	$\mathrm{molC\,mL^{-1}}$	DIC concentration
v	$\mathrm{mol\,mL^{-1}}$	Vitamin B_{12} concentration

Table 3.2 **Summary of model parameters**.

Parameter	Units	Description
μ_a	$\mathrm{h^{-1}}$	Maximum growth rate for algae
μ_b	$\mathrm{h^{-1}}$	Maximum growth rate for bacteria
K_a	$\mathrm{cells\,mL^{-1}}$	Algal carrying capacity
K_b	$\mathrm{cells\,mL^{-1}}$	Bacterial carrying capacity
K_v	$\mathrm{mol\,mL^{-1}}$	B_{12}-half-saturation constant for algal growth
K_c	$\mathrm{molC\,mL^{-1}}$	DOC-half-saturation constant for bacterial growth
$Y_{a,c}$	$\mathrm{cells\,molC^{-1}}$	Algal carbon yield
$Y_{a,v}$	$\mathrm{cells\,mol^{-1}}$	Algal B_{12} yield
$Y_{b,c}$	$\mathrm{cells\,molC^{-1}}$	Bacterial carbon yield
p_c'	$\mathrm{molC\,cell^{-1}\,h^{-1}}$	Algal DOC production rate
p_v	$\mathrm{mol\,cell^{-1}\,h^{-1}}$	Bacterial B_{12} production rate
ϕ_s		Fraction of algal carbon biomass that is 'stored'
η		Maximum bacterial growth efficiency i.e. $\eta' = \eta\left(1-\frac{b}{K_b}\right)$
X		Fraction of total bacterial carbon uptake coming from the DIC

3.2.6 Non-dimensional model

To understand the general behaviour of the co-culture model, the different variables were nondimensionalised, resulting in the definition of a set of non-dimensional parameters (table 3.3). The algal and bacterial cell densities were nondimensionalised using their carrying capacities: $a/K_a \rightarrow a$ and $b/K_b \rightarrow b$ respectively. The vitamin B_{12} concentration was rescaled using the half-saturation concentration for algal growth: $v/K_v \rightarrow v$. All the carbon concentrations were rescaled using the half-saturation concentration for bacterial growth: $c/K_c \rightarrow c$. To nondimensionalise time, the bacterial maximum growth rate was used: $t\ \mu_b \rightarrow t$. The set of non-dimensional ODEs, carbon biomass conversion relations and metabolite rates obtained from this rescaling are given in equations (3.26), (3.27) and (3.28) respectively.

Table 3.3 **Non-dimensional model parameters**.

Parameter	Definition	Description
ε	μ_a/μ_b	Ratio of growth rates
$k_{a,c}$	$K_a/\left(K_c\ Y_{a,c}\right)$	Algal carbon uptake parameter
$k_{a,v}$	$K_a/\left(K_v\ Y_{a,v}\right)$	Algal B_{12} uptake parameter
$k_{b,c}$	$K_b/\left(K_c\ Y_{b,c}\right)$	Bacterial carbon uptake parameter
s_v	$\left(p_v\ K_b\right)/\left(\mu_a\ K_v\right)$	B_{12} production strength
s'_c	$\left(p'_c\ K_a\right)/\left(\mu_b\ K_c\right)$	DOC production strength

Model ODEs

$$\frac{da}{dt} = \varepsilon\ a(1-a)\left(\frac{v}{1+v}\right) \tag{3.26a}$$

$$\frac{db}{dt} = b(1-b)\left(\frac{c_o}{1+c_o}\right) \tag{3.26b}$$

$$\frac{dc_o}{dt} = r_e - (1-X)\,r_u \tag{3.26c}$$

$$\frac{dc_i}{dt} = r_r - X\ r_u - r_p \tag{3.26d}$$

$$\frac{dv}{dt} = \varepsilon\ s_v\ b - r_v \tag{3.26e}$$

Carbon biomass relations

$$c_a = k_{a,c}\ a \tag{3.27a}$$

$$c_{a,s} = \phi_s\ c_a \tag{3.27b}$$

$$c_{a,p} = c_a - c_{a,s} \tag{3.27c}$$

$$c_b = k_{b,c}\, b \tag{3.27d}$$

Metabolite rates

$$r_s = \phi_s\, k_{a,c}\, \dot{a} \tag{3.28a}$$

$$r_e = (1-\phi_s)\; s'_c\, a \tag{3.28b}$$

$$r_p = k_{a,c}\, \dot{a} + r_e \tag{3.28c}$$

$$r_u = \frac{k_{b,c}\, b}{\eta}\left(\frac{c_o}{1+c_o}\right) \tag{3.28d}$$

$$r_r = (1-\eta\,(1-b))\, r_u \tag{3.28e}$$

$$r_v = \varepsilon\, k_{a,v}\, a\left(\frac{v}{1+v}\right) \tag{3.28f}$$

3.2.7 Isotope labelling dynamics

The atomic fraction of ^{13}C is defined as the concentration of ^{13}C relative to the total carbon concentration, i.e. $f = {}^{13}C/\left({}^{13}C + {}^{12}C\right)$. Each of the different carbon components of the model (bacterial carbon, DOC, DIC etc.) can be considered as a separate carbon pool. For a general case, I consider the *nth* carbon pool c_n with r_{gain}, the rate of carbon coming from the c_{n-1} pool and r_{loss}, the rate of carbon going to c_{n+1}. This can be summarised as

$$\mathrm{c}_{n-1} \xrightarrow{\mathrm{r_{gain}}} \mathrm{c}_n \xrightarrow{\mathrm{r_{loss}}} \mathrm{c}_{n+1}.$$

For example, when considering the DOC, $c_n = c_o$, then $c_{n-1} = c_{a,p}$ and $c_{n+1} = c_b$ (the photosynthetic component of algal carbon and the bacterial carbon respectively), $r_{gain} = r_e$ (the rate of DOC exudation by algae) and $r_{loss} = X\; r_u$ (the rate of DOC uptake by bacteria), giving

$$\mathrm{c}_{a,p} \xrightarrow{\mathrm{r}_e} \mathrm{c}_o \xrightarrow{\mathrm{X\ r}_u} \mathrm{c}_b.$$

The rate of change of the total carbon concentration for the *nth* carbon pool is

$$\frac{dc_n}{dt} = r_{gain} - r_{loss} \tag{3.29}$$

and the rate of change of the ^{13}C concentration for the *nth* carbon pool is

$$\frac{dc_n^{13}}{dt} = f_{n-1}\, r_{gain} - f_n\, r_{loss}, \tag{3.30}$$

where f_n is the atomic fraction of ^{13}C in the *nth* carbon pool and f_{n-1} is the atomic fraction of ^{13}C in the $(n-1)$ carbon pool. From equations (3.29) and (3.30), the rate of change of the atomic fraction of ^{13}C in the *nth* carbon pool was derived using the quotient rule and the result gave

$$\frac{df_n}{dt} = (f_{n-1} - f_n)\frac{r_{gain}}{c_n}. \tag{3.31}$$

This general result for the isotope labelling dynamics of a carbon pool assumes that isotopic fractionation is negligible, which corresponds to the assumption that the difference between the nutrient rates for the different carbon isotopes is negligible compared to the overall labelling rates. This assumptions leads to the conclusion that the rate of loss to the c_{n+1} carbon pool for the ^{13}C and ^{12}C isotopes are equal, meaning that the rate of isotope labelling is explicitly independent of r_{loss}. However, r_{loss} matters implicitly when comparing the growth and isotope labelling rates (i.e. substituting r_{gain} in equation (3.31) with $r_{gain} = \dot{c}_n + r_{loss}$ from equation (3.29) gives $\dot{f}_n = (f_{n-1} - f_n)(\dot{c}_n + r_{loss})/c_n$). If r_{loss} is neglected, then $\dot{f}_n$ would overestimate $\dot{c}_n$, i.e. the labelling rate would overestimate the growth rate.

The algal carbon biomass of the model has two different internal carbon components, meaning that the carbon isotope labelling dynamics for algae derived from the extended co-culture model (see section 3.2.6 for the non-dimensional model equations) does not follow the general case discussed above. In the model, the DOC produced by algae comes from only the photosynthetically active component of the algal biomass and therefore when $f_{a,s}$ is not equal to $f_{a,p}$, the rate of loss for ^{13}C and ^{12}C from the total algal biomass are not equal. As a result, the rate of change of the atomic fraction of ^{13}C in algae includes a term for the rate of carbon loss.

Taking into consideration the ^{13}C isotope labelling dynamics in the general case for the *nth* carbon pool and in the specific case for algae, the rate of change for the atomic fractions of ^{13}C in the co-culture were obtained for the non-dimensional model defined in section 3.2.6 and are given by the following equations

$$\frac{df_a}{dt} = (f_i - f_a)\,\varepsilon\,(1-a)\left(\frac{v}{1+v}\right) + (f_i - f_{a,p})\frac{(1-\phi_s)\,s_c'}{k_{a,c}}, \tag{3.32a}$$

$$\frac{df_{a,p}}{dt} = (f_i - f_{a,p})\left[\frac{\varepsilon\,(1-a)}{(1-\phi_s)}\left(\frac{v}{1+v}\right) + \frac{s_c'}{k_{a,c}}\right], \tag{3.32b}$$

$$\frac{df_{a,s}}{dt} = (f_{a,p} - f_{a,s})\,\varepsilon\,(1-a)\left(\frac{v}{1+v}\right), \tag{3.32c}$$

$$\frac{df_b}{dt} = (X\ f_i + (1-X)\,f_o - f_b)\,\frac{1}{\eta}\left(\frac{c_o}{1+c_o}\right), \tag{3.32d}$$

$$\frac{df_o}{dt} = (f_{a,p} - f_o)\,\frac{(1-\phi_s)\,s'_c\,a}{c_o}, \tag{3.32e}$$

$$\frac{df_i}{dt} = (f_b - f_i)\,\frac{(1-\eta\,(1-b))\,k_{b,c}\,b}{\eta\ c_i}\left(\frac{c_o}{1+c_o}\right), \tag{3.32f}$$

with f_a, $f_{a,p}$, $f_{a,s}$, f_b, f_o and f_i the atomic fractions of ^{13}C in the total algal carbon biomass, 'photosynthetically-active' algal carbon, 'stored' algal carbon, bacterial carbon, DOC and DIC respectively. This illustrates how the nutrient explicit model that has been developed in this chapter can be used to derive equations for isotope labelling dynamics, allowing the model to make predictions that can be experimentally tested.

3.2.8 Summary of model assumptions

Below is a list of the simplifying assumptions that have been made for the algal-bacterial co-culture model. These are considered both reasonable and necessary in order to obtain a tractable model, since the aim of constructing this nutrient-explicit model was not to describe all the biological processes in detail, but to capture the essential dynamics such that the mathematics is numerically and analytically tractable, and predictions can be qualitatively compared with experimental observations.

- The co-culture is well mixed such that it can be assumed that the transport of nutrients between algae and bacteria is not limiting, i.e. there is a uniform concentration of nutrients and cells throughout the culture.
- Population growth rate is defined by a Monod growth dependence on external vitamin B_{12} and DOC concentrations for algae and bacteria respectively.
- The recycling dynamics of vitamin B_{12} are not explicitly included in the model.
- Death rate is negligible compared to growth rate for both algae and bacteria. This corresponds to the case where $\delta_a \ll \mu_a\,(1-a/K_a)\,v/\,(K_v+v)$ for algae and similarly $\delta_b \ll \mu_b\,(1-b/K_b)\,c_o/\,(K_c+c_o)$ for bacteria.
- The effect of light has not been included in the model, which corresponds to a continuous light condition throughout the culture and assumes that the light intensity is

not limiting to algal growth. In the experiments discussed in chapter 2, a light-dark cycle was used, however only two time-points per day were sampled and therefore the assumption of continuous light should be sufficient for fitting this model to the experiments.

- The amount of carbon per cell is a constant for both algae and bacteria, which is defined by the carbon yield values $Y_{a,c}$ and $Y_{b,c}$ respectively.
- The DIC concentration is not limiting for the growth of both algae and bacteria.
- The DIC concentration in the media is considered as the effective total concentration of inorganic carbon (i.e. carbon dioxide and bicarbonate). Therefore, the DIC uptake by algae for photosynthesis does not explicitly consider the equilibrium between different forms of DIC and the carbon concentrating mechanism.
- The fraction of 'stored' carbon for the algal biomass ϕ_s is considered to be a constant.
- Algal respiration is negligible.
- The DOC production rate per algal cell is linearly proportional to the algal cell density. The constant of proportionality is defined as $(1-\phi_s)\,p'_c$, with p'_c a constant. This means that the DOC exudation rate is higher when the fraction of storage is smaller.
- DOC is modelled as an effective single carbon source.
- The bacterial growth efficiency (η') is the fraction of the total carbon uptake rate that contributes to an increase in bacterial carbon biomass. It is assumed that the bacterial growth efficiency is at its maximum in the exponential growth phase and tends to zero at carrying capacity (i.e. $\eta' = \eta\,(1-b/K_b)$).
- The respiration rate is equal to the difference between the total carbon uptake and the increase in bacterial carbon biomass, i.e. $r_r = r_u - \dot{c}_b$.
- The fraction of total carbon uptake by bacteria that comes from DIC is a constant, X.
- The vitamin B_{12} production rate per bacterial cell is a constant, p_v.
- Isotopic fractionation is negligible.
- The possible role of regulation has not included in the model, meaning that for a given algal-bacterial co-culture the parameters are constant such that the bacterial parameter values are not affected by the presence of algae and vice versa.

3.2.9 General behaviour of the model

In order to explore the general behaviour of the model a set of parameters were chosen that satisfy the inequality constraints obtained later in this chapter (see equation 3.34) and with orders of magnitude comparable to the parameters obtained by F. J. Peaudecerf *et al.* (2018) for the co-culture between the alga *L. rostrata* and the bacterium *M. loti*. The parameter values chosen were $\varepsilon = 0.5$, $k_{b,c} = 1$, $k_{a,c} = 1$, $k_{a,v} = 5$, $s_v = 1$, $s'_c = 0.02$, $\phi_s = 0.5$, $\eta = 0.5$ and $X = 0.01$. The initial conditions were chosen such that all carbon pools started with a carbon isotope fraction at natural abundance except for the DIC, which was 100 % ^{13}C-labelled. As expected, figures 3.6 and 3.7 show that as the model co-culture evolves the algal and bacterial populations grow. As bacteria grow, B_{12} production increases and with the current set of parameters the B_{12} concentration reaches a maximum, which is when algal uptake equals bacterial production. After this turning point, algal uptake becomes faster than bacterial production resulting in a decreasing B_{12} concentration. As algae grow, DOC is produced and the DOC concentration increases, but at a decreasing rate because as the bacterial population increases the bacterial DOC uptake starts to balance algal DOC production. The carbon dynamics within the co-culture are represented by the isotope fractions f_a, f_b and f_o for algae, bacteria and DOC respectively. First the algae become labelled due to photosynthetic assimilation of ^{13}C-labelled inorganic carbon. Then as algae become labelled and produce DOC, f_o increases, and when bacteria consume the labelled DOC they too become enriched with ^{13}C and f_b increases.

Introducing the storage fraction parameter ϕ_s has a minimal effect on algal growth (figure 3.6). However, increasing ϕ_s decreases the rate of isotope labelling of algae because a greater amount of initial unlabelled carbon is 'locked in' to the algal biomass. Increasing ϕ_s decreases the rate of DOC production, however the rate of DOC labelling increases because there is a smaller fraction of algal biomass that is 'photosynthetically active', which becomes quickly enriched with ^{13}C. The slower DOC production results in a decrease in bacterial growth and, despite the DOC becoming labelled more quickly, the labelling rate of bacteria also decreases.

Decreasing the bacterial growth efficiency parameter η corresponds to an increase in bacterial respiration, which mainly affects the DOC and bacterial dynamics of the model (figure 3.7). A smaller value for η means that bacteria respire more and therefore consume DOC more quickly, which causes the DOC concentration to decrease and the bacterial growth rate to slow down. The isotope fraction of bacteria f_b increases slightly more quickly for a model with smaller η because when bacterial respiration increases there is a faster turn around of bacterial carbon biomass.

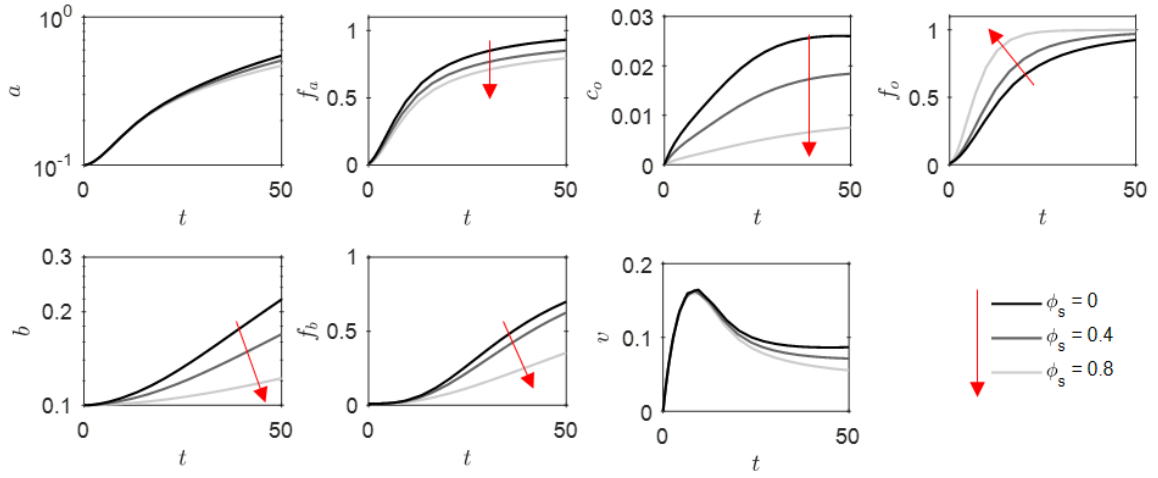

Figure 3.6 **General behaviour of the model and the effect of storage parameter ϕ_s.** Time evolution of model variables in non-dimensional units for different values of the storage parameter ϕ_s. The red arrows show the effect of increasing ϕ_s. The chosen set of parameter values were $\varepsilon = 0.5$, $k_{b,c} = 1$, $k_{a,c} = 1$, $k_{a,v} = 5$, $s_v = 1$, $s_c' = 0.02$, $\eta = 0.5$ and $X = 0.01$. The initial conditions were $a(0) = 0.1$, $b(0) = 0.1$, $c_o(0) = 0$, $v(0) = 0$, $c_i(0) = 50$, $f_a(0) = f_{a,p}(0) = f_{a,s}(0) = f_b(0) = f_o(0) = 0.0108$ and $f_i(0) = 1$.

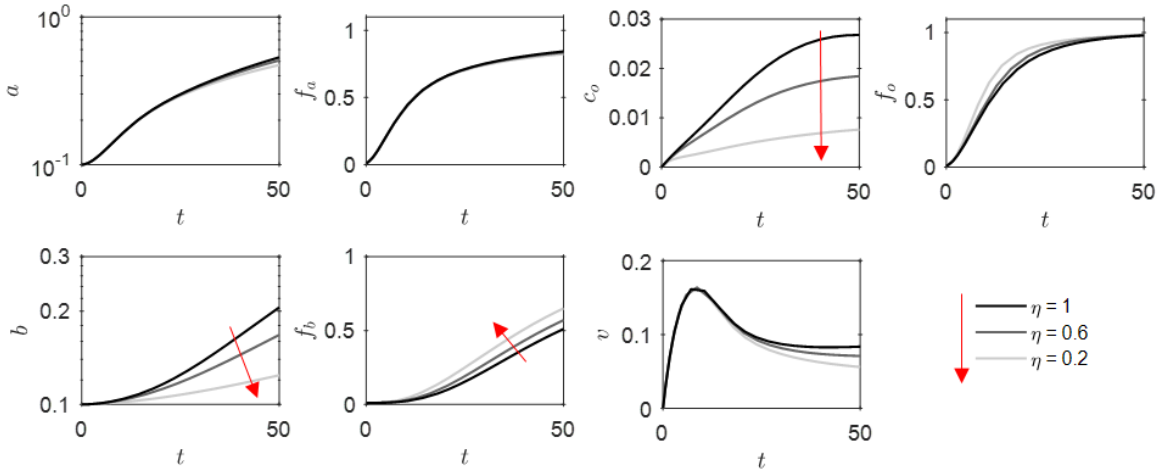

Figure 3.7 **General behaviour of the model and the effect of bacterial growth efficiency parameter η.** Time evolution of model variables in non-dimensional units for different values of the bacterial growth efficiency parameter η. The red arrows show the effect of decreasing η. The chosen set of parameter values were $\varepsilon = 0.5$, $k_{b,c} = 1$, $k_{a,c} = 1$, $k_{a,v} = 5$, $s_v = 1$, $s_c' = 0.02$, $\phi_s = 0.5$ and $X = 0.01$. The initial conditions were $a(0) = 0.1$, $b(0) = 0.1$, $c_o(0) = 0$, $v(0) = 0$, $c_i(0) = 50$, $f_a(0) = f_{a,p}(0) = f_{a,s}(0) = f_b(0) = f_o(0) = 0.0108$ and $f_i(0) = 1$.

3.3 Tractable analytical results

In general, numerical methods are required to solve the equations of the co-culture model in order to understand its behaviour and make specific predictions. However analytical results can aid understanding of the model dynamics and provide useful limits for interpreting the numerical results in chapter 4.

3.3.1 Model fixed point

The fixed point of the model's dynamical system of equations is a useful result to derive because it provides parameter constraints, which ensure that for long time periods the model will tend towards a positive value for the cell densities and the DOC and B_{12} concentrations. Additionally, the fixed point is helpful for studying the general behaviour of the model, since the trajectory of the co-culture through time towards the fixed point can be compared when the initial conditions or parameter values are changed. The approach taken here is based on the fixed point analysis described in François Peaudecerf's PhD thesis (F. Peaudecerf, 2016).

For the co-culture model (equations (3.26)), a non-zero fixed point exists where the algal cell density, bacterial cell density, DOC concentration and vitamin B_{12} concentration are all constant (i.e. at a^*, b^*, c_o^* and v^* respectively). The fixed point for the non-dimensional model is obtained by setting equations (3.26) equal to zero, which gives

$$a^* = 1 \tag{3.33a}$$

$$b^* = 1 \tag{3.33b}$$

$$r_e = (1-X)\, r_u \;\Rightarrow\; c_o^* = \frac{(1-\phi_s)\, s_c'}{(1-X)\, k_{b,c}/\eta - (1-\phi_s)\, s_c'} \tag{3.33c}$$

$$r_v = \varepsilon\, s_v\, b^* \;\Rightarrow\; v^* = \frac{s_v}{k_{a,v} - s_v}\,. \tag{3.33d}$$

At this fixed point, the algal and bacterial populations have reached carrying capacity, the rate of DOC production by algae is equal to the rate of DOC uptake by bacteria and the rate of B_{12} production by bacteria is equal to the rate of B_{12} uptake by algae. It is not relevant to consider the case where the DIC concentration is constant, because the model assumes that DIC is in excess and does not affect the rate of algal or bacterial growth.

In order for this fixed point to exist at positive values of c_o^* and v^*, the parameters of the model must satisfy the following inequality constraints

$$(1-X)\, k_{b,c}/\eta - (1-\phi_s)\, s_c' > 0 \tag{3.34a}$$

$$k_{a,v} - s_v > 0. \tag{3.34b}$$

The isotope labelling dynamics reach a fixed point when all the atomic fractions of ^{13}C are equal (i.e. $f_i^* = f_o^* = f_a^* = f_{a,p}^* = f_{a,s}^* = f_b^* = f^*$). This fixed point is defined as

$$f^* = \frac{f_i(0)\, c_i(0) + f_o(0)\, c_o(0) + f_a(0)\, c_a(0) + f_b(0)\, c_b(0)}{c_i(0) + c_o(0) + c_a(0) + c_b(0)}, \tag{3.35}$$

which can be intuitively understood as simply the weighted average of the initial atomic fractions of ^{13}C present in the system. This fixed point depends on the initial conditions, since it depends on the total amount of ^{13}C in the co-culture system.

Stability analysis

Using the extended co-culture model equations in their non-dimensional form (equations (3.26)), the Jacobian matrix

$$J = \begin{pmatrix} \frac{\varepsilon\,(1-2a)\,v}{(1+v)} & 0 & 0 & \frac{\varepsilon\,a\,(1-a)}{(1+v)^2} \\ 0 & \frac{(1-2b)\,c_o}{(1+c_o)} & \frac{b\,(1-b)}{(1+c_o)^2} & 0 \\ s_c'(1-\phi_s) & -\frac{(1-X)\,k_{b,c}\,c_o}{\eta\,(1+c_o)} & -\frac{(1-X)\,k_{b,c}\,b}{\eta\,(1+c_o)^2} & 0 \\ -\frac{\varepsilon\,k_{a,v}\,v}{(1+v)} & \varepsilon\, s_v & 0 & -\frac{\varepsilon\,k_{a,v}\,a}{(1+v)^2} \end{pmatrix} \tag{3.36}$$

was obtained for the ordinary differential equations describing the rate of change of the algal cell density, bacterial cell density, DOC concentration and vitamin B_{12} concentration. The atomic fraction of ^{13}C is not included in this analysis because the fixed point f^* in equation (3.35) and the fixed point for a^*, b^*, c_o^* and v^* defined in equations (3.33) are independent. In order to determine the stability of the fixed point associated with the population sizes and nutrient concentrations, the Jacobian matrix was evaluated at the fixed point (a^*, b^*, c_o^*, v^*) and the result is given by

$$J^* = \begin{pmatrix} -x_1 & 0 & 0 & 0 \\ 0 & -x_2 & 0 & 0 \\ y_1 & -y_1 & -x_3 & 0 \\ -y_2 & y_2 & 0 & -x_4 \end{pmatrix}, \tag{3.37a}$$

$$x_1 = \frac{\varepsilon\, s_v}{k_{a,v}}, \tag{3.37b}$$

$$x_2 = \frac{(1-\phi_s)\, s_c'}{(1-X)\, k_{b,c}/\eta}, \tag{3.37c}$$

$$x_3 = \frac{(1-X)\,k_{b,c}}{\eta}\left[1-\frac{(1-\phi_s)\,s_c'}{(1-X)\,k_{b,c}/\eta}\right]^2, \tag{3.37d}$$

$$x_4 = \varepsilon\, k_{a,v}\left[1-\frac{s_v}{k_{a,v}}\right]^2, \tag{3.37e}$$

$$y_1 = s_c'\,(1-\phi_s), \tag{3.37f}$$

$$y_2 = \varepsilon\, s_v. \tag{3.37g}$$

The eigenvalues of J^*, the Jacobian matrix at the fixed point defined by equations (3.37), were calculated by solving

$$det\,(J^* - I\lambda) = (-x_1-\lambda)\,(-x_2-\lambda)\,(-x_3-\lambda)\,(-x_4-\lambda) = 0, \tag{3.38}$$

resulting in four eigenvalues defined by

$$\lambda = -x_1,\ -x_2,\ -x_3 \text{ or } -x_4, \tag{3.39}$$

which are all found to be negative because x_1, x_2, x_3 and x_4 are strictly positive (equations (3.37)). Therefore the fixed point is asymptotically stable, meaning that any small perturbation will converge back to the fixed point (Terrell, 2009).

Phase diagrams and model trajectories towards the fixed point

For the set of parameters chosen in section 3.2.9 the fixed point is given by $a^* = 1$, $b^* = 1$, $c_o^* = 0.0051$ and $v^* = 0.25$ in dimensionless units. Using this same set of parameters the time evolution of the model variables over short time-periods and the long-term trajectories to the fixed point were determined for different initial cell densities (figure 3.8) and for different initial nutrient concentrations (figure 3.9).

Increasing the initial algal cell density $a\,(0)$ increases the rate of vitamin consumption and also increases the rate of DOC production, which in turn increases the rate of bacterial growth (i.e. compare the green dotted line and black solid line in figure 3.8). In terms of carbon isotope dynamics, a higher $a\,(0)$ means that overall there is a higher concentration of unlabelled algal biomass and therefore the rate of labelling for both algae and DOC decreases. However a minimal effect on the rate of isotope labelling of bacteria is observed, which is likely to be because the decreased DOC isotope fraction is balanced by an increase in the DOC uptake. The long-term trajectory towards the fixed point in the phase diagram for the microbial populations in figure 3.8b is minimally affected by the increase in $a\,(0)$. In the phase diagram of the nutrient concentrations in figure 3.8c the long-term trajectories

towards the fixed point show that an increase in $a(0)$ causes the DOC concentration to increase relatively rapidly beyond the fixed point value and diminishes the initial peak in B_{12} concentration. Increasing the initial bacterial cell density $b(0)$ increases the rate of DOC consumption and also increases the rate of vitamin production, which in turn increases the rate of algal growth (i.e. compare the red dotted line and black solid line in figure 3.8). Due to the faster algal growth, the isotope labelling rate of algae increases, which in turn results in a faster labelling rate of DOC. The labelling rate of bacteria is only minimally affected by the increase in $b(0)$, which is likely due to a balance between the increase in the atomic fraction of DOC and the higher initial amount of unlabelled bacterial biomass. The long-term trajectories towards the fixed point in the phase diagram for the microbial populations in figure 3.8b show that, for all the chosen combinations of initial cell densities, algae reach carrying capacity more quickly than bacteria. In the phase diagram of the nutrient concentrations in figure 3.8c the long-term trajectories show that an increase in $b(0)$ causes the initial peak B_{12} concentration to increase.

Compared to a co-culture with no initial DOC or B_{12}, when the initial DOC concentration $c_o(0)$ is greater than the fixed point value the initial bacterial growth rate is faster, but there is a negligible effect on all other model variables (i.e. compare the green dotted line and black solid line in figure 3.9). With the chosen set of parameters, the change in $c_o(0)$ has only a small effect on the model dynamics because the rate of DOC production by algae relatively quickly balances the rate of DOC consumption by bacteria. This results in the observed minimum in the DOC concentration, after which the DOC concentration is comparable to the case where $c_o(0) = 0$. Increasing the initial vitamin concentration $v(0)$ above zero and to a value greater than the fixed point, causes an increase in the algal growth rate, which increases the DOC production rate, and in turn increases bacterial growth (i.e. compare the red dotted line and black solid line in figure 3.9). In terms of the carbon isotope dynamics, the increase in algal growth rate means that the isotope labelling rate of both algae and DOC increases, which results in an increase in ^{13}C enrichment of bacteria. The long-term trajectories in the phase diagram for the microbial populations (figure 3.9b) are unaffected by the change in initial nutrient concentrations. Whereas, the long-term trajectories in the phase diagram for the nutrient concentrations (figure 3.9c) show that when $c_o(0)$ (or $v(0)$) is above the fixed point value, initially there is a decrease in the DOC (B_{12}) concentration while the B_{12} (DOC) concentration increases, after which the trajectory rejoins the case where the initial nutrient concentrations are zero, i.e. the DOC concentration increases then decreases, whereas the vitamin concentration decreases then increases.

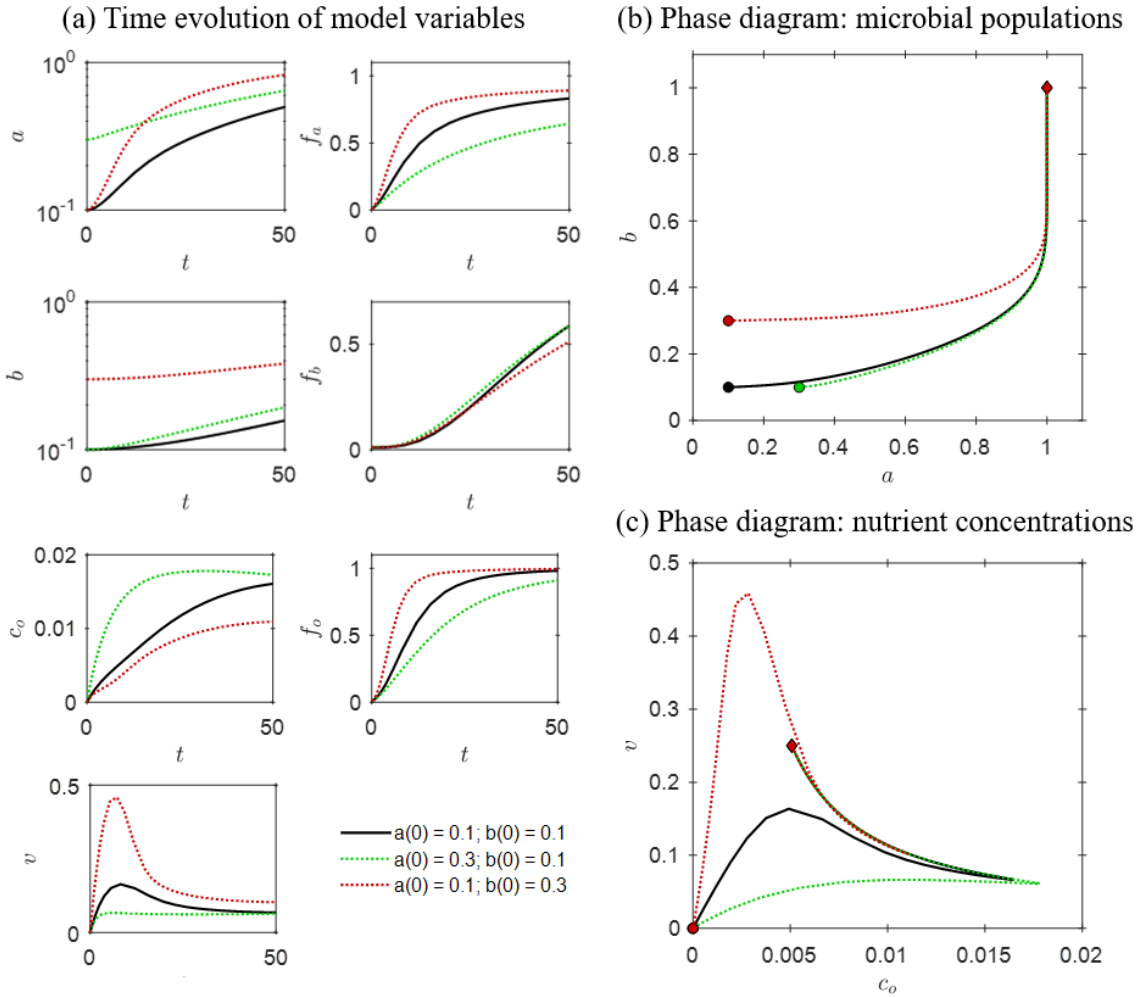

Figure 3.8 **Changing the initial algal and bacterial cell densities**. (a) Comparing the time evolution of model variables in dimensionless units for different initial algal and bacterial cell densities. The corresponding phase diagrams for (b) the algal and bacterial population sizes in non-dimensional units (a and b respectively) and (c) the DOC and B_{12} concentrations in non-dimensional units (c_o and v respectively). The phase diagrams show the different paths to the fixed point (diamonds) from different initial conditions (circles), but note that these trajectories occur over longer time-periods than the time-evolution plots in (a). The chosen set of parameter values were $\varepsilon = 0.5$, $k_{b,c} = 1$, $k_{a,c} = 1$, $k_{a,v} = 5$, $s_v = 1$, $s'_c = 0.02$, $\phi_s = 0.5$, $\eta = 0.5$ and $X = 0.01$. The initial conditions were $c_o(0) = 0$, $v(0) = 0$, $c_i(0) = 50$, $f_a(0) = f_{a,p}(0) = f_{a,s}(0) = f_b(0) = f_o(0) = 0.0108$ and $f_i(0) = 1$.

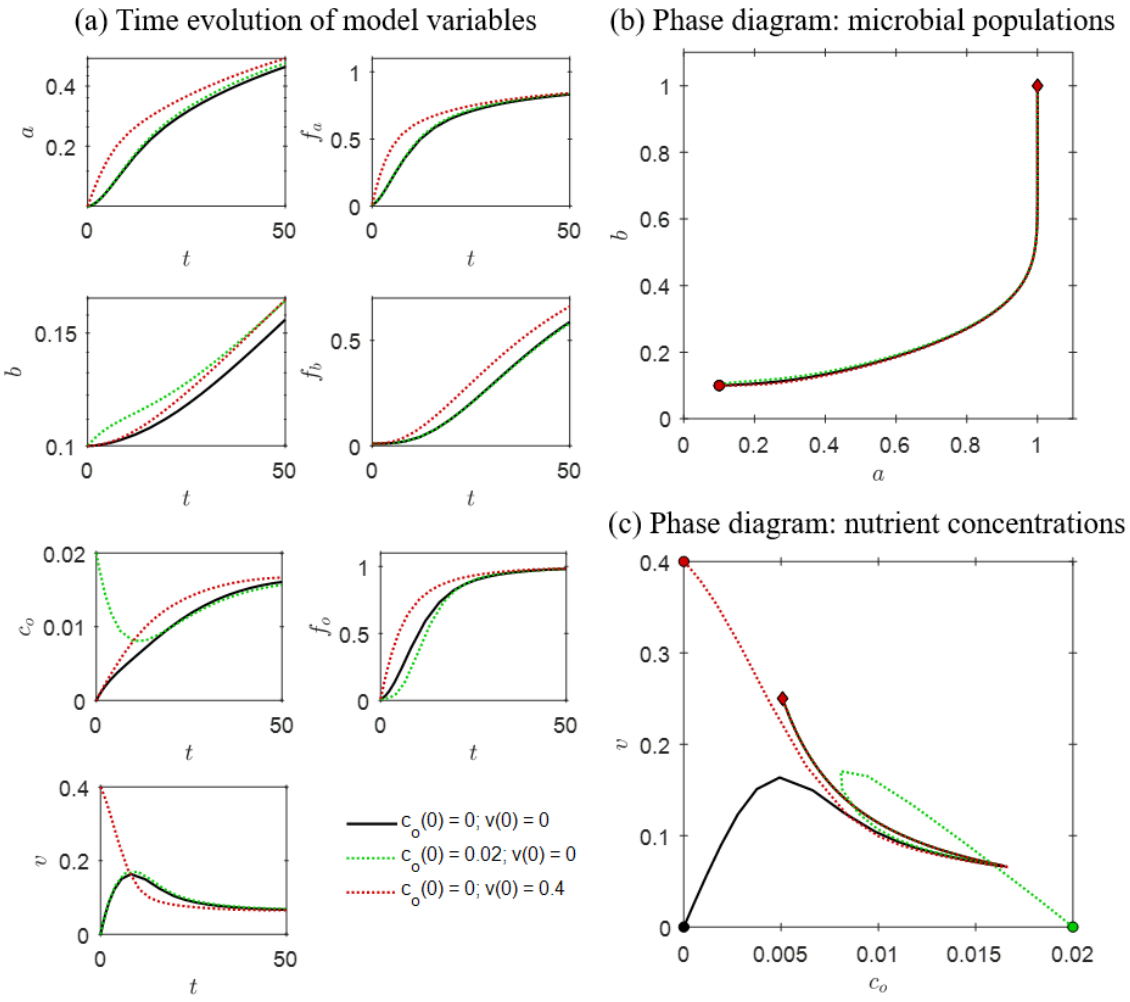

Figure 3.9 **Changing the initial DOC and B_{12} concentrations**. (a) Comparing the time evolution of model variables in dimensionless units for different initial DOC and B_{12} concentrations. The corresponding phase diagrams for (b) the algal and bacterial population sizes in non-dimensional units (a and b respectively) and (c) the DOC and B_{12} concentrations in non-dimensional units (c_o and v respectively). The phase diagrams show the different paths to the fixed point (diamonds) from different initial conditions (circles), but note that these trajectories occur over longer time-periods than the time-evolution plots in (a). The chosen set of parameter values were $\varepsilon = 0.5$, $k_{b,c} = 1$, $k_{a,c} = 1$, $k_{a,v} = 5$, $s_v = 1$, $s'_c = 0.02$, $\phi_s = 0.5$, $\eta = 0.5$ and $X = 0.01$. The initial conditions were $a(0) = 0.1$, $b(0) = 0.1$, $c_i(0) = 50$, $f_a(0) = f_{a,p}(0) = f_{a,s}(0) = f_b(0) = f_o(0) = 0.0108$ and $f_i(0) = 1$.

3.3.2 Analytical results for ^{13}C labelling dynamics

In this section certain instances are considered that allow for analytical results of the non-dimensional co-culture model to be obtained that relate the isotope labelling rate to growth rate for bacteria and algae. These results are interesting to consider because they allow for an improved understanding of how different parameters affect the isotope labelling dynamics and can therefore be helpful in interpreting results from parameter optimisations and numerical solutions to the model. The results discussed here use the non-dimensional form of the extended co-culture model defined in section 3.2.6.

Bacteria

Assuming exponential growth (i.e. $b \ll 1$) and a constant DOC concentration, which implies a constant growth rate $\mu_B = c_o/(1+c_o) = const.$, the bacterial population growth given by equation (3.26b) can be rewritten as

$$\dot{b} = b\ \mu_B, \tag{3.40a}$$

which can be integrated to give the bacterial population size as a function of time

$$b = b_0\ e^{\mu_B t}, \tag{3.40b}$$

with b_0 the initial bacterial population size. This can be rewritten as

$$\ln(b) = \ln(b_0) + \mu_B\ t. \tag{3.40c}$$

The atomic fraction of ^{13}C for the total carbon taken up by bacteria is given by

$$F = X\ f_i + (1-X)\ f_o \tag{3.41}$$

and if, in addition to the previously mentioned assumption of a constant growth rate, it is assumed that the atomic fractions of ^{13}C in the DOC and DIC are constant (i.e $\dot{F} = 0$), then the rate of change of the atomic fraction of ^{13}C in bacteria in equation (3.32d) can be rewritten as

$$\dot{f_b} = (F - f_b)\,\frac{\mu_B}{\eta}, \tag{3.42a}$$

which can be integrated to give the atomic fraction of ^{13}C as a function of time

$$f_b = F - \left(F - f_{b,0}\right) e^{-\mu_B t/\eta}, \tag{3.42b}$$

with $f_{b,0}$ the initial atomic fraction of ^{13}C in bacteria. This can be rewritten as

$$\ln\left(F - f_b\right) = \ln\left(F - f_{b,0}\right) - \frac{\mu_B\, t}{\eta}. \tag{3.42c}$$

The rate of carbon isotope labelling for bacteria decreases to zero as f_b approaches F. When $f_b \ll F$, the rate of change of the atomic fraction of ^{13}C in the bacterial carbon biomass is given by

$$\dot{f}_b = \frac{F\ \mu_B}{\eta}, \tag{3.43a}$$

which can be integrated to give the atomic fraction of ^{13}C as a function of time

$$f_b = f_{b,0} + \frac{F\ \mu_B\, t}{\eta}, \tag{3.43b}$$

which is linear in time. From these analytical results it can be seen that, for a constant exponential growth rate μ_B, f_b increases more quickly when the DIC and/or DOC have a higher atomic fraction of ^{13}C (i.e. higher F values). This is because when the DOC or DIC are more labelled, bacteria will take up a higher fraction of ^{13}C. A faster isotope labelling rate for bacteria is also predicted for a lower bacterial growth efficiency (i.e. smaller η). This is because a smaller η corresponds to a higher rate of respiration, which means that the bacteria turn over carbon more quickly and to achieve the same growth rate they need to take up more carbon. The estimated linear labelling rate from this approximation is given by $F\mu_B/\eta$.

Algae

Assuming exponential growth (i.e. $a \ll 1$) and a constant vitamin concentration, which implies a constant growth rate $\mu_A = \varepsilon\ v/\left(1+v\right) = const.$, the algal population growth given by equation (3.26a) can be rewritten as

$$\dot{a} = a\ \mu_A, \tag{3.44a}$$

which can be integrated to give the algal population size as a function of time

$$a = a_0\ e^{\mu_A t}, \tag{3.44b}$$

with a_0 the initial algal population size. This can be rewritten as

$$\ln\left(a\right) = \ln\left(a_0\right) + \mu_A\ t. \tag{3.44c}$$

The carbon isotope labelling dynamics of algae in the model depend on storage. To obtain some analytical results, the high and low limits of storage were considered.

High storage limit: For a high fraction of storage, $\phi_s \approx 1$, meaning that only a small component of the algal carbon biomass is photosynthetically active. As a result, the photosynthetically active component becomes labelled very quickly, reaching an equilibrium value of $f_{a,p} = f_i$, such that equation (3.32a) for the rate of change of f_a can be approximated as only dependent on growth rate and independent of the rate of DOC exudation. Therefore for the high storage limit, assuming a constant growth rate and a constant atomic fraction of ^{13}C in the DIC, the rate of change of the atomic fraction of ^{13}C in the algal carbon biomass is

$$\dot{f}_a = (f_i - f_a)\,\mu_A, \tag{3.45a}$$

which can be integrated to give the atomic fraction of ^{13}C as a function of time

$$f_a = f_i - (f_i - f_{a,0})\,e^{-\mu_A t}, \tag{3.45b}$$

with $f_{a,0}$ the initial atomic fraction of ^{13}C in algae. The rate of ^{13}C isotope labelling for algae decreases to zero as f_a approaches f_i. When $f_a \ll f_i$, the rate of change of the atomic fraction of ^{13}C in algae is

$$\dot{f}_a = f_i\,\mu_A, \tag{3.46a}$$

which can be integrated to give the atomic fraction of ^{13}C as a function of time

$$f_a = f_{a,0} + f_i\,\mu_A\,t, \tag{3.46b}$$

which is linear in time.

Low storage limit: For a low fraction of storage, $\phi_s \ll 1$ and the stored carbon component of algal biomass becomes negligible, meaning that $f_{a,p} \approx f_a$ and equation (3.32a) for $\dot{f}_a$ can be simplified. Assuming a constant growth rate and a constant atomic fraction of ^{13}C in the DIC, in the low storage limit the rate of change of the atomic fraction of ^{13}C in the algal carbon biomass is

$$\dot{f}_a = (f_i - f_a)\left(\mu_A + \frac{s'_c}{k_{a,c}}\right), \tag{3.47a}$$

which can be integrated to give the atomic fraction of ^{13}C as a function of time

$$f_a = f_i - (f_i - f_{a,0})\exp\left[-\left(\mu_A + \frac{s'_c}{k_{a,c}}\right)t\right]. \tag{3.47b}$$

Again, the rate of ^{13}C isotope labelling decreases to zero as f_a approaches f_i. When $f_a \ll f_i$, the rate of change of the atomic fraction of ^{13}C in the algal carbon biomass is

$$\dot{f}_a = f_i \left(\mu_A + \frac{s'_c}{k_{a,c}} \right), \tag{3.48a}$$

which can be integrated to give the atomic fraction of ^{13}C as a function of time

$$f_a = f_{a,0} + f_i \left(\mu_A + \frac{s'_c}{k_{a,c}} \right) t, \tag{3.48b}$$

which gives a linear isotope labelling rate.

These analytical expressions for the atomic fraction of ^{13}C in algae illustrate that, as expected, the algae become labelled more quickly when the DIC has a higher atomic fraction of ^{13}C. In addition, the analytical results indicate that for the high storage limit the rate of DOC exudation s'_c and the carbon uptake parameter $k_{a,c}$ do not affect the isotope labelling dynamics of algae. For a low storage fraction, the contribution of $s'_c/k_{a,c}$ increases the rate at which algae become labelled. Intuitively this can be understood by considering that as the fraction of stored carbon decreases, the rate of DOC export increases and therefore the rate of photosynthesis (and therefore the rate of DIC uptake) increases to allow for the same observed algal exponential growth rate μ_A. In addition, a smaller ϕ_s means that there is a smaller fraction of the initial algal biomass that is 'locked-in'. Both of these factors mean that for the same growth rate, the algal carbon turnover is faster and so the isotope labelling rate is faster when the fraction of storage is smaller. The effect of storage decreases when the DOC export parameter, s'_c, is small compared to the carbon uptake parameter, $k_{a,c}$, such that $s'_c/k_{a,c} \ll \mu_A$. In this case the linear approximation for the labelling rate of algae is given by $f_i\ \mu_A$ in both the high and low storage limits.

3.4 Biological interpretation of the co-culture model

In this chapter the additions made to the algal-bacterial model developed by F. J. Peaudecerf *et al.* (2018) aim to create a more realistic picture of the nutrient dynamics by considering some of the important carbon metabolic process within the co-culture; namely algal photosynthesis, the source of algal DOC exudation, bacterial growth efficiency and bacterial inorganic carbon assimilation. This extended co-culture model is summarised in figure 3.5 and sections 3.2.5 and 3.2.6.

The carbon metabolic fluxes associated with algal metabolism (outlined in section 1.2.2) could be approached mathematically in many ways, but for the purposes of the co-culture model the important features to consider are how algal metabolism accounts for the uptake of DIC and export of DOC. The model defines an algal population growth rate that is dependent on the external B_{12} concentration. A constant carbon yield (i.e. carbon per cell) is used to relate the algal carbon biomass growth to the population growth. The rate of DOC exuded from algal cells into the media is considered to be linearly dependent on the algal cell density, i.e. the DOC production rate increases as the number of algal cells increases. Algae are photosynthetic organisms, which means that they are able to harness light energy and fix carbon dioxide. *C. reinhardtii* also has a carbon concentrating mechanism (see figure 1.5 for details), meaning that it can utilise bicarbonate as a carbon source, but this is not incorporated into the model explicitly. For simplicity, the model considers carbon dioxide and bicarbonate as one entity (i.e. DIC), meaning that photosynthetic assimilation of DIC corresponds to the uptake of both forms of inorganic carbon. For the model, the rate of photosynthesis is analogous to the rate of DIC uptake and according to total carbon conservation this must be equal to the sum of the algal carbon biomass growth rate and DOC export rate (i.e. the carbon fluxes must balance so that the total amount of carbon is conserved within the system). One further consideration incorporated into the model is that there might be an unequal contribution to DOC exudation from different components of the algal biomass. Realistically, the DOC could originate from several components and until further work is done to identify the organic molecules being exuded by algae, the specific source of DOC exchanged between *C. reinhardtii metE7* and *M. loti* is unknown. There are several proposed mechanisms for the release of DOC from algal cells, including active and passive removal of excess carbon fixed during photosynthesis, passive diffusion driven by a concentration gradient across the cell membrane and release of organic material due to cell death (Fogg, 1983; Thornton, 2014). The mechanism for DOC production incorporated into the model is via excess photosynthate because the model considers cultures with a healthy population of cells such that cell death is assumed to be negligible. The parameter ϕ_s is introduced, which is named the storage parameter, and refers to the fraction of algal biomass that does not contribute to DOC export but is used by algae for their own biosynthesis pathways and for storage. Increasing ϕ_s decreases the DOC exudation rate and correspondingly also decreases the rate of photosynthesis. It is important to note that the labelling dynamics for algae and for DOC are affected by how DOC export is considered. For example, when the DIC is labelled, the DOC becomes labelled more quickly as ϕ_s increases, because the carbon contributing to DOC exudation (the 'photosynthetically active' carbon) makes up a smaller proportion of the algal biomass, meaning that it is more quickly replaced by labelled carbon from DIC.

Heterotrophic bacteria rely on an external source of organic carbon for their energy requirements and as an elemental building block for their cellular biomass growth and repair. Section 1.2.3 outlines the carbon metabolic processes of heterotrophic bacteria relevant to the co-culture model, i.e. growth, respiration and DIC assimilation. The model defines a bacterial population growth rate that is dependent on the external DOC concentration and uses a constant carbon yield to relate the bacterial carbon biomass growth to population growth. Due to the fact that bacteria must respire in order to produce the ATP required to drive cellular metabolism, a significant fraction of the carbon assimilated by bacteria will be transformed into carbon dioxide through respiration. To define how much carbon is used for respiration, η' is introduced, which is the bacterial growth efficiency defined as the amount of bacterial carbon biomass produced per unit of carbon consumed. In order for the carbon fluxes to remain balanced, while also maintaining an active carbon turnover at carrying capacity, the bacterial growth efficiency is a maximum in the exponential growth phase and decreases as the bacterial cell density increases, with $\eta' = 0$ at carrying capacity. Inorganic carbon assimilation by heterotrophic bacteria is included in the model through the parameter X, defined as the fraction of total carbon uptake by bacteria that comes from DIC.

The model provides a general description of the B_{12} kinetics, capturing the essential details that affect the co-culture dynamics. The B_{12} production rate is linearly proportional to the bacterial cell density, i.e. there is a constant production rate per bacterial cell. The B_{12} uptake rate by algae is defined by considering the uptake required to account for the B_{12}-dependent growth rate and using a constant for the amount of B_{12} per cell.

Overall, the co-culture model results in an algal growth that is dependent on the B_{12} produced by bacteria, with photosynthetic uptake of DIC accounting for the algal carbon biomass growth and DOC exudation. The bacterial growth is dependent on the DOC produced by algae, respiration produces carbon dioxide (DIC) and provides the bacteria with the energy they require to grow. In addition to DOC uptake, bacteria are also able to assimilate DIC as a source of carbon. From this simplified interpretation of microbial metabolism within an algal-bacterial co-culture, equations for the carbon isotope labelling dynamics were obtained assuming that isotopic fractionation has a negligible effect (see section 3.2.7 for details).

3.5 Conclusion and outlook

F. J. Peaudecerf *et al.* (2018) developed a mutualism at a distance model to study an algal-bacterial mutualism in which bacteria provide algae with vitamin B_{12} and algae provide bacteria with an organic carbon source. The model developed by F. J. Peaudecerf *et al.* (2018) considers the nutrient exudation and uptake dynamics, together with the nutrient diffusion between spatially separated populations of algae and bacteria. The zero-distance limit of this model is comparable to a mixed co-culture in which the algae and bacteria are grown together in a well mixed flask, as was performed in the experiments described in chapter 2. In this chapter, the zero-distance limit of the mutualism at a distance model was taken as a starting point for considering the carbon isotope labelling dynamics for an algal-bacterial co-culture. The extended model developed in this chapter incorporates the carbon dynamics associated with algal photosynthesis, DOC exudation originating from excess algal photosynthate, bacterial respiration and bacterial assimilation of inorganic carbon. Nondimensionalising the model variables allowed for the determination of characteristic dimensionless model parameters. The growth and nutrient dynamics of the extended model were used to obtain equations for the carbon isotope labelling dynamics for an algal-bacterial co-culture, illustrating that without taking into account the rate of loss from a particular carbon pool, the labelling rate would overestimate the growth rate.

A positive, non-zero fixed point was determined for the model, which resulted in the determination of two inequality constraints for the model parameters. The fixed point stability was assessed using the Jacobian matrix and was found to be asymptotically stable.

For constant exponential growth rates, analytical solutions for the atomic fractions of ^{13}C in algae and bacteria were obtained. The analytical result for bacteria illustrated that a higher atomic fraction of ^{13}C for the inorganic and organic carbon in the media or a lower bacterial growth efficiency (i.e. higher rate of respiration) increases the isotope labelling rate for bacteria. For algae, the analytical results considered the limits of high and low carbon storage, which suggest that for an increase in the fraction of stored carbon, it is expected that the isotope labelling rate for algae decreases. However, this effect of storage is minimal when the organic carbon exudation parameter is small compared to the carbon uptake parameter.

The co-culture model developed in this chapter, and the isotope labelling dynamics associated with it, is tested in chapter 4, where parameter optimisations are carried out using the experimental results presented in chapter 2. The general principles used in this chapter to construct the co-culture model could be extended to model other microbial mutualisms with different nutrient exchanges.

Chapter 4

Parameter optimisations and model predictions

4.1 Introduction

This chapter brings together the experimental observations from chapter 2 and the mathematical model developed in chapter 3 for an algal-bacterial co-culture in which B_{12} and carbon are exchanged between the two microorganisms. The aim of this chapter is to obtain a full set of model parameters and to test the validity of the model by seeing how well it captures the experimentally observed growth and labelling dynamics.

Estimating model parameters: least squares method

The ultimate test of a model's validity is its predictive ability and whether its behaviour is in agreement with experiment, but since simplifying assumptions are required when constructing any mathematical description of a biological system, some divergence between the model and data is expected (Allman *et al.*, 2018). Testing how well a model describes a set of data points typically involves determining the free parameter values that bring the model results closest to the experimental observations. The least squares analysis provides estimates of model parameters by minimising the sum of the squared deviations of the observations from the model predictions (Brown *et al.*, 1993), i.e. minimising

$$r^2 = \sum_t \left(y_{exp}(t) - y_{model}(t)\right)^2, \tag{4.1}$$

which is a sum over all time points in the experiment, with y_{exp} and y_{model} the experimentally observed and model values respectively. This analysis determines the parametrisation of the model that gives the best fit with experimental observations.

Applications of dynamic models in biology

A dynamic model consists of equations that describe the processes thought to account for experimental observations, which is different to a descriptive model that only aims to reproduce observations without the need for mechanistic detail (Ellner *et al.*, 2006). In this chapter two advantages of having a dynamic model for an algal-bacterial co-culture are explored:

- *To develop scientific understanding*. A model encodes a hypothesis and makes experimentally testable predictions, meaning that it provides a practical method for comparing a hypothesis with observation. In this chapter, parameter optimisation is used to test if the model is capable of capturing both the growth and carbon isotope labelling dynamics measured experimentally in chapter 2. Additionally, the model is used to generate hypotheses for what the main contributing factors are for the observed distributions in the single cell results for the atomic fractions of ^{13}C for bacteria in both axenic and co-culture populations.
- *To make predictions*. Once a model has been parametrised satisfactorily, it can be used to make predictions for different scenarios. This chapter explores how changing an initial condition or model parameter impacts the expected growth and nutrient dynamics. Such predictions could be extended to more complex systems that involve several interacting microorganisms and could therefore be helpful in understanding the contribution of algal-bacterial interactions to the carbon cycle or when designing synthetic microbial communities.

4.2 Parameter optimisations

In chapter 3 a mathematical model was developed to capture the essence of the growth and nutrient dynamics for an algal-bacterial co-culture, in which bacteria provide B_{12} to algae and algae provide organic carbon to bacteria. The co-culture model in its non-dimensional form is outlined in section 3.2.6 and the corresponding isotope labelling dynamics are defined in section 3.2.7. The equations of the model have several free parameters that determine its behaviour. In order to test how effectively the model represents the algal-bacterial carbon dynamics, the experimental results described in chapter 2 for *C. reinhardtii metE7* and *M. loti*

grown alone and in co-culture were used to parametrise the model. In order for experimental data to adequately constrain the model during parameter optimisations the number of free parameters should be less than the number of experimental data points, which is true for all parameter optimisations performed in this work.

4.2.1 Methods

Estimating parameters using the basic model

Several of the parameters for a co-culture between *C. reinhardtii metE7* and *M. loti* were obtained by François Peaudecerf (at the time a PhD student at the Department of Applied Mathematics and Theoretical Physics, University of Cambridge), who used the basic co-culture model (section 3.2.1) to run a global fit of three independent co-culture experiments that were performed by Freddy Bunbury (at the time a PhD student at the Department of Plant Sciences, University of Cambridge), see figure 4.1 for the experimental and fit results. The experiments measured colony forming units, particle counts and vitamin B_{12} concentrations for three independent co-cultures between *C. reinhardtii metE7* and *M. loti*. The parameters obtained are listed in table 4.1, but there were some parameters of the model that remained unknown because the experiments did not measure carbon explicitly. Estimates for the carbon yield of algae and bacteria ($Y_{a,c}$ and $Y_{b,c}$ respectively) were obtained in this work from dry mass measurements and isotope ratio mass spectrometry (IRMS) results (see appendix C for more details). From these carbon yield values the remaining parameters of the basic co-culture model (i.e. without photosynthesis, algal carbon storage, bacterial respiration and bacterial DIC uptake) were estimated and are listed in table 4.1.

Parameter optimisations for the extended model

In order to minimise the number of free parameters, the parameters obtained for the basic model (table 4.1) were used in the parameter optimisations for the extended model (i.e. the model that includes photosynthesis, algal storage, bacterial respiration and bacterial DIC uptake). Table 4.1 shows that the estimated value for the DOC production strength for algae is $s_c = 0.021$, but when photosynthesis and storage are introduced into the model (section 3.2.2) the DOC production strength becomes dependent on the fraction of storage, i.e. $s_c = s_c'(1-\phi_s)$, therefore the parameter optimisations discussed in this chapter had s_c' as a free parameter. Additionally, the parameters K_b, μ_b, K_c and $k_{b,c}$ were included as free parameters for the axenic cultures of bacteria, i.e. they were not taken as the values in table 4.1 determined from co-culture experiments, because it is reasonable to expect that these parameters might be different for *M. loti* grown axenically and in a co-culture.

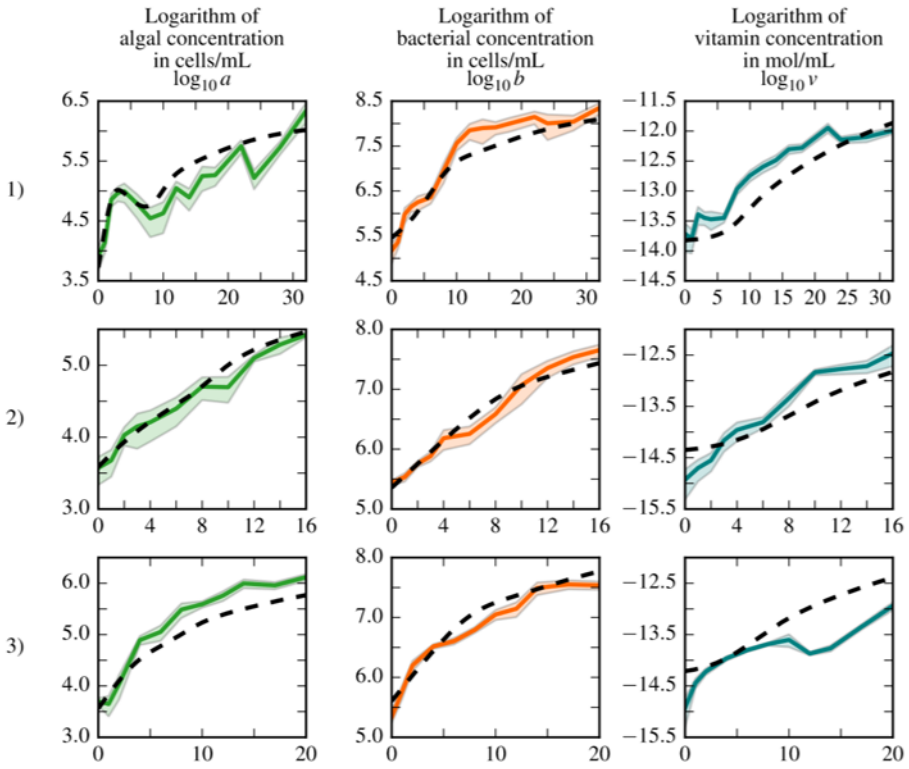

Figure 4.1 **Parameter optimisation for the Peaudecerf co-culture model, i.e. the 'basic model'**. Fit of data obtained for co-cultures of *C. reinhardtii metE7* and *M. loti*. Each row of plots corresponds to an independent experiment, with the first column the evolution of algal density, in the second column the evolution of bacterial density and in the third column the evolution of vitamin concentration as determined by bioassy. The mean of each variable appears as a continuous line, with the shaded region showing the standard deviation. The global fit with a unique set of parameters for the three independent experiments is shown in black dashed lines. This figure was created by François Peaudecerf.

Parameter optimisations were performed by fitting the mathematical model to the experimental results for the stable isotope labelling cultures of both algae and bacteria alone and in co-culture. Growth was measured using viable counts and the atomic fractions were taken as the mean value of the dilution corrected, single cell measurements obtained using SIMS (chapter 2). Experimental errors were not included as weights in the objective function of the parameter optimisations because they were relatively small. The Matlab ordinary differential equation solver *ode45* was used to numerically solve the model equations. The parameter optimisations were performed as a global search of the parameter space, meaning that several minimisations were run with different starting points in order to obtain the best estimate for the set of parameters that minimise the deviation of the model from experiment and that satisfy the boundary conditions (table 4.2) and inequality constraints (table 4.3). The

Table 4.1 **Basic model parameter values**. Model parameter values for the co-culture were obtained from a global fit of the basic model (section 3.2.1), which was performed by Fançois Peaudecerf using three independent co-culture experiments done by Freddy Bunbury. The carbon yield values were estimated from dry mass measurements and IRMS analysis, details of which are given in appendix C.

Parameter value		Units	Definition
K_a	$2.3 \times 10^{6\dagger}$	cells mL^{-1}	Algal carrying capacity
K_b	$1.14 \times 10^{9\dagger}$	cells mL^{-1}	Bacterial carrying capacity
K_v	$2.6 \times 10^{-14\dagger}$	mol mL^{-1}	B_{12} half-saturation concentration for algae
μ_b	$0.42^{\dagger}$	h^{-1}	Maximum bacterial growth rate
ε	$0.51^{\dagger}$		Ratio of maximum growth rates; μ_a/μ_b
$k_{a,v}$	$7.8^{\dagger}$		Algal B_{12} uptake parameter; $K_a/(K_v\, Y_{a,v})$
$k_{b,c}$	$3.6^{\dagger}$		Bacterial carbon uptake parameter; $K_b/\left(K_c\, Y_{b,c}\right)$
s_c	$0.021^{\dagger}$		DOC production strength; $(p_c\, K_a)\,/\,(\mu_b\, K_c)$
s_v	$4.2^{\dagger}$		B_{12} production strength; $(p_v\, K_b)\,/\,(\mu_a\, K_v)$
$Y_{a,c}$	4×10^{12} ‡	cells molC^{-1}	Algal carbon yield
$Y_{b,c}$	5×10^{14} ‡	cells molC^{-1}	Bacterial carbon yield
K_c	6.3×10^{-7} •	molC mL^{-1}	DOC half-saturation concentration or bacteria
$k_{a,c}$	0.91^{*}		Algal carbon uptake parameter; $K_a/(K_c\, Y_{a,c})$

† From François Peaudecerf's fit to Freddy Bunbury's data.
‡ From IRMS samples (appendix C).
• Calculated using $K_c = K_b/(Y_{b,c}\, k_{b,c})$.
* Calculated using $k_{a,c} = (K_a\, Y_{b,c}\, k_{b,c})\,/\,(K_b\, Y_{a,c})$.

boundary conditions for ϕ_s, η and X constrained these parameters to values between 0 and 1, as required by their definitions. Other boundary conditions were chosen in order to reduce the parameter search space to biologically reasonable values and save computation time. The inequality constraints came from the positive fixed point existence criterion discussed in section 3.3.1. Global parameter optimisations were done using the *GlobalSearch* and *createOptimProblem* functions in Matlab's global optimisation toolbox, with *fmincon* as the solver for each minimisation. The *fmincon* solver is a gradient-based, first-order iterative optimisation algorithm for finding the local minimum of a function by following a gradient descent method that takes steps proportional to the negative of the gradient of the function. The *GlobalSearch* algorithm in Matlab is a type of basin-hopping algorithm that repeatedly runs the *fmincon* local solver using different starting points and thus generates a list of local minima while aiming to locate the solution with the lowest objective function value. All default settings were used except for the *StartPointsToRun* property of the *GlobalSearch* function, which was selected to run with the *bounds-ineqs* option, meaning that all starting

points for the minimisations had to lie within the boundary conditions (table 4.2) and satisfy the inequality constraints (table 4.3). The *GlobalSearch* algorithm can be briefly summarised as:

- Run *fmincon*: the local minimisation solver *fmincon* is run from the given start point. If this run converges, *GlobalSearch* records the final objective function value for use in the score function (for points that lie within the boundary constraints the score function is equal to the objective function value).
- Generate trial points: a set of trial points, i.e. potential start points, are generated using a scatter search algorithm.
- Stage 1: the score function is evaluated for a subset of the trial points. Then *fmincon* is run using the point with the best score as the starting point and the subset of trial points are removed from *GlobalSearch*'s list of points to examine.
- Stage 2: one at a time, the remaining trial points are examined to determine if a local minimisation using *fmincon* reveals a new local minimum.
- Output: after reaching a maximum time threshold or running out of trial points, *GlobalSearch* creates a vector of local minima ordered by their objective function value, from lowest (best) to highest (worst).

The minimised objective function value (i.e. the residual sum of squares) was used as an estimate for the goodness of fit. Errors for individual parameters were not provided by the output of the *GlobalSearch* algorithm. For future work, if estimates for the individual errors are required, two methods that could be employed are described by Meisl *et al.* (2014). The first approach uses Markov chain Monte Carlo, which involves sampling points in the parameter space close to the found minimum, and quantifying how much of an effect on the minimised objective function each parameter has. The result estimates how strongly the given dataset constrains the parameters to their fitted values and provides estimates for the individual errors. This method was not used for this work because it would have required an extensive amount of additional code. The alternative approach used by Meisl *et al.* (2014) estimates how much experimental variation influences the fitted parameters by running separate fits for data from different experimental replicas. Not enough replicas were performed in this work, so this second method could also not be used to estimate the individual errors.

Table 4.2 **Boundary conditions for the parameter optimisations**. These were the boundary conditions used for the various free parameters and free initial conditions of the parameter optimisations run for axenic algae, axenic bacteria and the co-culture. When units are not specified the parameter/initial condition is in dimensionless units (see section 3.2.6 for details of the nondimensionalisation). These boundary conditions for ϕ_s, η and X came from their definition requiring these parameters to be between 0 and 1. Other boundary conditions were chosen to ensure that the parameter optimisation results were reasonable when considering their biological interpretation.

	Boundary condition					Units
All parameter optimisations:	0	$\leq$	ϕ_s	$\leq$	0.99	
	0.01	$\leq$	η	$\leq$	1	
	0	$\leq$	X	$\leq$	1	
Axenic algae:	0	$\leq$	s_c'	$\leq$	10	
	0	$\leq$	$v(0)$	$\leq$	5	
	0.001	$\leq$	$a(0)$	$\leq$	0.01	
	0	$\leq$	$f_i(0)$	$\leq$	1	
Axenic bacteria:	1×10^{7}	$\leq$	$b(0)$	$\leq$	1×10^{8}	cells mL^{-1}
	1×10^{8}	$\leq$	K_b	$\leq$	1×10^{13}	cells mL^{-1}
	0.01	$\leq$	μ_b	$\leq$	2	h^{-1}
	1×10^{-10}	$\leq$	K_c	$\leq$	1×10^{-4}	molC mL^{-1}
Axenic bacteria, no glycerol:	0	$\leq$	$c_o(0)$	$\leq$	4×10^{-7}	molC mL^{-1}
Co-culture:	0	$\leq$	s_c'	$\leq$	10	
	0.001	$\leq$	$a(0)$	$\leq$	0.01	
	0.001	$\leq$	$b(0)$	$\leq$	0.03	
	1×10^{-5}	$\leq$	$c_o(0)$	$\leq$	0.5	
	0.0108	$\leq$	$f_o(0)$	$\leq$	1	

Table 4.3 **Non-linear constraints for parameters of the co-culture model**. The parameters of the model must satisfy these inequality constraints in order for a fixed point to exist at positive values for the concentration of DOC c_o^* and B_{12} v^* (see section 3.3.1).

Non-linear constraint	Comment
$(1-\phi_s)\ s_c'\ \eta - k_{b,c}(1-X) < 0$	Ensures a positive value of c_o^*
$s_v - k_{a,v} < 0$	Ensures a positive value of v^*

4.2.2 Axenic algae

From the non-dimensional co-culture model given in section 3.2.6, an axenic algal culture can be modelled by setting the initial bacterial concentration to zero (i.e. $b(0) = 0$). Two parameter optimisations for the model of axenic algae were performed using the experimental results from the axenic culture of *C. reinhardtii metE7* detailed in section 2.3.5, one included storage in the model (i.e. ϕ_s was a free parameter) and the other neglected storage (i.e. $\phi_s = 0$). The objective function minimised by these parameter optimisations is given by

$$r^2(a, f_a) = \sum_t \left(\frac{a_{model}(t) - a_{exp}(t)}{a_{exp}(t)} \right)^2 + \left(\frac{f_{a,model}(t) - f_{a,exp}(t)}{f_{a,exp}(t)} \right)^2, \qquad (4.2)$$

which gives a measure for the deviation of the model from the experiment for both the algal cell density a and atomic fraction of ^{13}C for the algal biomass f_a. In equation (4.2) the sum corresponds to the sum over all time-points in the experiment, the subscript 'model' refers to the value obtained from the model and the subscript 'exp' refers to the value measured experimentally. Since two experimental variables were used to fit the model, a modified version of the least squares method was used, meaning that the terms in the sum correspond to the deviation of the model from experiment taken relative to the experimental values, which ensure that the two variables contribute equally to r^2 (equation (4.2)). This relative weighting in r^2 also ensures that every time point contributes to the same extent, for example without this weighting the deviation of cell numbers in early exponential phase would be negligible compared to a small relative deviation in late exponential phase.

Free parameters and initial conditions

In addition to the free parameters ϕ_s and s'_c, some initial conditions were unknown and therefore kept free for the parameter optimisations. For the experiment, it was assumed that initially there was no DOC in the media, the DIC was in excess and the algae were initially unlabelled, therefore initial conditions of the model were fixed at $c_o(0) = 0$, $c_i(0) = 5$, $f_a(0) = 0.0108$ and $f_o(0) = 0.0108$. No reliable measurement for the initial algal cell density was obtained and although the initial B_{12} concentration was $100\,\mathrm{ng\,L^{-1}}$, the model for algal growth neglects the internal B_{12} recycling dynamics and so the B_{12} concentrations in the model do not necessarily correspond to the quantitative values of the experiment, therefore the initial algal cell density and B_{12} concentration were free in the parameter optimisations. As discussed in section 2.2.3, although the ^{13}C-bicarbonate used for the stable isotope labelling cultures had 98 atom% ^{13}C, due to the equilibria between different forms of inorganic carbon, the actual atomic fraction of ^{13}C for the DIC assimilated by the algae is

unknown, therefore the initial condition $f_i(0)$ was also free in the parameter optimisations. Overall there were 5 free parameters and initial conditions, which was less than the number of experimental data points (i.e. 9 data points: 5 f_a and 4 a measurements).

Discussion of the parameter optimisation results

The results for the two parameter optimisations, one with storage (ϕ_s is a free parameter), one without ($\phi_s = 0$), showed that in both cases the minimised r^2 values were similar with only a small improvement for the model with storage (see table 4.4 and figure 4.2). The main difference between the two sets of results was in the value of the DOC production strength s'_c. The analytical results for the low and high storage limits in section 3.3.2 show that the algal labelling rate is affected by the value of s'_c more significantly in the low storage limit (i.e. $\phi_s \to 0$). This means that both increasing the storage fraction (i.e. $\phi_s \to 1$) or decreasing the DOC production strength (i.e. $s'_c/k_{a,c} \to 0$) have the overall effect of decreasing the isotope labelling rate of algae towards the limit $f_a \to (f_i - f_a)\ \varepsilon\ (1-a)\ v/(1+v)$. When $s'_c/k_{a,c} \ll \varepsilon\ (1-a)\ v/(1+v)$, meaning the DOC production strength relative to the carbon uptake for algae is small compared to the growth rate, the storage fraction has little effect on the isotope labelling. However, for higher values of $s'_c/k_{a,c}$, increasing the storage fraction decreases the rate of isotope labelling. This interconnected effect of s'_c and ϕ_s on the isotope labelling dynamics is illustrated in figure 4.2 using the parameter optimisation results, and shows that the parameter optimisations achieved a reasonable fit to experiments by either decreasing s'_c or increasing ϕ_s. In order to confidently parametrise the DOC exudation rate determined by $s_c = s'_c(1-\phi_s)$, measurements of the DOC concentration would be necessary in addition to measurements of algal growth and isotope labelling. The value of $s_c = s'_c(1-\phi_s)$ obtained from the fit results for the model with storage was greater than for the model without storage (i.e. 0.277 compared with 0.041), meaning that the storage model predicted a higher DOC exudation rate. Algal carbon storage is likely to be something that is important, and there is some indication of this in the SIMS analysis of algal cells, which show heterogeneity in the distribution of ^{13}C (sections 2.2.6 and 2.3.1). Therefore, the results with storage were chosen to be carried forward. In particular, the result for the initial atomic fraction of ^{13}C for the DIC, $f_i(0) = 0.65$, was used for axenic bacteria and the co-culture.

Table 4.4 **Parameter optimisation results for axenic algae**. Results for two optimisations, one with storage (ϕ_s as a free parameter), one without ($\phi_s = 0$), using SIMS results for *C. reinhardtii metE7*. The parameter s'_c was free, and the free initial conditions were $a(0)$, $v(0)$ and $f_i(0)$. All other parameter values used were as specified in table 4.1. The fixed initial conditions were $c_o(0) = 0$, $c_i(0) = 5$, $f_a(0) = 0.0108$ and $f_o(0) = 0.0108$, since in the experiment it was assumed that initially there was no DOC in the media, the DIC was in excess and the algae were initially unlabelled. The value $r^2(a, f_a)$ is the residual sum of squares for the fit, meaning it gives a measure for the goodness-of-fit.

Fit	ϕ_s	s'_c	$a(0)$	$v(0)$	$f_i(0)$	$r^2(a, f_a)$
With storage	0.87	2.13	0.0032	0.374	0.65	0.313
Without storage	0	0.041	0.0032	0.379	0.60	0.323

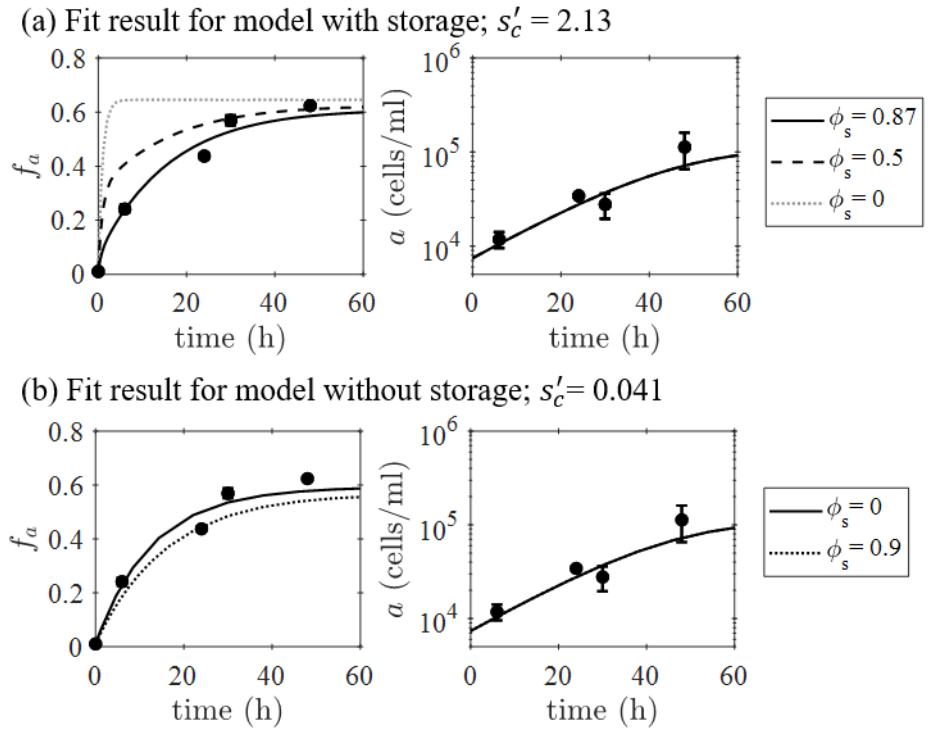

Figure 4.2 **Parameter optimisation results for axenic algae and the effect of the storage fraction parameter** ϕ_s. The solid black lines show the fit results for two parameter optimisations performed for an axenic culture of *C. reinhardtii metE7*, (a) including storage (i.e. with ϕ_s as a free parameter, which gave $s'_c = 2.13$) and (b) neglecting storage (i.e. with $\phi_s = 0$, which gave $s'_c = 0.041$). The parameter optimisations used the experimental data points (circles) of both the isotope fraction f_a and the algal population size a, with the full results given in table 4.4. The dotted and dashed lines show how ϕ_s affects the two different results. (a) For the fit result obtained for the model with ϕ_s as a free parameter, a decrease in ϕ_s would increase the rate of labelling but has no affect on the growth rate. (b) If storage is re-introduced to the fit result for the model without storage (i.e. $\phi_s = 0$), there is only minimal change in the time evolution of the model variables. This illustrates that the model is more sensitive to the value of ϕ_s when s'_c is small.

4.2.3 Axenic bacteria

An axenic culture of bacteria can be modelled using the set of equations that come from the non-dimensional co-culture model given in section 3.2.6 and setting the initial algal cell density to zero (i.e. $a(0) = 0$). A global parameter optimisation was performed for axenic bacteria using the experimental results of four cultures of *M. loti*, each grown with a different concentration of glycerol (section 2.3.4). The objective function minimised by the global parameter optimisation is given by

$$r^2(b, f_b) = \sum_{all\ cultures} \sum_{t} \left(\frac{b_{model}(t) - b_{exp}(t)}{b_{exp}(t)} \right)^2 + \left(\frac{f_{b,model}(t) - f_{b,exp}(t)}{f_{b,exp}(t)} \right)^2, \qquad (4.3)$$

with the sum over *all cultures* indicating that the aim was to minimise the difference between the model and the experimental results for the bacterial cell density b and the atomic fraction of ^{13}C for bacteria f_b for all four axenic cultures simultaneously.

Free parameters and initial conditions

The model parameters for axenic bacteria were considered as global parameters, with the exception of η and X that could have values specific to the different cultures. The carrying capacity, maximum growth rate and carbon uptake parameter for bacteria (K_b, μ_b and $k_{b,c}$ respectively) in table 4.1 were obtained for *M. loti* in co-culture with *C. reinhardtii metE7*, however these might not be the same as for *M. loti* grown in axenic cultures in which the bacteria were grown with glycerol as their organic carbon source. Therefore K_b, μ_b and K_c were kept as free global parameters for axenic bacteria. Using $Y_{b,c} = 5 \times 10^{14}\,\text{cells}\,\text{molC}^{-1}$ obtained from dry mass measurements and IRMS results (see appendix C), the value for the carbon uptake parameter $k_{b,c}$ was updated throughout the parameter optimisation as K_b and K_c changed, according to the parameter definition $k_{b,c} = K_b / \left(Y_{b,c} K_c\right)$.

For the experiments it was assumed that the DIC was in excess and had an atomic fraction of ^{13}C taken as the estimate obtained from the parameter optimisation for axenic algae, meaning $c_i(0) = 5$ and $f_i(0) = 0.65$ (see section 4.2.2). Initially, there was no B_{12} in the media, the bacteria were at natural abundance and the glycerol was unlabelled; therefore the corresponding initial conditions of the model for all four cultures of axenic bacteria were fixed at $v(0) = 0$, $f_b(0) = 0.0108$ and $f_o(0) = 0.0108$. The initial DOC concentrations were calculated for 0.1 %, 0.01 % and 0.001 % glycerol concentrations to be 4×10^{-5}, 4×10^{-6} and $4 \times 10^{-7}\,\text{molC}\,\text{mL}^{-1}$ respectively, using the molar mass of glycerol, $92.09\,\text{g}\,\text{mol}^{-1}$, and its density, $1.26\,\text{g}\,\text{mol}^{-1}$. Although it is expected that the axenic culture grown without glycerol had no DOC in the media, the experimental results suggest that there is still a

small amount of bacterial growth (section 2.3.4), which could be due to the bacteria from the pre-culture having an internal store of organic carbon. In order to account for this observation, $c_o(0)$ for the 'no glycerol' culture was kept free, but was constrained to be less than 4×10^{-7} molC mL^{-1} (i.e. 0.001 % glycerol). No reliable measurement for the initial bacterial cell density was obtained experimentally, therefore $b(0)$ for each of the cultures was kept free during the global parameter optimisation. This means that in total there were 16 free parameters and initial conditions, which was less than the number of experimental data points (i.e. 30 data points: 14 f_b and 16 b measurements).

Table 4.5 **Parameter optimisation results for axenic bacteria**. Results for the global parameter optimisation performed for the four axenic cultures of *M. loti* grown with 0.1 %, 0.01 %, 0.001 % and no glycerol, with global free parameters K_b, μ_b and K_c. The free parameters and initial conditions that were permitted to be different for the different cultures were η, X and $b(0)$. The initial DOC concentration $c_o(0)$ for the culture grown without glycerol was also included as a free parameter. All other parameter values used were as specified in table 4.1. The fixed initial conditions were $c_i(0) = 5$, $v(0) = 0$, $f_b(0) = 0.0108$, $f_o(0) = 0.0108$ and $f_i(0) = 0.65$, since for the experiments it was assumed that the DIC was in excess, initially there was no B_{12} and the bacteria had natural abundance, the glycerol was unlabelled and the atomic fraction of ^{13}C in the DIC was taken as the estimate obtained from the parameter optimisation for axenic algae (see section 4.2.2). The residual sum of squares for this global parameter optimisation result was 2.55, whereas when respiration is not included in the model it was 4.31.

Global parameters

K_b cells mL^{-1}	μ_b h^{-1}	K_c molC mL^{-1}	$k_{b,c}$ †
1.2×10^{12}	0.138	1.2×10^{-6}	1982

Culture specific parameters

culture	$c_o(0)$ molC mL^{-1}	η	X	$b(0)$ cells mL^{-1}
0.1 %	4×10^{-5} ‡	0.52	0.048	1.0×10^7
0.01 %	4×10^{-6} ‡	0.14	0.042	1.4×10^7
0.001 %	4×10^{-7} ‡	0.33	0.021	1.7×10^7
no glycerol	1.3×10^{-7}	0.79	0.010	1.4×10^7

† Calculated using $k_{b,c} = K_b / (Y_{b,c} K_c)$ and $Y_{b,c} = 5 \times 10^{14}$ cells molC^{-1}.
‡ Not free in the parameter optimisation, calculated from the % glycerol concentration using the molar mass of glycerol, 92.09 g mol^{-1}, and its density, 1.26 g mol^{-1}.

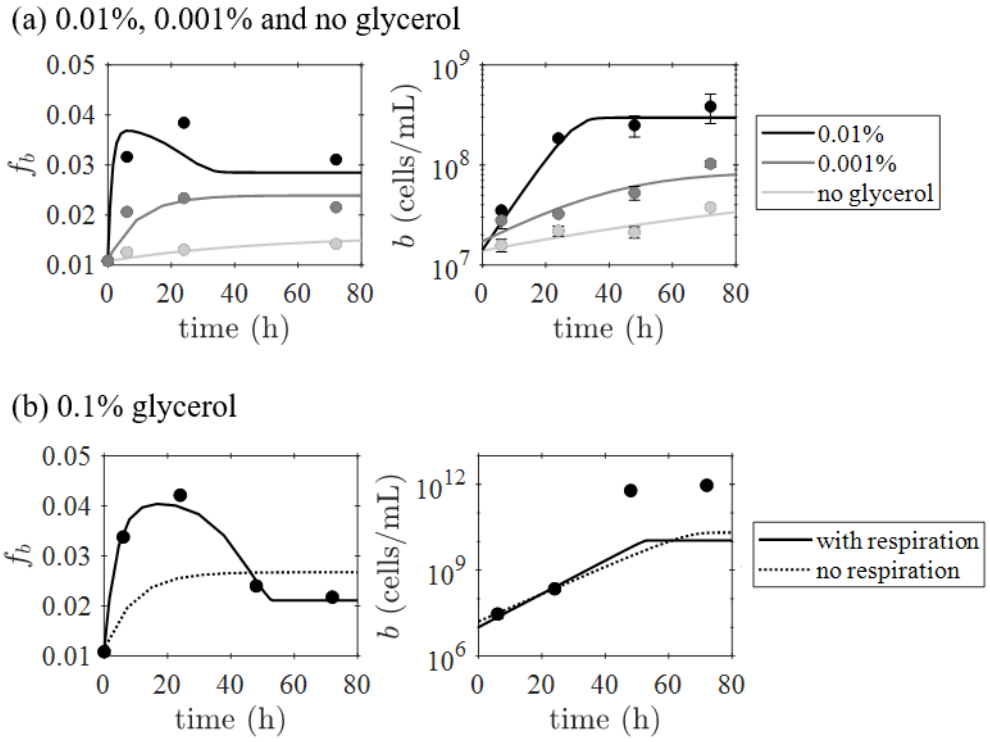

Figure 4.3 **Parameter optimisation results for axenic bacteria**. (a) The parameter optimisation results for the axenic cultures of *M. loti* grown with 0.01 %, 0.001 % and no glycerol (see table 4.5). (b) Comparison of the parameter optimisation result with and without respiration for the axenic culture of *M. loti* grown with 0.1 % glycerol. The circles are experimental data points and the lines indicate the parameter optimisation results. For the model that includes respiration the parameter results are given in table 4.5. The global parameter optimisation that neglected respiration (i.e. $\eta' = 1$) gave parameter values: $K_c = 7.6 \times 10^{-6}\,\mathrm{molC\,mL^{-1}}$, $K_b = 1.2 \times 10^{11}\,\mathrm{cells\,mL^{-1}}$, $\mu_b = 0.132\,\mathrm{h^{-1}}$ and $b(0) = 1.6 \times 10^{7}\,\mathrm{cells\,mL^{-1}}$ and $X = 0.025$ for the 0.1 % glycerol culture.

Discussion of the parameter optimisation results

The results from the global parameter optimisation show a good agreement between the model and experiment (see table 4.5 and figure 4.3). Large ranges for the bacterial growth efficiency, η', are quoted in the literature, for example 0.05-0.6 in Giorgio *et al.* (1998). The inorganic carbon assimilation is expected to be small relative to the total carbon biomass, for example approximately 1.4-6.5% of bacterial carbon biomass was estimated to be derived from carbon dioxide in Roslev *et al.* (2004). The results for the bacterial growth efficiency η and inorganic carbon uptake parameter X in table 4.5 correspond well with these observations from the literature.

If the inorganic carbon uptake by bacteria were not included in the model (i.e. $X = 0$), f_b would be expected to remain at natural abundance because the glycerol was unlabelled. For the model that neglects respiration (i.e. $\eta' = 1$), the global parameter optimisation results could not reproduce the experimentally observed peak in f_b (see figure 4.3b), which is likely to be because only with respiration is there a feedback loop of carbon from bacteria to DIC. These results illustrate that the model successfully describes bacterial DIC uptake and respiration, which are both necessary to account for the experimental observations for the axenic cultures of bacteria.

No overall trend was observed for the bacterial growth efficiency η as the concentration of glycerol increases (table 4.5). However, table 4.5 and figure 4.4 suggest that for a higher initial concentration of glycerol, the bacteria assimilate a higher fraction of inorganic carbon, i.e. X increases. A fit of the equation

$$X = m \ln(c_o(0)) + n \tag{4.4}$$

was performed in Microsoft Excel, with results $m = 0.0067 \pm 0.0012$ and $n = 0.120 \pm 0.017$, which is plotted in figure 4.4.

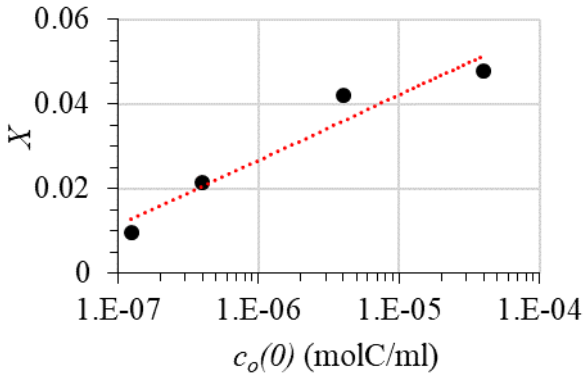

Figure 4.4 **DIC uptake parameter depends on the initial DOC concentration**. The relationship between the fraction of total carbon uptake by bacteria that comes from DIC, X, and the initial DOC concentration was approximated with a logarithmic fit using the equation $X = m \ln(c_o(0)) + n$, giving $m = 0.0067 \pm 0.0012$ and $n = 0.120 \pm 0.017$.

4.2.4 The algal-bacterial co-culture

In order to test whether the co-culture model defined in chapter 3 is able to capture, at least qualitatively, the SIMS results for the co-culture between *C. reinhardtii metE7* and *M. loti* (section 2.3.6), a series of different parameter optimisations were performed, and the results are compared in table 4.6. The objective function minimised by the parameter optimisations is given by

$$r^2(a,b,f_a,f_b) = \sum_t \left(\frac{a_{model}(t)-a_{exp}(t)}{a_{exp}(t)}\right)^2 + \left(\frac{b_{model}(t)-b_{exp}(t)}{b_{exp}(t)}\right)^2 + \left(\frac{f_{a,model}(t)-f_{a,exp}(t)}{f_{a,exp}(t)}\right)^2 + \left(\frac{f_{b,model}(t)-f_{b,exp}(t)}{f_{b,exp}(t)}\right)^2, \tag{4.5}$$

which gives a measure for the deviation of the model from the experiment for both the cell densities (a and b for algae and bacteria respectively) and the atomic fractions of ^{13}C (f_a and f_b for algae and bacteria respectively).

Free parameters and initial conditions

Initial conditions were fixed at $c_i(0) = 5$ and $v(0) = 0$ because the DIC was in excess and there was no B_{12} added to the media. The initial value used for the atomic fraction of ^{13}C for the DIC was the estimate obtained from the parameter optimisation for axenic algae in section 4.2.2, i.e. $f_i(0) = 0.65$. The co-culture was inoculated with pre-labelled algae, therefore the 48 h time-point of the pre-labelling culture was used to estimate the initial ^{13}C atomic fractions in the algae and DOC in the co-culture. Using the axenic algae model that includes storage and the parameter results in section 4.2.2, estimates for the initial conditions $f_a(0) = 0.59$, $f_{a,p}(0) = 0.65$ and $f_o(0) = 0.64$ for the co-culture were obtained. The bacteria started the co-culture at natural abundance and so $f_b(0) = 0.0108$. The initial conditions that remained free during the parameter optimisations were $a(0)$, $b(0)$ and $c_o(0)$, with $f_o(0)$ also included as a free initial condition for some optimisations (i.e. fit 4 in table 4.6).

The majority of the model parameters were fixed with values as defined in table 4.1, apart from s_c', which was included as a free parameter. For the parameters ϕ_s, η and X, three different scenarios were considered. Fit 1 considered the basic model, which does not include algal storage, bacterial DIC uptake or respiration, meaning that $\phi_s = 0$, $\eta' = \eta(1-b) = 1$ and $X = 0$. Fits 2, 3 and 4 considered the extended co-culture model, with fit 2 including ϕ_s, η and X as free parameters, and fits 3 and 4 using estimates of ϕ_s, η and X obtained from considering the parameter optimisation results for the axenic cultures.

The result $\phi_s = 0.9$ was obtained from the parameter optimisation for axenic algae (see section 4.2.2). For axenic bacteria, there was no overall trend that could relate glycerol concentration or growth rate to the bacterial growth efficiency, so to estimate the expected growth efficiency of bacteria in the co-culture, the results from the global parameter optimisation of the four axenic cultures of bacteria (see section 4.2.3) were used to calculate the mean and standard error $\eta = 0.44 \pm 0.14$. The results for axenic bacteria in section 4.2.3 suggested that X increases for higher initial concentrations of glycerol, which implies that a faster growth rate corresponds to a higher value of X. Figure 2.21 in chapter 2 plots the result of an exponential growth rate fit for bacteria in the co-culture, which gives estimates for the initial bacterial cell density $b(0) = 1.2 \times 10^7 \pm 1.5 \times 10^5$ cfu mL^{-1} and the exponential growth rate $\mu_B = 0.022 \pm 0.005$ h^{-1} (section 3.3.2 details an analytical result for bacteria in the exponential growth phase). An estimate for the initial DOC concentration, $c_o(0) = 2.2 \times 10^{-7}$ molC mL^{-1}, that would account for the observed growth rate of bacteria in the co-culture was obtained using $c_o(0) = K_c \ \mu_B/(\mu_b - \mu_B)$, with $K_c = 1.2 \times 10^{-6}$ molC mL^{-1} and $\mu_b = 0.14$ h^{-1} from the parameter optimisation for axenic bacteria in section 4.2.3. A linear fit for X against $\ln(c_o(0))$ gave a gradient of $m = 0.0067 \pm 0.0012$ and an intercept $n = 0.120 \pm 0.017$ (see equation (4.4) and figure 4.4), which was used to obtain the estimate $X = 0.017 \pm 0.006$ for bacteria in the co-culture.

Overall, for all the different co-culture fits, there were at most 8 free parameters and initial conditions, which was less than the number of experimental data points (i.e. 26 data points: 7 f_a, 7 f_b, 6 a and 6 b measurements).

Discussion of the parameter optimisation results

The parameter optimisation results showed a good agreement between model and experiment for f_a, f_b and a, but they also illustrated some of the limitations of the co-culture model, in particular with respect to the bacteria (see table 4.6 and figure 4.5). Fits 1, 2 and 3 all gave similar parameter optimisation results, which implied that the model was in a regime where the sensitivity to the parameters ϕ_s, η and X was low. This could be because the co-culture experiment did not give sufficient evidence of the different carbon metabolic processes considered and so the basic model was enough to account for the experimental measurements.

The algae were pre-labelled such that it was likely that in the co-culture they had reached an equilibrium in their isotope labelling dynamics, meaning that the experimental results for the co-culture might not give enough detail to be able to estimate ϕ_s effectively. Additionally, the value for s_c' in the parameter optimisation results (see table 4.6) were relatively small and so, as discussed in section 3.3.2, this implies that storage has a small effect on the algal

labelling rate. However the SIMS results suggested that the carbon isotope distribution within an algal cell was not homogeneous (see section 2.3.1), which implies that there are metabolic processes within algae that resemble carbon storage and therefore it was reasonable to continue to include ϕ_s in the model. For subsequent discussions and model predictions the estimate of $\phi_s = 0.9$ from the result for axenic algae in section 4.2.2 was used.

When η was included as a free parameter, the optimisation maximised η (see the result for fit 2 in table 4.6) and therefore implied that bacterial respiration was negligible in the exponential growth phase. In reality, this is unlikely to be the case because respiration is an important component of bacterial metabolism that provides bacteria with the energy needed to grow. By considering the analytical result for bacteria derived in section 3.3.2, it can be seen that for a given exponential growth rate, increasing η decreases the bacterial labelling rate. Therefore, this unrealistic result for η in fit 2 is likely to be the result of a discrepancy between the model and the experimental results for the relationship between growth and isotope labelling.

Including the inorganic carbon metabolism of bacteria had little effect on the co-culture model results because both the DOC and DIC were expected to be labelled and therefore the model could not easily distinguish between uptake of DOC and DIC, unlike for the axenic bacteria grown with unlabelled glycerol and labelled sodium bicarbonate. Therefore it was more challenging to estimate X using the co-culture experiment than for axenic bacteria.

The results for the axenic bacteria clearly showed the necessity of including bacterial respiration and inorganic carbon metabolism in the model (see section 4.2.3), therefore for bacteria in a co-culture the estimated values carried forward were $\eta = 0.44$ and $X = 0.017$, which were estimated by considering the parameter optimisation results for axenic bacteria. Figure 4.5 illustrates the results of the parameter optimisations that used the fixed parameters $\phi_s = 0.9$, $\eta = 0.44$ and $X = 0.017$ (fits 3 and 4 in table 4.6).

The co-culture fit was improved (i.e. $r^2(a,b,f_a,f_b)$ is smallest) when the parameter optimisation included $f_o(0)$ as a free initial condition (fit 4 in table 4.6). This illustrates a trade-off between bacterial growth and isotope labelling that appears to have limited the effectiveness of the co-culture parameter optimisations. When the initial atomic fraction of ^{13}C for DOC was fixed at $f_o(0) = 0.64$, which was the expected value according to the pre-labelling culture of algae, the bacterial growth was negligible compared to the experiment (see fit 3 in figure 4.5). In contrast, when $f_o(0)$ was free the result for the bacterial growth was much improved, but the value for $f_o(0)$ obtained was close to natural abundance (see fit 4 in figure 4.5 and table 4.6). The DOC was expected to have a high atomic fraction of ^{13}C because it was originating from labelled algae. This suggests that there is likely to be something missing from the model or that an unsuitable assumption has been made.

For example, isotopic fractionation was not considered for the bacterial carbon metabolic processes or the carbon yield for bacterial cells $Y_{b,c}$ might not be a constant. In chapter 2 bacterial growth was observed for the axenic culture grown in the absence of an organic carbon substrate, which implies that there are internal carbon dynamics contributing to bacterial growth that were not included in the model (i.e. bacterial growth in the model depends on the external DOC concentration). In future, it would therefore be interesting to try bacterial pre-cultures with lower glycerol concentrations in order to see if the agreement between the model and experiment could be improved by inoculating the co-culture with bacteria that are carbon starved and thus minimising the internal carbon contribution to growth. Moreover, the SIMS results discussed in chapter 2 showed that not all the algal cells were actively turning over carbon, meaning that it was likely that there were dead algal cells in the co-culture with a low ^{13}C content. Bacteria could have used these dead algal cells as a source of organic carbon, which would have diluted the atomic fraction of ^{13}C for the organic carbon metabolised by bacteria and therefore could account for the difficulty of the co-culture parameter optimisation to satisfactorily fit the bacterial growth together with the isotope labelling. This suggests that in future work it would be interesting to explore algal cell death as a source of DOC or alternative carbon biomass conversion relations as further extensions to the co-culture model.

Overall, the co-culture parameter optimisation results were able to achieve a reasonable qualitative agreement between the model and experiments, but they were not enough to obtain quantitative results. In particular, the co-culture was in a regime where the sensitivity to the parameters ϕ_s, η and X was low and so these parameters were estimated using results from the axenic cultures. Additionally, the results for bacterial growth and isotope labelling suggest that there is something in the co-culture model that is missing or has been misinterpreted. Despite these limitations, fit 3 achieved a good qualitative agreement with experimental data and so the parameter results from fit 3 are used in section 4.3 for making model predictions and to observe qualitative trends in the model results.

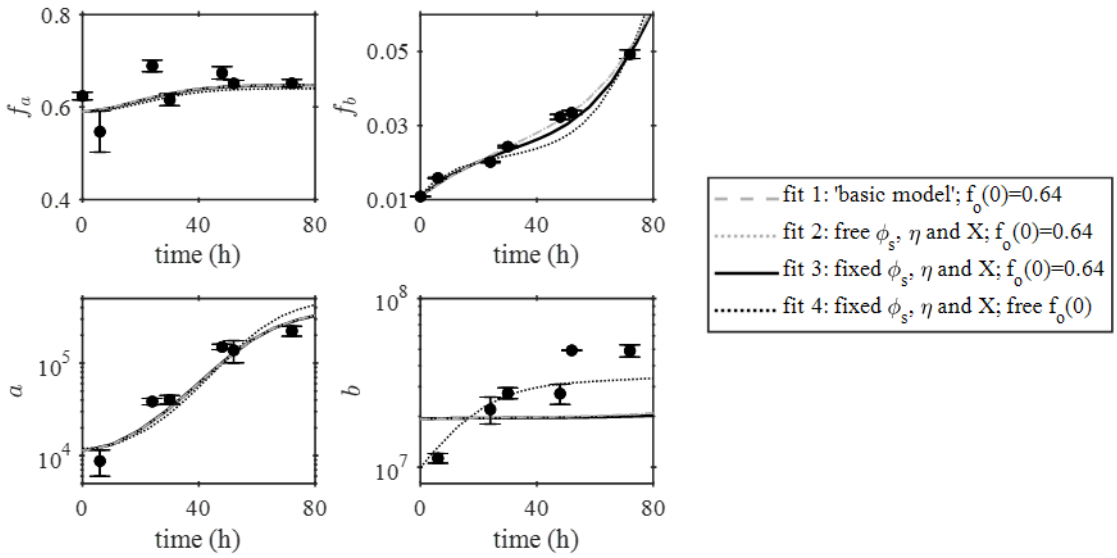

Figure 4.5 **Parameter optimisation results for the algal-bacterial co-culture**. The circles are experimental data points (with error bars corresponding to the standard errors) and the lines indicate the parameter optimisation results. Several different parameter optimisations were performed for the algal-bacterial co-culture and the results for fits 1, 2, 3 and 4 (see table 4.6) are plotted here. Fit 1 used the 'basic model' for the co-culture (i.e. no algal storage, no bacterial respiration and no bacterial DIC uptake), whereas fits 2-4 all used the extended co-culture model. Fit 2 included the storage fraction ϕ_s, bacterial growth efficiency η and DIC uptake fraction X as free parameters, whereas fits 3 and 4 used the parameter estimates $\phi_s = 0.9$, $\eta = 0.44$ and $X = 0.017$ obtained using fit results for the axenic cultures. Fits 1-3 all fixed the initial isotope fraction for DOC $f_o(0) = 0.64$, which was estimated from the parameter optimisation results for axenic algae, and the time evolution of the model variables f_a, f_b, a and b using these fit results are very similar. In contrast, fit 4 kept $f_o(0)$ free.

Table 4.6 **Parameter optimisation results for the algal-bacterial co-culture**. Results of different parameter optimisation results for the co-culture between *C. reinhardtii metE7* and *M. loti*. The parameters not included as free parameters in the optimisation had values as specified in table 4.1. The fixed initial conditions were $c_i(0) = 5$ (i.e. DIC concentration in excess), $v(0) = 0$ (i.e. initially no B_{12} in the media), $f_a(0) = 0.59$ and $f_{a,p}(0) = 0.65$ (i.e. from pre-labelling axenic algae), $f_b(0) = 0.0108$ (i.e. bacteria initially have natural abundance), and $f_i(0) = 0.65$ (i.e. estimate obtained from the parameter optimisation for axenic algae).

Fit	ϕ_s	η	X	s'_c	$a(0)$	$b(0)$	$c_o(0)$	$f_o(0)$	r^2
$1^{\dagger\ddagger}$	0	n.a.	0	0.006	0.005	0.017	0.0022	$0.64^{\ddagger}$	1.927
$2^{\bullet\ddagger}$	0.86	1.00	0.0004	0.043	0.005	0.017	0.0022	$0.64^{\ddagger}$	1.929
$3^{*\ddagger}$	0.9^{*}	0.44^{*}	0.017^{*}	0.046	0.005	0.017	0.0013	$0.64^{\ddagger}$	1.963
4^{*}	0.9^{*}	0.44^{*}	0.017^{*}	0.070	0.005	0.009	0.1407	0.0120	1.309

† Basic model fit that does not include storage, respiration or bacterial DIC uptake.

‡ Initial atomic fraction of ^{13}C for the DOC, $f_o(0) = 0.64$, estimate obtained using the parameter optimisation result for axenic algae.

$^{\bullet}$ Extended co-culture model fit, including ϕ_s, η and X as free parameters.

* Extended co-culture model fit; $\phi_s = 0.9$, $\eta = 0.44$, $X = 0.017$ from axenic cultures.

4.3 Model predictions

The parameter optimisation results obtained in the previous section provide a full set of model parameters that can be used to make experimentally testable predictions. In this section, the results of different types of model predictions are discussed. Firstly, using the parameter optimisation results for the axenic cultures of *M. loti* and for the co-culture, the effect of different model parameters are investigated in order to identify which parameters best account for the experimentally determined single cell distributions of the atomic fraction of ^{13}C in bacteria. The results provide potential mechanistic interpretations of the observed single cell heterogeneity of carbon isotope labelling within the bacterial populations of the different cultures. Secondly, the model is used to make predictions for the effect of changing an initial condition on the growth and ^{13}C-labelling dynamics in a co-culture. The effect of changing different model parameters is also explored, which corresponds to changing the experimental conditions or microbial species used. These results are examples of how the model can be used to make experimentally testable predictions and therefore aims to reveal opportunities for using this type of nutrient explicit co-culture model to guide future experiments.

4.3.1 Single cell heterogeneity

SIMS is able to achieve isotope measurements at single cell resolution. The SIMS results in chapter 2, plotted as histogram distributions, showed that SIMS can be used to investigate the single cell heterogeneity that exists within a microbial population. The experiments alone imply the presence of heterogeneity, but are not enough to indicate what the heterogeneity in atomic fraction measurements is due to. I will only discuss the bacterial heterogeneity because the SIMS results gave a more complete picture of the single cell distributions for bacteria than for algae (for each time-point more than 80 bacterial cells were analysed, whereas for algae it was only 5-29 cells). Many metabolic processes contribute to the carbon dynamics of the co-culture and differences in any of these processes between different cells could have contributed to the observed single cell distributions of f_b. This is an example of how having a mathematical model of the carbon dynamics is helpful for interpreting data, and specifically here for predicting potential origins of the observed temporal evolution for the distributions of single cell f_b values. In section 4.2 parameter optimisations were performed by fitting the model to the mean values of f_b from the SIMS experiments for axenic cultures and a co-culture. This section explores the effect of different parameters on the model predictions for the bacterial labelling dynamics and how this could relate to the observed single cell distributions. Starting from the parameter optimisation results in table 4.5 for

axenic bacteria and from fit 3 in table 4.6 for the co-culture, different model parameters were considered in turn, a range was arbitrarily chosen either side of the optimisation result and the model was solved for the parameter values at the boundaries of this range. The resulting temporal evolution for the ranges of f_b values predicted by the model for the different cultures were compared with the standard deviations of the SIMS single cell measurements.

Figure 4.6a illustrates how, for axenic bacteria grown with unlabelled DOC and labelled DIC, the parameter X affected the height of the peak that appears in a plot of f_b against time. This means that for when different cells within an axenic bacterial population assimilate different amounts of DIC (i.e. different X), the model predicts the same trends of broadening and narrowing for the distributions of f_b as was measured experimentally by the increasing and decreasing standard deviation values (figure 4.6a). A similar agreement between model and experiment was not observed for a distribution of X within the co-culture (figure 4.6a), which is likely to be because in the co-culture the DIC and DOC were both expected to be labelled and therefore X had a smaller impact on the labelling dynamics than for the axenic cultures, in which only the DIC was labelled.

For axenic bacteria, the model suggests that when the bacterial growth efficiency increases (respiration decreases), it takes longer for the bacteria to reach the maximum value of f_b. For a distribution of η within a population of axenic bacteria the model was unable to reproduce the experimentally observed trend for the f_b distributions (figure 4.6b). A distribution broadening for f_b that approximately resembled the results from the co-culture experiments was observed when the co-culture model was considered to have a distribution of η (figure 4.6b). However, the distribution width stabilised relatively quickly for the model in comparison to the experiment, meaning that the model for a range of η in the co-culture did not reproduce the experimentally observed *divergent* broadening for the distribution of f_b.

The effect of a faster bacterial growth rate on the isotope labelling dynamics of the model can be investigated by considering an increase in the maximum growth rate μ_b or a decrease in the DOC half saturation constant K_c. Figures 4.6c and 4.6d show the model predictions for the effect of a distribution of single cell growth rates on the isotope labelling of bacteria by considering μ_b and K_c respectively. Both show poor agreement between the model and experiment for the axenic cultures of bacteria. The model results for the 0.1 % and 0.01 % glycerol cultures implied that the most distribution broadening occurs after the peak in f_b, whereas the experimental measurements showed the most broadening over the first 24 h of the axenic cultures. In contrast, there was a good agreement between the co-culture experiment and the predicted effect of a single cell bacterial growth rate distribution on the distribution of f_b for the co-culture. The co-culture experiments showed a distribution broadening with a

divergent standard deviation for f_b, which the model was able to reproduce for a distribution in either μ_b or K_c (see figures 4.6c and 4.6d respectively).

The carbon yield, $Y_{b,c}$, measures the number of bacterial cells per mole of carbon, which means that bacteria with a smaller $Y_{b,c}$ have more carbon per cell and reach a lower maximum cell density in axenic cultures with the same starting concentration of glycerol, i.e. for the same growth in cell density, glycerol is depleted more quickly. This effect can be seen in figure 4.6e, which shows that a distribution of $Y_{b,c}$ for axenic bacteria would correspond to a distribution broadening for f_b at later times than what was observed experimentally. For the co-culture a distribution in $Y_{b,c}$ was predicted to have a good agreement with the experimental measurements of the single cell distributions in f_b (see figure 4.6e). The effect of $Y_{b,c}$ was comparable to the effect of K_c (figure 4.6d), which is likely to be because both of these parameters are related to the bacterial carbon uptake parameter, $k_{b,c} = K_b / \left(K_c\, Y_{b,c}\right)$, and therefore affect the bacterial growth rate in a similar way.

Overall, this work to investigate the potential origins of the single cell heterogeneity for the experimental measurements of the atomic fraction of ^{13}C in bacteria illustrates the potential of having a mathematical model to describe microbial carbon dynamics. The results for the axenic bacteria suggest that a distribution in the single cell values of X can best predict the experimental observations. In contrast, a distribution in parameters related to bacterial growth rate like μ_b, K_c and $Y_{b,c}$, gave a model prediction for the divergent distribution broadening observed for the bacteria in co-culture with pre-labelled algae. These results suggest that the axenic bacteria have a well-defined growth rate, whereas more variation in the single cell growth rate is expected for the co-cultured bacteria. This could be because the axenic cultures were grown with a single organic carbon substrate (glycerol) but in the co-culture the organic carbon substrate for bacterial growth came from algal DOC exudation, which is likely to produce a complex mix of molecules, creating a heterogeneous carbon environment for the bacteria.

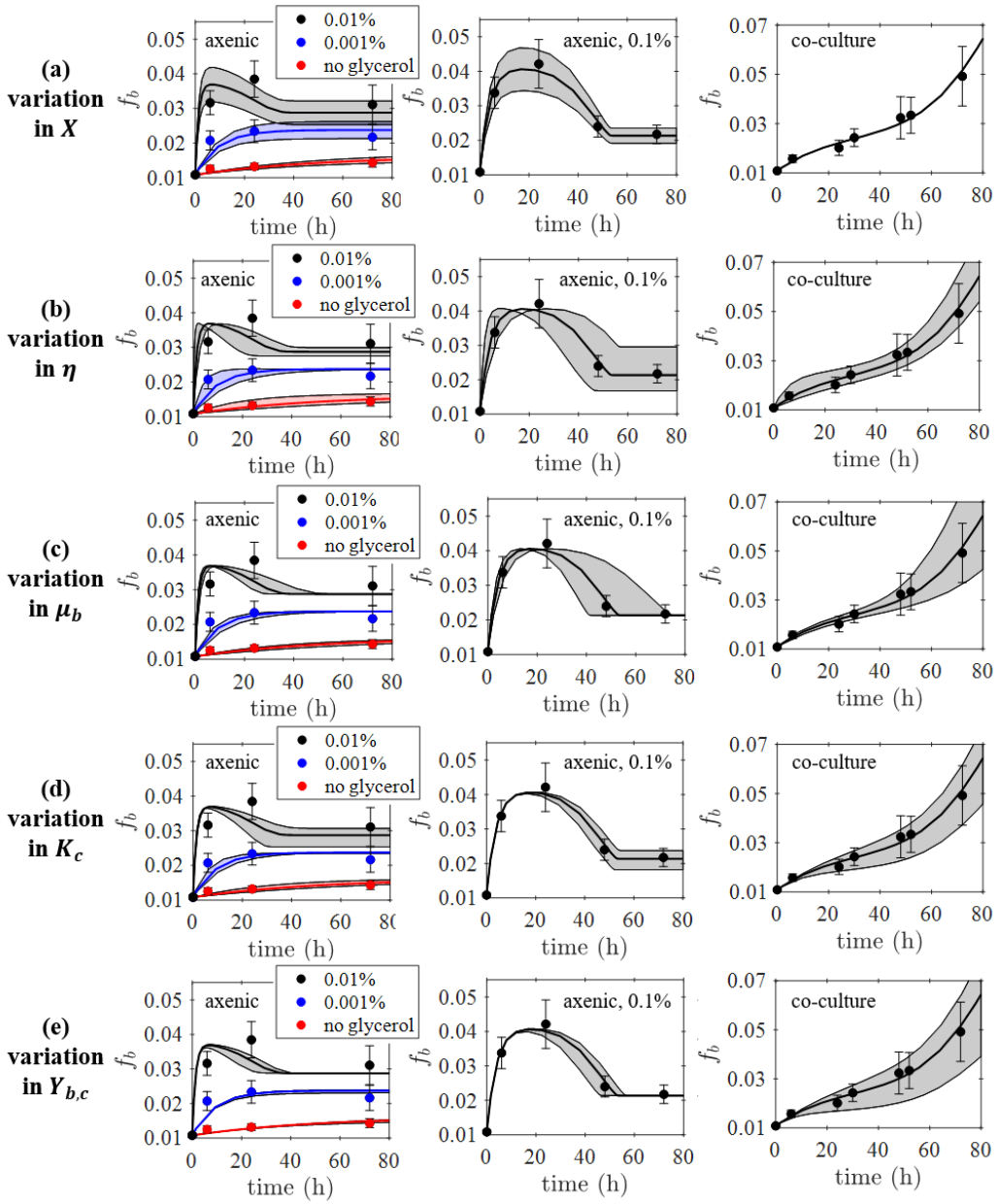

Figure 4.6 **Comparison of single cell heterogeneity predicted by the model and measured experimentally with SIMS**. The mean for the dilution-corrected results for f_b obtained using SIMS are plotted as circles with error bars indicating the standard deviation of the single cell values. The results of the model fit to the experiments are shown as solid lines and the shaded regions correspond to the predicted range of f_b values when a range in a specific model parameter is considered, i.e. range in the (a) DIC uptake parameter X, (b) maximum bacterial growth efficiency η, (c) maximum bacterial growth rate μ_b (d) DOC half-saturation concentration K_c and (e) bacterial carbon yield $Y_{b,c}$. For the 0.1 %, 0.01 %, 0.001 % and no glycerol cultures of axenic bacteria (a) $X \in [0.038, 0.058]$, $[0.034, 0.050]$, $[0.017, 0.025]$ and $[0.008, 0.012]$ respectively, and (b) $\eta \in [0.22, 0.82]$, $[0.04, 0.24]$, $[0.13, 0.53]$ and $[0.59, 0.99]$ respectively. For the co-culture (a) $X \in [0.014, 0.020]$ and (b) $\eta \in [0.14, 0.74]$. (c) For the axenic cultures $\mu_b \in [0.10, 0.18]$ and for the co-culture $\mu_b \in [0.34, 0.50]$ in units h^{-1}. (d) For the axenic cultures $K_c \in \left[0.7 \times 10^{-6}, 1.7 \times 10^{-6}\right]$ and for the co-culture $K_c \in \left[3.3 \times 10^{-7}, 9.3 \times 10^{-7}\right]$ in units $\mathrm{molC\,mL^{-1}}$. (e) For the axenic cultures and the co-culture $Y_{b,c} \in \left[2 \times 10^{14}, 8 \times 10^{14}\right]$ in units $\mathrm{cells\,molC^{-1}}$.

4.3.2 Changing an initial condition or model parameter

This section examines some model predictions for changes in an initial condition or model parameter. The non-dimensional form of the model was used for these predictions because it was the general qualitative trends that were of interest. Unless otherwise stated, the initial conditions used were those given in table 4.7 and the parameter values were based on the parameter optimisation results for the co-culture, which are summarised in table 4.8.

Table 4.7 **The initial conditions used for model predictions**. Unless stated otherwise, these are the non-dimensional initial conditions used for the model predictions. These values correspond to relatively low initial algal and bacterial cell densities, which are sampled from pre-cultures that have been washed before inoculating the co-culture, meaning that no DOC or B_{12} is present in the media.

Initial condition	Value	Comment
$a(0)$	0.05	
$b(0)$	0.05	
$c_o(0)$	0	No DOC added to the media
$v(0)$	0	No B_{12} added to the media
$c_i(0)$	50	DIC is in excess
$f(0)$	0.0108	Atomic fractions start at natural abundance unless otherwise stated

Table 4.8 **The parameter values used for model predictions**. This table lists the values for the non-dimensional model parameters used for making model predictions and briefly explains how these were obtained, more details of which can be found in the sections listed.

Parameter	Value	Source	Section
ε	0.51	Fit by FP using co-culture data obtained by FB	4.2.1
$k_{b,c}$	3.6	Fit by FP using co-culture data obtained by FB	4.2.1
$k_{a,c}$	0.91	Fit by FP using co-culture data obtained by FB & IRMS results	4.2.1
$k_{a,v}$	7.8	Fit by FP using co-culture data obtained by FB	4.2.1
s_v	4.2	Fit by FP using co-culture data obtained by FB	4.2.1
s'_c	0.046	Fit 3 result for the algal-bacterial co-culture	4.2.4
ϕ_s	0.9	Fit result for the axenic culture of algae	4.2.2
η	0.44	Estimated using the fit results for axenic bacteria	4.2.4
X	0.017	Estimated using the fit results for axenic bacteria	4.2.4

FP: François Peaudecerf
FB: Freddy Bunbury

Changing the initial conditions

The most intuitive alterations that can be made both in the model and experimentally are to change initial conditions. In chapter 2 the co-culture was inoculated with pre-labelled algae and unlabelled bacteria, and was grown in media with labelled bicarbonate (DIC), however it is interesting to consider how the labelling dynamics change when different carbon components of the co-culture are initially labelled. Figure 4.7 illustrates some examples of this, showing that if at the start of the co-culture only the DIC is labelled then it was predicted that f_a and f_o increase to a constant value and f_b increases continuously throughout the time-period plotted. In contrast, if only the algae are initially labelled the model predicted that the values for f_a and f_o will decay monotonically, while a non-monotonic peak is expected in f_b (figure 4.7). Alternatively, the bacteria could be labelled, however since the DIC is in excess, as the bacteria respire and f_b decreases, the amount of ^{13}C entering the DIC is negligible compared with the total DIC concentration and therefore the model predicted negligible changes in f_a and f_o overtime (figure 4.7). Therefore the most interesting cases to consider for further model predictions are when initially only the DIC or only the algal biomass is labelled. With labelled DIC it is the rate of increase for f_a and f_b, along with the maximum value of f_a that are the key features that can be compared between different experiments. When algae are labelled it is the rate of decay for f_a and the peak height and width for f_b that can be compared. Experiments could test whether these features can be observed.

As well as changing the origin of ^{13}C enrichment, the initial cell numbers or the nutrient availability can be changed. Table 4.9 summarises the predicted effect on the growth and labelling dynamics when the initial cell densities ($a(0)$ and $b(0)$) increase or if additional nutrients are added to the media (increasing $c_o(0)$ or $v(0)$). For example, when the initial algal cell density increases the model predicted an increasing exudation of DOC and therefore the lag time for bacterial growth was predicted to decrease due to the faster availability of organic carbon, but after this lag period the bacterial growth rate was predicted to be unaffected by $a(0)$ (see figure 4.8). Vitamin B_{12} was predicted to have a smaller peak value when $a(0)$ increases, which is likely to be because when the algal cell density is higher, the algae will consume the B_{12} produced by bacteria more quickly. If the DIC is initially labelled, when $a(0)$ increases, the model suggested that the rate of labelling decreases for algae, but the lag time observed for f_b decreases, mirroring the predicted bacterial growth. When the algae are labelled instead, for an increase in $a(0)$, the model predicted that f_a will decay more slowly and f_b will have a higher peak.

The effect of adding additional DOC or B_{12} to the media is interesting to investigate because it can test how well the model is able to capture the nutrient dynamics within the

algal-bacterial co-culture. For example, if a known concentration of a known, unlabelled organic carbon source is added to the media, this would correspond to a non-zero value for $c_o(0)$ in the model. This type of experiment would test how well the model is able to capture the DOC uptake dynamics for bacteria when an additional DOC source is available as well as the DOC produced by algae. Figure 4.9 illustrates that for an increasing $c_o(0)$, the model predicted that both the algal and bacterial growth rate should increase. When the DIC is initially labelled, the model suggested that the algae become labelled more quickly when $c_o(0)$ increases, corresponding to the faster algal growth rate. In this case, f_b is expected to increase more quickly initially, but have a slower labelling rate in the long-term. In contrast, when only the algae are labelled initially, it was predicted that f_a decays more quickly and the maximum f_b is smaller.

Table 4.9 **An overview of how different initial conditions affect the expected growth and isotope labelling dynamics**. This table summarises the effect of increasing (↑) different initial conditions on the algal and bacterial growth (a and b respectively), and on the labelling dynamics for algae and bacteria (f_a and f_b respectively). Two potential initial conditions for the atomic fractions of ^{13}C were explored, either only the DIC or only the algae were initially labelled (i.e. $f_i(0) = 1$ or $f_a(0) = f_{a,p}(0) = 1$). These observations were made for results obtained by numerically solving the model equations with different initial conditions.

Initial condition	a	b	**Labelled DIC**		**Labelled algae**	
			f_a	f_b	f_a	f_b
↑ $a(0)$	slower	shorter lag time	slower	shorter lag time	slower decay	higher peak
↑ $b(0)$	faster		faster	slower	faster decay	smaller peak
↑ $c_o(0)$	faster	faster	faster	faster (short term), slower (long term)	faster decay	smaller peak
↑ $v(0)$	faster	faster	faster	slower	faster decay	smaller peak

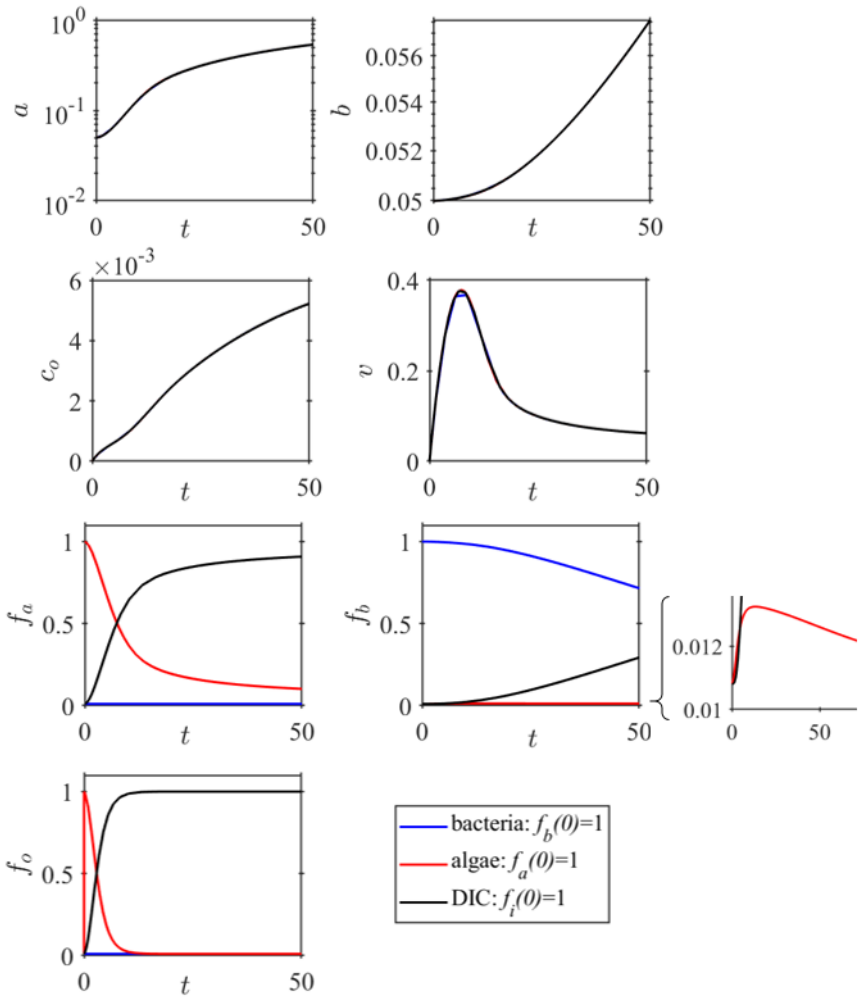

Figure 4.7 **The labelling dynamics for different initial atomic fractions of ^{13}C**. The results of the model using the initial conditions and parameters in tables 4.7 and 4.8 respectively. All the atomic fractions start at natural abundance, with the exception of $f_b(0) = 1$, $f_a(0) = 1$ or $f_i(0) = 1$ for the blue, red and black lines respectively. All variables are in their dimensionless form (see section 3.2.6 for details).

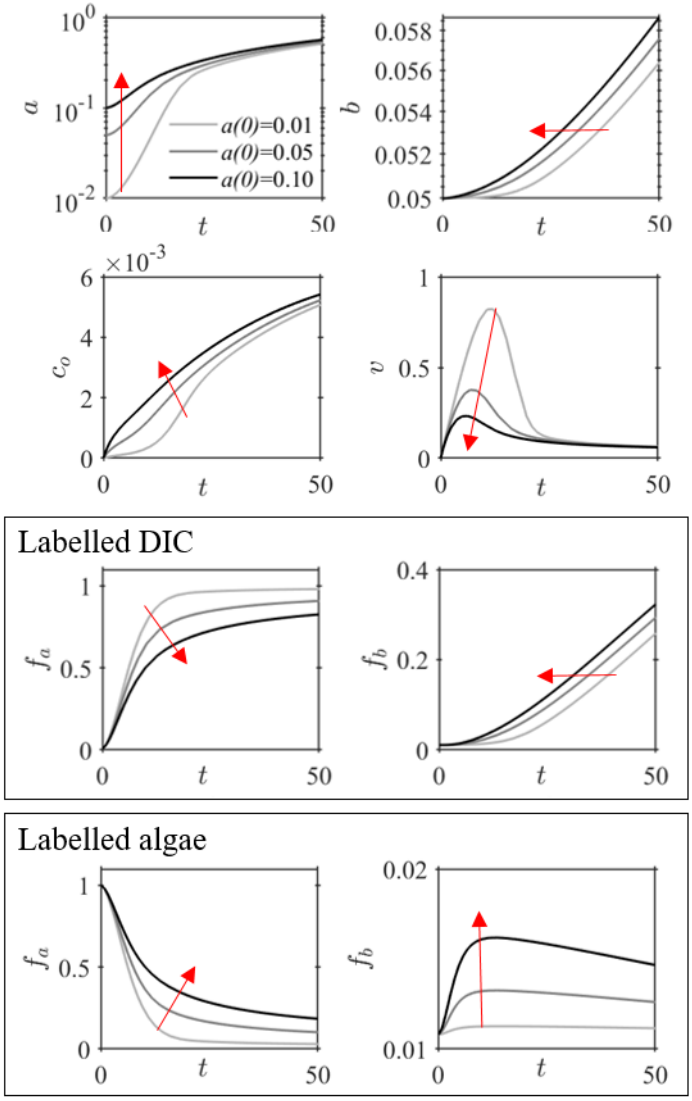

Figure 4.8 **The effect of increasing the initial algal cell density on the growth, nutrient and labelling dynamics**. The model results for different initial algal cell densities, $a(0) = 0.01,\ 0.05,\ 0.10$, with the other initial conditions defined in table 4.7 and using the parameter values given in table 4.8. Two potential initial conditions for the atomic fractions of ^{13}C were explored, either only the DIC or only the algae were initially labelled (i.e. $f_i(0) = 1$ or $f_a(0) = f_{a,p}(0) = 1$). All variables are in their dimensionless form (see section 3.2.6 for details). The red arrows indicate the effect of increasing $a(0)$.

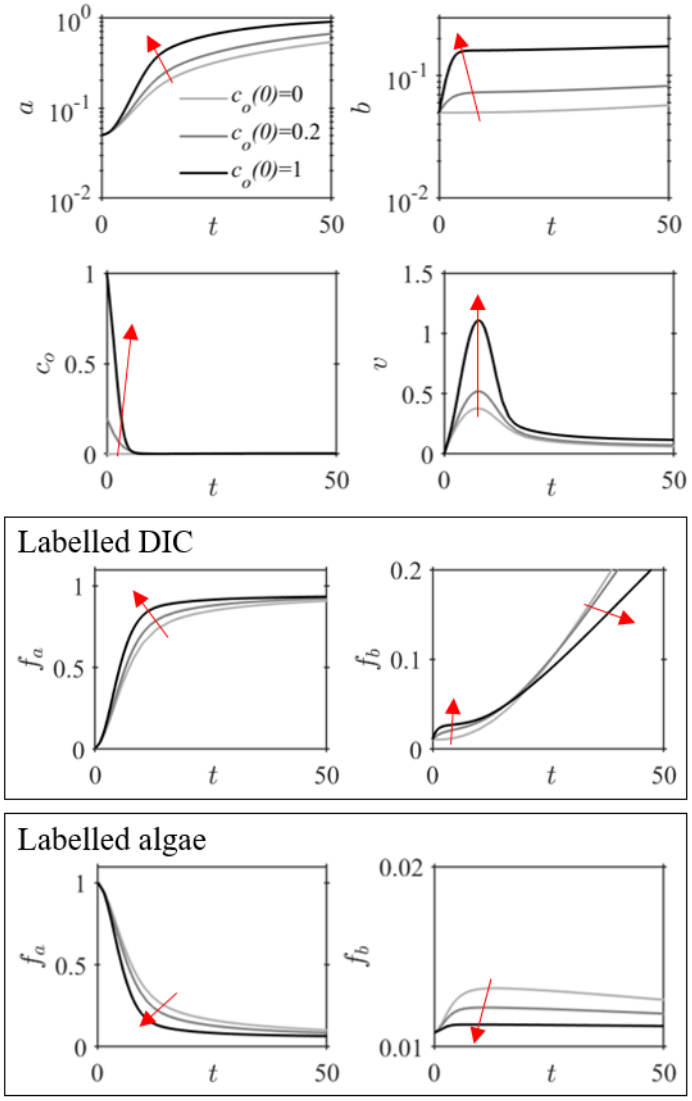

Figure 4.9 **The effect of increasing the initial DOC concentration on the growth, nutrient and labelling dynamics**. The model results for different initial DOC concentrations, $c_o(0) = 0,\ 0.2,\ 1$, with the other initial conditions defined in table 4.7 and using the parameter values given in table 4.8. Two potential initial conditions for the atomic fractions of ^{13}C were explored, either only the DIC or only the algae were initially labelled (i.e. $f_i(0) = 1$ or $f_a(0) = f_{a,p}(0) = 1$). All variables are in their dimensionless form (see section 3.2.6 for details). The red arrows indicate the effect of increasing $c_o(0)$.

The effect of different model parameters

Table 4.10 summarises how an increase in the different non-dimensional parameters of the model were predicted to affect the growth and labelling dynamics. These predictions could be tested by changing experimental conditions, using different species of algae and bacteria or using synthetic mutants. Suggested experimental interpretations for changes in the different parameters are listed below, although it should be noted that changing the algal or bacterial species is unlikely to be restricted to a change in a single parameter.

- DOC export parameter s_c': this could correspond to a change in photosynthesis rate, which could be tested experimentally by changing the light conditions or using photosynthesis mutants of *C. reinhardtii*, for example, mutants with a disrupted carbon concentrating mechanism (Jungnick *et al.*, 2014; Spalding *et al.*, 2002).

- Fraction of 'stored' carbon in algae ϕ_s: this is another way that the photosynthesis rate of the model can be modified. It could be interesting to see whether results from a change in light conditions fit better with a change in ϕ_s or s_c'.

- B_{12} export parameter s_v: this could be tested by using a synthetic mutant of *M. loti* that is unable to export B_{12}, or by using different bacterial species that produce B_{12} at different rates. For example, the rhizobial species *M. loti*, *Rhizobium leguminosarum* and *Sinorhizobium meliloti* have been shown to support the growth of B_{12}-dependent algae to different extents (Kazamia *et al.*, 2012b).

- Carbon uptake parameter for bacteria $k_{b,c}$: this could be tested for axenic bacteria by changing the organic carbon source added to the media, which would have the effect of changing K_c, and therefore changing $k_{b,c}$, which is inversely proportional to K_c. For the co-culture, the effect of $k_{b,c}$ would be most easily tested experimentally by considering different species of bacteria such that there is a change in their carbon requirement.

- Carbon uptake parameter for algae $k_{a,c}$: this would be most easily tested experimentally by considering a different algal species that has a different carbon yield or carrying capacity.

- B_{12} uptake parameter for algae $k_{a,v}$: this could be tested by comparing the wild-type, B_{12} independent strain of *C. reinhardtii* with the B_{12} dependent *C. reinhardtii metE7*, as well as the B_{12} dependent alga *L. rostrata*.

- Ratio of growth rates ε: this would require the maximum growth rate of either the bacteria or the algae to be different, which could be achieved by using different species.

Figure 4.10 illustrates that for an increase in s'_c the model predicts a minimal effect on algal growth and labelling dynamics. It also shows that the bacterial growth rate is expected to increase, which is likely to be the result of an increase in the DOC exudation by algae. The model predictions also show that when initially only the DIC is labelled, it is expected that an increase in s'_c results in an increase in the rate of ^{13}C enrichment for bacteria. Alternatively, when initially only the algae are labelled, the model predicts that the maximum f_b is higher and decays more quickly when s'_c increases.

An increase in $k_{a,v}$ is expected to decrease the algal growth rate (see figure 4.11), which is because a higher $k_{a,v}$ corresponds to algae having a higher B_{12} requirement. As a result, the model predicts that there is less DOC being produced and therefore slower bacterial growth is expected. This implies that when the DIC is initially labelled, the labelling rate for both algae and bacteria is slower. When initially only algae are labelled, the model predicts that the decay of f_a is slower and the f_b peak is slightly higher and has a slower decay.

4.4 Successes and limitations of the model

The co-culture model was able to successfully capture the general features observed for the growth and labelling dynamics for *C. reinhardtii metE7* and *M. loti* both grown axenically and in co-culture (see figures 4.2, 4.3 and 4.5). The model achieved a particularly good fit for the axenic bacterial cultures, showing that the parameters η and X, introduced to include respiration and DIC assimilation respectively, were sufficient and necessary to capture the experimentally determined non-monotonic bacterial labelling dynamics. The model was also able to suggest potential mechanistic origins for the experimentally observed single cell distributions of f_b. This chapter has also demonstrated the predictive power of the model, showing that it can make experimentally testable predictions for changes in either an initial condition or model parameter.

Although the model has generally performed well in reproducing the experimental results, there have been some limitations. It was challenging to obtain a satisfactory quantitative result for the parameter optimisations of the co-culture (see section 4.2.4). This could be due to how the model describes the DOC production by algae or how the model connects DOC assimilation to bacterial growth. The experiments were unable to measure the DOC concentrations and isotope measurements because TRIS buffer, used in the growth media, is an organic buffer that created a high background of carbon. Further experiments that included DOC measurements would be beneficial to improve the parametrisation of the model by obtaining improved estimates for the algal DOC export parameter s'_c and the bacterial carbon uptake parameter $k_{b,c}$.

Table 4.10 **An overview of the predicted effect of different model parameters on the growth and labelling dynamics**. This table summarises the effect on algal and bacterial growth (a and b respectively), and on the labelling dynamics for algae and bacteria (f_a and f_b respectively) when a single model parameter increases (↑), while all others were constant (table 4.8). The initial conditions were set to the values in table 4.7 and two potential initial conditions for the atomic fractions of ^{13}C were explored, either only the DIC or only the algae were initially labelled (i.e. $f_i(0) = 1$ or $f_a(0) = f_{a,p}(0) = 1$). These observations were made for results obtained by changing the value for each parameter in turn and numerically solving the model equations.

Parameter	a	b	**Labelled DIC**		**Labelled algae**	
			f_a	f_b	f_a	f_b
↑ s'_c		faster		faster		faster, higher peak
↑ s_v	faster	faster	faster	faster	faster decay	smaller peak
↑ $k_{b,c}$		slower		slower		smaller peak
↑ $k_{a,c}$						higher peak
↑ $k_{a,v}$	slower	slower	slower	slower	slower decay	slightly higher peak, slower decay
↑ ε	faster	faster	faster	faster	faster decay	smaller peak
↑ ϕ_s	slightly slower	slower	slightly slower	slower	slower decay	smaller peak
↑ η		faster		slightly slower		slightly slower
↑ X		very slightly faster		very slightly faster		

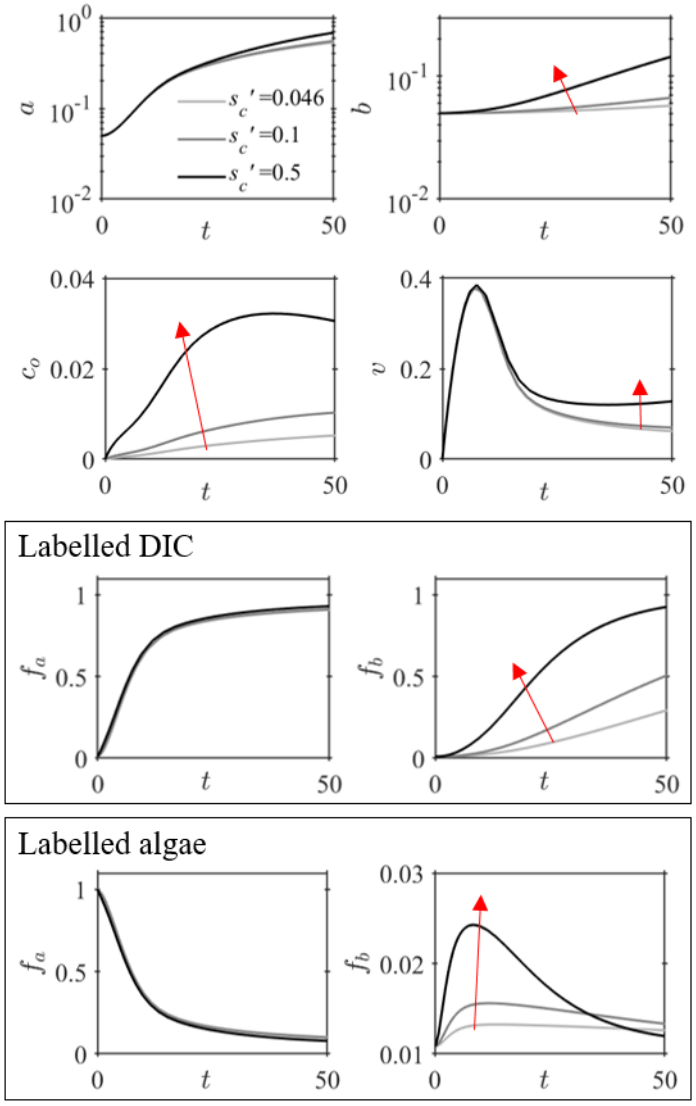

Figure 4.10 **The effect of increasing the DOC export parameter, s_c', on the growth, nutrient and labelling dynamics**. The model results for different values of the DOC export parameter, $s_c' = 0.046,\ 0.1,\ 0.5$, with the other parameter values defined in table 4.8 and using the initial conditions defined in table 4.7. Two potential initial conditions for the atomic fractions of ^{13}C were explored, either only the DIC or only the algae were initially labelled (i.e. $f_i(0) = 1$ or $f_a(0) = f_{a,p}(0) = 1$). All variables are in their dimensionless form (see section 3.2.6 for details). The red arrows indicate the effect of increasing s_c'.

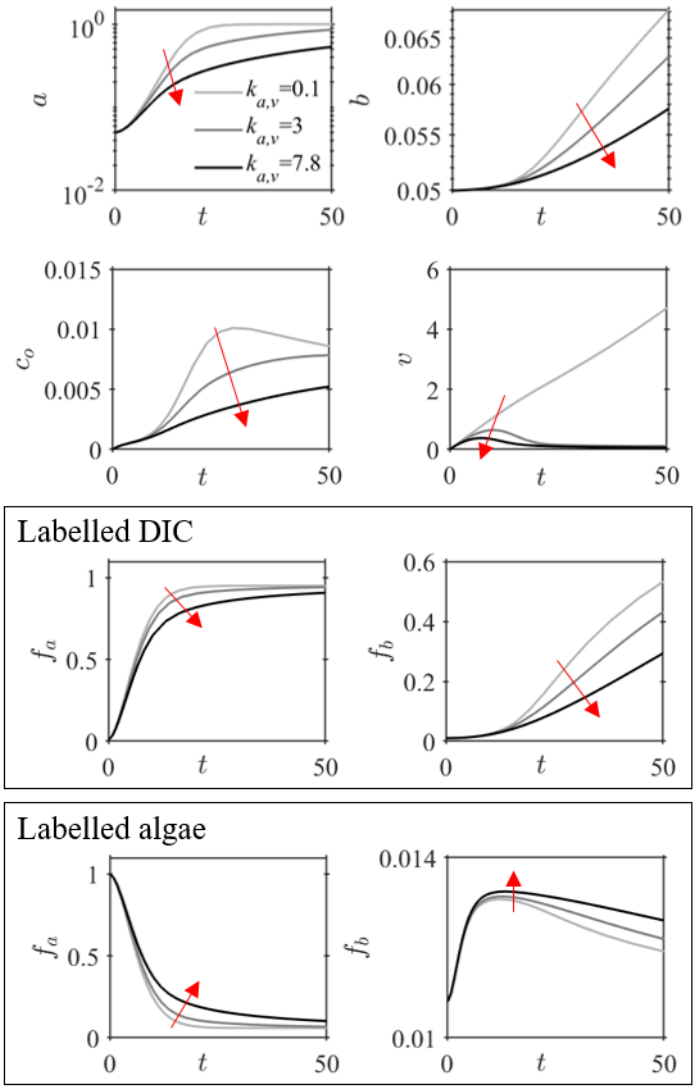

Figure 4.11 **The effect of increasing the B_{12} uptake parameter, $k_{a,v}$, on the growth, nutrient and labelling dynamics**. The model results for different values of the B_{12} uptake parameter, $k_{a,v} = 0.1,\ 3,\ 7.8$, with the other parameter values defined in table 4.8 and using the initial conditions defined in table 4.7. Two potential initial conditions for the atomic fractions of ^{13}C were explored, either only the DIC or only the algae were initially labelled (i.e. $f_i(0) = 1$ or $f_a(0) = f_{a,p}(0) = 1$). All variables are in their dimensionless form (see section 3.2.6 for details). The red arrows indicate the effect of increasing $k_{a,v}$.

4.5 Conclusion and outlook

This chapter tested the validity of the nutrient explicit co-culture model developed in chapter 3 by analysing its behaviour in comparison with the experimental results presented in chapter 2. The parameter optimisation results showed that the mathematical model achieves a reasonably good fit to the experimental measurements for population growth and ^{13}C enrichment for the alga *C. reinhardtii metE7* and the bacterium *M. loti* grown alone and in co-culture. The model fit for the axenic cultures of bacteria suggested that the model incorporating bacterial respiration and DIC assimilation was necessary and sufficient for interpreting the experimental data. These results also suggest that a higher fraction of DIC is assimilated by bacteria when grown with a higher concentration of glycerol. The results for the axenic algae and co-culture implied that the model was not able to quantitatively capture the DOC dynamics, possibly because DOC measurements could not be used to parametrise the model. Alternatively, the model might improve if missing processes, such as algal cell death or bacterial carbon storage, were included. Despite these limitations, the model qualitatively captured the general growth and labelling dynamics of both algae and bacteria grown alone and in co-culture.

In this chapter the predictive power of the model was demonstrated by investigating possible mechanistic explanations for the observed heterogeneity in the SIMS results for the atomic fraction of ^{13}C in bacterial cells. Single cell distributions of f_b could occur due to the heterogeneity of several of the carbon metabolic processes within a population. The model predicted that the main contributing factor for the distributions of f_b determined using SIMS for the axenic cultures of bacteria, was a distribution in the DIC uptake ratio X. In contrast, the divergent broadening observed for f_b in the co-culture was most convincingly reproduced by the model when a distribution in parameters related to growth rate were considered (i.e. the maximum growth rate μ_b, DOC half-saturation concentration K_c or bacterial carbon yield $Y_{b,c}$).

This chapter also used the co-culture model and parameter optimisation results to predict the effect of changing an initial condition or model parameter in order to explore opportunities for future experiments that could further test the model and develop our understanding of the interdependent growth and nutrient dynamics within an algal-bacterial co-culture. In terms of isotope labelling, rather than using a ^{13}C-enriched source of DIC at a high concentration that acts as a continuous source of ^{13}C, it would be interesting to consider 'pulse-chase' experiments. For example, if ^{13}C-enriched algae are grown with unlabelled DIC and unlabelled bacteria, a 'pulse' of ^{13}C would be expected to transfer from the algae to the bacteria. If in a co-culture only the algae are labelled, the model predictions presented in this chapter illustrate that the isotope labelling dynamics could potentially provide more

characteristic features to compare between different experimental conditions than when the DIC is labelled. For example, the atomic fraction of ^{13}C in bacteria plotted over time gives a peak, for which the peak height, width and decay rate are defining features.

Nutrient dynamics can be difficult to access experimentally and so mathematical predictions of population dynamics are more easily tested, meaning that models of microbial interactions often rely on the inferences that come from measuring microbial growth. However, microbial interactions are influenced by nutrient exchange and therefore it is important to have methods for testing model predictions of the nutrient dynamics that underpin microbial communities. The work presented in this chapter demonstrates the potential of using isotope labelling experiments to test nutrient explicit models. There is a wealth of information that can be obtained from isotope labelling experiments and a mathematical model provides an aide for interpreting the data and can be used to investigate single cell heterogeneity within a microbial population.

Chapter 5

Conclusion and future directions

5.1 Conclusion

Due to the complexity of microbial communities, a combined experiment-theory approach using a two-species system can provide insights that contribute to a mechanistic understanding of ecological interactions between microorganisms and improve methods for modelling and interpreting larger-scale situations (Clark *et al.*, 2017; Widder *et al.*, 2016; Zaccaria *et al.*, 2017). This thesis combined experiments and mathematical modelling to examine the carbon fluxes in an algal-bacterial co-culture. The specific co-culture studied used the experimentally evolved, B_{12}-dependent alga *C. reinhardtii metE7* (Helliwell *et al.*, 2015) and the B_{12}-producing, heterotrophic bacterium *M. loti*. This thesis makes steps towards integrating a mechanistic understanding of carbon dynamics with kinetic models of microbial growth and cross-feeding interactions.

Stable isotope labelling combined with SIMS can provide a wealth of data to uncover nutrient fluxes and metabolic activities at the single cell level and therefore is of particular interest for studies in microbial ecology (Abreu *et al.*, 2016; Gao *et al.*, 2015; Herrmann *et al.*, 2007; Musat *et al.*, 2016). Chapter 2 used this experimental approach to obtain time-resolved, single cell measurements of the ^{13}C enrichment of bacteria grown alone and in co-culture with pre-labelled algae. The results were able to demonstrate the bacterial assimilation of algal photosynthate within a co-culture and showed that, for axenic cultures, the extent of inorganic carbon assimilation by bacteria depends on organic carbon availability.

In chapter 3 a co-culture model was developed to connect algal-bacterial carbon dynamics to our understanding of key metabolic processes, without going into precise detail of the chemical reactions involved. A kinetic model approach was used to describe the nutrient dependent population growth of algae and bacteria. The nutrient dynamics were included in a way that extends the typical approach of using nutrient yields (i.e. a constant value for

the amount of carbon per cell defines the carbon uptake) to consider metabolic processes more explicitly. The approach used can be considered as a population level stoichiometric model that ensured the overall nutrient fluxes were balanced. However, detailed chemical reactions were not considered, instead the model equations originated from a more coarse-grained interpretation of carbon fluxes. While aiming to maintain conceptual simplicity and computational tractability, this approach allowed a nutrient explicit model to be developed that incorporates algal photosynthesis, DOC exudation due to excess algal photosynthate, bacterial respiration and inorganic carbon assimilation by bacteria. The resulting model is able to provide dynamical predictions for the population growth, nutrient fluxes and ^{13}C enrichment dynamics, which can be tested experimentally.

Chapter 4 examined the ability of the co-culture model from chapter 3 to test the consistency of our assumed understanding of key metabolic processes with the observed carbon isotope labelling dynamics in chapter 2. The parameter optimisation results gave good agreement with experiments, but also highlighted some limitations. The results showed an increase in relative inorganic carbon uptake by *M. loti* when grown with a higher concentration of glycerol. One of the limitations was that, for axenic algae, the experimental results were not enough to clearly distinguish between the model with and without algal storage. The parameter optimisation results also highlighted a discrepancy between bacterial growth and bacterial ^{13}C assimilation in the co-culture, which was also seen in chapter 2 where estimates for net carbon assimilation accounted for only about 6% of bacterial population growth. These results appear to imply that there are mechanisms for bacterial growth that have not been considered by the model. For example, the pre-cultured bacteria were not completely carbon starved and therefore could grow using internal stores of organic carbon. There could also have been an unlabelled organic carbon source in the co-culture originating from dead algal cells.

A particular success of the model was its ability to investigate potential origins of the single cell heterogeneity observed experimentally for the axenic and co-cultured bacteria. In chapter 4 the effect of different model parameters were compared with the SIMS results from chapter 2. The results illustrated that a distribution in inorganic carbon uptake within a bacterial population gave the best agreement with experiment for axenic cultures, whereas a distribution in parameters related to bacterial growth rate best accounted for the co-culture results. Chapter 4 also showed the predictive power of the model by providing examples of how the growth and labelling dynamics are predicted to change as either an initial condition or model parameter is altered. Experimental interpretations of these predictions were also discussed, suggesting that the effect of changing the light conditions, the algal and bacterial

strains used or which carbon component of the co-culture is labelled could all be interesting avenues to explore with future experiments.

5.2 Recommendations for future research

In hindsight, there were some aspects of the work presented in this thesis that could have been improved and could have simplified the interpretation of results. Future work would likely benefit from further consideration of:

- Bacterial pre-cultures: the bacterial pre-cultures used in this work were grown with a high concentration of glycerol, i.e. 0.1 %. As demonstrated by the axenic culture grown in the absence of an organic carbon substrate, this choice of pre-culture condition meant that bacteria were able to grow on internal organic carbon reserves. Future work would therefore benefit from additional experiments with bacteria in different concentrations of glycerol to determine a suitable concentration that allows sufficient growth in the pre-culture but once inoculated into fresh media in the absence of organic carbon the bacteria are unable to grow.

- DOC analysis: Isotope analysis of DOC was unsuccessful because the TRIS buffer used in the growth media is an organic buffer, which created a high background of carbon. Carbon isotope enrichment measurements for DOC would have enhanced the results of this work and therefore in future it would be good to explore other options for the growth media.

- Initial conditions: Unfortunately I was not able to obtain reliable measurements of the initial cell densities because my focus during sample preparation was on preparing samples for SIMS and IRMS analysis. However, when it came to the model parametrisations it would have been helpful to have the experimental measurements of $a\,(0)$ and $b\,(0)$. For future work I would therefore emphasise the importance of initial conditions and recommend to take care to obtain reliable measurements of them.

- Light conditions: In this work a 12 h-12 h light-dark cycle was used for the experimental cultures, however the model assumed continuous light and the sample frequency was not sufficient to be able to clearly distinguish between the isotope labelling kinetics of the light and dark periods. For future experiments I would suggest careful consideration of the light conditions, perhaps using continuous light in order to simplify the experimental design or focusing on shorter time-periods with more frequent sampling to investigate differences between the light and dark periods of a day-night cycle.

- More extensive IRMS analysis: IRMS is a widely available technique, so it would be interesting to explore its potential use in providing more extensive data for the parametrisation of nutrient-explicit models. The main challenges to obtaining IRMS measurements for microbial samples are to obtain enough biomass and to separate the biomass components of different species in a mixed co-culture. Therefore, I would suggest that the most beneficial experiments using IRMS analysis would be for axenic cultures grown in different conditions (e.g. nutrient concentrations, light intensity, temperature).

5.3 Future directions

Nutrient-explicit models and isotope labelling experiments

Recent review articles (Clark *et al.*, 2017; Widder *et al.*, 2016; Zaccaria *et al.*, 2017) have highlighted the need for combining experimental and theoretical approaches in microbial ecology. This thesis provides an example study of how experimental data can be integrated into the development of mathematical models of microbial interactions. In particular, the results highlight the potential of using isotope labelling experiments and mathematical modelling to advance our understanding of nutrient fluxes in synthetic microbial communities. Momeni *et al.* (2017) demonstrated the importance of nutrient-explicit models for describing the full diversity of microbial interactions. The work described in this thesis shows that isotope labelling dynamics can be derived from nutrient-explicit models, meaning that, in addition to growth measurements, isotope labelling experiments offer valuable data for parametrising and testing nutrient-explicit models. For example, carbon isotope labelling could provide an additional layer of information for testing the kinetic model developed by Bai *et al.* (2015) to study the effect of carbon re-mineralisation on algal growth.

Typical approaches to analysing isotope labelling experiments, particularly for SIMS studies in microbial ecology, involve estimating net nutrient assimilation rates (Montoya *et al.*, 1996; Popa *et al.*, 2007). These calculations have been used to estimate carbon and nitrogen fixation rates for cyanobacteria (Eichner *et al.*, 2017; Foster *et al.*, 2013) and to study the effect of temperature on nutrient fluxes between phytoplankton and bacteria (Arandia-Gorostidi *et al.*, 2016). These calculations are useful for short time-periods or when only one time-point is analysed, but they assume a linear increase in nutrient assimilation overtime. Therefore, nutrient-explicit dynamic models can be particularly useful for analysing isotope labelling experiments when time-course data is available and non-linear labelling dynamics are expected.

Additionally, nutrient explicit models offer opportunities to explore the effect of nutrient availability on microbial interactions by considering the effect of different initial nutrient concentrations. For example, a nutrient-explicit co-culture model, like the one developed in this thesis, combined with isotope labelling experiments could provide new insight into how interaction outcomes depend on specific nutrient conditions, which have previously been studied for algal-bacterial co-cultures using growth experiments, B_{12} concentration measurements and pairwise co-culture models (Grant *et al.*, 2014; Kazamia *et al.*, 2012b).

More broadly, combining experiments with mathematical models can have applications in synthetic ecology, which aims to design, construct and understand engineered microbial communities that could have biotechnological potential (Kazamia *et al.*, 2012a; Zomorrodi *et al.*, 2016). A combined experiment-theory approach could help create predictive models for developing synthetic microbial communities that are grown as efficiently as possible for their designed purpose (Kazamia *et al.*, 2012a; Zomorrodi *et al.*, 2016).

Opportunities for further development of the co-culture model

There are several opportunities to further test and build on the co-culture model developed in this thesis in order to improve understanding of microbial carbon dynamics and nutrient exchange interactions. For example, stable isotope labelling experiments using algal species with different B_{12} requirements, like the B_{12}-independent *C. reinhardtii* and B_{12}-dependent *C. reinhardtii metE7*, could be used to investigate how B_{12} dynamics affect algal photosynthesis and DOC exudation.

It would also be interesting to compare different approaches to modelling the carbon fluxes due to algal photosynthesis and consider different mechanisms for DOC dependent bacterial growth that do not rely on using a constant value for the amount of carbon per cell. Thornton (2014) provides a detailed overview of different mechanisms for the dissolved organic matter release by phytoplankton. A set of mathematical models could be developed to capture these different proposed mechanisms and their relative validity under different conditions could be compared by fitting the models to results of growth and isotope labelling experiments.

Additionally, the co-culture model could be further extended to include more species in order to investigate ecological processes like leakiness (Morris, 2015) and cheating (Jones *et al.*, 2015; Stump *et al.*, 2018). Leakiness is when organisms produce public goods, i.e. metabolites that are available to all members of a community. A cheater benefits from an existing mutualism or shared public good, but they do not pay the cost of helping their interaction partner(s) (Bronstein, 2001; Morris, 2015). Cross-feeding mutualisms are vulnerable to cheaters and it would be interesting to use the experiment-theory approach

developed in this thesis to investigate a tri-culture for an algal-bacterial mutualism, in which a bacterial cheater that does not produce B_{12} but does use the DOC produced by algae is added. For example, if the B_{12}-producing rhizobial species *Sinorhizobium meliloti* is used, then synthetic mutants of this species that cannot produce B_{12} (Campbell *et al.*, 2006; Taga *et al.*, 2007) could be used as cheaters. The challenge for such tri-cultures would be distinguishing between the different bacteria in the SIMS results and therefore genetic techniques like fluorescence in situ hybridisation would be required (Abreu *et al.*, 2016; Musat *et al.*, 2012).

Bacterial growth efficiency and heterotrophic DIC assimilation

As was observed in this thesis, it can be valuable to consider the carbon dynamics in axenic cultures of bacteria. The bacterial growth efficiency is affected by several different factors including temperature, nutrient limitation and energetic quality of the organic carbon substrate (Carlson *et al.*, 2007; Hofmann *et al.*, 2018). Studies have also shown that the extent of inorganic carbon assimilation by heterotrophic bacteria depends on what organic carbon substrate is used (Hesselsoe *et al.*, 2005; Roslev *et al.*, 2004). The model for DOC dependent bacterial growth presented in this thesis offers a tractable model that incorporates both bacterial growth efficiency and DIC uptake. By fitting this model to results of ^{13}C labelling experiments, the effect of different environmental conditions on these metabolic processes of bacteria could be explored. Further work could also integrate this understanding into more complex community models that asses the general impact of bacterial respiration and DIC assimilation on the carbon cycle.

Microfluidics and SIMS

Microfluidic and microfabrication technologies can create physical structures, manipulate fluid flows and generate precisely controlled chemical environments on a microscopic scale (Rusconi *et al.*, 2014). These technologies can be used to create microscopic habitats for microorganisms, which are ideal for investigating cell-cell and cell-environment interactions (Aleklett *et al.*, 2018; Nagy *et al.*, 2018; Rusconi *et al.*, 2014). Microfluidics is often combined with video, time-lapse and fluorescence microscopy, for example to study chemotaxis of bacteria towards phytoplankton (Smriga *et al.*, 2016), the effect of microscale spatial structure on microbial communities (Kim *et al.*, 2008) or single-cell stochasticity of gene expression and growth rate (Kiviet *et al.*, 2014). Moreover, an emerging area of interest in microbial ecology is the region around phytoplankton cells called the phycosphere, which is considered to be of ecological importance and microfluidics offers an ideal platform to study this microenvironment (Seymour *et al.*, 2017). Microfluidics could be used to cultivate

microorganisms in precise environments with isotope labelled substrates, such that the cells could be analysed using SIMS to obtain spatial measurements of single-cell metabolic activity. Several technical challenges would need to be overcome for this to be possible. Firstly, in order to effectively correlate microscopy images with SIMS measurements it would be desirable to use SIMS to analyse specific cells from a microfluidic device. Moreover, SIMS requires samples to be flat, conductive and stable in a high vacuum (Musat *et al.*, 2012; Watrous *et al.*, 2011). Many of these requirements are the same as for electron microscopy and so the microfluidic platform created by Mukhitov *et al.* (2016), used to prepare samples for transmission electron microscopy, could be a suitable starting point for designing a microfluidic device that could be used for preparing samples for SIMS analysis. Combining microfluidics, microscopy and SIMS would offer a wide range of possibilities to correlate single-cell analysis of growth rate, gene-expression or chemotaxis with metabolic activity.

References

Abreu, N. A. and M. E. Taga (2016). "Decoding molecular interactions in microbial communities". *FEMS Microbiology Reviews* 40.5, pp. 648–663.

Aleklett, K., E. T. Kiers, P. Ohlsson, T. S. Shimizu, V. E. Caldas, and E. C. Hammer (2018). "Build your own soil: Exploring microfluidics to create microbial habitat structures". *ISME Journal* 12.2, pp. 312–319.

Allman, E. S. and J. A. Rhodes (2018). "Curve Fitting and Biological Modeling". *Mathematical Models in Biology: An Introduction*. Cambridge University Press.

Amin, S. A., M. S. Parker, and E. V. Armbrust (2012). "Interactions between diatoms and bacteria." *Microbiology and Molecular Biology Reviews* 76.3, pp. 667–84.

Andrews, J. H. (2017). *Comparative Ecology of Microorganisms and Macroorganisms*. 2nd ed. Springer.

Antwis, R. E., S. M. Griffiths, X. A. Harrison, P. Aranega-Bou, A. Arce, A. S. Bettridge, F. L. Brailsford, A. de Menezes, A. Devaynes, K. M. Forbes, E. L. Fry, I. Goodhead, E. Haskell, C. Heys, C. James, S. R. Johnston, G. R. Lewis, Z. Lewis, M. C. Macey, A. McCarthy, J. E. McDonald, N. L. Mejia-Florez, D. O'Brien, C. Orland, M. Pautasso, W. D. Reid, H. A. Robinson, K. Wilson, and W. J. Sutherland (2017). "Fifty important research questions in microbial ecology". *FEMS Microbiology Ecology* 93.5, fix044.

Arandia-Gorostidi, N., P. K. Weber, L. Alonso-Sáez, X. A. G. Morán, and X. Mayali (2016). "Elevated temperature increases carbon and nitrogen fluxes between phytoplankton and heterotrophic bacteria through physical attachment." *The ISME journal* 11.3, p. 641.

Atlas, R. M. and R. Bartha (1998). *Microbial Ecology: Fundamentals and Applications*. Vol. 4th ed. Benjamin/Cummings.

Bai, X., P. Lant, and S. Pratt (2015). "The contribution of bacteria to algal growth by carbon cycling." *Biotechnology and Bioengineering* 112.4, pp. 688–95.

De-Bashan, L. E., X. Mayali, B. M. Bebout, P. K. Weber, A. M. Detweiler, J.-. P. Hernandez, L. Prufert-Bebout, and Y. Bashan (2016). "Establishment of stable synthetic mutualism without co-evolution between microalgae and bacteria demonstrated by mutual transfer of metabolites (NanoSIMS isotopic imaging) and persistent physical association (Fluorescent in situ hybridization)". *Algal Research* 15, pp. 179–186.

Bertrand, E. M., D. M. Moran, M. R. McIlvin, J. M. Hoffman, A. E. Allen, and M. A. Saito (2013). "Methionine synthase interreplacement in diatom cultures and communities : implications for the persistence of B12 use by eukaryotic phytoplankton". *Limnology and Oceanography* 58.4, pp. 1431–1450.

Bjørnsen, P. K. (1988). "Phytoplankton exudation of organic matter: Why do healthy cells do it?" *Limnology and Oceanography* 33.1, pp. 151–154.

Boschker, H. T. S. and J. J. C. N. .-.-. M. 2. Middelburg (2002). "Stable isotopes and biomakers in microbial ecology". *FEMS Microbiology Ecology* 40.August, pp. 85–95.

Boxer, S. G., M. L. Kraft, and P. K. Weber (2009). "Advances in imaging secondary ion mass spectrometry for biological samples." *Annual Review of Biophysics* 38, pp. 53–74.

Brenna, J. T., T. N. Corso, H. J. Tobias, R. J. Caimi, and B. E. T. Al (1997). "High-precision continuous-flow isotope ratio mass spectrometry". *Mass Spectrometry Reviews* 16, pp. 227–258.

Bronstein, J. L. (2001). "The exploitation of mutualisms". *Ecology Letters* 4.3, pp. 277–287.

Brown, D. and P. Rothery (1993). *Models in Biology: Mathematics, Statistics and Computing*. John Wiley & Sons Ltd.

Brussaard, C. P. D., K. D. Bidle, C. Pedrós-alió, and C. Legrand (2016). "The interactive microbial ocean". *Nature Microbiology* 2, p. 16255.

Buchan, A., G. R. LeCleir, C. A. Gulvik, and J. M. González (2014). "Master recyclers: features and functions of bacteria associated with phytoplankton blooms." *Nature Reviews Microbiology* 12.10, pp. 686–98.

Butler, J. N. (1991). *Carbon Dioxide Equilibria and Their Applications*. CRC Press.

Campbell, G. R. O., M. E. Taga, K. Mistry, J. Lloret, P. J. Anderson, J. R. Roth, and G. C. Walker (2006). "Sinorhizobium meliloti bluB is necessary for production of 5,6-dimethylbenzimidazole, the lower ligand of B12". *Proceedings of the National Academy of Sciences* 103.12, pp. 4634–4639.

Carlson, C., P. del Giorgio, and G. Herndl (2007). "Microbes and the Dissipation of Energy and Respiration: From Cells to Ecosystems". *Oceanography* 20.2, pp. 89–100.

Clark, T. J., C. A. Friel, E. Grman, Y. Shachar-Hill, and M. L. Friesen (2017). "Modelling nutritional mutualisms: challenges and opportunities for data integration". *Ecology Letters* 20.9, pp. 1203–1215.

Cole, J. J. (1982). "Interactions Between Bacteria and Algae in Aquatic Ecosystems". *Annual Review of Ecology and Systematics* 13.1, pp. 291–314.

Craig, H. (1957). "Isotopic standards for carbon and oxygen and correction factors for mass-spectrometric analysis of carbon dioxide". *Geochimica et Cosmochimica Acta* 12.1-2, pp. 133–149.

Croft, M. T., A. D. Lawrence, E. Raux-Deery, M. J. Warren, and A. G. Smith (2005). "Algae acquire vitamin B12 through a symbiotic relationship with bacteria." *Nature* 438.7064, pp. 90–3.

Deline, V. R. (1983). "Instrumental cross-contamination in the Cameca IMS-3F secondary ion microscope". *Nuclear Instruments and Methods in Physics Research* 218.1, pp. 316–318. DOI: https://dx.doi.org/10.1016/0167-5087(83)90998-5.

Doucette, J. (2004). ©Woods Hole Oceanographic Institution, created by Jayne Doucette in 2004 for use in Oceanus magazine Vol. 42, No. 2, April 2004.

Droop, M. R. (1968). "Vitamin B12 and Marine Ecology. IV. The kinetics of uptake, growth and inhibtition in Monochrysis lutheri". *Journal of the Marine Biological Association of the United Kingdom* 48.1968, pp. 689–733.

Durham, B. P., S. Sharma, H. Luo, C. B. Smith, S. A. Amin, S. J. Bender, S. P. Dearth, B. A. S. Van Mooy, S. R. Campagna, E. B. Kujawinski, E. V. Armbrust, and M. A. Moran (2015). "Cryptic carbon and sulfur cycling between surface ocean plankton." *Proceedings of the National Academy of Sciences of the United States of America* 112.2, pp. 453–7.

Eichner, M. J., I. Klawonn, S. T. Wilson, S. Littmann, M. J. Whitehouse, M. J. Church, M. M. M. Kuypers, D. M. Karl, and H. Ploug (2017). "Chemical microenvironments and single-cell carbon and nitrogen uptake in field-collected colonies of Trichodesmium under different pCO2". *Nature Publishing Group* 11.6, pp. 1305–1317.

Ellner, S. P. and J. Guckenheimer (2006). *Dynamic Models in Biology*. Princeton University Press.

Falkowski, P. G. (1994). "The role of phytoplankton photosynthesis in global biogeochemical cycles". *Photosynthesis Research* 39.3, pp. 235–258.

Falkowski, P. and J. Raven (2007). "Carbon Acquisition and Assimilation". *Aquatic Photosynthesis*. 2nd ed. Princeton University Press. Chap. Chapter 5, pp. 156–201.

Farquar, G. D., J. R. Ehleringer, and K. T. Hubrick (1989). "Carbon Isotope Discrimination and Photosynthesis". *Annual Review of Plant Physiology and Plant Molecular Biology* 40, pp. 503–537.

Faust, K. and J. Raes (2012). "Microbial interactions: from networks to models". *Nature Reviews Microbiology* 10.8, pp. 538–550.

Flynn, K. J. (2008). "Use, Abuse, Misconceptions and Insights from Quota Models - the Droop Cell Quota Model 40 Years on". *Oceanography and Marine Biology: An Annual Review* 46, pp. 1–23.

Fogg, G. E. (1983). "The ecological significance of extracellular products of phytoplankton photosynthesis". *Botanica marina* 26.1, pp. 3–14.

Foster, R. A., S. Sztejrenszus, and M. M. M. Kuypers (2013). "Measuring carbon and N2 fixation in field populations of colonial and free-living unicellular cyanobacteria using nanometer-scale Secondary Ion Mass Spectrometry". *Journal of Phycology* 516, pp. 502–516.

Gao, D., X. Huang, and Y. Tao (2015). "A critical review of NanoSIMS in analysis of microbial metabolic activities at single-cell level". *Critical Reviews in Biotechnology* 36.5, pp. 884–890.

Giorgio, P. A. del and J. J. Cole (1998). "Bacterial Growth Efficiency in Natural Aquatic Systems". *Annual Review of Ecology and Systematics* 29.1, pp. 503–541.

Goers, L., P. Freemont, and K. M. Polizzi (2014). "Co-culture systems and technologies: taking synthetic biology to the next level." *Journal of the Royal Society, Interface* 11.96.

Grant, M. A., E. Kazamia, P. Cicuta, and A. G. Smith (2014). "Direct exchange of vitamin B12 is demonstrated by modelling the growth dynamics of algal–bacterial cocultures". *The ISME Journal* 8.7, pp. 1418–1427.

Greenwood, N. N. and A. Earnshaw (1997). *Chemistry of the Elements.* Vol. 2nd ed. Butterworth-Heinemann.

Grossart, H. and M. Simon (2007). “Interactions of planktonic algae and bacteria: effects on algal growth and organic matter dynamics”. *Aquatic Microbial Ecology* 47.2, pp. 163–176.

Gurung, T. B., J. Urabe, and M. Nakanishi (1999). “Regulation of the relationship between phytoplankton Scenedesmus acutus and heterotrophic bacteria by the balance of light and nutrients”. *Aquatic Microbial Ecology* 17.1, pp. 27–35.

Harris, E. (2009). *The Chlamydomonas Sourcebook (Second Edition)*. Academic Press.

Hellebust, J. A. (1958). “Excretion of some organic compounds by marine phytoplankton”. *Limnology and Oceanography* 10.2, pp. 192–206.

Helliwell, K. E., S. Collins, E. Kazamia, S. Purton, G. L. Wheeler, and A. G. Smith (2015). “Fundamental shift in vitamin B12 eco-physiology of a model alga demonstrated by experimental evolution”. *The ISME Journal* 9.6, pp. 1446–1455.

Helliwell, K. E., M. A. Scaife, S. Sasso, A. P. U. Araujo, S. Purton, and A. G. Smith (2014). “Unraveling Vitamin B12-Responsive Gene Regulation in Algae”. *Plant Physiology* 165.1, pp. 388–397.

Helliwell, K. E., G. L. Wheeler, K. C. Leptos, R. E. Goldstein, and A. G. Smith (2011). “Insights into the Evolution of Vitamin B12 Auxotrophy from Sequenced Algal Genomes”. *Molecular Biology and Evolution* 28.10, pp. 2921–2933.

Helliwell, K. E., G. L. Wheeler, and A. G. Smith (2013). “Widespread decay of vitamin-related pathways: coincidence or consequence?” *Trends in Genetics* 29.8, pp. 469–478.

Hellweger, F. L., R. J. Clegg, J. R. Clark, C. M. Plugge, and J. U. Kreft (2016). “Advancing microbial sciences by individual-based modelling”. *Nature Reviews Microbiology* 14.7, pp. 461–471.

Herrmann, A. M., K. Ritz, N. Nunan, P. L. Clode, J. Pett-Ridge, M. R. Kilburn, D. V. Murphy, A. G. O’Donnell, and E. A. Stockdale (2007). “Nano-scale secondary ion mass spectrometry — A new analytical tool in biogeochemistry and soil ecology: A review article”. *Soil Biology and Biochemistry* 39.8, pp. 1835–1850.

Hesselsoe, M., J. L. Nielsen, P. Roslev, and P. H. Nielsen (2005). “Isotope labeling and microautoradiography of active heterotrophic bacteria on the basis of assimilation of 14CO(2).” *Applied and Environmental Microbiology* 71.2, pp. 646–55.

Hobbs, P. V. (2000). *Introduction to Atmospheric Chemistry*. Cambridge University Press.

Hoek, T. A., K. Axelrod, T. Biancalani, E. A. Yurtsev, J. Liu, and J. Gore (2016). "Resource Availability Modulates the Cooperative and Competitive Nature of a Microbial Cross-Feeding Mutualism". *PLoS Biology* 14.8, e1002540.

Hofmann, R. and C. Griebler (2018). "DOM and bacterial growth efficiency in oligotrophic groundwater: Absence of priming and co-limitation by organic carbon and phosphorus". *Aquatic Microbial Ecology* 81.1, pp. 55–71. ISSN: 09483055. DOI: 10.3354/ame01862.

Holland, J. N. and D. L. Deangelis (2009). "Consumer-resource theory predicts dynamic transitions between outcomes of interspecific interactions". *Ecology Letters* 12.12, pp. 1357–1366.

Holland, J. N. and D. L. Deangelis (2010). "A consumer-resource approach to the density-dependent population dynamics of mutualism". *Ecology* 91.5, pp. 1286–1295.

Holling, C. S. (1973). "Resilience and Stability of Ecological Systems". *Annual Review of Ecology and Systematics* 4.1, pp. 1–23.

Hom, E. F., P. Aiyar, D. Schaeme, M. Mittag, and S. Sasso (2015). "A Chemical Perspective on Microalgal–Microbial Interactions". *Trends in Plant Science* 20.11, pp. 689–693.

Housecroft, C. E. and A. G. Sharpe (2008). *Inorganic Chemsitry*. Vol. 3rd ed. Pearson Education UK.

Hummert, S., K. Bohl, D. Basanta, A. Deutsch, S. Werner, G. Theißen, A. Schroeter, and S. Schuster (2014). "Evolutionary game theory: Cells as players". *Molecular BioSystems* 10.12, pp. 3044–3065.

Jett, B. D., K. L. Hatter, M. M. Huycke, and M. S. Gilmore (1997). "Simplified agar plate method for quantifying viable bacteria." *Biotechniques* 23.4, pp. 648–50.

Jiang, H., E. Favaro, C. N. Goulbourne, P. D. Rakowska, G. M. Hughes, M. G. Ryadnov, L. G. Fong, S. G. Young, D. J. Ferguson, A. L. Harris, and C. R. Grovenor (2014). "Stable isotope imaging of biological samples with high resolution secondary ion mass spectrometry and complementary techniques". *Methods* 68.2, pp. 317–324.

Jones, E. I., M. E. Afkhami, E. Akçay, J. L. Bronstein, R. Bshary, M. E. Frederickson, K. D. Heath, J. D. Hoeksema, J. H. Ness, M. S. Pankey, S. S. Porter, J. L. Sachs, K. Scharnagl, and M. L. Friesen (2015). "Cheaters must prosper: reconciling theoretical and empirical perspectives on cheating in mutualism." *Ecology letters* 18, pp. 1270–1284.

Jungnick, N., Y. Ma, B. Mukherjee, J. C. Cronan, D. J. Speed, S. M. Laborde, D. J. Longstreth, and J. V. Moroney (2014). "The carbon concentrating mechanism in Chlamydomonas reinhardtii: finding the missing pieces." *Photosynthesis Research* 121.2-3, pp. 159–73.

Kaneko, T., Y. Nakamura, S. Sato, E. Asamizu, T. Kato, S. Sasamoto, A. Watanabe, K. Idesawa, A. Ishikawa, K. Kawashima, T. Kimura, Y. Kishida, C. Kiyokawa, M. Kohara, M. Matsumoto, A. Matsuno, Y. Mochizuki, S. Nakayama, N. Nakazaki, S. Shimpo, M. Sugimoto, C. Takeuchi, M. Yamada, and S. Tabata (2000). "Complete genome structure of the nitrogen-fixing symbiotic bacterium Mesorhizobium loti". *DNA RESEARCH* 7, pp. 331–338.

Kazamia, E., D. C. Aldridge, and A. G. Smith (2012a). "Synthetic ecology - A way forward for sustainable algal biofuel production?" *Journal of Biotechnology* 162.1, pp. 163–169.

Kazamia, E., H. Czesnick, T. T. V. Nguyen, M. T. Croft, E. Sherwood, S. Sasso, S. J. Hodson, M. J. Warren, and A. G. Smith (2012b). "Mutualistic interactions between vitamin B12-dependent algae and heterotrophic bacteria exhibit regulation". *Environmental Microbiology* 14.6, pp. 1466–1476.

Kim, H. J., J. Q. Boedicker, J. W. Choi, and R. F. Ismagilov (2008). "Defined spatial structure stabilizes a synthetic multispecies bacterial community". *Proceedings of the National Academy of Sciences* 105.47, pp. 18188–18193.

Kiviet, D. J., P. Nghe, N. Walker, S. Boulineau, V. Sunderlikova, and S. J. Tans (2014). "Stochasticity of metabolism and growth at the single-cell level". *Nature* 514.7522, pp. 376–379.

Kolter, R. (1993). "The stationary phase of the bacterial life cycle". *Annual Review of Microbiology* 47.1, pp. 855–874.

Kouzuma, A. and K. Watanabe (2015). "Exploring the potential of algae/bacteria interactions". *Current Opinion in Biotechnology* 33, pp. 125–129.

Kropat, J., A. Hong-Hermesdorf, D. Casero, P. Ent, M. Castruita, M. Pellegrini, S. S. Merchant, and D. Malasarn (2011). "A revised mineral nutrient supplement increases biomass and growth rate in Chlamydomonas reinhardtii". *The Plant Journal* 66.5, pp. 770–780.

Kurepin, L. V., A. G. Ivanov, M. Zaman, R. P. Pharis, V. Hurry, and N. P. Hüner (2017). *Photosynthesis: Structures, Mechanisms, and Applications*. Ed. by H. J. M. Hou, M. Mahdi Najafpour, G. F. Moore, and S. I. Allakhverdiev. Springer.

Larsson, U. and A. Hagström (1979). "Phytoplankton exudate release as an energy source for the growth of pelagic bacteria". *Marine Biology* 52, pp. 199–206.

Liu, H., Y. Zhou, W. Xiao, L. Ji, X. Cao, and C. Song (2012). "Shifting nutrient-mediated interactions between algae and bacteria in a microcosm: Evidence from alkaline phosphatase assay". *Microbiological Research* 167.5, pp. 292–298.

Madigan, M. T., K. S. Bender, D. H. Buckley, W. Matthew Sattley, and D. A. Stahl (2019). *Brock Biology of Microorganimsms*. Vol. 15th ed. Pearson.

May, R. M. (1973). "Qualitative Stability in Model Ecosystems". *Ecology* 54.3, pp. 638–641. ISSN: 00129658. DOI: 10.2307/1935352. URL: http://doi.wiley.com/10.2307/1935352.

McPhail, D. and M. Dowsett (2009). *Dynamic SIMS*. John Wiley and Sons, pp. 207–268. ISBN: 9780470017630. DOI: https://dx.doi.org/10.1002/9780470721582.ch5.

Meisl, G., X. Yang, E. Hellstrand, B. Frohm, J. B. Kirkegaard, S. I. A. Cohen, C. M. Dobson, S. Linse, and T. P. J. Knowles (2014). "Differences in nucleation behavior underlie the contrasting aggregation kinetics of the Aβ40 and Aβ42 peptides". *Proceedings of the National Academy of Sciences* 111.26, pp. 9384–9389. DOI: 10.1073/pnas.1401564111.

Momeni, B., C.-C. Chen, K. L. Hillesland, A. Waite, and W. Shou (2011). "Using artificial systems to explore the ecology and evolution of symbioses." *Cellular and Molecular Life Sciences* 68.8, pp. 1353–68.

Momeni, B., L. Xie, and W. Shou (2017). "Lotka-Volterra pairwise modeling fails to capture diverse pairwise microbial interactions". *eLife* 6, e25051.

Monod, J. (1949). "The growth of bacterial cultures". *Annual Review of Microbiology* 3, pp. 371–394.

Montoya, J. P., M. Voss, P. Kahler, and D. G. Capone (1996). "A Simple, High-Precision, High-Sensitivity Tracer Assay for N2 Fixation". *Applied and Environmental Microbiology* 62.3, pp. 986–993.

Mook, W. G., J. C. Bommerson, and W. H. Staverman (1974). "Carbon isotope fractionation between dissolved bicarbonate and gaseous carbon dioxide". *Earth and Planetary Science Letters* 22.2, pp. 169–176.

Morris, J. J. (Aug. 2015). "Black Queen evolution: the role of leakiness in structuring microbial communities." *Trends in genetics : TIG* 31.8, pp. 475–82.

Muccio, Z. and G. P. Jackson (2009). "Isotope ratio mass spectrometry". *Analyst* 134, pp. 213–222. DOI: 10.1039/b808232d.

Mukhitov, N., J. M. Spear, S. M. Stagg, and M. G. Roper (2016). "Interfacing Microfluidics with Negative Stain Transmission Electron Microscopy". *Analytical chemistry* 88, pp. 629–634.

Murray, J. D. (2002). *Mathematical Biology I: An Introduction*. Vol. 3rd ed. Springer.

Musat, N., R. Foster, T. Vagner, B. Adam, and M. M. M. Kuypers (2012). "Detecting metabolic activities in single cells, with emphasis on nanoSIMS." *FEMS Microbiology Reviews* 36.2, pp. 486–511.

Musat, N., F. Musat, P. K. Weber, and J. Pett-Ridge (2016). "Tracking microbial interactions with NanoSIMS". *Current Opinion in Biotechnology* 41, pp. 114–121.

Musat, N., H. Stryhanyuk, P. Bombach, L. Adrian, J. N. Audinot, and H. H. Richnow (2014). "The effect of FISH and CARD-FISH on the isotopic composition of 13C- and 15N-labeled Pseudomonas putida cells measured by nanoSIMS". *Systematic and Applied Microbiology* 37.4, pp. 267–276.

Nagy, K., Á. Ábrahám, J. E. Keymer, and P. Galajda (2018). "Application of microfluidics in experimental ecology: The importance of being spatial". *Frontiers in Microbiology* 9.

Navarro Llorens, J. M., A. Tormo, and E. Martínez-García (2010). "Stationary phase in gram-negative bacteria". *FEMS Microbiology Reviews* 34.4, pp. 476–495.

Ohkouchi, N., N. O. Ogawa, Y. Chikaraishi, H. Tanaka, and E. Wada (2015). "Biochemical and physiological bases for the use of carbon and nitrogen isotopes in environmental and ecological studies". *Progress in Earth and Planetary Science* 2.1, pp. 1–17.

Okuyama, T. and J. N. Holland (2008). "Network structural properties mediate the stability of mutualistic communities". *Ecology Letters* 11.3, pp. 208–216.

Orphan, V. J. and C. H. House (2009). "Geobiological investigations using secondary ion mass spectrometry: microanalysis of extant and paleo-microbial processes". *Geobiology* 7.3, pp. 360–372.

Peaudecerf, F. (2016). "The role of spatial structure in microbial mutualisms of model associations between algae and bacteria". PhD thesis. University of Cambridge.

Peaudecerf, F. J., F. Bunbury, V. Bhardwaj, M. A. Bees, A. G. Smith, R. E. Goldstein, and O. A. Croze (2018). "Microbial mutualism at a distance: The role of geometry in diffusive exchanges". *Physical Review E* 97.2, p. 022411.

Peterson, B. J. and B. Fry (1987). "Stable isotopes in ecosystem studies". *Annual Review of Ecological Systematics* 18, pp. 293–320.

Phelan, V. V., W.-T. Liu, K. Pogliano, and P. C. Dorrestein (2012). "Microbial metabolic exchange–the chemotype-to-phenotype link." *Nature Chemical Biology* 8.1, pp. 26–35.

Popa, R., P. K. Weber, J. Pett-Ridge, J. A. Finzi, S. J. Fallon, I. D. Hutcheon, K. H. Nealson, and D. G. Capone (2007). "Carbon and nitrogen fixation and metabolite exchange in and between individual cells of Anabaena oscillarioides." *The ISME Journal* 1.4, pp. 354–60.

Raina, J. B., P. Clode, S. Cheong, J. Bougoure, M. R. Kilburn, A. Reeder, S. Forêt, M. Stat, V. Beltran, P. Thomas-Hall, D. Tapiolas, C. M. Motti, B. Gong, M. Pernice, C. E. Marjo, J. R. Seymour, B. L. Willis, and D. G. Bourne (2017). "Subcellular tracking reveals the location of dimethylsulfoniopropionate in microalgae and visualises its uptake by marine bacteria". *eLife* 6.

Ramanan, R., B.-H. Kim, D.-H. Cho, H.-M. Oh, and H.-S. Kim (2016). "Algae–bacteria interactions: Evolution, ecology and emerging applications". *Biotechnology Advances* 34.1, pp. 14–29.

Roslev, P., M. B. Larsen, D. Jørgensen, and M. Hesselsoe (2004). "Use of heterotrophic CO2 assimilation as a measure of metabolic activity in planktonic and sessile bacteria." *Journal of Microbiological Methods* 59.3, pp. 381–93.

Rusconi, R., M. Garren, and R. Stocker (2014). "Microfluidics Expanding the Frontiers of Microbial Ecology". *Annual Review of Biophysics* 43, pp. 65–91.

Samo, T. J., J. A. Kimbrel, D. J. Nilson, J. Pett-Ridge, P. K. Weber, and X. Mayali (2018). "Attachment between heterotrophic bacteria and microalgae influences symbiotic microscale interactions". *Environmental Microbiology*.

Seymour, J. R., S. A. Amin, J.-B. Raina, and R. Stocker (2017). "Zooming in on the phycosphere: the ecological interface for phytoplankton–bacteria relationships". *Nature Microbiology* 2, p. 17065.

Shou, W., C. T. Bergstrom, A. K. Chakraborty, and F. K. Skinner (2015). "Theory, models and biology". *eLife* 4, pp. 1–4.

Slade, H., H. G. Wood, A. O. Nier, A. Hemingway, and C. H. Werkman (1942). "Assimilation of heavy carbon dioxide by heterotrophic bacteria". *The Journal of Biological Chemistry* 143, pp. 133–145.

Smith, H. J., R. A. Foster, D. M. McKnight, J. T. Lisle, S. Littmann, M. M. M. Kuypers, and C. M. Foreman (2017). "Microbial formation of labile organic carbon in Antarctic glacial environments". *Nature Geoscience* 10.5, pp. 356–361.

Smriga, S., V. I. Fernandez, J. G. Mitchell, and R. Stocker (2016). "Chemotaxis toward phytoplankton drives organic matter partitioning among marine bacteria." *Proceedings of the National Academy of Sciences of the United States of America* 113.6, pp. 1576–1581.

Song, H.-S., W. Cannon, A. Beliaev, and A. Konopka (2014). "Mathematical Modeling of Microbial Community Dynamics: A Methodological Review". *Processes* 2.4, pp. 711–752.

Spalding, M. H., K. Van, Y. Wang, and Y. Nakamura (2002). "Acclimation of Chlamydomonas to changing carbon availability". *Functional Plant Biology* 29.2-3, pp. 221–230.

Stowers, M. D. (1985). "Carbon Metabolism in Rhizobium Species". *Annual Reviews in Microbiology* 39, pp. 89–108.

Stump, S. M. C., E. C. Johnson, and C. A. Klausmeier (2018). "Local interactions and self-organized spatial patterns stabilize microbial cross-feeding against cheaters". *Journal of the Royal Society Interface* 15.140.

Taga, M. E., N. A. Larsen, A. R. Howard-Jones, C. T. Walsh, and G. C. Walker (2007). "BluB cannibalizes flavin to form the lower ligand of vitamin B12". *Nature* 446.7134, pp. 449–453.

Takahashi, K., E. Wada, and M. Sakamoto (1991). "Relationship between Carbon Isotope Discrimination and the Specific Growth Rate of Green Alga Chlamydomonsa reinhardtii". *Japanese Journal of Limnology* 52.2, pp. 105–112.

Terrell, W. J. (2009). *Stability and Stabilization : An Introduction*. Princeton University Press.

Thornton, D. C. (2014). "Dissolved organic matter (DOM) release by phytoplankton in the contemporary and future ocean". *European Journal of Phycology* 49.1, pp. 20–46.

Van den Meersche, K., J. J. Middelburg, K. Soetaert, P. van Rijswijk, H. T. S. Boschker, and C. H. R. Heip (2004). "Carbon-nitrogen coupling and algal-bacterial interactions

during an experimental bloom: Modeling a 13 C tracer experiment". *Limnology and Oceanography* 49.3, pp. 862–878.

Wagner, M. (2009). "Single-Cell Ecophysiology of Microbes as Revealed by Raman Microspectroscopy or Secondary Ion Mass Spectrometry Imaging". *Annual Review of Microbiology* 63.1, pp. 411–429.

Warren, M. J., E. Raux, H. L. Schubert, and J. C. Escalante-Semerena (2002). "The biosynthesis of adenosylcobalamin (vitamin B12)". *Natural Product Reports* 19.4, pp. 390–412. ISSN: 02650568. DOI: 10.1039/b108967f.

Watrous, J. D. and P. C. Dorrestein (2011). "Imaging mass spectrometry in microbiology." *Nature reviews. Microbiology* 9.9, pp. 683–694.

Werkman, C. H. and H. G. Wood (1942a). "Heterotrophic Assimilation of Carbon Dioxide". *Advances in Enzymology and Related Areas of Molecular Biology* 2, pp. 135–182.

Werkman, C. H. and H. G. Wood (1942b). "On the Metabolism of Bacteria". *Botanical Review* 8.1, pp. 1–68.

Wessel, A. K., L. Hmelo, M. R. Parsek, and M. Whiteley (2013). "Going local: technologies for exploring bacterial microenvironments". *Nature Reviews Microbiology* 11.5, pp. 337–348.

Widder, S., R. J. Allen, T. Pfeiffer, T. P. Curtis, C. Wiuf, W. T. Sloan, O. X. Cordero, S. P. Brown, B. Momeni, W. Shou, H. Kettle, H. J. Flint, A. F. Haas, B. Laroche, J.-U. Kreft, P. B. Rainey, S. Freilich, S. Schuster, K. Milferstedt, J. R. van der Meer, T. Groβkopf, J. Huisman, A. Free, C. Picioreanu, C. Quince, I. Klapper, S. Labarthe, B. F. Smets, H. Wang, and O. S. Soyer (2016). "Challenges in microbial ecology: building predictive understanding of community function and dynamics". *The ISME Journal* 10.11, p. 2557.

Yukalov, V. I., E. P. Yukalova, and D. Sornette (2012). "Modeling symbiosis by interactions through species carrying capacities". *Physica D: Nonlinear Phenomena* 241.15, pp. 1270–1289.

Zaccaria, M., S. Dedrick, and B. Momeni (2017). "Modeling Microbial Communities: A Call for Collaboration between Experimentalists and Theorists". *Processes* 5.4, p. 53.

Zomorrodi, A. R. and D. Segrè (2016). "Synthetic Ecology of Microbes: Mathematical Models and Applications". *Journal of Molecular Biology* 428.5, pp. 837–861.

Appendix A

Growth media

A.1 TRIS-minimal media (TRISmin)

Table A.1 gives the recipe for TRISmin growth media. The different components were added to water and then water was added to reach a final volume of 1 L. The TRISmin growth media was autoclaved in order to ensure that it was sterile. However, vitamin B_{12} and sodium bicarbonate are not stable at high temperatures and therefore would degrade during the autoclaving process. If vitamin B_{12} and/or sodium bicarbonate were required in the media, then the stock solutions of B_{12} and sodium bicarbonate were filter sterilised and the required amount added after autoclaving.

The 1 M TRIS stock solution was prepared by dissolving 121.14 g TRIS in approximately 600 mL of water. The solution was then titrated to pH 7.2 by adding concentrated HCl and water was added to reach a final volume of 1 L. The pH was measured and if required, the solution was again titrated to pH 7.2 with concentrated HCl.

Tables A.2 and A.3 give the recipes for the stock solution of salts and phosphates respectively. Table A.4 gives details of the seven separate trace element solutions required for TRISmin media. These have been adapted from Kropat *et al.* (2011) to include a seventh solution containing cobalt. Cobalt is required as the central ion of vitamin B_{12}. The cobalt concentration was chosen to be the same as is used in the Hutner's trace elements (Harris, 2009; Kropat *et al.*, 2011). EDTA only dissolves at pH 8, meaning that when preparing the trace element solutions that contain EDTA, the pH was adjusted using HCl and NaOH as required.

Table A.1 **TRISmin growth media**. Recipe for 1 L of TRISmin growth media. The different components were added to water in the required quantities and then water was added to reach a final volume of 1 L.

	Quantity
1 M TRIS solution	20 mL
Salt solution	25 mL
Phosphates	1 mL
Trace element solutions 1-7	1 mL each

Table A.2 **TRISmin salts**. Recipe for 1 L of the stock solution of salts for TRISmin growth media. The chemical components were weighed out and dissolved in water. Water was then added to reach a final volume of 1 L.

	Quantity
NH_4Cl	15.0 g
$MgSO_4 \cdot 7\,H_2O$	4.0 g
$CaCl_2 \cdot 2\,H_2O$	2.0 g

Table A.3 **TRISmin phosophates**. Recipe for 100 mL phosphate solution for TRISmin growth media. The chemical components were weighed out and dissolved in water. Water was then added to reach a final volume of 100 mL.

	Quantity
K_2HPO_4	10.8 g
KH_2PO_4	5.6 g

Table A.4 **TRISmin trace elements**. The concentrations of the different chemical components and the masses required for preparing 50 mL of each of the seven trace element stock solutions.

Number	Chemical Component	Concentration	Mass per 50 mL stock
1	$EDTA \cdot Na_2 \cdot 2H_2O$	25 mM	0.465 g
2	$(NH_4)_6Mo_7O_{24} \cdot 4H_2O$	32 µM	0.002 g
3	$CuCl_2 \cdot 2H_2O$	1.4 mM	0.017 g
	EDTA	2 mM	0.029 g
4	$ZnSO_4 \cdot 7H_2O$	2.5 mM	0.036 g
	EDTA	2.7 mM	0.040 g
5	$MnCl_2 \cdot 4H_2O$	6 mM	0.059 g
	EDTA	6 mM	0.088 g
6	$FeCl_3 \cdot 6H_2O$	20 mM	0.270 g
	EDTA	22 mM	0.321 g
	Na_2CO_3	22 mM	0.116 g
7	$CoCl_2 \cdot 6H_2O$	7 mM	0.083 g

A.2 TY media

TY agar plates were used for viable count measurements of algal and bacterial population growth. Table A.5 gives the recipe for preparing TY growth media with 1.5 % agar.

Table A.5 **TY solid growth media**. Recipe for 1 L of TY solid growth media with 1.5 % agar. The chemical components were weighed out and dissolved in water. Water was then added to reach a final volume of 1 L

	Quantity
Tryptone	5.0 g
Yeast extract	3.0 g
$CaCl_2 \cdot H_2O$	0.875 g
Agar	15 g

Appendix B

Preliminary SIMS results

A preliminary experiment for stable isotope labelling and SIMS analysis was done for an algal pre-labelling culture, a labelled co-culture and an axenic culture of bacteria with 0.1 % glycerol. Figures B.1, B.2, B.3 and B.4 show the preliminary results and also compares them with the results from the final SIMS experiment. The SIMS results shown here have not been dilution corrected.

The results from the preliminary SIMS experiment show the same trends in the isotope labelling dynamics as those observed for the final SIMS experiment. This illustrates the repeatability of the measurements obtained. It was also from the preliminary results that the DIC uptake by bacteria was observed and so it became interesting to investigate further the axenic bacterial cultures in different concentrations of glycerol. Lastly, unlabelled control cultures for the axenic algal culture and the co-culture were included in the preliminary experiments and showed the expected result of natural abundance for both the algae and bacteria.

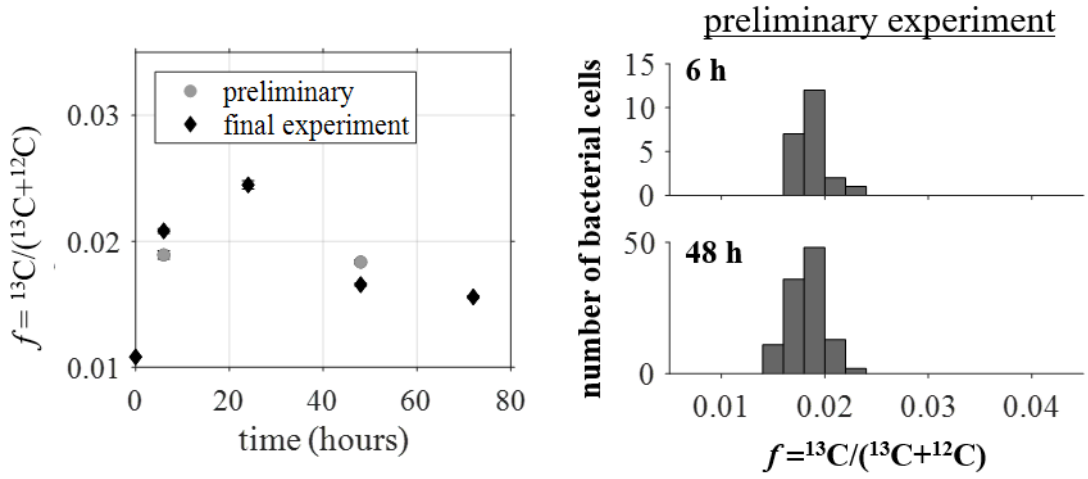

Figure B.1 ***M. loti* grown axenically with** 0.1 % **glycerol**. Preliminary SIMS results for the mean carbon isotope fraction are compared with the results from the final experiment for axenic cultures of bacteria grown with 0.1 % glycerol and 5 mM $NaH^{13}CO_3$. The standard error values are small compared to the size of the plotted points and therefore the error bars are not visible. Histogram plots of the results from the preliminary SIMS experiment show the distributions for the carbon isotope fraction values of single cells for bacteria sampled at two time-points.

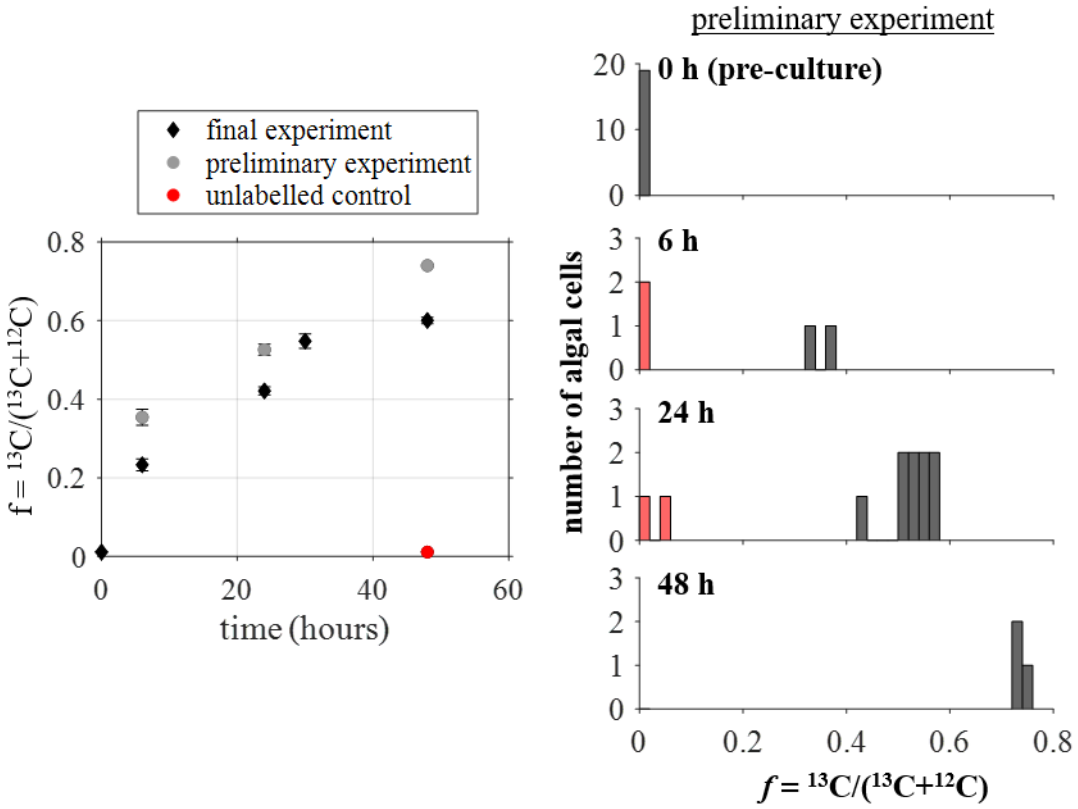

Figure B.2 **Pre-labelling culture of axenic *C. reinhardtii metE7***. Preliminary SIMS results for the mean carbon isotope fraction are compared with the results from the final experiment for the pre-labelling cultures of algae grown with 5 mM $NaH^{13}CO_3$. Error bars are not visible when the standard error in the mean is smaller than the plotted point. In the preliminary experiment, a control culture of axenic algae was grown with 5 mM unlabelled $NaHCO_3$ and a sample at 48 h was taken and analysed using SIMS to show that the algae remained at natural abundance (red circle). Histogram plots of the results from the preliminary SIMS experiment show the distributions for the carbon isotope fraction values of single cells for algae sampled from the pre-labelling culture. In the preliminary experiment only one SIMS measurement was obtained, whereas for the final experiment the values plotted represent the mean value for algal cells where the single cell values are the mean of 2-3 repeated SIMS measurements taken at the same location on the filter. The red bars indicate the algal cells that were not included in the calculation of the mean because they gave isotope fraction values close to natural abundance and therefore were considered inactive.

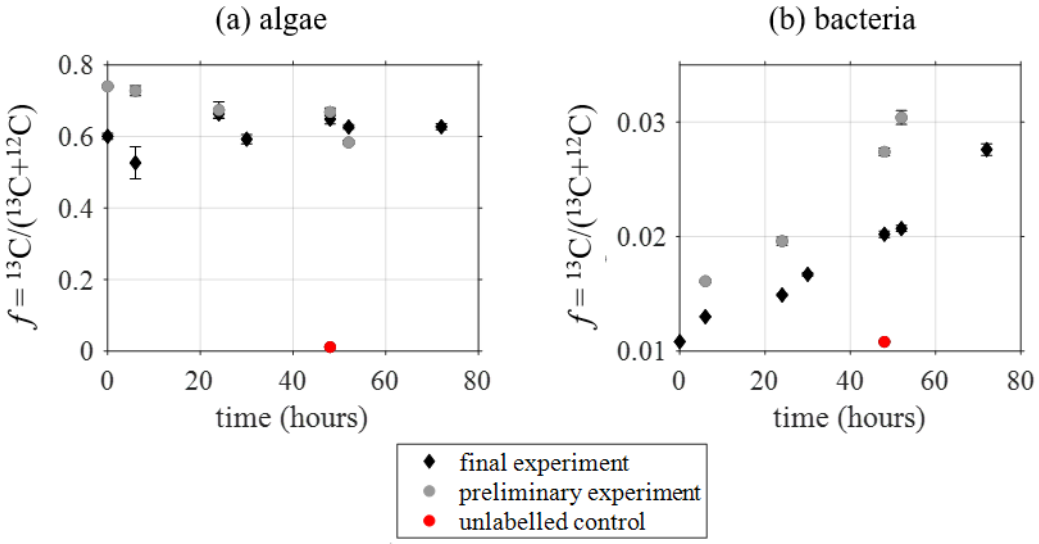

Figure B.3 **SIMS results for the co-culture between *M. loti* and pre-labelled *C. reinhardtii metE7***. SIMS results for the preliminary and final experiment are compared in the plots for the mean and standard error of the carbon isotope fraction of (a) algal and (b) bacterial cells. In the preliminary experiment, a control co-culture was grown with unlabelled algae and unlabelled $NaHCO_3$. A sample at 48 h was taken from this unlabelled co-culture and analysed using SIMS to show that the algae and bacteria remained at natural abundance (red circle). In the preliminary experiment only one SIMS measurement was obtained, whereas for the final experiment the values plotted represent the mean value for algal cells where the single cell values are the mean of three repeated SIMS measurements taken at the same location on the filter.

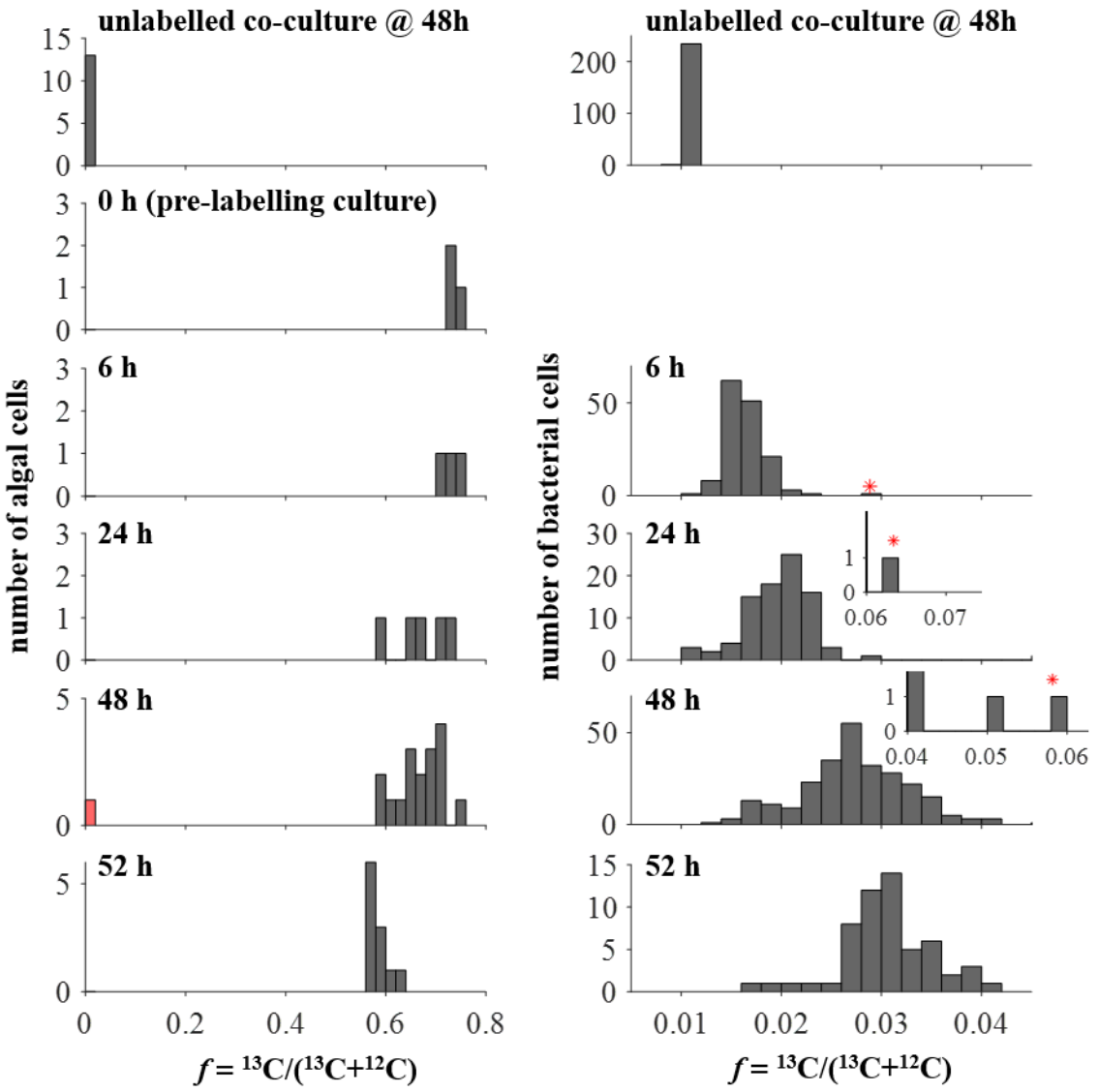

Figure B.4 **Distributions of ^{13}C-isotope fractions for algae and bacteria in the co-culture**. Histogram plots of the results from the preliminary SIMS experiment show the distributions for the carbon isotope fraction values of (left) algal and (right) bacterial cells for samples from the ^{13}C-labelled co-culture. Unlike for the final SIMS experiment, for which the carbon isotope fraction of algal cells was calculated as the mean of 2-3 repeated SIMS measurements, in the preliminary experiment only one SIMS measurement was obtained for each algal cell. The red bar indicates the algal cell that was not included in the calculation of the mean for the 48 h sample because it is close to natural abundance and therefore the algal cell is considered inactive. The red circles indicate the bacterial cells that were considered outliers from the distribution and therefore excluded from the calculation of the mean (i.e. 1 point for the 6 h, 24 h and 48 h samples).

Appendix C

Isotope Ratio Mass Spectrometry

Isotope Ratio Mass Spectrometry (IRMS) was used to analyse bulk samples of the algal and bacterial biomass to give estimates for the carbon isotope content. IRMS also measures the total carbon and nitrogen content, which was used to calculate the C-N ratio and, together with the dry mass and cell density measurements, were used to estimate the carbon yield (i.e. cells $\mathrm{mol}C^{-1}$) for algae and bacteria.

Sample Preparation

Figure C.1 gives an overview of the steps required to prepare samples for IRMS analysis. First the biomass was concentrated using centrifugation. For co-cultures, additional steps were required to separate the bacterial and algal biomass fractions. First a slow centrifugation step was used to concentrate the algal cells as a pellet at the bottom of the culture. The supernatant was passed through a 3 µm filter in order to ensure that the algal cells were completely removed. In this way the filtrate provided the bacterial fraction of the culture biomass, which was concentrated into a pellet by centrifugation. Once the concentrated biomass samples were obtained, they were transferred to eppendorfs and dried overnight in an oven at 50 °C. To remove any excess $NaH^{13}CO_3$ that could contaminate the biomass sample and give falsely high isotope fraction values, the samples were placed in a desiccator with 32 % HCl for acid fumigation. The dry mass of the samples was measured and the required amount for IRMS analysis was weighed out and encapsulated in tin. It was not possible to collect enough dry mass for IRMS analysis at every time-point. For samples where enough dry mass was obtained, 1-4 sub-samples were analysed.

The samples were sent to the Godwin lab at the Department of Earth Sciences, University of Cambridge for IRMS analysis using the Thermo Delta V Plus and Costech. The bulk material is converted to gaseous products and N_2 masses at 28, 29 and 30 are monitored

for nitrogen measurements and CO_2 masses at 44, 45 and 46 are for carbon measurements. IRMS analysis measures the carbon and nitrogen content as a percentage of the total dry mass (%AmtC and %AmtN) using the peaks at mass 44 and 28 respectively. From these results, the C:N ratio can be calculated. IRMS results of the isotope analysis are given as $\delta^{13}C$ readings, which is defined by the equation

$$\delta^{13}C = \left(\frac{R_{sample}}{R_{standard}} - 1 \right) 1000\,‰. \tag{C.1}$$

This is a measure of the isotope ratio relative to a standard, i.e. the Pee Dee Belemnite (PDB) standard that has an isotope ratio value $R_{standard} = 0.01124$. Isotope ratio is defined as $R = {}^{13}C/{}^{12}C$, and the isotope fraction is given by $f = {}^{13}C/\left({}^{12}C + {}^{13}C\right) = R/(1+R)$.

C-N Content and Carbon Yield

Table C.1 summarises the estimates for the carbon and nitrogen content and the carbon yield obtained from the IRMS results for samples of *M. loti* and *C. reinhardtii metE7* taken from the different stable isotope labelled cultures described in chapter 2. For samples of algal biomass, 8 samples gave suitable results for measurements of C-N content. The mean and standard error for %AmtC was 35 ± 4 % and for %AmtN was 8 ± 1 %. Taking the ratio of the percentage measurements for the individual sample results and then calculating the mean and standard error gives a C:N ratio of 4.4 ± 0.1 for *C. reinhardtii metE7*. For samples of bacterial biomass, 13 samples gave suitable results for measurements of C-N content. The mean and standard error for %AmtC was 39 ± 2 % and for %AmtN was 11 ± 1 %. Taking the ratio of the percentage measurements for the individual sample results and then calculating the mean and standard error gives a C:N ratio of 3.71 ± 0.03 for *M. loti*.

To calculate the carbon yield for algal cells (i.e. $Y_{a,c}$, the number of cells per mole of carbon) the following equation was used

$$Y_{a,c} = M_r \, \frac{a \cdot V \cdot 100}{m \cdot \%\text{AmtC}}, \tag{C.2}$$

with a the algal cell density in cells mL^{-1} measured using the Coulter counter, V the sample volume in mL, m the sample dry mass in g, %AmtC the percent of dry mass that is carbon and M_r the molar mass of carbon in g mol^{-1}. The value for the molar mass depends on the atomic fraction of ^{13}C and therefore M_r was calculated using

$$M_r = 12 \cdot (1 - f) + 13 \cdot f, \tag{C.3}$$

with f the atomic fraction of ^{13}C obtained from IRMS analysis. There were four algal samples that had suitable dry mass and IRMS measurements to be able to estimate the carbon yield. From these four estimates the carbon yield for algal cells was found to be $4 \times 10^{12} \pm 1 \times 10^{12}$ cells molC^{-1}. The carbon yield for bacterial cells, $Y_{b,c}$, was calculated in the same way, but using the viable count measurement of cell density in cfu mL^{-1}. There were ten bacterial samples that had suitable dry mass and IRMS measurements to be able to estimate the carbon yield. From these ten estimates the carbon yield for bacterial cells was found to be $5 \times 10^{14} \pm 1 \times 10^{14}$ cells molC^{-1}.

Carbon Isotope Results

Figures C.2, C.3 and C.4 give the results for the ^{13}C-isotope fraction values obtained by IRMS analysis which show the same trends as observed using SIMS analysis. Figure C.2 shows that a higher concentration of glycerol results in a higher isotope fraction and for the 0.1 % glcyerol culture a peak in the carbon isotope fraction is observed, i.e. the carbon isotope fraction decreases when the bacteria are in the stationary phase. Figure C.3 shows the increasing carbon isotope fraction of algae in the pre-labelling culture and figure C.4 shows the IRMS measurements of the carbon isotope fraction for the algal and bacterial fractions of the co-culture biomass.

Table C.1 **C-N content and carbon yield**. Summary of the IRMS results for the carbon and nitrogen content and the carbon yield. The table gives the mean, standard error and the number of samples included in the mean (n).

		Mean	Standard error	n
Algae	%AmtC	35	4	8
	%AmtN	8	1	8
	C:N ratio	4.4	0.1	8
	$Y_{a,c}$ (cells molC^{-1})	4×10^{12}	1×10^{12}	4
Bacteria	%AmtC	39	2	13
	%AmtN	11	1	13
	C:N ratio	3.71	0.03	13
	$Y_{b,c}$ (cfu molC^{-1})	5×10^{14}	1×10^{14}	10

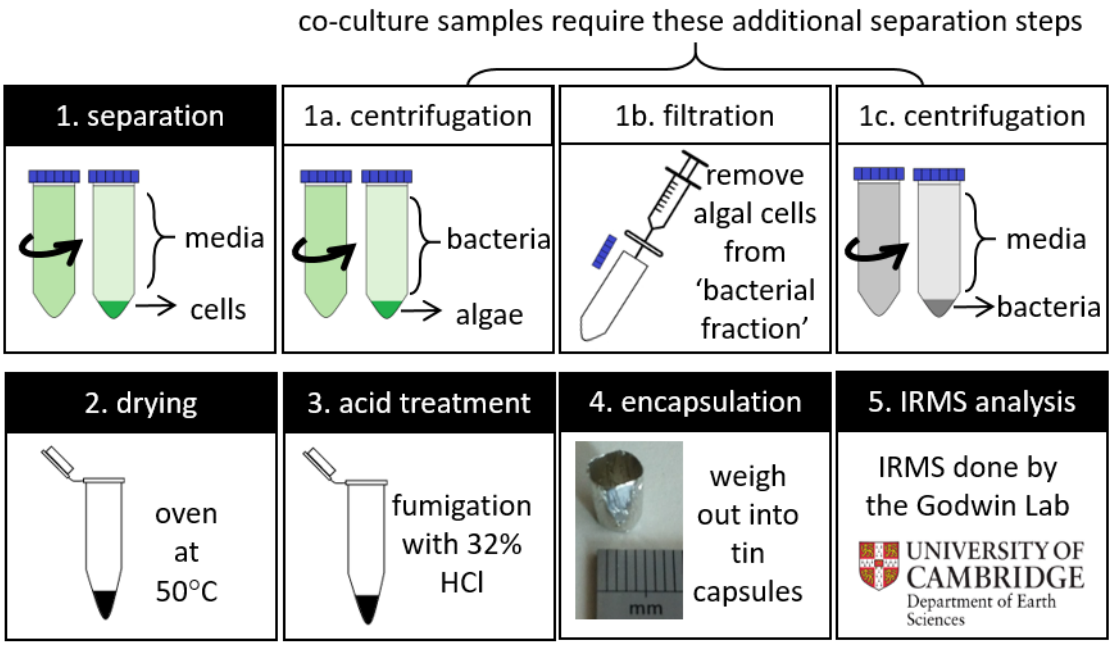

Figure C.1 **Sample preparation for IRMS**. An overview of the steps involved in preparing microbiological samples for analysis by Isotope Ratio Mass Spectrometry. (1) For axenic cultures, centrifugation was used to concentrate the cells. The supernatant was taken as the media fraction of the culture. (1a, b, c) For co-cultures, additional steps were required to separate the bacterial and algal biomass fractions. First a slow centrifugation step was used to concentrate the algal cells as a pellet. The supernatant was passed through a 3 µm filter in order to ensure that the algal cells were completely removed. In this way the filtrate provides the bacterial fraction of the culture biomass, which was concentrated into a pellet by centrifugation. (2) The concentrated pellets were transferred to an eppendorf and left in a 50 °C oven overnight to dry. (3) The samples were then placed in a desiccator with 32 % HCl for acid fumigation. (4) Samples were encapsulated in tin. (5) IRMS analysis was done by the Godwin lab at the Department of Earth Sciences, University of Cambridge.

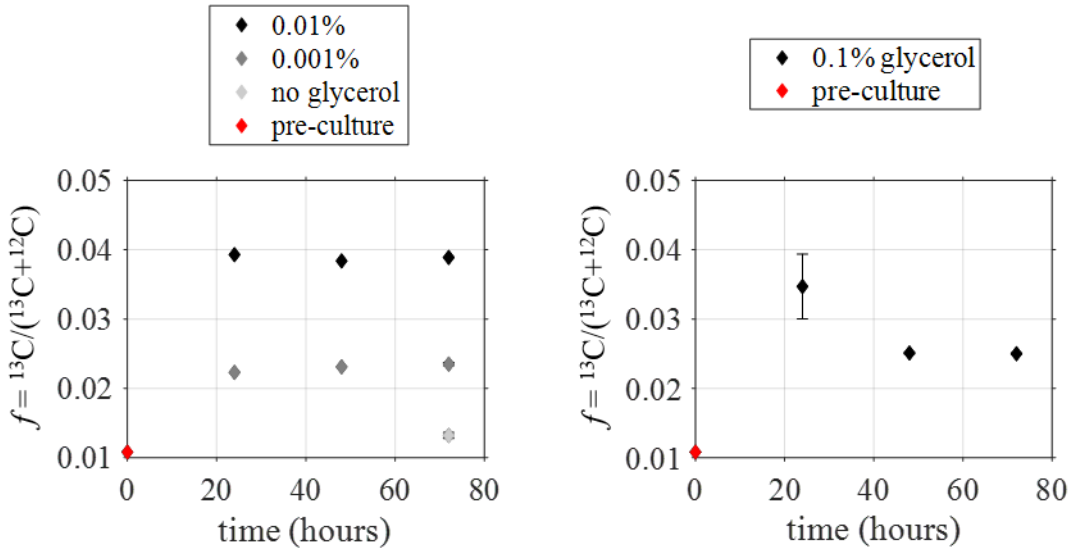

Figure C.2 **IRMS results for bacteria in axenic cultures with different concentrations of glycerol**. The ^{13}C-isotope fraction values obtained by IRMS analysis for samples taken at different time-points of the bacterial cultures grown axenically in different concentrations of unlabelled glycerol and 5 mM $NaH^{13}CO_3$. The number of measurements taken per sample was restricted by the amount of dry mass obtained. For the 24 h and 48 h samples from the 0.01 % and 0.001 % glycerol cultures only one measurement was obtained. For the other samples between 2-4 measurements were obtained and the plots show the mean and standard error for these points. In most cases the standard error is smaller than the point, except for the 24 h sample of the 0.1 % glycerol culture.

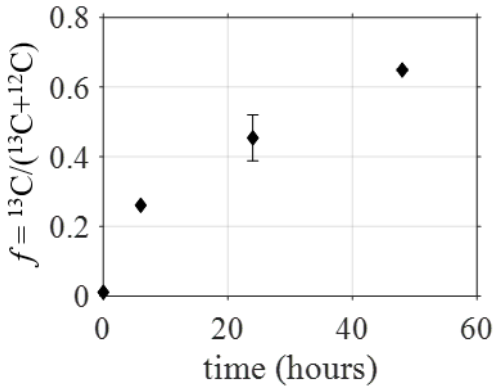

Figure C.3 **IRMS results for the pre-labelling culture of algae**. The ^{13}C-isotope fraction values obtained by IRMS analysis for samples taken at different time-points of the pre-labelling culture of algae, grown with 5 mM $NaH^{13}CO_3$. The number of measurements taken per sample was restricted by the amount of dry mass obtained. For the zero time-point sample from the pre-culture and the 6 h sample from the pre-labelling culture only one measurement was taken. For the 24 h and 48 h samples 4 and 3 measurements were taken respectively. For points with repeated measurements the mean was calculated and the error bars show the standard error in the mean.

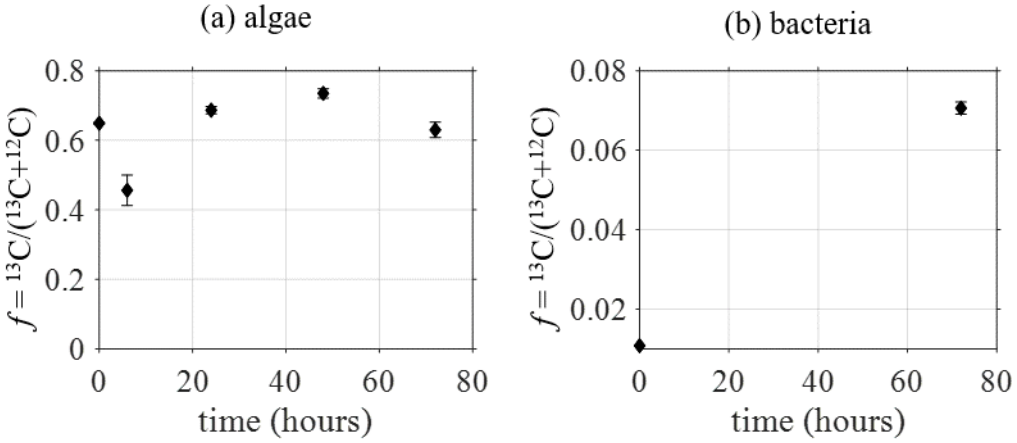

Figure C.4 **IRMS results for the co-culture**. The ^{13}C-isotope fraction values obtained by IRMS analysis for (a) the algal fraction and (b) the bacterial fraction of samples taken at different time-points of the co-culture. The plots give the mean and standard error of repeated measurements. For points where the error bars are not visible, the standard error is smaller that the point. The number of measurements taken per sample was restricted by the amount of dry mass obtained. For the samples of the algal fraction, 2-3 measurements were taken per sample. For the bacterial fraction of the co-culture, only the 72 h sample gave enough dry mass for IRMS analysis, for which 2 measurements were obtained. The zero time-point for the bacteria is the IRMS result for the unlabelled bacterial pre-culture, for which 3 measurements were taken. The error bars show the standard error in the mean.

Appendix D

Comparing growth rate and net carbon assimilation rate

Exponential growth of a bacterial population is given by the equation

$$b = b(0)\ e^{\mu_B t}, \tag{D.1}$$

with b and $b(0)$ the bacterial population size at time t and at time zero respectively, and μ_B the exponential growth rate. To relate population growth to the bacterial carbon biomass, it is assumed that

$$c_b = \frac{b}{Y_{b,c}}, \tag{D.2}$$

with c_b the bacterial biomass in $\mathrm{molC\,mL^{-1}}$ and $Y_{b,c}$ a constant that defines the bacterial carbon yield in $\mathrm{cells\,molC^{-1}}$. Substituting equation (D.1) into equation (D.2) gives an exponential growth equation for the bacterial carbon biomass

$$c_b = c_b(0)\ e^{\mu_B t}, \tag{D.3}$$

with $c_b(0)$ the initial bacterial carbon biomass concentration. The change in carbon biomass concentration is defined as

$$\Delta c_b = c_b - c_b(0). \tag{D.4}$$

Using equation (D.3), equation (D.4) can be rewritten as

$$\Delta c_b = c_b(0)\left(e^{\mu_B t} - 1\right), \tag{D.5}$$

which can be approximated for short time periods, assuming $\mu_B t \ll 1$, as

$$\Delta c_b \approx c_b(0)\,\mu_B t. \tag{D.6}$$

Rearranging, gives an expression for the exponential growth rate accounted for by carbon assimilation

$$\mu_B = \frac{\Delta c_b}{t\ c_b(0)}. \tag{D.7}$$

If bacteria loose carbon from their biomass due to respiration and take up carbon for growth and as an energy source, the net change in carbon biomass concentration can be defined as

$$\Delta c_b = \Delta c^+ - \Delta c^- \tag{D.8}$$

with Δc^+ the concentration of carbon biomass taken up and Δc^- the concentration of carbon biomass lost from bacterial biomass. The fraction of carbon in the sampled bacteria taken up from the labelled carbon source can be approximated as

$$F_s = \frac{\Delta c^+}{c_b}. \tag{D.9}$$

The fraction of carbon in the sampled bacteria from the initial carbon content can be approximated as

$$F_i = \frac{c_b(0) - \Delta c^-}{c_b} \tag{D.10}$$

According to the definition of net carbon assimilation $Fx_{net} = F_s/F_i$ (see equation (1.13) in section 1.4.2) and using equations (D.9) and (D.10), the net carbon assimilation can be approximated as

$$Fx_{net} = \frac{\Delta c^+}{c_b(0) - \Delta c^-}. \tag{D.11}$$

In order to compare net carbon assimilation with growth rate it is assumed that $\Delta c^- \ll \Delta c^+$, such that $\Delta c_b \approx \Delta c^+$, which gives

$$Fx_{net} \approx \frac{\Delta c_b}{c_b(0)}. \tag{D.12}$$

Therefore $\Delta c_b \approx Fx_{net} c_b(0)$, which can be substituted into equation (D.7) to give

$$\mu_B \approx \frac{Fx_{net}}{t}. \tag{D.13}$$

In summary, the above discussion shows that Fx_{net}/t is a reasonable approximation to the population growth rate when $t \ll 1/\mu_B$, $\Delta c^- \ll \Delta c^+$ and a linear relationship between population size and carbon biomass is assumed.